REPUBLIQUE DU CAMEROUN
Paix – Travail – Patrie
****
UNIVERSITE DE YAOUNDE I
****
FACULTE DES SCIENCES
****
CENTRE DE RECHERCHE ET DE FORMATION DOCTORALE EN SCIENCES, TECHNOLOGIE ET GEOSCIENCES
****
UNITE DE RECHERCHE ET DE FORMATION DOCTORALE PHYSIQUE ET APPLICATIONS
****
B.P 812 Yaoundé
Email: crftstg@uyi.uninet.cm Email:

REPUBLIC OF CAMEROON
Peace – Work – Fatherland
****
UNIVERSITY OF YAOUNDE I
****
FACULTE OF SCIENCES
****
POSTGRADUATE SCHOOL OF SCIENCE, TECHNOLOGY AND GEOSCIENCES
****
RESEARCH AND POSTGRADUATE TRAINING UNIT FOR PHYSICS AND APPLICATIONS
****
P.O. Box 812 Yaoundé
Email: crfd_stg@uy1.uninet.cm

Laboratory of Nuclear, Atomic, Molecular Physics and Biophysics

Study of the correlations between ^{226}Ra and ^{222}Rn in the soil and in dwellings at the bauxite bearing area of Fongo-Tongo, Western Cameroon

Submitted and defended in fulfilment of the requirements for the award of the Degree of **Doctorat/Ph.D in Physics**

Specialty Nuclear Physic, Dosimetry and Radiation Protection

By :

DJEUFACK Léonard Boris

Registration Number : **12W0080**

Master of Science in Physics

Under the supervision of

SAÏDOU

Professor

University of Yaoundé I

YEAR : 2024

UNIVERSITE DE YAOUNDE I
UNIVERSITY OF YAOUNDE I

FACULTE DES SCIENCES
FACULTY OF SCIENCE

DEPARTEMENT DE PHYSIQUE
DEPARTMENT OF PHYSICS

ATTESTATION DE CORRECTION DE LA THESE DE DOCTORAT/Ph.D

Nous, Professeurs **DJUIDJE KENMOE Germaine, BEN-BOLIE Germain Hubert** et Professeur, **NDJAKA Jean Marie Bienvenu** respectivement Examinateurs et Président du jury de la thèse de Doctorat/Ph.D de Monsieur **DJEUFACK Léonard Boris** Matricule **12W0080**, préparée sous la direction du Professeur **SAÏDOU,** intitulée « **Study of the correlations between ^{226}Ra and ^{222}Rn in the soil and in dwellings at the bauxite bearing area of Fongo-Tongo, western Cameroun** », soutenue le **Mardi 21 Mai 2024**, en vue de l'obtention du grade de Docteur/Ph.D en Physique, spécialité Physique Nucléaire, Atomique, Moléculaire et Biophysique, option Physique Nucléaire, Dosimétrie et Radioprotection, attestons que toutes les corrections demandées par le Jury de soutenance ont été effectuées.

En foi de quoi, la présente attestation lui est délivrée pour servir et valoir ce que de droit.

Fait à Yaoundé le 21 MAI 2024

Examinateurs

Pr DJUIDJE KENMOE Germaine,

Pr BEN-BOLIE Germain Hubert

Le Président du Jury

Pr NDJAKA Jean Marie Bienvenu

Le Chef de Département de Physique

UNIVERSITE DE YAOUNDE I ★ FACULTE DES SCIENCES ★ DEPARTEMENT DE PHYSIQUE
Le Chef de Département

Ndjaka Jean-Marie Bienvenu
Professeur

Study of the correlations between ^{226}Ra and ^{222}Rn in soil and in dwellings at the bauxite bearing area of Fongo-Tongo, western Cameroon

Laboratory of Nuclear, Atomic, Molecular Physics and Biophysics

THESIS

Submitted and defended in fulfillment of the requirements for the award of the Degree of

Doctorat/Ph.D in Physics

Nuclear Physics; Dosimetry and Radiation protection

By

DJEUFACK Léonard Boris

Registration number: 12W0080

Master of Science in Physics

Under the supervision of

Saïdou

Professor

UYI

May 22, 2024

Dedication

I dedicate this thesis to my late father **Mr. DJEUFACK Léonard**.

Acknowledgements

First and foremost, I express my gratitude to God Almighty for creating me and enabling me to undertake this work under excellent conditions and good health.

This thesis is the result of a collaboration between the University of Yaoundé I and the Institute of Geological and Mining Research (IRGM) through the Research Center for Nuclear Science and Technology. I extend my sincere appreciation for the invaluable collaboration, guidance, genuine scientific input, and relevance that this research has garnered. I am deeply thankful for all the material, financial, and human resources provided for the completion of this scientific endeavor.

I am immensely grateful to my advisor, Professor Saïdou, for supervising this thesis. He skillfully defined a research topic that was not only highly relevant to the set objectives but also profoundly enriching in its multidisciplinary scope. His dedicated involvement struck a perfect balance between meticulous oversight of my work and granting me the freedom to navigate the scientific process. This approach nurtured the genesis of ideas and the evolution of my research quest. I am honored by the trust he placed in me and his unwavering support, including the opportunities to present my work at various meetings, working groups, and congresses. Moreover, I appreciate his efforts in facilitating my professional integration. I must emphasize his exceptional human qualities, which significantly contributed to the successful completion of this thesis.

I extend a special thank-you to him for graciously welcoming me into his team of researchers at the Research Center for Nuclear Science and Technology. The knowledge and guidance gained from him over the years greatly enriched this thesis. His insights played a pivotal role in my growth within the laboratory and the fruition of this inspired and thought-provoking thesis.

I express my gratitude to all the members of the jury who evaluated this work, including the President and all other members.

I am thankful to Professor Ndjaka Jean Marie Bienvenu, Head of the Department of Physics at the University of Yaoundé I, for his guidance and supervision on academic and administrative matters. I commend him for his approachability and simplicity.

I also acknowledge Professor Ben-Bolie Germain Hubert, Head of the Laboratory of Nuclear Physics, for his excellent teaching, kindness, availability, and encouragement.

I extend my appreciation to Professor Kofane Timoléon Crépin, Head of the Laboratory of Mechanics, Materials, and Structures, for his visionary leadership in advancing science.

Special thanks are due to Wafo Paul for his outstanding teaching, kindness, availability, and encouragement.

I also express my gratitude to Professor Vondou Derbetini Appolinaire for his teaching, encouragement, and moral support.

My sincere thanks go to Professor Tchawoua Clément, Professor Djuidje Germaine, Professor Ekobéna Fouda, and Professor Bodo Bertrand for their contributions to this Ph.D. thesis.

I extend my heartfelt thanks to all the teachers at the Department of Physics of the University of Yaoundé I, especially those at the Laboratory of Nuclear, Atomic, Molecular, and Biophysical Physics, for their dedication to student training.

I am particularly grateful to the Institute of Geological and Mining Research of Cameroon (IRGM), particularly its Director General, Dr. Hell Joseph Victor, for granting me unconditional access to the Research Centre for Nuclear Science and Technology at the IRGM laboratory, where the practical part of this thesis was conducted. The conducive working environment provided an excellent opportunity for achieving high-quality results, for which I am immensely grateful.

I extend my thanks to the entire team at the Research Center for Nuclear Sciences and Technology of the IRGM of Cameroon for their contributions to this thesis.

I am thankful to the populations of the Dschang and Fongo-Tongo localities for welcoming us and allowing us to conduct this study. I also appreciate the support of the administrative and traditional authorities in facilitating the experimental part of this work.

For their advice, guidance, moral support, and encouragement throughout my Ph.D. studies, I am grateful to Dr. Bineng Guillaume Sammuel. His support and constructive advice were invaluable during the preparation of this thesis.

I also sincerely thank Dr. Takoukam Soh Didier and Dr. Hamadou Issa for their support and guidance over the years.

My gratitude extends to my academic mentors for their moral support, encouragement, social interactions in the laboratory, and sharing of scientific experiences.

I express my sincere gratitude to Dr. Zora S. Zuni from the Institute of Nuclear Sciences and Technology in Vin?a, Belgrade, Serbia, and Dr. Mikhail Zhukovsky from the Institute of Industrial Ecology of the Ural Branch of the Russian Academy of Sciences in Yekaterinburg, Russia, for their collaboration and review of my manuscript. I have learned significantly from their insights and am grateful for their contributions.

I am thankful to my classmates and colleagues for their assistance, intellectual contributions, and solidarity, which created a conducive and harmonious social environment for the completion of this thesis.

I extend my sincere thanks to Mr. Narcisse Aubin Kenang Kemassong for his support and assistance during the experimental phase of this work, as well as to Mr. and Ms. Kenfack Vouffo Vincent for their

hospitality and support.

To my late father, Mr. Djeufack Léonard, and my dear mother, Ms. Demmeze Elise, I honorably acknowledge your guidance, sacrifices, and prayers, which have contributed to the completion of this intellectual work. Your names will forever remain inscribed among those who have fulfilled their duties commendably.

I also express my gratitude to all my family members for their support, encouragement, and advice.

For his guidance, encouragement, and financial support since my enrollment at the University, I extend my thanks to Mr. Vandi Yeta Mathieu, CEO of the Société Générale des Technologies BTP. I also appreciate the moral support of Ing. Ngonou Ndassi Kevin and Ing. Betchen Prince.

I extend my endless gratitude to the entire family of the Centre Chrétien pour toutes les Nations for their prayers and guidance. I am particularly thankful to Dr. Tchuela Loic Josué for his advice, moral support, and financial assistance.

Numerous individuals have supported me throughout my academic journey and during the completion of this thesis. I express my deep gratitude to all of them, whether mentioned or not, and to all souls of goodwill who have contributed to this thesis in one way or another. May God bless each one of you.

Contents

Abstract

The aim of the current work is to study the correlations between ^{226}Ra and ^{222}Rn in soil, ^{222}Rn in soil and in dwellings a view to better predict the radiological risk of a locality. For this purpose, ^{222}Rn was measured at a depth of one meter from the ground surface using a Markus 10 detector. Activity concentrations of ^{226}Ra,^{232}Th and ^{40}K were measured in soil by *in situ* and laboratory γ spectrometry with the NucScout detector and a NaI (Tl) model 802 detector respectively. ^{222}Rn, ^{220}Rn and thoron progeny were measured in dwellings using RADTRAK^{2}®, RADUET and thoron progeny monitor detectors. ^{226}Ra, ^{232}Th and ^{40}K activity concentrations obtained by *in situ* γ spectrometry were 129 $\pm$ 22 Bq kg^{-1}, 205 $\pm$ 61 Bq kg^{-1}, and 224 $\pm$ 39 Bq kg^{-1} respectively, while those obtained by laboratory γ spectrometry were 129 $\pm$ 23 Bq kg^{-1}, 205 $\pm$ 61 Bq kg^{-1} and 224 $\pm$ 39 Bq kg^{-1} respectively. The mean values of ^{222}Rn concentrations in soil ranged from 35 kBq m^{-3} to 255 kBq m^{-3} with a geometric mean of 67 (18) kBq m^{-3}. In addition, 99% of ^{222}Rn measurement points in soil showed concentrations above 40 kBq m^{-3}, the recommended limit value according to the Swedish Radiation Protection Institute Regulations for classification of risk levels. The minimum and maximum values of ^{226}Ra obtained by laboratory and *in situ* measurement are respectively, three and five times higher than the world average value of 35 Bq kg^{-1} given by the United Nations Scientific Committee on the Effects of Atomic Radiation **(UNSCEAR)**. Moreover, ^{222}Rn concentrations in dwellings obtained with RADTRAK^{2}® detector varied from 85 Bq m^{-3} to 410 Bq m^{-3}, with a geometric mean of 152 (26) Bq m^{-3}. Those measured with RADUET detectors range from 31 to 123 Bq m^{-3} with a geometric mean of 60 (14) Bq m^{-3}. These indoor ^{222}Rn concentration values are higher than 100 Bq m^{-3}, the World Health Organization **(WHO)** reference value. ^{220}Rn concentrations and EETC varied from 36 to 688 Bq m^{-3} and from 1 to 22 Bq m^{-3} with a geometric mean of 241 (21) Bq m^{-3} and 8 (2) Bq m^{-3} respectively. However, a strong correlation between ^{222}Rn and ^{226}Ra activity concentrations determined by *in situ* and laboratory γ spectrometry measurements (R^2 = 0.86 and R^2 = 0.88, respectively) was found. When there was not a good air flow between the outside and inside of the dwelling, the correlation coefficients between ^{222}Rn concentrations in soil and in the dwellings were R^2 = 0.82 and R^2 = 0.73, respectively, for the earthen and concrete dwellings. Under the best natural ventilation conditions, these correlation coefficients decrease significantly. Their values were R^2 = 0.54 and R^2 = 0.34 for earthen and concrete dwellings respectively. In addition, a RadonEye+2 detector showed a daily accumulation of ^{222}Rn reaching values of 800 Bq m^{-3} in some dwellings when all doors and windows were closed. Architecturally, dwellings built with impervious

materials such as cement and concrete do not facilitate ^{222}Rn diffusion. They had lower ^{222}Rn concentrations and effective dose than those made of earth or mud brick. These results show that ^{222}Rn level in soil and those in the confined air of dwellings are strongly correlated.

Keywords: *Radium-226; Radon-222; Correlation; inhalation dose; Life Excess Cancer Risk; Lifetime Excess Absolute Risk.*

Résumé

Le but de ce travail est d'étudier les corrélations entre ^{226}Ra et ^{222}Rn dans le sol et, le ^{222}Rn dans le sol et ses concentrations dans les habitations en vue de mieux prédire le niveau de risque radiologique d'une localité. Le ^{222}Rn a été mesuré dans le sol à une profondeur d'un mètre de la surface par le biais d'un détecteur de type Markus 10. Les concentrations du ^{226}Ra, ^{232}Th et ^{40}K ont été mesuré dans le sol par spectrometrie γ *in situ* et en laboratoire, en utilisant respectivement les détecteurs de type NucScout et un scintillateur NaI(Tl) model 802. Par ailleurs, le ^{222}Rn, ^{220}Rn et les descendants du thoron ont été mesurées dans les habitations avec les détecteurs de types RADTRAK$^{2®}$, RADUET et les moniteurs des descendants de thoron respectivement. Les concentrations de ^{226}Ra, ^{232}Th et ^{40}K obtenues par spectrométrie γ *in situ* ont été respectivement de 129 $\pm$ 22 Bq kg^{-1}, 205 $\pm$ 61 Bq kg^{-1} et 224 $\pm$ 39 Bq kg^{-1} tandis qu'en spectrométrie γ en laboratoire elles ont été de 129 $\pm$ 23 kg^{-1}, 205 $\pm$ 61 kg^{-1} et 224 $\pm$ 39 kg^{-1} Bq kg^{-1} respectivement. Les concentrations de ^{222}Rn dans le sol étaient comprises entre 35 kBq m^{-3} et 255 kBq m^{-3} avec une moyenne géométrique de 67 (18) kBq m^{-3}. Par ailleurs, 99% des points de mesure de ^{222}Rn dans le sol ont présenté des concentrations supérieures à 40 kBq m^{-3}, la valeur limite recommandée selon le critère suédois de classification des niveaux de risque. De plus les concentrations de ^{222}Rn dans les habitations obtenues avec les détecteurs RADTRAK$^{2®}$ ont été entre 85 Bq m^{-3} et 410 Bq m^{-3}, avec une moyenne géométrique de 152 (26) Bq m^{-3}. Celles mesurées avec les détecteurs RADUET sont comprises entre 31 à 123 Bq m^{-3} avec une moyenne géométrique de 60 (14) Bq m^{-3}. Ces valeurs moyennes des concentrations de radon sont supérieures à 100 Bq m^{-3}, la valeur de référence de l'organisation mondiale de la santé **(OMS)**. D'autres part, les concentrations de ^{220}Rn et les EETCs ont variés de 36 à 688 Bq m^{-3} et de 1 à 22 Bq m^{-3} avec une moyenne géométrique de 241 (21) Bq m^{-3} et de 8 (2) Bq m^{-3} respectivement. Cependant, une forte corrélation entre les concentrations de ^{222}Rn et ^{226}Ra déterminées par mesures *in situ* et en laboratoire (R^2 = 0,86 et R^2 = 0,88, respectivement) a été observée. Lorsqu'il n'y avait pas une bonne circulation de l'air entre l'extérieur et l'intérieur de l'habitation, les coefficients de corrélation entre les concentrations de ^{222}Rn dans le sol et dans les habitations sont respectivement de R^2 = 0,82 et R^2 = 0,73 pour les logements en terre et en béton. Dans les meilleures conditions de ventilation naturelle, ces coefficients de corrélation ont diminué de manière significative. Leurs valeurs sont de R^2 = 0,54 et de R^2 = 0,34 respectivement pour les habitations en terre et en béton. De plus un détecteur RadonEye+2 a révélé une accumulation quotidienne de ^{222}Rn atteignant des valeurs de 800 Bq m^{-3} dans certaines habitations lorsque toutes les portes et fenêtres étaient

fermées. Sur le plan architectural, les logements construits avec des matériaux étanches tels que le ciment et le béton ne facilitent pas la diffusion du ^{222}Rn. Ils ont donc des concentrations en ^{222}Rn et une dose efficace plus faibles que ceux en terre ou en brique de terre. Ces résultats montrent que les concentrations de ^{222}Rn dans le sol et celles dans l'air confiné des habitations sont fortement corrélés.

Mots clés: *Radium-226; Radon-222; Corrélation; Inhalation dose; Excès de Risque de Cancer au cours de la vie ; Excès de risque absolu au cours de la vie.*

List of abbreviations and symbols

Rn : Radon

RnP : Radon progeny

Tn : Thoron

TnP : Thoron progeny

$\mathbf{F}_{Rn}$: Radon Equilibrium Factor

$\mathbf{F}_{Tn}$: Thoron Equilibrium Facto

$\mathbf{C}_{Rn}$: Radon concentration

$\mathbf{C}_{Tn}$: Concentration of thoron

$\mathbf{C}_{TnP}$: Concentration of thoron progeny

RADTRAK : Radon Track Detector

RADUET : Passive Integrated Radon-Thoron Discriminative Detectors

E-PERM : Electret-Passive Environmental Radon Monitor

EAED : External Absorbed Effective Dose

EEAD : External Absorbed Dose rate in air at 1 m from the ground

DNA : Deoxyribonucleic Acid

$\mathbf{D}_{Rn}$: Effective dose due to radon inhalation

$\mathbf{D}_{RnP}$: Effective dose due to the inhalation of radon progeny

$\mathbf{D}_{TnP}$: Effective dose due to the inhalation of Thoron progeny

$\mathbf{D}_{Tn}$: Effective dose due to thoron inhalation

DSTN : Solid state nuclear trace detector

$\mathbf{E}_{ext}$: Effective dose by external irradiation

$\mathbf{H}_{ext}$: External risk index

$\mathbf{H}_{in}$: Internal risk index

$\mathbf{I}_{\gamma}$: Radioactivity level index

$\mathbf{I}_{\alpha}$: Alpha Radiation Hazard Index

EETC : Equivalent concentration of thoron at equilibrium

Kerma : Kinetic Energy Released in Matter

IAEA : International Atomic Energy Agency

ICRP : International Commission on Radiological Protection

EPA: : Environmental Protection Agency

GPS : Global Positioning System

ICRU : International Commission on Radiation Units and Measurements

IEC : International Electrotechnical Commission

IRGM : Institut de Recherches Géologiques et Minières

IRSN : Institut de Radioprotection et de Sûretéé Nucléaire

ISO : International Organization for Standardization

WHO : World Health Organization

NORM : Naturally Occurring Radioactive Materials

OECD : Organization for Economic Cooperation and Development

UNSCEAR : United Nation Scientific Committee On the Effects of Atomic radiation

US EPA : United States Environmental Protection Agency

CRSTN : Centre de Recherche en Sciences et Techniques Nucléaires

List of Tables

List of Figures

General Introduction

Human beings are constantly exposed to both natural and man-made sources of ionizing radiation. These sources include cosmic rays from outer space and terrestrial radiation from the Earth, the latter being generated by various radioelements present in the Earth's crust [1]. The level of exposure to natural sources depends on the geological composition of the soil in a particular area. Natural and anthropogenic radioactivity can lead to significant public health concerns due to the emission of ionizing radiation. Radioactive elements such as ^{238}U and ^{232}Th are typically evenly distributed in soil, but certain geological and hydrogeological conditions can cause their accumulation in specific regions. When these enriched areas come into contact with the biosphere, there's a risk of dispersing these natural radionuclides into the environment [2].

Exposure to natural radioactivity, especially radon and its progeny, presents a public health challenge. Protecting individuals from the health effects of this radioactivity begins with monitoring radiation levels in the environment and identifying the sources responsible for exposure. This involves implementing an environmental sampling plan followed by on-site or laboratory radioactivity measurements. The aim of these measurements is to determine the activity levels of naturally occurring radionuclides, including α, β, or γ emitters. The selection of measurement methods depends on their capability to measure all radionuclides in the natural series of ^{238}U, ^{235}U, ^{232}Th, and ^{40}K, ideally [2].

Regions with mining potential are particularly important for environmental monitoring. Activities such as exploration and ore mining can lead to surface contamination by radioactive materials like ^{238}U, ^{232}Th, and ^{40}K, collectively known as Naturally Occurring Radioactive Materials (NORM) [3]. This contamination may contribute to environmental pollution and increase the exposure of local residents to natural radiation. The content and distribution of radioactive elements depend on the underlying bedrock [4, 5], varying from one environment to another based on geological structure, mineral composition, and soil depth [1].

Radon, a naturally occurring radioactive gas, can seep from rocks into the atmosphere through cracks and accumulate in confined spaces like homes. Notably, ^{222}Rn and ^{220}Rn, along with their progeny, contribute significantly to human exposure from natural radiation sources [6]. Radon is a recognized pulmonary carcinogen, second only to tobacco in its carcinogenic potential [7].

Numerous studies on natural radioactivity have been conducted globally, revealing high levels of radioactivity in specific areas, particularly those with mining potential [11, 12, 13, 14, 15]. These studies

have shown elevated concentrations of ^{238}U, ^{232}Th, and ^{40}K in soil, as well as high levels of ^{222}Rn and ^{220}Rn in homes compared to international standards set by organizations like UNSCEAR, ICRP, and WHO [16, 17, 18]. Correlations have been observed between the activity concentrations of ^{238}U and ^{232}Th in soil and ^{222}Rn and ^{220}Rn in dwellings in certain areas [20, 21]. Factors such as soil porosity, permeability, climatic conditions, and dwelling architecture influence the migration and accumulation of radon and its progeny [5, 16, 17, 20, 24, 25, 37, 38].

Assessing the risk of public exposure to radon and its progeny often faces challenges, including limited access to detection instruments in the field and public reluctance regarding the importance of radiation measurements. Mapping radon levels is crucial for identifying high-risk areas and implementing remediation plans, as seen in projects like CMR9009 in Cameroon. Overcoming logistical and deployment challenges in field measurements requires alternative methods, such as estimating radon exposure and risk without direct field measurements, based on relevant parameters.

In this study, we aimed to investigate correlations between ^{226}Ra and ^{222}Rn concentrations in soil, as well as between ^{222}Rn concentrations in soil and dwellings. We used both in-situ and laboratory gamma-ray spectrometry to measure ^{226}Ra, ^{232}Th, and ^{40}K concentrations in soil, along with solid nuclear track detection for ^{222}Rn and its progeny in dwellings. Our results, presented in three chapters, provide insights into natural radioactivity's impact on human health and correlations between radioelements in various environmental settings.

Chapter 1

Literature review

Introduction

Radiation is energy, in the form of particles or electromagnetic rays released in general by radioactive atoms. The three most common types of radiation are alpha particles, beta particles and gamma rays. Exposure to radiation is called irradiation. Irradiation occurs when all or part of the body is exposed to radiation from a source. Irradiation can lead to gene mutations and increases the risk of cancer (long term exposure) or radiation sickness depending on the amounts of radiation. This chapter provides some background on natural radioactivity and its origins, describes the various interactions of photons with matter, and briefly describes geology and radioactivity in the rock, some important phenomena and quantities which explain radiation exposure and its effects on the body.

1.1 Geology and radioactivity in the rocks

Natural radioactivity comes from the earth, mainly in the soil. It is non-uniformly distributed according to the pedological, mineralogical and geological characteristics of the different environments. The radioactive atoms present in the environment, such as ^{238}U, ^{232}Th and their progeny, which constitute **NORM** are also distributed in varying amounts in the geological matrix of the earth's crust. These atoms are permanently formed in soil or in the rock from cosmic radiation or sufficiently enriched under certain geological and hydrological conditions that can lead to a uranium, thorium or potassium mining deposit.

According to their nature, the grounds and the rocks have a specific radioactivity that allows them to be differentiated Table 1.1 presents the level of radioactivity in the different types of rocks. The detailed analyses by nuclear plates allowed to establish three origins of the radioactivity which are[42]:

- **Inclusions**: These may include other minerals or rocks, a liquid, a gas, or any other form embedded in the host mineral. There are two types of inclusions, depending on when they appear in the host

mineral: primary inclusions, which appear during the hydrothermal phase of crystallization in the fractures of the mineral, and secondary inclusions, which are formed after the crystallization of the mineral [42].

- **Fissures**:

  Under the action of the excessive rise in temperature and pressure, begin to crack, thus promoting the circulation of hot water or steam within it. The intensification of this phenomenon dissolves a lot of elements which are carried towards the empty zones generated by the fissures. The rock around the latter is mineralized to form crystals whose nature will depend on the initial rock, on the temperature, and on the pressure. The presence of radioelements such as ^{238}U, ^{232}Th and ^{40}K in the micro-fractures can thus induce a radioactivity with sometimes very high levels [42].

- **Dispersion in the essential minerals**

  In this case, All rocks are therefore likely to be radioactive, due to the general dissemination of the three natural radionuclides,^{238}U, ^{232}Th and ^{40}K . However, they are preferentially fixed on the fine sediments, so that the latter are more radioactive than the coarser sediments. When radioactivity is distributed in the essential minerals, it is contemporaneous with the rock.

  ^{40}K is an element that is very present in minerals essential to ^{238}U, ^{232}Th, they are in very small quantities and frequently associated with minerals such as rare earth and elemnts zirconium. In the minerals, they are present as traces or impurities. Zircons, allanites and monazites are the main radioactive accessory minerals found as microscopic inclusions in rocks. Zircons are commonly found in granites, pegmatites or syenites, gneisses and biotite contained in rocks. Allanites are present in some granites and pegmatites. Monazites are found in biotite granitoids and their pegmatites [42].

  A moderate uranium content is found in magma rocks. Analysis of several samples of acidic rocks (granites and granulite) revealed fairly high uranium and thorium contents. [5, 42]. Moreover, a high uranium and thorium activity concentration has been observed in granites and syenites, while they are lower in basalts and very low in peridotites [4, 42]. In the basic rocks, radioactivity level due to uranium and thorium is about three times lower than in the acid rocks. The average contents vary between 1 and 2 ppm in uranium, 3 and 4 ppm in thorium. In certain rocks such as gabbros, radioactivity due to uranium and thorium is very low. In diorites, it is average, whereas it is high in acidic rocks. In volcanic rocks, the primordial radioactive elements ^{238}U, ^{232}Th and ^{40}K are present, but at variable levels according to their nature [42]. In the sedimentary rocks, the radioactivity is lower because of the radioelement's dispersion.

  In addition, microscopic uranium and thorium minerals are not resistant to erosion. Nevertheless, inclusions such as zircons and many others rich in thorium such as monazite, apatite, and xenotime are resisting it and manage to accumulate in the placers. Unlike thorium, uranium is destroyed in an

oxidizing environment because of its chemical properties. It is therefore less present in sedimentary rocks [43]. Accordind to Table1.1, the sedimentary rock's radioactivity varies according to the kind and origin of the rock. In carbonaceous rocks and hydrocarbons such as asphalts, petroleum, mineral waxes and gases, uranium is present in varying levels. Its content is high in phosphates, low in phosphate clays and limestone, absent in clays. Thorium is absent in limestone, clays and phosphates [43].

Table 1.1: Radioactivity content level in some rock

Type of rocks	Radioactivity level in the rock		
	High	Medium	low
Sedimentary rock	Black shales	sandstones and sands	Simple limestones
	Phosphates	Gneiss	Coal
	Potassic evaporite	-	evaporites sans potation
	some sand basic	-	basic and ultra-basic rocks
Metamorphic rock	Quartz schist	-	granulite gneiss
	Black Schist	schists	amphibolite
	Maber	Silicate limestone	Eclogite
	-	Amphibolite	-
Magmatic rock	acidic rocks (granite family)	intermediate rocks (di-arist)	-

1.2 Radium

1.2.1 Discovery and historical context

Radium was discovered by Pierre and Marie Curie in 1898. This was a period of scientific emulation: Röntgen discovered X-rays in 1895. Henri Becquerel became interested in this phenomenon and discovered that uranium salts emit rays that are different from X-rays. They are called uranic rays. However, Marie Curie, interested in this discovery, studied uranium salts. She deduced from her experiments that the intensity of the radiation was proportional to the quantity of uranium. Moreover, this radiation is independent of external factors (light, temperature, etc.). She soon realized that this radiation was an atomic property,

specific to the atom. This is how she discovered that thorium is like uranium. Marie Curie called this phenomenon radioactivity. Once she had studied uranium salts and oxides, she turned her attention to the minerals containing uranium. She then discovered that certain minerals, including pitchblende (Figure 3), had a much higher radioactivity than expected. After much checking, she concluded that pitchblende contains an unknown element that has a much higher radioactivity than uranium [44].

Figure 1.1: Pitchblende sample [44].

Pierre and Marie Curie combined their efforts to isolate this element. Pitchblende is an ore of known composition, so they gradually separate the various constituents using known treatments. They succeeded in isolating two highly radioactive fractions: they concluded that two new elements had been discovered. Thus, in July 1898, they announced the discovery of polonium and in December of the same year, that of radium. But the scientific community remained perplexed and asked to see their elements [44]. The Curie duo then divided the work between them: Pierre Curie studied radioactivity while Marie isolated radium. Thus began a four-year period of work, during which they published some thirty articles and several memoirs. Finally, Marie Curie isolated 0.1 g of pure radium salt and determined the molar mass of radium: 226 g.mol^{-1}. Pierre Curie, for his part, discovered numerous phenomena associated with the radioactivity of radium, notably the emission of gas (radon), light and heat. He also discovered more general phenomena such as the existence of 3 types of radiation, which were later called α, β and γ [45].

1.2.2 Radium Physico-chemical properties

Radium is only bivalent. Its chemical properties are very close to those of its counterpart, barium, because, due to the lanthanide contraction, the radius of the Ra^{2+} ion (0.139 nm) differs very little from that of the Ba2+ ion (0.133 nm). Radium salts are isomorphic to the corresponding barium salts. Freshly

prepared, pure radium is white and bright, but it darkens when exposed to air (probably by formation of nitride Ra_3N_2. Its density is 5.5 g cm^3, higher than that of barium [45]. The precipitation of radium in the sulphate state, possibly in the presence of barium serving as an entrainer, makes it possible to separate it from almost all the elements. Lead, whose sulphate and nitrate are isomorphous to those of radium, can also be used as a carrier. It has the advantage that it can be easily separated in the halide or sulfide state because, in this form, it does not sy-crystallize with radium. The very low solubility of radium chloride and radium nitrate in concentrated solutions of the corresponding acid is also taken advantage of to perform certain separations. Thus, radium can be purified from the ?-emitters that accompany it in nature by precipitating it in a mixture of concentrated hydrochloric acid and ether, after the addition, if necessary, of a few milligrams of $BaCl_2$ as an entrainer [46].

The tendency of radium to form complexes is even lower than that of barium. The pK of the citric and tartaric complexes are, at 25^0C, 2.36 and 1.24, respectively. However, the complex with ethylene-diamine-tetra acetic acid is strong enough to inhibit the precipitation of radium sulphate.

1.2.3 Uses of radium: Medical field and industrialization

Thanks to its radioactive properties, radium aroused enthusiasm until the 1940s. It was used in various fields such as radiotherapy, pharmacology, industry and in everyday life. In 1900, two Germans, Walkhoff and Giesel, discovered that radium had physiological properties. Thus, Pierre Curie, in collaboration with leading physicians, decided to study its effects on animals. They found that radium could heal wounds and even tumours. In June 1901, Pierre Curie and Henri Becquerel published a note together on "the physiological effects of radium rays": this was the beginning of radiotherapy, which was called radium therapy or curietherapy at the time. Thus, doctors used radium needles or applicators, "bandages, poultices (Figure 7)" to treat tumors and other skin diseases. The results on dermatological diseases as well as on skin cancers are very promising. This is why radiotherapy was subsequently tested on many incurable diseases of the time (cancer, tuberculosis...) [46].

Radium was also used during the First World War to take X-rays in order to precisely locate bullets inside the wounded and thus to facilitate surgical operations. Following the 1903 Nobel Prize and the success of "radium therapy", radium became more widely available and its extraordinary properties were widely promoted. Thus, from the beginning of the 20th century, radium was used to produce radio luminescent paints. Indeed, the radium salts associated with zinc sulfidic in a varnish constitute a paint that emits a continuous light not very intense. Therefore, the watch industry will use these paints to make fluorescent clocks and clocks. The radio fluorescent properties of radium were also used for night lighting. A little later, manufacturers of pharmaceutical products distributed many products containing radium with miraculous virtues, which are not medically proven. This is how radon emanators, ointments, compresses, ampoules, drinkable potions, wool and food supplements for animals appeared [47].

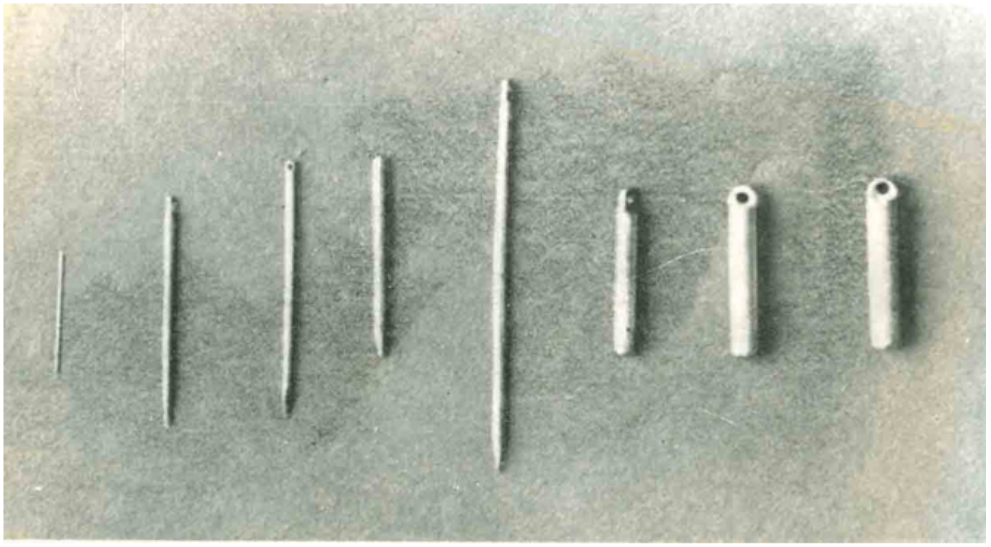

Figure 1.2: Needles and tubes used in radiotherapy [44].

1.2.4 Radium isotopes

In 1934, Irène and Frédéric Joliot discovered artificial radioactivity, thus showing that radionuclides not present in nature could be created, and received the Nobel Prize in Chemistry in 1935. In the medical field, radium was officially abandoned in 1976 for radioprotection reasons and was replaced by Iridium-192 and cesium-137 in radiotherapy. The use of radium left many polluted sites (sites where the soil or buildings were contaminated by radium) and radioactive objects. Moreover, radium has no stable isotope, and therefore no standard atomic mass can be assigned to it. The longest-lived isotope, and the most common, is radium-226 which has a half-life of 1600 years. In addition, four of its 25 possible isotopes exist in nature in trace amounts: ^{223}Ra, ^{224}Ra, ^{226}Ra and ^{228}Ra, all four radioactive and all derived from the radioactive decay of other naturally occurring radioisotopes [44, 45].

♣ → **Radium 223**: It is an alpha emitter with a half-life of 11 days. It was historically referred to as actinium X, since it is the daughter isotope of actinium 227 in the decay chain of uranium 235.

♣ → **Radium 224**: It is, along with radium 228, traditionally associated with thorium, as it is part of the decay chain of ^{232}Th. It was historically referred to as thorium X, as it is the direct descendant of ^{228}Th. Along with radium 225, it is considered a potential candidate for nuclear medicine applications because of its short half-life (3.62 days) and the four alpha emitters present in its decay chain.

♣ → **Radium 225**: It has a half-life of 15 days, it is the precursor of actinium 225, which decays in a chain emitting a total of four alpha particles1, making it an interesting candidate for applications in alpha-immunotherapy. Radium itself is difficult to complex and the lack of a suitable ligand limits its applications.

To overcome this difficulty, alternative ways of binding radium are being studied.

♣ → **Radium 226**: It is the most common isotope of radium, representing more than 99% of the radium naturally present on Earth, the other isotopes being present only in trace amounts. The average content of radium 226 in soil is about 0.7 ng/kg (0.7 ppt). Radium-226 is present on Earth as a decay product that is part of the uranium-238 decay chain (often called the radium series). With a half-life of 1600 years,it is very highly radioactive, with a specific activity of 36.6 GBq g^{-1}. This activity is practically that of the old curie unit, conventionally equal to 37 GBq. It decays by alpha radioactivity, with an energy of 4,784 keV (94%) or 4,602 keV (6%), and by emitting γ radiation of 186.211 keV (Intensity 3.555%). Its γ-radiation (direct, or via its progeny) makes a small contribution to the terrestrial exposure to which individuals are naturally subjected. The decay energy of pure radium gives off a specific power of 28 W/kg, which rises to 160 W/kg when added after a few days to that of its short-lived progeny, which rapidly reach secular equilibrium [47].

♣ → **Radium 228** is naturally present in soil in small quantities (of the order of 5 ppq) as a descendant of thorium 232. It is in equilibrium in this chain with actinium 228, more easily detected by gamma spectrometry. Because of its presence in this decay chain, it was historically called mesothorium I when it was discovered in 1907 by Otto Hahn. It is marketed under the brand name **Xofigo** and as radium chloride for medical application against bone metastases of prostate cancer. It binds to bone because of its chemical analogy with calcium [46].

1.2.5 Health effects and risks due to radium

It was only gradually after its discovery that the danger of radium radiation became apparent. The first to be alerted were the radium workers. For example, several deaths were observed at the Radium Institute in London, dedicated to medical applications. This is why, in 1921, a series of recommendations and protection rules were published: the walls of radiotherapy rooms were henceforth lined with lead and radium handling required the use of special precautions. However, these protections were not sufficient; industry, on the other hand, did not seem to be really concerned about the potential danger of radiation and working conditions in the factories remained dangerous. In 1917, several cancers were reported among female workers who used radium-based luminescent paint and refined their brushes by mouth: this was the trial of the Radium Girls. In 1937, radium was banned for non-medical use [48]. Radium emits α and γ radiation. The α radiation corresponds simply to the emission of helium atoms during the disintegration of the nucleus. The γ radiation, on the other hand, is made up of photons, like visible light or X-rays, but these carry a much higher energy, which makes them dangerous. There is also another type of emission: β radiation. It can be broken down into β^+ radiation (positron emission) and β^- radiation (electron emission). It should be noted that radium and its descendants are practically not affected by this last type of radiation [48].

1.3 Radon

After the discovery of radium by Pierre and Marie Curie, other natural radioelements were discovered, including radon. In 1900, the German Friedrich Ernst Dorn demonstrated that air in contact with radium compounds becomes radioactive and that this phenomenon is due to a gaseous emanation from radium, which is radon. The same year, Rutherford showed that this gas is formed during the radon decay with the emission of an alpha particle. Radon and its progeny measurement in the environment has become an important mission for environmental radioactivity analysis and measurement laboratories in recent years. It is estimated that this element is the main source of natural radiological exposure for humans [1, 7].

1.3.1 Physico-chemical properties and radon isotopes

Etymologically, radon derived from radium. radon in the past was called nitens, which means bright, indoor, colourless, tasteless and radioactive. It is invisible and was historically called emanation. Radonn is a rare inert gas, of natural origin, it is the heaviest gas, density 9,72 kg m $^{-3}$ to 273^{o}K that is to say 8 times denser than the air. It liquefies at 68°C and solidifies at 71°C. Radon is measured according to its activity. The Curie (Ci) and the Becquerel (Bq) tell us how much a radioactive material is decaying every second 1Ci = 37109Bq = 37 billion curies per second). The radiation dose from radon and its progeny is measured in terms of the energy they transmit to tissues (in units called gray) [49]. Radon has 33 radioactive isotopes, of which thirty are artificial and only three are in the natural state with a range of atomic masses from 195 to 228, these are:

- Radon: ^{222}Rn ($T_{1/2}$= 3.8 days),
- Thoron: ^{220}Rn ($T_{1/2}$ = 54.2 seconds),
- Actinon: ^{219}Rn ($T_{1/2}$ = 3.92 seconds)

They differ from the physical parameter "$T_{1/2}$" and decay by alpha emission leading to unstable polonium isotopes. The three radon isotopes (radon, thoron and actinon) belong to the natural radioactive families of uranium ^{238}U, thorium ^{232}Th and uranium ^{235}U respectively. ^{222}Rn belongs to the decay chain of ^{238}U, ^{220}Rn belongs to the decay chain of ^{232}Th and ^{219}Rn belongs to the decay chain of ^{235}U respectively [2, 39]. In these three families, the three parent elements have a very long half-life and generate a series of radioactive decay products until the appearance of a stable element: lead isotope. The different radioelements formed are solids (at normal temperature and pressure) with the exception of one per family which is the radon isotope.

1.3.2 Radon dispersion in the environnement

Dispersion of radon in the environment depends strongly on atmospheric conditions, and the resulting distribution is far from being homogeneous: over the continents, the radon activity decreases with increasing altitude. There is thus a quasi-exponential profile characterized by a decrease of a factor of 2.3 when the altitude increases by 3.7 km [50]. During the night, the temperature inversions strongly decrease the atmospheric diffusion. Radon then stagnates at the ground level. Its concentration in the air can thus increase by a factor of 10 to 100. To model, in a simplified way, radon dispersion over the continents, one generally considers a sufficiently extended zone with a supposedly uniform flux C. The distribution of radon and radon progeny activity in air can then be expressed only as a function of the height above ground. It is governed, in steady state, by the following differential equations:

$$\frac{d}{dz}[K(z)\frac{dC_0}{dz}] - \lambda_0 C_0 = 0 \tag{1.1}$$

$$\frac{d}{dz}[K(z)\frac{dC_j}{dz}] - \lambda_j C_j - \lambda_{j-1} C_{j-1} \tag{1.2}$$

where j is: when j=0, the radon, and for j going from 0 to 4 its different progeny (^{218}Po, ^{214}Pb, ^{214}Bi, ^{214}Po). C_j is the concentration of radionuclide j in the air at altitude z [Bq m $^{-3}$], λ_j is the radioactive decay constant of j [s^{-1}], K(z) is the diffusion coefficient [m^2 s^{-1}], it increases with height.

1.3.3 Dispersion of natural radon isotopes

The low content of ^{235}U in the earth's crust (on average 0.7% of total uranium) leads to a limited production of ^{219}Rn. Its short half-life also limits the distance travelled before decay. ^{219}Rn is therefore practically absent in our environment. Even if it is produced in larger quantities, the fast decay of ^{220}Rn induces mostly low volume activities of this isotope in the atmosphere. In contrast, more significant amounts of ^{222}Rn can migrate to the air.radon concentration in the ground varies in space, in particular according to a vertical gradient, and in time, mainly according to the meteorological conditions (temperature, precipitation, barometric pressure) and the intrinsic characteristics of the ground (geology, paedology) [50].

1.3.4 Radon in soil-atmosphere interface

Radon concentration in soils varies in space, notably according to a vertical gradient, and in time, mainly as a function of meteorological conditions (temperature, precipitation, barometric pressure) and intrinsic soil characteristics (geology, pedology). The amount of radon that comes to the soil-atmosphere interface per unit of time and per unit of area is called the exhalation flux. Figure 1.3 show the process of radon emanation in the ground to the exhalation in the atmosphere. Radon exhalation flux depends on the volume activity of radon in soil, and the meteorological conditions. the average flux at the earth's surface is estimated at

2×10^{-2} Bq m^{-2} s^{-1}. As with radon concentrations in soils, radon exhalation flux varies in a temporal manner. At the earth's surface, the average volume activity of ^{222}Rn is 400 Bq m^{-3} [50]. Radon level in the dwellings

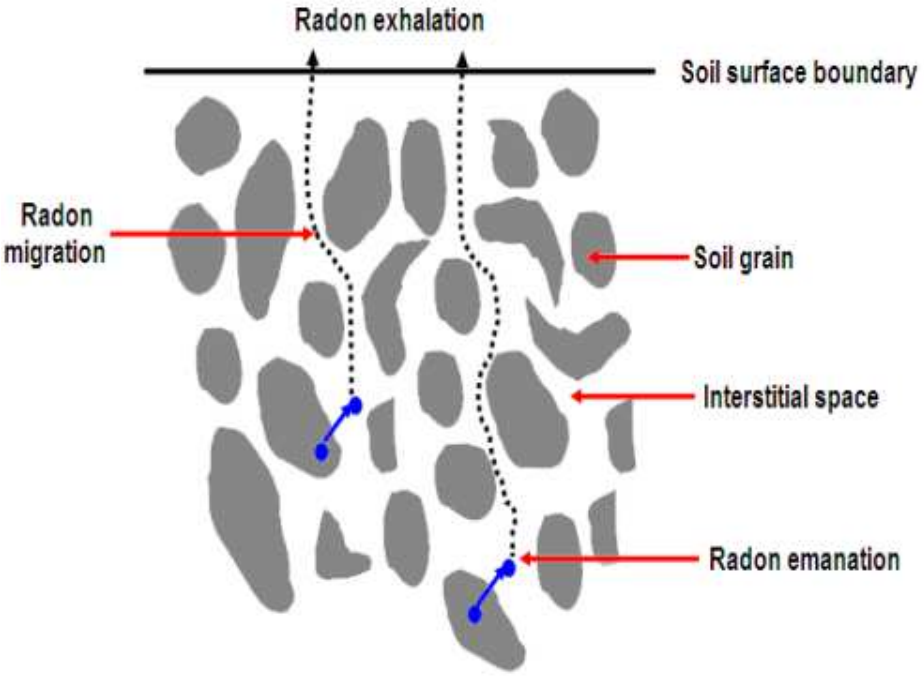

Figure 1.3: Schematic representation of the radon emanation [1]

According to Figure 1.4 ^{222}Rn infiltration in the house is favoured by convection phenomena induced by the temperature difference between the inside and the outside of the dwelling or by a pressure difference existing between the air in the house and the air in the ground. In fact, radon originates in soil gas located under the dwellings and in some cases, in the building materials. The radon concentrations are also dependent on the characteristics of the dwelling: - existing transfer pathways (staircase, pipe passage...), - ventilation rate and occupants' routines [6]. Some studies have shown that the ^{222}Rn concentrations in water vary greatly. They can sometimes contribute strongly to the entry of ^{222}Rn into a room by outgassing [51]. Surface water does not contribute significantly to airborne ^{222}Rn concentrations; on the contrary, groundwater can be a higher contributor, especially deep wells. These results highlight the accumulation of radon inside the dwelling when there is no human activity, corresponding to a confined environment, i.e., at night, doors and windows. The decrease in radon concentration is correlated with the resumption of human activities in the house. During the day this concentration does not exceed 200 Bq m^{-3} with an average value of 100 Bq m^{-3}.

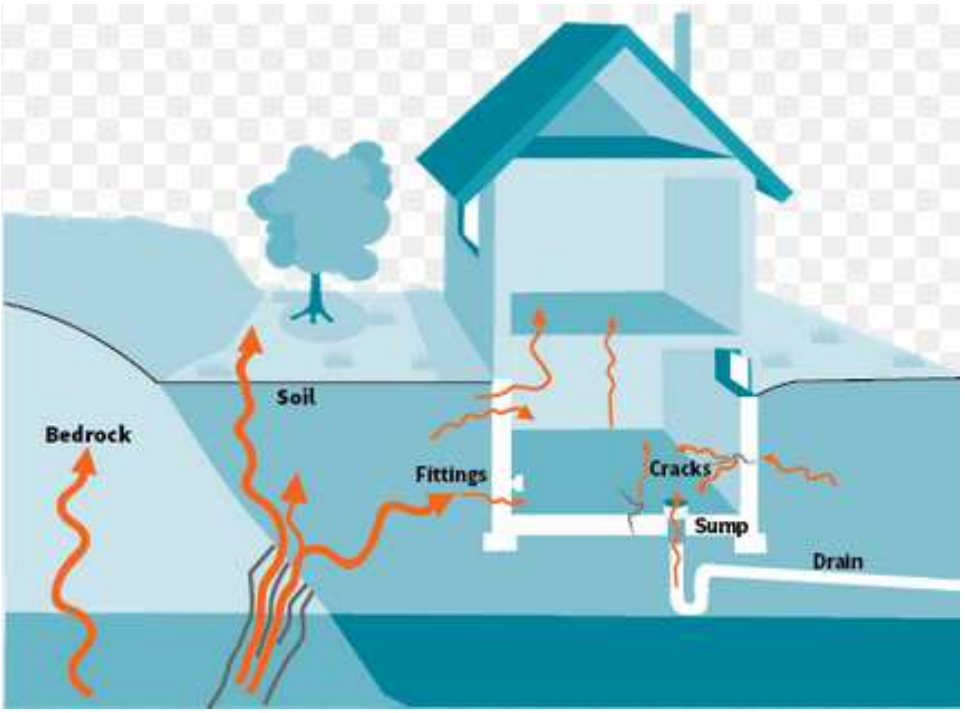

Figure 1.4: Radon ingress in a dwelling [1].

1.4 Human exposure to ionising radiations

1.4.1 Natural radiation exposure sources

These sources are different in nature depending on the physical form of the earth and its physical and chemical constitution:

- **Cosmic radiation**: Cosmic radiation], of galactic or solar origin, is composed of charged particles, mainly protons, but also α particles and heavier nuclei. These highly energetic particles (average energy of 10 GeV) interact with the nuclei of atoms in the atmosphere by spallation and produce secondary particles that initiate further cascade reactions, resulting in the presence of a variety of particles: protons, neutrons, pions, kaons, muons, electrons, neutrinos and photons. The composition of cosmic rays (in particular the ratio of directly ionizing particles to neutrons), their energy and intensity are strongly dependent on altitude. The intensity of cosmic rays depends to a lesser degree on other factors such as geographic latitude (due to the influence of the Earth's magnetic field) and solar activity [1].

- **Terrestrial radiation**: The natural radioactivity of the ground comes from its content of ^{40}K as well as uranium and thorium progeny. Their concentrations vary from one area to another and is a few hundred Bq kg^{-1} for ^{40}K and a few tens of Bq kg^{-1} for ^{238}U and ^{232}Th daughters. The effective

dose from γ-rays inside a home is on average 1.5 times greater than in the open air. According to **UNSCEAR 2000**, the world average effective dose is 0.5 mSv/year [1].

- **Proper radiation**: ^{40}K is found in relatively large quantities in plants and in food. Its concentration is of the order of 100 Bq.kg^{-1} for cereals (dry matter) and 30 to 60 Bq l^{-1} of milk. At equilibrium, the human body contains 3000 to 6000 Bq of ^{40}K. Other radioelements, such as ^{210}Pb, ^{210}Bi and ^{210}Po are also present in the body, but in much smaller quantities. The world average value of the committed dose according to **UNSCEAR 2000** is 0.3 mSv, of which nearly 60% is due to potassium-40 [1].

1.4.2 Artificial radiation sources

Exposure to artificial sources is generally observed in the workplace or by the general public in the event of a nuclear accident:

- **Occupational sources**: Occupational exposure is constantly monitored by the Commission or by the radiation protection service in some states, which publishes an annual report on this subject. Occupational radiation concerns four sectors of activity: medicine, research, nuclear power stations, industry and public services. The medical sector is characterized by a large number of people monitored and a relatively low collective dose, while the situation is reversed in the field of nuclear power stations [52].

- **Medical radiation sources**: The distribution of doses in the body in the case of medical applications is very heterogeneous. Moreover, the doses vary greatly from person to person and are also dependent on age and sex. A worldwide survey has been conducted to assess the doses received by the population from medical applications [1]. In the analysis of the results of this survey, countries were grouped into four health levels that differ significantly in both the frequency of radiological procedures and the doses received.

- **Radiation from other artificial sources**: The public is also subject to the following sources of radiation: Radioactive releases into the environment from companies (hospitals, nuclear power stations, industrial companies) using ionizing radiation. External exposure in companies or public places (hospitals) where ionizing radiation generating installations or sealed radioactive sources are handled. Food contamination; Various contributions; these are minor contributions due to smoking, high altitude flights, small sources used in consumer products (watches); the irradiation is difficult to quantify, but is on average less than 0.1 mSv/year [1].

1.4.3 Types of radiation exposure

As presented in Figure 1.5, human exposure to radiation that reaches the body can be external or internal depending on whether the source is outside or inside the body.

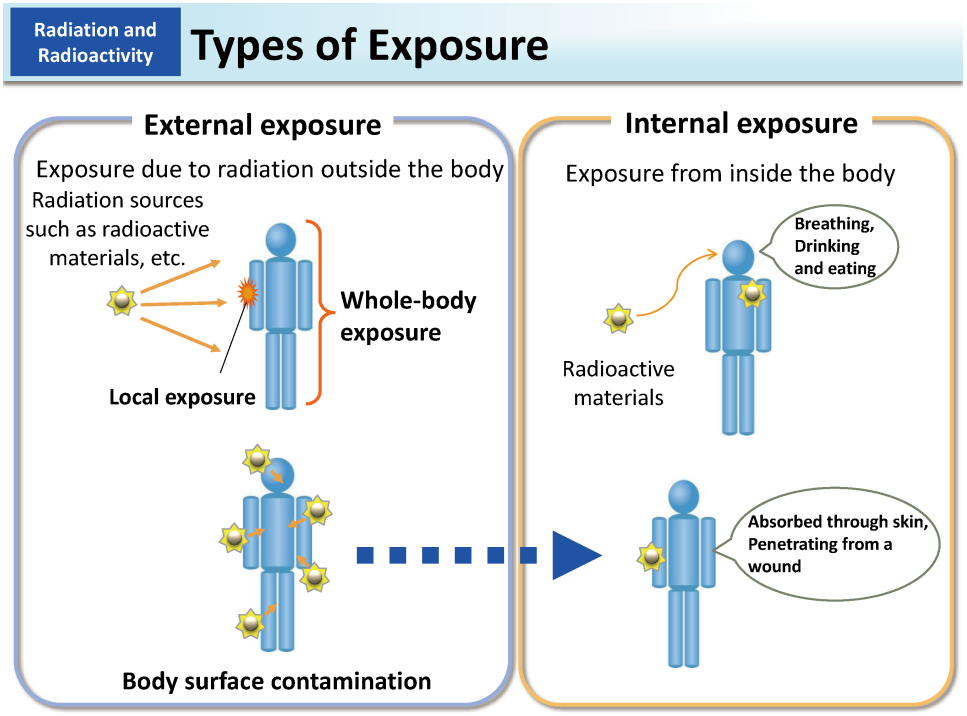

Figure 1.5: Type of exposure to radioactivity.

a → External exposure

When one is near a radioactive source or when it is in direct contact with the skin, it is called irradiation or external exposure. External exposure is therefore related to irradiation from a distance or by skin contact, by beams of β, γ, X or neutron radiation emitted by radionuclides present in the environment. It can come from a gaseous or particulate plume where the individual is evolving, from a deposit of these particles on the ground or at depth, or from contamination of the skin by direct contact or by immersion in water. It ceases when the source of exposure is eliminated or sufficiently distant. External exposure can be grouped into three main categories such as cosmic radiation exposure, terrestrial radiation exposure and proper radiation exposure.

b → Internal exposure

Inhaling or swallowing radioactive substances, or when these substances enter the body through a wound or through the skin, this is called contamination or internal exposure [52]. Internal exposure can result from incorporation of radioactive substances through inhalation, ingestion, skin contamination or injury. In the workplace, ingestion is very rare, while respiratory contamination is the most common. Although it also

remains very rare, contamination by injury remains a constant concern for protection services because the contamination it causes can be significant. Cutaneous contamination, on healthy skin, has few consequences except for tritiated compounds that can cross the skin barrier. Irradiation linked to contamination inside the body does not cease with the end of exposure to the pollutant; it will continue as long as the radionuclide is present in the body.

- **Incorporation through inhalation**

  Subjects immersed in a radioactive plume or in air contaminated with radioactivity can be exposed internally as a result of inhalation of airborne radioactive materials. Inhaled radionuclides irradiate tissues of the respiratory system as well as other organs. The committed effective dose to a subject is determined by many physical, chemical, and biological factors, including the amount and type of material inhaled, its deposition and retention in the respiratory system, and the subject's breathing rate [53].

- **Incorporation through ingestion**

  Ingestion is the main route of intake for the public through contamination of food and water. This contamination comes from either atmospheric emission falling to the ground or from liquid discharges from factories. Contrary to the other routes of entry, the contamination of populations by ingestion generally involves only infinite quantities of radionuclides that always stay at trace levels. This route of intake also involves inhaled radionuclides that "reach" the gastrointestinal tract. Passing through the skin or incorporation by injection It is a risk only related to a professional activity. Generally speaking, healthy skin is an effective barrier to the transit of substances, whether radioactive or not, and the risk is eliminated by wearing waterproof gloves and prohibiting workers using unsealed sources from handling in case of skin lesions. Transfer of contamination through healthy skin will be encountered primarily through contact with tritiated water. Wounding is a less common route of entry than inhalation, but is generally more serious in terms of the level of contamination generated. Radioelements in the body release energy as they decay. This released energy will disturb the atoms constituting the organs and tissues through many interactions [1].

1.5 Dosimetry and protection quantities

1.5.1 Absorbed dose

The activity of a radioactive source is expressed in Becquerel (Bq) which is also the number of nuclei that spontaneously transform per second. When radiation interacts with matter, it transmits energy to it. This transfer is defined by the absorbed dose of which the unit is gray (Gy) which is also the deposit of 1 J kg^{-1}. The energy deposited at a point makes it possible to define the importance of an irradiation. The absorbed

dose Dabs or radiation at a point, corresponds to the energy which is deposited (dE) per unit mass (dm). The absorbed dose is given by the following relation:

$$D_{abs} = \frac{dE}{dm} \tag{1.3}$$

The activity of a source is not directly related to the absorbed dose because D_{abs} varies according to the radioelements and therefore the nature of the emitted radiation. Depending on the type of radiation, it is possible to obtain different biological effects at equivalent absorbed dose [52]. For example, when α-beams enter the material, they are braked more rapidly by the γ or X radiation. They are therefore more disruptive because they spread less their energy deposition. To take into account the nature of the radiation emitted, it is therefore necessary to use an equivalent dose.

1.5.2 Absorbed dose rate

The absorbed dose rate, Dabs (nGy h^{-1}) is the quotient of dD by dt, where dD is absorbed dose increment during the corresponding dt time interval:

$$\dot{D_{abs}} = \frac{dD}{dt} \tag{1.4}$$

1.5.3 Equivalent dose

Biological detriment to an organ depends not only on the physical average dose received by the organ but also on the pattern of the dose distribution that results from the radiation type and energy [49]. For the same dose to the organ a or neutron radiation will cause greater harm compared to γ-rays or electrons. Effectiveness of the given radiation in inducing health effect is expressed in equivalent dose. Equivalent dose H_T as per equation 1.5 is the product of the absorbed dose D and the radiation weighting factor of the radiation [19]. The radiation weighting factors are related to the particular type of radiation and depend on the ionizing capacity and density.

$$H_T = \sum_R W_R D_{T,R} \tag{1.5}$$

where $D_{(T,R)}$ is the absorbed dose in tissue T due to radiation R. In 2007, the ICRP defined W_R values that are grouped in the table. The equivalent dose rate (H_T) is the equivalent dose based on the exposure time (Sv yr^{-1}).

1.5.4 Effective dose

Various organs and tissues in the body differ in their response to radiation. For the same equivalent dose, the detriments from the exposure of different organs or tissues are different. Equivalent dose in each tissue

Table 1.2: Tissue weighting factors according to ICRP [53], (*) Remaining tissues: Adrenals, extrathoracic region, gall bladder, heart, kidneys, lymphatic nodes, muscle, oral mucosa, pancreas, prostate (man), small intestine, spleen, thymus, uterus/cervix (woman)

Tissue	Tissue weighting factor W_T	$\sum W_T$
Bone-marrow (red), colon, lung, stomach, breast, remaining tissues (*)	0.12	0.72
Gonads	0.08	0.08
Bladder, Oesophagus, Liver, Thyroid	0.04	0.16
Bone surface, Brain, Salivary glands, Skin	0.01	0.04
	Total	1

or organ is multiplied by a tissue weighting factor W_T and the sum of these products over the whole body is the effective dose, given by following equation [19].

$$E = \sum_T W_T H_T = \sum_T W_T \sum_R W_R D_{T,R} \tag{1.6}$$

The effective equivalent dose rate (E) is also the effective dose based on the exposure time (Sv yr^1). These factors were obtained from a reference population of equal numbers of men and women ranging in age. Because of the normalization of all tissue weighting factor values is unity, the effective dose equals a uniform equivalent dose over the whole body. The SI unit of effective dose is also the Sievert (Sv). Table 1.2 lists the tissue weighting factors for tissues and organs of the human body.

1.6 Biological effects of radiation

Radiation effects on an organism are physical, chemical, and biological in nature (Figure 1.6). Physical effects are the result of energy transfer by ionization or excitation and are immediate (on the order of 10^{-15} seconds). These effects trigger chemical changes by atomic modification or molecular bond breaking, which result in the activation or modification of chemical reactions. This step takes about 10-6 seconds [54]. The biochemical changes produce modifications on the structures and the vital functions which extend over a period ranging from one second to several years. In some cases, these changes can be corrected by molecular or cellular mechanisms, thus recovering normal functions. The effect of radiation is therefore variable and ranges from faithful repair of a cell-to-cell death. There is a great disproportion between the number of ionizations and excitations produced by the radiation and its biological effect. Indeed, a dose of 10 Gy,

lethal in whole-body irradiation for humans and most mammals, corresponds to an energy absorption of 10 J per kilogram of tissue, or a temperature rise of only 2 thousandths of a degree, or 2×10^{18} ionizations. Thus, only 2 out of 10^7 water molecules are affected by the ionization process [52].

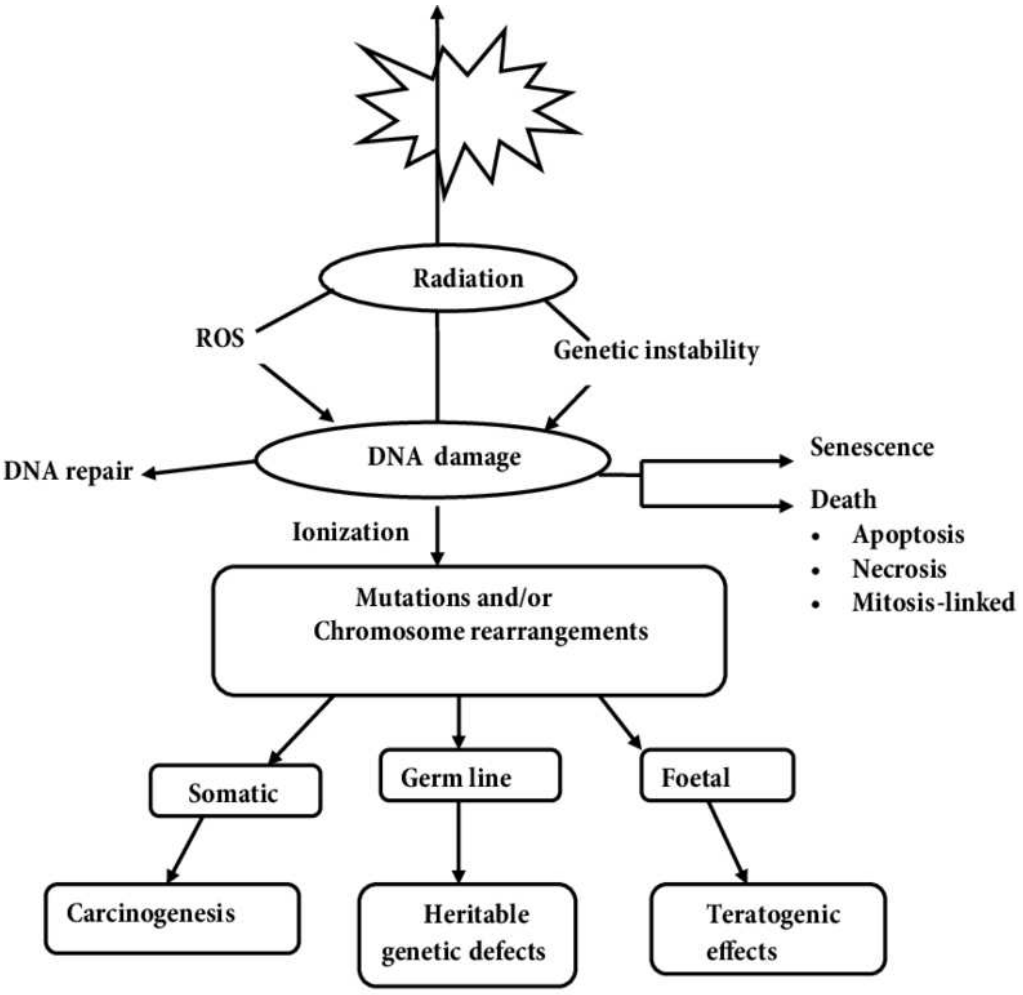

Figure 1.6: Paradigm for the biological effects of ionizing radiation exposure at cellular level.

1.6.1 Cellular effects

The biological effects of irradiation depend on (1) the energy transmitted, (2) the type of radiation, (3) the nature and radiosensitivity of the affected cells and (4) their physiological conditions. There is a great disproportion between the number of ionizations and excitations produced by the radiation and its biological effect. The latter are quantified by measuring cell mortality based on the cell survival curve, which makes it possible to study the radiosensitivity of cells as well as the influence of physical, chemical or biological parameters on the radiation effects. [54]. Indeed; the Temperature Effect results from the increase in radiosensitivity with temperature. This is due to the acceleration of biochemical processes that lead to increased free radicals and incorrect repair. While for high TEL radiation, on the one hand a strong increase in sensitivity, on the other hand a reduction in the shoulder of the curve, i.e., reduced cell repair capacity.

The radiosensitivity also depends on the biochemical composition of the cell at the time of exposure and varies according to the phase of the cell cycle [54].

1.6.2 DNA and organ effects

The incorporated radioactive material decays by emitting ionizing radiation within the body. Therefore, the radiation would affect the atoms in living cells and thereby damage their genetic material (DNA). Fortunately, the living cells are extremely efficient at healing this damage. However, if the damage is not fixed correctly, a cell may die or eventually become cancerous. Exposure of high level of radiation over a short period of time could lead to some symptoms such as nausea and vomiting within hours and could sometimes result in death over the following days or weeks. This is known as acute radiation syndrome. A low level of radiation exposure does not cause immediate health effects, it could increase the risk of cancer over a lifetime. Interaction of radiation with DNA could be a direct or indirect process [52]. In the direct process, radiation would break strands of DNA. However, in the indirect process, radiation would break water molecules surrounding the DNA (Figure 1.7). Afterwards, the broken water molecules produce free radicals unstable oxygen molecules. The new created oxygen molecules would damage cells and organ. The cell damage would repair itself and go back to normal or the cell damage is not repaired or is incorrectly repaired creating a changed cell which may eventually lead to cancer, or the cell is badly damage causing the death of this cell. When cells die there is two options: The body will recover and there is no risk of those cells potentially turn into cancer (a few radiations damaged), and the high radiation dose could cause widespread cell death which can lead to organ failure. All those effects described below are classified in two types; Deterministic effects and stochastic effects [53].

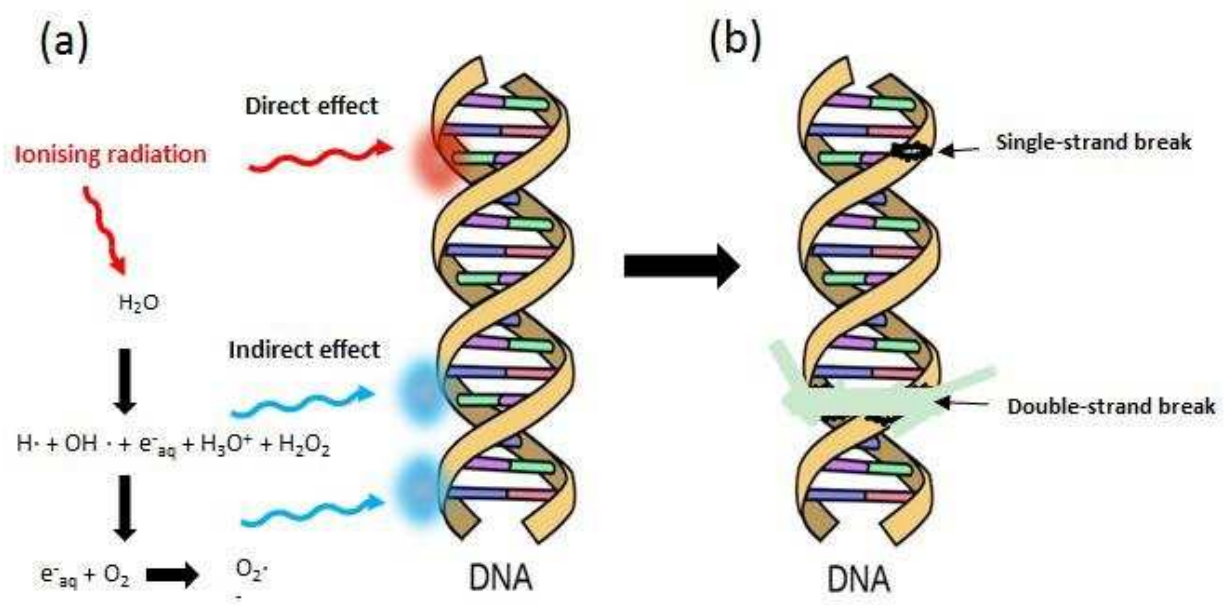

Figure 1.7: Schematic-of-how-ionising-radiation-utilised-for-radiotherapy-can-damage-DNA.

Deterministic effects or tissue reactions of ionising radiation are referred directly to the absorbed radiation dose and the severity of the effect increases as the dose increases. A deterministic effect typically has a threshold below which the effect does not occur [53]. Stochastic effects of ionising radiation are chance events, with the probability of the effect increasing with dose, but the severity of the effect is independent of the dose received. These type effects are assumed to have no threshold. Cancer risk and hereditary disorders are stochastic effects [53]. The main stochastic effects are induction of: (1) cancers in the irradiated subject, if the mutation is induced in some somatic cell genes, (2) genetic diseases in the offspring, if the mutation is induced in the germ cells, (3) cardiovascular diseases.

1.7 Environnemental radioactivity measurement techniques

Radioactivity has always posed serious problems to man and the environment when it is misused or misunderstood. The techniques used to measure environmental radioactivity are dependent on the nature and type of radiation emitted. In this section, we will limit ourselves only to the techniques used in this study to measure radioactivity. These are in situ γ-spectrometry and laboratory γ-spectrometry for measuring natural radioactivity in soil and nuclear trace detection for measuring concentrations of ^{222}Rn, ^{220}Rn, and their associated progeny in dwellings. The measuring instruments used for this purpose require prior calibration in energy and efficiency for the energy range covering the lines of the radionuclides considered. The main cause of human external exposure to natural radioactivity is the uranium and thorium series, and the ^{40}K. Soils, rocks and building materials contain radioactivity at varying levels due to their mineralogical composition [28]. In principle, the quantities to be measured are usually concentrations of the primordial radionuclides such as ^{238}U, ^{232}Th and ^{40}K. NaI (Tl) scintillators (thallium-doped sodium iodide) have been used for this purpose.

1.7.1 Techniques for measurement natural radioactivity in soil

a $\rightarrow$ *In situ* measurement

In situ γ-ray spectrometry is a technique that involves direct measurement of radioactivity at the site. *In situ* measurement of radionuclide activity in soil is more sensitive and provides more representative data than data obtained from soil sample collection and subsequent laboratory analysis. In emergency situations, it is crucial to assess contamination. For rapid assessment of deposited activity, a direct measurement of ambient γ radiation is used [28]. This method allows rapid determination of activity levels of γ-emitting radionuclides at a site and the corresponding free air dose rates. Such measurements can be used to guide further actions including, for example, radiological assessments, sampling and measurement programs [29]. It is more easily and less expensively to make *In situ* sample measurements. Consequently, it is easy to see that the measurements taken on the site cover a large area (10 m radius and more). This gives the *In situ* results more

reliability with respect to the overall radiological behaviour of the site under study. The counting statistics in in situ measurement are obtained in a very small time [30]. *In situ* γ-spectrometry is based on the analysis of spectra obtained from a detector. The mechanisms dealing with the radiation-matter interaction remain valid as well as the internal operation of the detector. In practice, on-board measurements (carbon survey) and *In situ* γ-ray spectrometry are common methods that have proven to be effective for direct dose assessment in the field. Over the past few decades, many research teams around the world have used these methods to quickly learn about the levels of radioactivity in a large environment. Examples include Brunei [31], Turkey [32], and Japan [44, 45], where several rounds of natural and artificial radioactivity measurements have been made. The conditions must remain good (sunny) during the whole measurement period so that the estimated air Kerma levels are not affected by precipitation. The air Kerma rate due to natural γ radiation energy can thus be considered as almost equivalent to the absorbed dose rate in air at 1 m above ground level. Other instruments have been developed for the measurement of primordial radionuclides by *In situ* γ-ray spectrometry. These are less bulky than the one using the carbon survey technology and are also very sensitive to γ radiation. This is the case of the miniature NucScout detector of the Sarad company (see section 1 of chapter 2) and the RADEYEE PRD-ER (Appendix II) pocket flowmeter which has been the subject of several dose rate monitoring works has led to satisfactory results [44].

b $\rightarrow$ Laboratory measurement

Conventional γ-ray spectrometry methods, known as laboratory methods, require the collection of samples on site for analysis in a controlled environment. Although this has potential advantages in terms of accuracy for individual results, when the sample is distributed over a large area that is limited to one soil sample per 1 m2 of surface. For γ spectrometry in the laboratory, measurements of radioactivity in soil samples are made using a Canberra NaI (Tl) detector. Data processing is performed by the GENIE 2000 software [**?**]. The efficiency calibration of the detector is performed using aqueous solutions of ^{60}Co, ^{241}Am, ^{109}Cd, ^{57}Co, ^{139}Ce, ^{137}Cs and ^{88}Y whose emitted photon energy varies in the range 59-1836 keV. The energy calibration of the detector is performed with the reference sources ^{60}Co (1173.23 and 1332.5 keV), ^{133}Ba (383.9 keV), ^{54}Mn (834.9 keV), ^{22}Na (511 and 1274.5 keV), ^{137}Cs (661.6 keV) from the International Atomic Energy Agency, Vienna [47].

Only ^{40}K is directly measured by the NaI (Tl) detector because it is a gamma emitter. The activities of ^{232}Th and ^{238}U not being easy to determine directly by γ spectrometry, their descendants with which they are in secular equilibrium have been used for this purpose. For ^{232}Th, the 911.1 and 969.1 keV energy lines of ^{228}Ac are used. On the other hand, the 1764.5, 1120 and 609.3 keV lines of ^{214}Bi are used to determine the specific activity of ^{226}Ra.

1.7.2 Techniques for indoor radon, thoron and thoron progeny measurement

The measurements quantities are usually the activity concentration of radon and thoron gas and the concentration of alpha potential energy by volume. There are many techniques for measuring indoor radon, thoron and their progeny concentrations. They can be classified into three categories according to the characteristics of the air detector; the latter can be active or passive (no pump, no power supply) [27].

a → Spot measurement techniques

They consist of a detector carried out over a short period of time (of the order of a few minutes or less). The count is carried out quickly afterwards.

b → Continuous measurement techniques

Sampling is carried out continuously. Simultaneous or slightly different analysis allows to record the temporal variations of the concentration.

c → The techniques giving integrated measurements

It is a detector carried out over a long period (from a few days to a year). In this case, the measurement provides a value that is globally representative of the concentration during the period considered. This classification is convenient, even if the limits are sometimes badly fixed, both for radon measurements and for those of the descendants. The measurement of radon in dwellings or in a confined atmosphere is always accompanied by the information p concerning the duration, the period of measurement and the altitude where the measurement was made. This is due to the fact that radon concentrations vary according to the above-mentioned parameters. The measurement must be made at a location whose location relative to nearby natural or artificial landforms places them outside a cone with a vertical axis and an angle at the apex of at least 1400, of which the detector point is the apex. The measurement should be carried out at a height of between 1 and 2 meters from the ground [27].

As measuring devices, the solid nuclear trace detectors (LR115 and CR-39) and the Teflon ionization chamber (electret) are used for this purpose. A nuclear trace is a damage zone created along the trajectories of these particles in materials . There are two types of DSTNs:

- **The massive DSTN:** they are polycarbonates. Here, we used CR-39. They are sheets of Plexiglas more or less flexible of thickness of the order of millimeters this technique was used in this work. The traces look like cones of different sizes. These detectors record alpha particles with an angle of incidence of 750 and an energy between 0 and 20 MeV.

- **The DSTN in thin layers:** it is the KODAK film type LR115. It is made of a nitrocellulose strongly tinted in red. It can record alpha particles of energy between 1.4 and 4.7 MeV with angle of incidence

up to 500.

The Teflon ionization chamber: it is a passive detection system for the integrated measurement of of radon in air. A Teflon disk, heated to a negative potential of about 200 V, is inserted into an electret ionization chamber made of conductive plastic material of a certain volume. The electrostatic field thus created inside the chamber allows to collect on this disk the ions formed during the decay of radon and descending. As a result of this ion collection, the potential of the disk decreases with the radon concentration. An electrometer is used to measure this potential difference which is directly proportional to the concentration of radon observed over the exposure period. Teflon ionization chambers were used in the first phase of this work by means of E-perm detectors.

The measurement of radon gas does not allow direct access to the health risk. Only a dosimetric model or the use of the equilibrium factor can be used to estimate the risk. Because the health risk is not due to the radon gas itself, but to its decay products. With the radon equilibrium factor, we can easily access these decay products. In homes the average equilibrium factor varies between 0.3 and 0.6 with an average value of 0.4; in the absence of an exact value, it is commonly accepted as equal to 0.4 [26]. This approach is not valid for thoron progeny, because the concentration of thoron in a house varies considerably with the floor/wall position relative to the detector. For this reason, it is more appropriate for health risk studies to measure the concentration of thoron progeny directly over periods of several weeks. For studies of a phenomenological nature, the determination of the concentration of gases and progeny is recommended [27]. The average value of the equilibrium factor recommended for thoron is 0.02 [26].

In epidemiology, the health risk is studied as a function of cumulative exposure over 20 to 40 years. Thus, a measurement over 6 months or 1 year is often recommended in the home for the most accurate most accurate estimation of individual exposure to radon [27]. However, in this study, the devices used were designed for a period of 1 to 3 months. The results of the measurement of the concentrations of radon, thoron or their progeny at a given location are only meaningful if they are accompanied by: $\rightarrow$ the detector modes (point, integral, or continuous);
$\rightarrow$ the duration of the detector;
$\rightarrow$ the period of measurement in the year;
$\rightarrow$ the meteorological conditions.

1.8 Current situation of Monitoring to natural radioactivity exposure in Cameroon

Studies on the exposure and measurement of natural radioactivity in Cameroon are significantly more advanced than in other sub-Saharan African countries in general and in the sub-region (Central Africa) in particular. To date, this work is conducted on all ten regions of our country. In fact, the work recently carried

out by Ndjana Nkoulou *et al* [56], and Ngachin *et al* [57] presented a study on external exposure to building materials used in Cameroon. This study revealed that all the materials examined could be used as building materials according to the criteria of the Organization for Economic Cooperation and Development [58].

Ben-Bolie *et al* [58], Mvondo *et al* [59, 60], measured the concentrations of ^{238}U, ^{235}U, ^{234}U, ^{232}Th, ^{230}Th, ^{228}Th, ^{226}Ra and ^{210}Po in soil samples, agricultural crops and some plants collected in the localities of Ngombas, Awanda, Bikoué and Melondo. They showed that the soil-plant transfer factor values were higher than those proposed by the IAEA. In addition, results from measurements made in the same localities and at Ngombas in the southwestern region of Cameroon by Ele Abiama *et al* [61] and Beyala Ateba *et al* [62] confirmed these high activity concentrations of ^{238}U, ^{232}Th and ^{40}K at some points and also measured activity concentration of ^{238}U in rocks and soils collected at locations where a radiometric anomaly had been detected in a survey respectively. These studies reported that the areas studied have a very high level of radioactivity and therefore present a uranium mining potential.

Furthermore, a set of work on radioactivity measurements and dose assessment was conducted in the uranium mining areas of Poli in northern Cameroon. Most of the total dose assessed was attributed to radon exposure and elevated levels of ^{210}Po and ^{210}Pb in vegetables and foodstuffs [63]. A comparative study of public exposure to natural radiation in the uranium and oil producing areas of Cameroon was also carried out [23]. It showed that radiation dose and radiological risk in each of theses localities are higher than the world average values. In addition, an assessment of public exposure to natural radiation in the gold mining areas of eastern Cameroon showed that the soils can be safely used for building materials. Nevertheless, some recommendations have been made to stretching environmental protection in these mining areas [64].

Recently, measurements of ^{222}Rn concentrations in the Bauxite zone of southern Adamoua showed high values at the threshold of 300 Bq m^{-3} in some dwellings [16]. A study carried out in the same region by Bachirou *et al* showed that the area is a radon prone area [65]. On the other hand, several measurements of ^{222}Rn and ^{220}Rn concentrations have also been carried out in dwellings in some localities in Cameroon. In the Poli and Lolodorf uranium areas, results obtained with Electret ionization chambers (Eperm) have shown high levels of ^{222}Rn in many dwellings [11]. High ^{222}Rn and ^{220}Rn concentrations were also observed in most dwellings in the Bikoué and Ngombas uranium- and thoron-potential areas using RADUET detectors [22]. The work done by Bineng *et al* in these localities confirmed that the risk related to ^{222}Rn is very high [20]. These and other studies have shown that the contribution of thoron should no longer be neglected when assessing inhalation dose. A similar study was conducted by Takoukam *et al* in the economic capital of Cameroon Douala. [12, 25]. It revealed the presence of radioactivity at high concentrations at some points in the city.

In addition, soil samples taken from the bauxite ore deposit in the Menoua division, West of Cameroon, also showed the presence of primary radionuclides at high levels. These results have called into question the use of soil as a building material that may lead to increased exposure (external and internal) of the public to natural radioactivity [13, 14]. Recent work on indoor ^{222}Rn and radioactivity monitoring in the Far North

region by Awé *et al* [66] and Koyang *et al* [67] have respectively shown that ^{40}K is the main contributor to the external radiation dose to the public and that the risk from ^{222}Rn is relatively low compared to the values recommended by international bodies. The conclusion is reported by Sadjo *et al*. in the work investigated in the northern region of Cameroon, where they also showed that radon concentrations vary during the day [68].

Finally, Mbida *et al*. found very high concentrations in some dwellings in the town of Ebolowa in the south of Cameroon [69]. Moreover, despite all the knowledge available on ^{222}Rn, ^{220}Rn and their associated descendants, the natural radioactivity measured elsewhere and in Cameroon as presented above are so far limited for the most part to the evaluation of the effective dose by inhalation, by external irradiation and by ingestion.

These studies do not take into account the correlations between the concentrations of the parents in soil and those of ^{222}Rn and its progeny in the dwellings on the one hand and the correlation between the concentrations of ^{222}Rn in soil and in the dwellings on the other hand. Nevertheless, Gondji et al recently examined this correlation in and showed that it is a function of the soil geology. This study in addition to assessing the dose by inhalation and external irradiation of the public of the bauxite areas of Fongo-Tongo has also studied these correlations which can be a major asset to establish a radon mapping based on a number of parameters that are described in the rest of this thesis.

Conclusion

This chapter presented some basics on natural radioactivity and its origins in soil and rock. The interactions between photons and matter, human exposure to natural radiation sources and the effects of these radiations are also described and presented. A status report on the monitoring of natural radioactivity exposure in Cameroon was then presented and interest in the study of correlations between radionuclides in soil and in confined spaces was found

Chapter 2

Material and Methods

Introduction

This chapter outlines the equipment and methods used in conducting this study. It describes the sampling techniques and procedures for determining the activity concentrations of α and γ emitting natural radionuclides. The experimental devices employed, such as γ spectrometry detectors with NaI(Tl) detectors for in-situ measurements, and the analysis of soil samples in the laboratory, are discussed. Additionally, RADTRAK^{2}® and RADUET detectors for ^{222}Rn measurements, simultaneous measurements of ^{222}Rn and ^{220}Rn, and thoron progeny monitors for associated thoron progeny measurements are presented and detailed. Furthermore, the various components of public radiation dose from different radiation types and associated exposure risks are also addressed.

2.1 Study Area

2.1.1 Location and Overview

The study areas, depicted in Figure 2.1, are situated in the Menoua subdivision of the Western Region of Cameroon. The urban core consists of Dschang and Fongo-Tongo, with an average altitude of approximately 1600 m. These areas are located on the southwestern slopes of the Bamboutos Mountains, characterized by low plateaus dissected by small, occasionally swampy valleys [70]. The climate is sub-equatorial Cameroonian, typically cold, humid, and heavily influenced by altitude, featuring a long rainy season (March to November) and a short dry season (December to February). The average annual temperature is 22.5°C, with an average rainfall of 1364.4 mm. The vegetation is influenced by anthropogenic activities and cultivated crops [70].

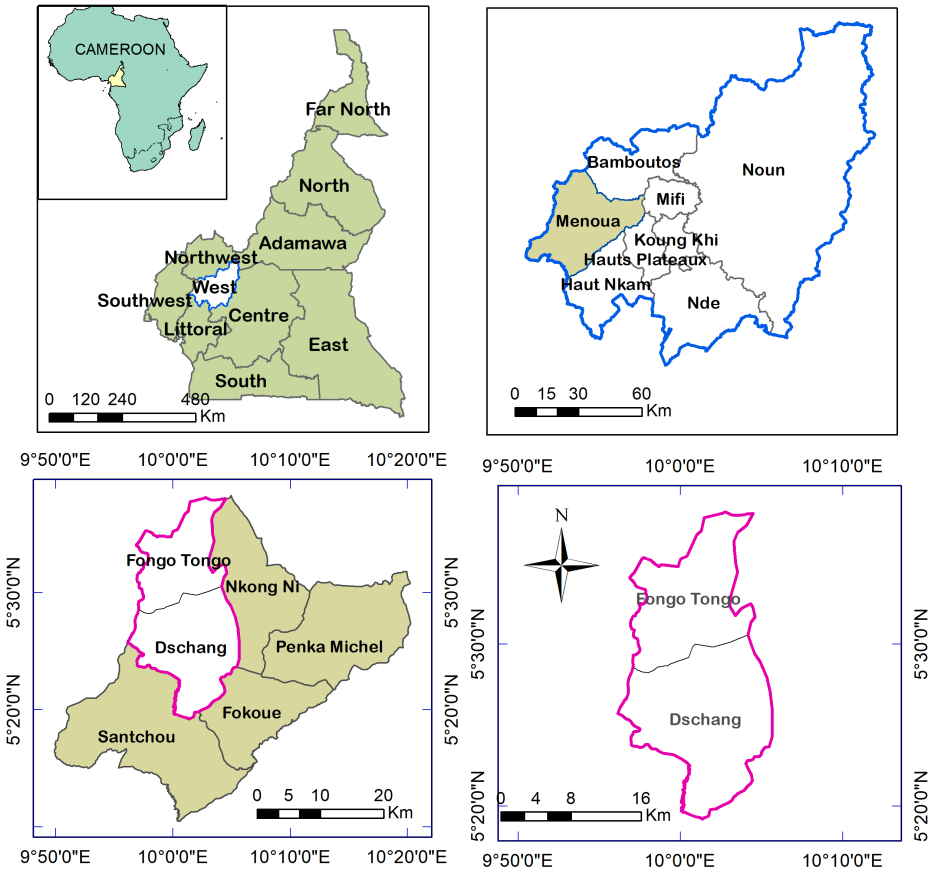

Figure 2.1: Location of the study areas indicating the two investigated localities.

2.1.2 Geology and Mineralogy

The area exhibits various volcanic activities and products of different facies [71]. It is underlain by an extensive loose mantle on trachyte and forms a differentiated geological profile (including basalts, trachytes, phonolites, rhyolites, and ignimbrites), with deposits of new bauxite minerals. Fongo-Tongo hosts a substantial bauxite ore deposit, explored since 1950 by the French Geological and Mining Research Bureau (FGMRB) [72]. Discovered in 1957 by BUMIFOM prospectors [37, 38], this deposit is one of the region's major bauxite reserves, estimated at 45 million tons and integral to Cameroon's geological resources [37, 39]. The soils are primarily granite and orthogenetic basement formations, forming the granite-gneiss complex [13, 16]. Bauxite ore deposits in the area originate from aphyric or porphyry mid-oscine basalts, with an average chemical composition of approximately 15.9% Al_2O_3, 13.5% FeO_3, and 44.6% SiO_2 [75]. Figure 2.2 illustrates the geological map of the study area.

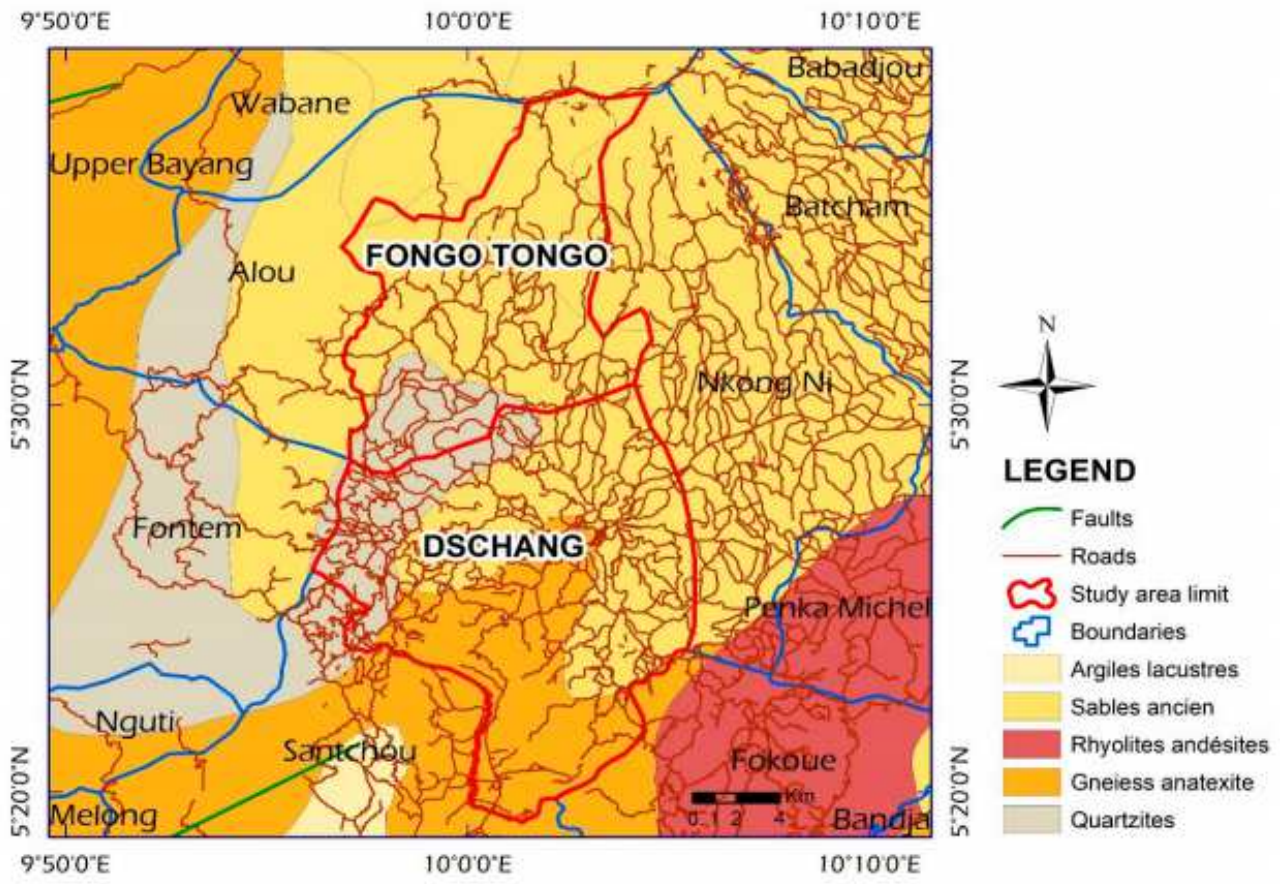

Figure 2.2: Soil characteristics map of the study area.

2.1.3 Dwelling Characteristics

The monitored dwellings are constructed using earth bricks or cement. Cement dwellings feature concrete floors and walls made of earth bricks or covered with cement, with some built using cinder blocks. These dwellings are well-ventilated with large openings, although some remain closed. In this agricultural area, farming and livestock raising are predominant activities. Most houses utilize the main room for multiple purposes, including storage, kitchen, and a warm space during cold weather. The study conducted measurements during the dry season (December to February), with dwellings typically having one front door and one or more windows. Detectors were positioned 80 cm from walls and at a height of 150 cm from the floor surface, suspended from the ceiling using strings.

2.2 ^{226}Ra, ^{232}Th, and ^{40}K Measurements in Soil by In-Situ γ-Spectrometry with NucScout

γ-ray spectrometry is a non-destructive measurement method used in nuclear physics to quantify various radionuclides by analyzing emitted γ-rays' energy. This technique, based on semiconductor physics, generates energy spectra, identifying and quantifying radionuclides based on their characteristic emission lines. High-resolution γ-ray spectrometry is an effective tool for environmental measurements.

2.2.1 In-Situ γ-Spectrometry with NucScout

In radiological site characterization and nuclear facility dismantling, in-situ measurements are crucial. This method involves using a miniature NaI (Tl) spectrometer, such as the NucScout, to identify and quantify radionuclides on-site.

2.2.2 Measurement Device

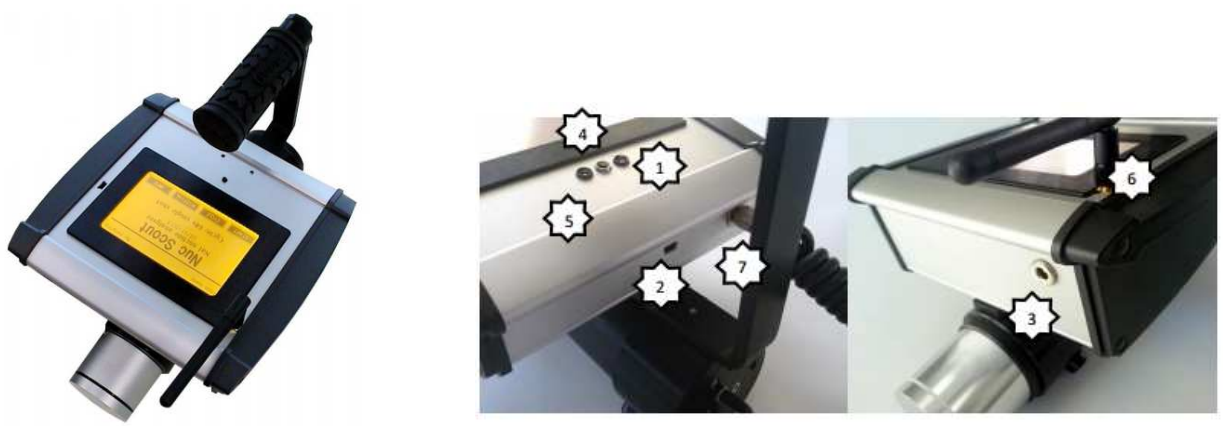

Figure 2.3: NucScout gamma monitor.

The NucScout monitor measures local dose rates and the activity of up to 28 user-selectable nuclides. It records results over time and can adjust sampling intervals. The unit includes a GPS receiver for data localization, can be user-calibrated, and has a rugged NaI $2" \times 2"$ detector for low detection limits.

2.2.3 Operating principle

Figure 2.4: Principle of sampling with NucScout detector.

The "Power Off" cycle can be selected and initiated to shut down the instrument. To restart the instrument, the power adapter must be briefly plugged in. The instrument operates on an internal rechargeable NiMH battery, and a power adapter for battery charging is included in the package. It should be connected to socket **(3)** on the rear panel of the NucScout. While charging, the indicator **(1)** illuminates, turning off when the charging is complete. To prevent deep discharge, a safety circuit disconnects the electronics from the battery if the voltage drops below 10.5V, independent of the main switch. The instrument is operational once the battery voltage reaches 11.5V. Other components include: **3)** Power adapter connector, **4)** Standby mode exit button, **5)** Alert indicator (red LED), **6)** Wireless communication antenna, and **7)** Gamma probe connector [76].

2.2.4 Measurement Principle

Measurements were conducted randomly at different points in the area, one meter above ground on a dry wooden support, with each sample point measured for exactly 45 minutes. Data from these measurements were stored on a USB or memory card and transferred to a PC for analysis using dvision software [77]. Calibration of the detector was done using dconfig software when connected to a PC. The detector was

positioned at a height of one meter on a dry bench for measurements. Concentrations of ^{226}Ra, ^{232}Th, and ^{40}K were determined using gamma lines at 609.3 Kev for ^{214}Bi, 2614 Kev for ^{208}Tl, and 1461 Kev for ^{40}K, respectively.

2.3 ^{226}Ra, ^{232}Th, and ^{40}K Measurements by Laboratory γ-Spectrometry

γ-ray spectrometry based on NaI (Tl) detectors is a powerful method for photon detection, utilized in part of this thesis work.

2.3.1 Soil Sampling

Sampling of environmental samples like soil is essential for natural radioactivity measurement. Given the complex morphology of soils in the study area, random sampling was adopted to ensure representativeness. A one-meter square area was defined on a vegetation-free surface, and samples were collected at each vertex and the center of the square, to a depth of 5 cm, resulting in a sample of approximately 1 kg. Samples from the square were placed in labeled and sealed plastic bags for analysis.

2.3.2 Preparation and Conditioning of Soil Samples

After sampling, conditioning was performed at the Research Center for Nuclear Science and Technology of the Institute of Geological and Mining Research (CRSTN/IRGM) in Yaoundé. Samples weighing about 1 kg were dried in an oven at 70°C for 48 hours, crushed to a particle size of 1 mm, and transferred to 500 cm^3 plastic boxes (Marinelli beakers) with space for gaseous releases. The boxes were sealed to prevent radon leakage and stored for at least 40 days for secular equilibrium between ^{226}Ra and its progeny before γ-spectrometry analysis [2].

2.3.3 Experimental Devices

The previous section outlined the main steps and equipment used to obtain and analyze spectra. Radioactivity measurements in soil samples were conducted using a Canberra NaI(Tl) detector Model 802 from CRSTN/IRGM, featuring a crystal measuring 7.6 cm $\times$ 7.6 cm. It boasts a relative efficiency of 7.5% with a resolution of 667 keV. The associated electronics include a Canberra preamplifier and an Accuspec-type acquisition card. Figure 2.5 illustrates the measurement device used for acquisition and spectrum analysis using the GENIE 2000 software (Canberra) [83].

Figure 2.5: Experimental device for acquisition and analysis of emission spectra in laboratory soil samples.

2.3.4 Acquisition Chain in γ-Spectrometry

The γ-spectrometry measurement chain comprises several components:

- **Preamplifier**: Integrates the input signal to correlate with the energy deposited in the crystal, facilitating energy measurement.
- **Amplifier**: Shapes and amplifies the signal to minimize noise and obtain a Gaussian signal.
- **Analog-to-Digital Converter (ADC)**: Converts signal amplitude into a proportional number representing the energy deposited in the crystal, creating a continuous signal.
- **Multi-Channel Analyzer (MCA)**: Collects, classifies, and records information in different channels, correlating energy deposited in the crystal with channel numbers.

The purpose of this chain is to convert the electrical signal into energy and count the different energies obtained. Figure **??** depicts a simplified diagram of the γ-spectrometry measurement chain.

Energy calibration is crucial for accurate measurements, involving a multi-line standard source or several standard sources with energies close to those to be measured. The efficiency calibration of the NaI (Tl) detector in this study utilized a polynomial approximation method, typically a second-degree polynomial, as shown in Equation (1), where $E(x)$ represents the energy of the γ-photon and x denotes a channel of the detector.

$$E(x) = a_1 + a_2 x + a_3 x^2 \tag{2.1}$$

The coefficients a_1, a_2, and a_3 are determined through a fit algorithm, as illustrated in Figure 2.6 displaying the energy calibration curve of the detector.

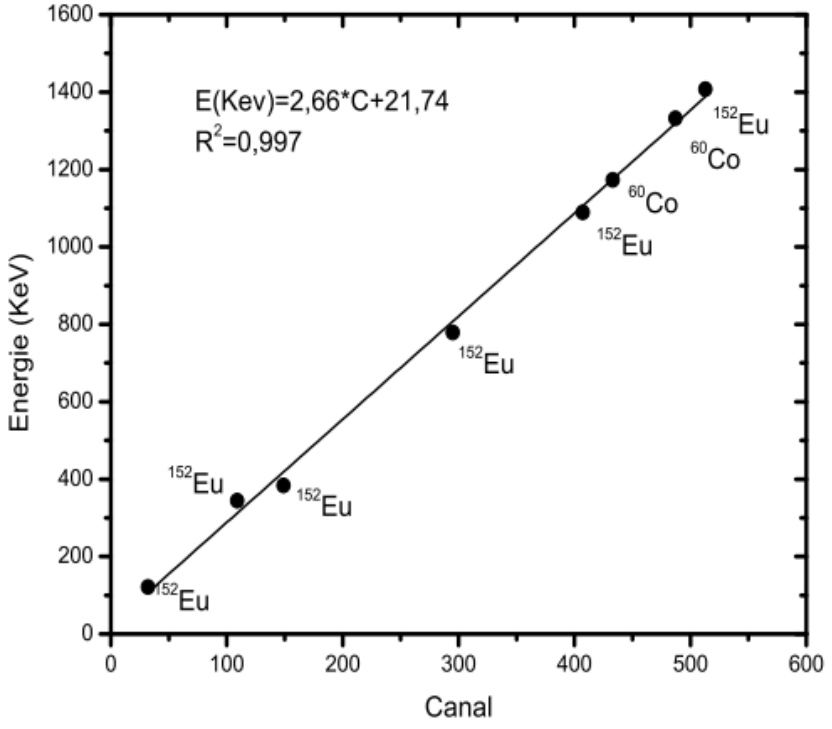

Figure 2.6: Energy calibration curve.

2.3.5 Efficiency Calibration

Within the emitted radiation from a source, only a fraction is captured by the measurement system (detector + associated electronics). Efficiency (ε) quantifies the likelihood of a gamma photon being fully absorbed in the detector's sensitive volume, contributing to the total absorption peak. Efficiency is defined in two ways by equations 2.2 and 2.3 [80, 83]:

Absolute efficiency: This ratio represents the number of photons recorded relative to the total emitted photons by the source (in all directions). Intrinsic efficiency: This ratio signifies the number of recorded photons compared to those reaching the detector.

$$\begin{aligned} \varepsilon(E_\gamma) &= \eta\,\varepsilon_i(E_i) \\ \eta &= \frac{4\pi}{\Omega} \end{aligned} \tag{2.2}$$

Here, Ω denotes the solid angle at which the detector views the source, considering intrinsic properties. The efficiency calibration in this study employed a fourth-order polynomial approximation, given by:

$$\log \varepsilon = a_0 + a_1 \log(E_\gamma) + a_2 \log(E_\gamma)^2 + a_3 \log(E_\gamma)^3 + \ldots + a_3 \log(E_\gamma)^n \tag{2.3}$$

To calibrate the detector's efficiency, a multi-energy standard was used under the same experimental conditions as the samples. This standard comprised various radioactive sources with energies ranging from 59.54 to 1836 keV, including ^{60}C, ^{88}Y, ^{137}Cs, ^{152}Eu, and ^{241}Am. Figure 2.5 illustrates the experimental efficiency curve characterizing our detector based on energy E_γ.

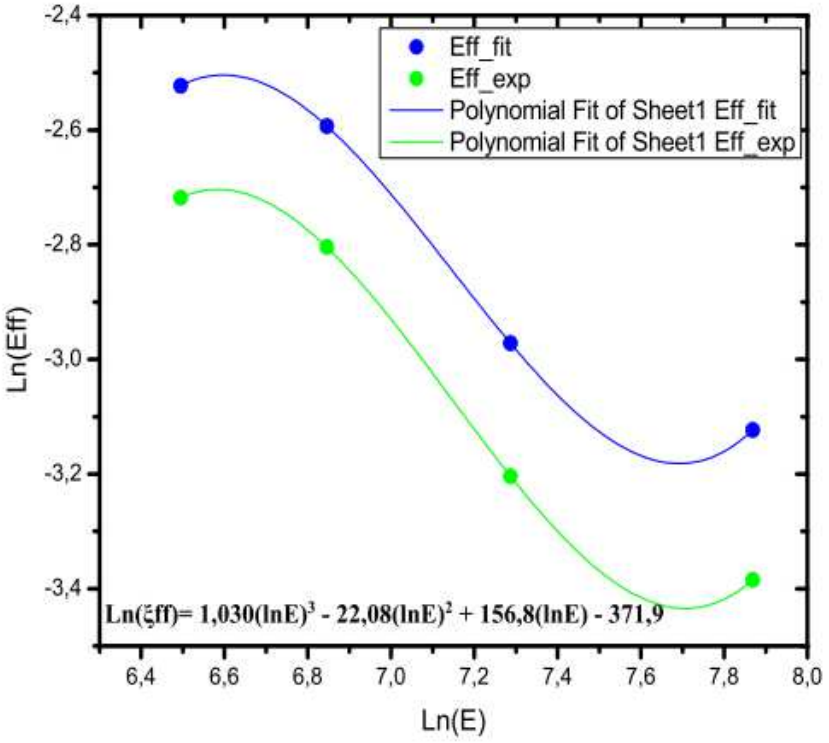

Figure 2.7: Experimental efficiency curve for the detector at different gamma energies.

2.3.6 Activity Concentrations of ^{226}Ra, ^{232}Th, and ^{40}K in Soil Samples

Determining the activity concentration of ^{226}Ra in environmental samples can be approached in two ways. The first method involves direct determination without sample pre-treatment using the 186.2 keV emission line, although this method requires corrections due to potential interference with the 185.7 keV line of ^{235}U and is therefore infrequently used [84]. Instead, the 609.3 keV line is commonly utilized [80, 85, 86].

The short half-lives of ^{234}Th (T1/2 = 24.1 days) and ^{234m}Pa (T1/2 = 1.17 minutes) are advantageous as secular equilibrium with ^{238}U is achieved approximately six months after sampling for ^{234}Th and ten minutes for ^{234m}Pa. However, the 766.4 keV line of ^{234m}Pa may interfere with the 768.3 keV line of ^{214}Bi. In environmental samples, the 1001.0 keV line is less affected by self-absorption but has a low emission

probability [69, 74, 75]. Table 2.1 presents the energy lines used to determine activity concentrations for ^{226}Ra, ^{232}Th, and ^{40}K.

Table 2.1: Summary of the different energy lines used to determine activity concentrations.

^{238}U-Serie	^{234}Th	63.3(4.5)	92.6(5.4)		
	^{234m}Pa	765(0.21)	1001(0.7)		
	^{226}Ra	186(3.3)			
	^{214}Pb	242(7.43)	295.2(19.2)	351.8(37.2)	
	^{214}Bi	609.3(46.6)	1120.3(15.1)	1764(15.9)	
	^{210}Pb	46.5(4.1)			
^{232}Th-Serie	^{228}Ac	38.3(11.4)	911.6(27.7)	969.1(16.6)	940.3(44.3)
	^{212}Pb	238.5(43.6)	300.1(3.23)		
	^{212}Bi	7.2(6.7)	72 1620.6(1.5)		
	^{208}Tl	510.8(21.6)	583(86.3)	860.4(12.5)	2614.7(100)
other	^{40}K	1460.8(10.7)			

Activity concentration, expressed in Becquerel per kilogram, is determined according to the international standard NT ISO 18589-3 [46]. The concentration is calculated using Equation (4), where N_P represents the number of counts in a given peak area at energy E, $\varepsilon(E_\gamma)$ is the detection efficiency at energy E, $I_\gamma(E_\gamma)$ is the number of gamma rays per decay for that nuclide at energy E, t_c is the counting time (100,000 seconds), and M is the mass of the sample in kilograms. The uncertainty in activity concentration (ΔA) is determined using Equation (5).

2.3.7 Activity Corrections

The total absorption peak can result from the simultaneous detection of several emission lines' total absorption peaks or from one total absorption peak and the Compton background of another (or vice versa). This can create background interference between the lines, leading to underestimation or overestimation of counts, necessitating correction [80, 89, 90].

a $\rightarrow$ Self-absorption Correction

Self-absorption causes pulse loss, leading to underestimation or overestimation of efficiency, which varies with photon energy, detector volume, effective charge, and density. Environmental samples often differ in density from the calibration source, typically water, complicating efficiency comparisons. Self-absorption correction becomes crucial, particularly for photons with energies E$\gamma \leq$ 200 keV, where the effect is significant [86, 90].

The correction for self-absorption in a solid sample's energy line is the ratio of the efficiency for a reference source to the detector's efficiency for the solid sample. This correction is applied to the activity determined for each radionuclide line, calculated using GENIE 2000. After correction, the weighted average activity of a non-interfering nuclide, with multiple energy lines, is determined using the formula:

$$A = \frac{\sum_{i=1}^{N} \frac{A_j}{\sigma_i^2}}{\sum_{i=1}^{N} \frac{1}{\sigma_i^2}} \tag{2.4}$$

Where A_i is the corrected activity of the nth nuclide line, N is the number of lines identified and not marked by a function, and σ_{Ai} is the uncertainty of A_i. The uncertainty in activity is calculated as:

$$\sigma_{Ai} = \sqrt{\frac{1}{\sum_{i=1}^{N} A_i}} \tag{2.5}$$

b $\rightarrow$ Coincidence Summation Correction

Coincidence summation occurs when at least two γ photons from a cascade decay of an excited nucleus are simultaneously detected. The correction for this effect is the ratio of counts determined with and without the summation effect [91].

c $\rightarrow$ Threshold and Detection Limit

When measurement results are close to background or very low, determining the minimum detectable quantity is crucial. The decision threshold (SD) is used for this purpose, with a detection limit (LD) corresponding to twice the decision threshold. The gamma spectrum's representation involves total absorption peaks superimposed on a continuous distribution. The net area of the total absorption peak and the continuous background under the peak can be determined using a Gaussian curve for the peak and a polynomial function for the background. SD is calculated as:

$$SD = 4.4\sqrt{R.B} \tag{2.6}$$

Where R is the total width at half height of the peak (in keV), and B is the average background amplitude (in pulses. KeV^{-1}). LD is calculated as:

$$LD = \frac{8.8\sqrt{R.B}}{\varepsilon(E,\nu) \times I \times t} \tag{2.7}$$

Where $\varepsilon(E,\nu)$ represents the total absorption efficiency for a given energy E and geometrical conditions, I is the intensity of the emission line (%), and t is the acquisition time (in seconds). The detection limit for a

multi-gamma emitter is the lowest among the detection limits calculated for its different γ lines. This value can be determined for de-ionized water filled in a Marinelli beaker and calculated using:

$$MDA = \frac{LD}{\varepsilon \times \gamma \times t} \tag{2.8}$$

Where ε is the emission probability per disintegration of the selected γ-ray line, ε is the absolute efficiency of the corresponding gamma line, and t is the live time of the spectrum. MDA is calculated in terms of activity (Becquerel), dependent on the γ-ray energies of the sample and the counting efficiency of the detector.

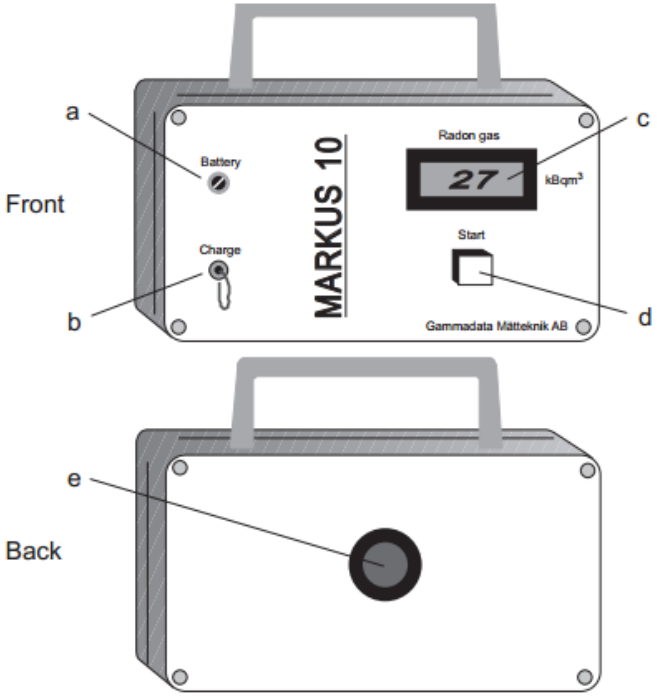

Figure 2.8: Instrument for determining the radon content in soil Markus 10 detector.

b → Operating principle

The measurement with the instrument is done in two steps. The first is the pumping step. The instrument pumps the air contained in soil through the probe into the measuring chamber. The pumping time (about 30 seconds) ensures that the chamber is completely filled. The detector is equipped with a pressure sensor. The instrument can automatically decide to stop the pump if the pressure measured in the probe drops below a given value of 0.91l. When the pressure rises, the pump starts again. For each measurement performed, the pump's running time is always the same, guaranteeing a constant volume of air in the chamber for each measurement.

After the pumping phase, the measurement phase begins. The instrument automatically switches on

the measuring chamber. The electric field thus created directs the electrically charged radioactive radon progeny to the sensor. The detector records the alpha radiation from the radon progeny. The electric pulses delivered by the sensor are amplified then filtered in the analysis channel which allows only the counting of the pulses corresponding to the energy coming from the ^{218}Po. This filtering principle allows to ignore the pulses coming from the ^{214}Po, slower to occur and which can create a latent measurement background in the chamber [94].

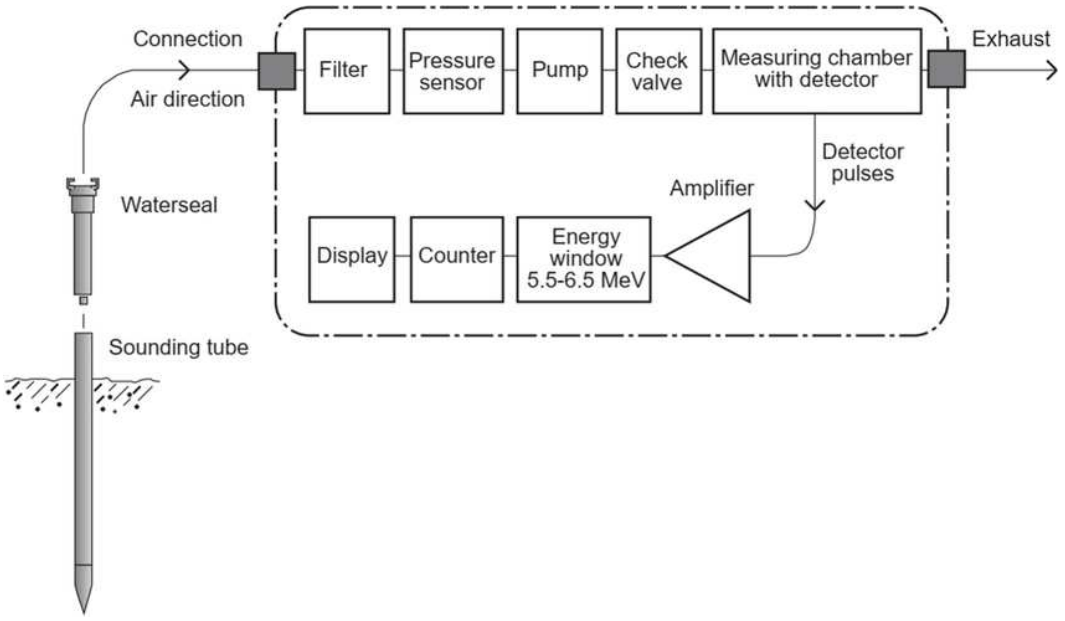

Figure 2.9: schematic process of ^{222}Rn measurement with Markus 10 detector.

2.3.8 Geogenic radon potential (GRP)

Geogenic radon potential (GRP) is the parameter that quantifies the rate of radon escaping from the adjacent geological formation to the atmosphere. It is an indicator of the potential of soil to be a source of indoor radon [102]. Considering the ground of the area as highly permeable (in the order of 10^{-11}, 10^{-12} and 10^{-13}), the geogenic radon potential was evaluated on the basis of the formula proposed by Neznal, defined in the following equation [103, 104, 105]:

$$GRP = \frac{C_{Rn}}{-log_{10}k - 10} \tag{2.9}$$

Where C_{Rn} (kBq m^{-3}) is the radon concentration in soil gas and k (m^2) is the soil permeability. High average values of geogenic radon potential imply a greater potential for radon migration into the soil [106]. Radon-prone areas are generally classified using the radon index (RI) based on geogenic radon potential values. Many years of extensive research in the Czech Republic have classified radon-prone areas into three categories based on geogenic radon potential values: low RI (GRP $\leq$ 10), medium RI (10 < GRP < 35) and high RI (GRP > 35) [103].

2.3.9 Assessment of outdoor ^{222}Rn concentration

Estimation of ^{222}Rn in soil gases and in the atmosphere has been proposed as a tool for many research purposes such as uranium exploration, earthquake prediction, groundwater transport and geothermal resource assessment [107]. If the soil is sufficiently porous, diffusion proceeds as if the soil were absent. From production to exhalation into the atmosphere [108], ^{222}Rn concentration C'_{Rn} (Bq m^{-3}) in air near the ground surface is estimated by the equation (7) [19, 42]

$$C'_{Rn} = C_{sg}\sqrt{\frac{d}{D}} \tag{2.10}$$

Where C_{sg} is ^{222}Rn concentration gas in soil in kBq m^{-3}, d is the exhalation diffusion constant (= 0.05 cm^2 s^{-1}) and D is the diffusion coefficient (5×10^4 cm^2 s^{-1}).

2.3.10 ^{222}Rn concentration measurements in dwellings with RADTRAK^{2}® detectors

The detector housing shown in Figure 2.10 was made of electrically conductive plastic. Through a small slit (filter), ^{222}Rn gas entered the detector. The trace detection material (film) inside the detector is then subjected to the alpha particles generated by the radon gas entering the container and the decay products formed from it. On the film, the alpha particles form small traces that are enlarged by chemical etching and then counted under a microscope to determine radon exposure. The lowest detection limit for a tree month measurement period is 10 Bq m^{-3}.

Figure 2.10: RADTRAK^{2}® passive radon detector.

Thirty detectors were deployed in Dschang and 20 in Fongo-Tongo, over a three-month exposure period. After the exposure, the detectors were collected and returned to the RADONOVA laboratories in Uppsala,

Sweden for analysis. The measurements were made in accordance with the standard. However, the arithmetic mean of the radon activity concentration (Bq m^{-3}) is given as follows [95]:

$$\begin{aligned} \bar{C} &= (n_g - \bar{n}_b)\frac{1}{t.S_{SSNTD}.F_C} = (n_g - \bar{n}_b).\omega \\ \omega &= \frac{1}{t.S_{SSNTD}.F_C} \end{aligned} \tag{2.11}$$

Where n_g is the number of traces after exposure, nb is the average number of traces due to background radiation, t is the sampling time, F_c is the calibration factor, ω is the correction factor related to the calibration factor and sampling time, and S_{SSNTD} is the detector area used to count the number of etched traces in cm^2. To obtain the most accurate value, n_b is determined experimentally by reading n detectors that have not been exposed to radon and have been processed under the same physicochemical and counting conditions. Physicochemical and counting conditions. The value of nb can also be given by the manufacturer. The standard uncertainty of C is given as follows:

$$\begin{aligned} u(\bar{C}) &= \sqrt{(n_g - \frac{\bar{n}_b}{n})^2 + \bar{C}^2 u^2_{(rel)}(\omega)} \\ u^2_{(rel)}(\omega) &= u^2_{(rel)}(F_C) + u^2_{(rel)}(S) \end{aligned} \tag{2.12}$$

Where $u_{(rel)}$ represented the relative standard uncertainty, the sampling time uncertainty is not taken into account and is therefore considered negligible.

2.3.11 Daily variations of indoor ^{222}Rn concentration

Figure 2.11: Real-time radon detector RadonEyes+[2], for the instantaneous measurement of indoor radon levels.

According to Figure 2.11, RadonEye+[2] is an active detector for indoor radon measurement based on the ionization principle. It measures radon levels quickly and accurately. The RadonEye RD200 PLUS2 is a high-quality instrument for use in homes or buildings with multiple occupants. It is up to 20 times more sensitive than other consumer instruments. Dosimeters should be ordered to measure the annual average radon value. Measuring in this way provides an accredited and approved result, which is a potential requirement of municipalities.

The measurement updates automatically every ten minutes and displays the result of the previous hour's measurement on the screen. The maximum concentration that the device can measure in a home is 37000 Bq m^{-3} [96]. The RadonEye RD200 PLUS2 measures radon levels quickly and accurately. For a normal indoor ^{222}Rn level, the measurement uncertainty is about 10% for one hour of measurement. The measured value displayed on the screen updates every 10 minutes and is based on the measurement recorded during the last hour. The measurement data is sent via WiFi, which allows to read the data on the instrument in real time. The have many option of transferring data from the device by connecting it to your smartphone via Bluetooth. An excellent tool for homeowners and consultants who want to determine the radon concentration in a building with multiple occupants, for example.

2.3.12 Simultaneous measurements of ^{222}Rn and ^{220}Rn concentrations in dwellings with RADUET detectors

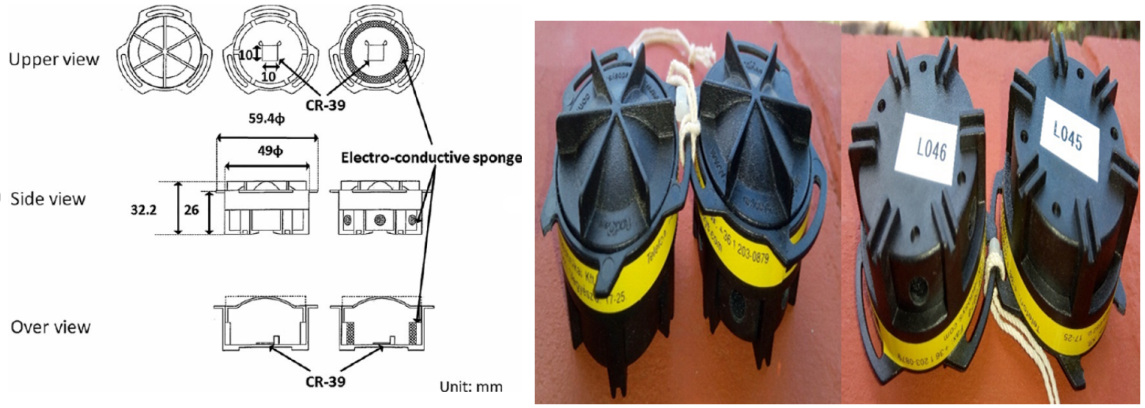

Figure 2.12: RADUET Monitor for simultaneous measurement of ^{222}Rn and ^{220}Rn.

Using commercially available passive radon-thoron discriminant detectors (RADUET), radon and thoron concentrations were measured simultaneously. Each detector was associated with a thoron progeny monitor. The RADUET detector is designed with two separate low and high diffusion chambers. With a different air change rate for each chamber [97]. Each chamber contains a CR-39 chip with a size of 10×10 mm^2 (Figure 2.12). The CR-39 detector records the trace of alpha particles, especially those emitted by ^{212}Po (8.78 MeV) [98]. The low scattering chamber is made of electrically conductive plastic with an interior volume of 30

cm^3. The high scattering chamber is the one used for measuring ^{222}Rn and ^{220}Rn concentrations. It contains six 6-mm-diameter holes open in the chamber wall and covered with an electrically conductive sponge to prevent the ^{222}Rn and ^{220}Rn progeny from easily entering the chamber [97]. Thoron progeny measurements were performed using a deposition rate detector. This detector consists of CR-39 chips that are coated with a 71 mm-thick aluminized Mylar film (Figure 2.12) in air for discrimination of high-energy alpha particles.

A total of 50 RADUET detectors were deployed in dwellings in the bauxite area of Fongo-Tongo. The dwellings selected were those that had elevated concentrations ($\geq$200Bq m^{-3}) during previous measurements with RADTRAK$^{2\textcircled{R}}$ detectors. This measurement phase was done during the period from July to September, considered the rainy season due to the climate of the area and the heavy rainfall recorded during the deployment of these instruments. Figure 3 shows a sample of this detector and its different parts. RADUET detector depletion rate CR-39 chips were chemically etched for 24 h in a 6 M NaOH solution at 60°C (4). Formed alpha tracks were taken by digital photographs using a microscope. Then, the alpha track etched on each of the photographs was evaluated using the JAVA-based image processing software IMAGE-J developed at the National Institutes of Health. Using the alpha track densities of low and high air change rooms and conversion factors for ^{222}Rn and ^{220}Rn, the average radon and thoron activity concentrations were calculated as follows [99]:

$$\begin{aligned}\bar{C}_{Rn} &= (d_L-\bar{b})\frac{f_{Tn2}}{t.(f_{Rn1}.f_{Tn2}-f_{Rn2}.f_{Tn1})} - (d_H-\bar{b})\frac{f_{Tn1}}{t.(f_{Rn1}.f_{Tn2}-f_{Rn2}.f_{Tn1})} \\ &= (d_L-\bar{b}).\omega_1 - (d_H-\bar{b})\omega_2\end{aligned} \tag{2.13}$$

With $\omega_1 = \frac{f_{Tn2}}{(t.\varepsilon)}$ et $\omega_2 = \frac{f_{Tn1}}{(t.\varepsilon)}$ o? $\varepsilon = f_{Rn1}.f_{Tn2} - f_{Rn2}.f_{Tn1}$

$$\begin{aligned}\bar{C}_{Tn} &= (d_H-\bar{b})\frac{f_{Tn1}}{t.(f_{Rn1}.f_{Tn2}-f_{Rn2}.f_{Tn1})} - (d_L-\bar{b})\frac{f_{Tn2}}{t.(f_{Rn1}.f_{Tn2}-f_{Rn2}.f_{Tn1})} \\ &= (d_H-\bar{b}).\omega_3 - (d_L-\bar{b})\omega_4\end{aligned} \tag{2.14}$$

With $\omega_3 = \frac{f_{Tn1}}{(t.\varepsilon)}$ et $\omega_4 = \frac{f_{Tn2}}{(t.\varepsilon)}$

Where d_L and dH represent the trace densities of alpha particles for a low and high air exchange rate chamber in traces per square centimeters (tracks cm^{-2}) respectively. $\bar{b}$ is the trace density due to background in (tracks cm^{-2}). t(h) sampling time; f_{Rn1} and f_{Tn1}, the respective calibration factors for radon and thoron in a low air exchange rate chamber in tracks cm^{-2} h^{-1})/ (Bq m^{-3}), respectively. f_{Rn2} and f_{Tn2} are the respective calibration factors for ^{222}Rn and ^{220}Rn in a high air exchange rate chamber in tracks cm^{-2} h^{-1})/ (Bq m^{-3}).

According to the ISO/IEC 98-3 guide [99], the uncertainty in the concentration (C_{Rn}) is given by the following equation:

$$\tilde{u}(\tilde{C}_{Rn}) = (\omega_1^2(u^2(d_L) - u^2(\bar{b})) - 2\omega_1\omega_2 u^2(\bar{b}) + \omega_2^2(u^2(d_H) + u^2(\bar{b})) + \frac{(d_H^2 - 2d_H\bar{b} + \bar{b}^2)\omega_2^2 + \tilde{C}_{Rn}(2d_H + 2\bar{b})\omega_2 + \tilde{C}_{Rn}^2}{\omega_1^2} u^2(\omega_1) + (-d_H + \bar{b})^2 u^2(\omega_2))^{-1/2} \quad (2.15)$$

with

$$\tilde{u}(\tilde{C}_{Tn}) = (\omega_3^2(u^2(d_H) - u^2(\bar{b})) - 2\omega_3\omega_4 u^2(\bar{b}) + \omega_4^2(u^2(d_L) + u^2(\bar{b})) + \frac{(d_L^2 - 2d_L\bar{b} + \bar{b}^2)\omega_4^2 + \tilde{C}_{Tn}(2d_L + 2\bar{b})\omega_4 + \tilde{C}_{Tn}^2}{\omega_1^2} u^2(\omega_3) + (-d_L + \bar{b})^2 u^2(\omega_4))^{-1/2} \quad (2.16)$$

The detection limit $\bar{C}_{Rn}^*$ and $\bar{C}_{Tn}^*$ are obtained from the formulas of ω_3,ω_4 and $\bar{C}_{Rn}$ for $\tilde{C}_{Rn} = 0$,$u^2(d_L) = 0$, $\tilde{C}_{Tn} = 0$ and $u^2(d_H) = 0$ (ISO 11929).

We then obtained :

$$\bar{C}_{Rn}^* = k_{1-\alpha}\tilde{u}(0) = k_{1-\alpha}(\omega_1^2 u^2(\bar{b}) - 2\omega_1\omega_2 u^2(\bar{b}) + \omega_2^2(u^2(d_H) + u^2(\bar{b})) + \frac{(d_H^2 - 2d_H\bar{b} + \bar{b}^2)\omega_2^2}{\omega_1^2} u^2(\omega_1) + (-d_H + \bar{b})^2 u^2(\omega_2))^{-1/2} \quad (2.17)$$

$$\bar{C}_{Tn}^* = k_{1-\alpha}\tilde{u}(0) = k_{1-\alpha}(\omega_3^2 u^2(\bar{b}) - 2\omega_3\omega_4 u^2(\bar{b}) + \omega_4^2(u^2(d_L) + u^2(\bar{b})) + \frac{(d_L^2 - 2d_L\bar{b} + \bar{b}^2)\omega_4^2}{\omega_3^2} u^2(\omega_3) + (-d_L + \bar{b})^2 u^2(\omega_4))^{-1/2} \quad (2.18)$$

$\alpha = 0.05$ avec $k_{1-\alpha} = 1.65$ are often chosen by default.

The decision limit $\bar{C}_{Rn}^{\#}$ of ^{222}Rn and $\bar{C}_{Tn}^{\#}$ of ^{220}Rn sont are calculated by the following formula given by ISO 11929 :

$$\bar{C}_{Rn}^{\#} = \bar{C}_{Rn}^* + k_{1-\beta}(\omega_1^2(u^2(d_L) - u^2(\bar{b})) - 2\omega_1\omega_2 u^2(\bar{b}) + \omega_2^2(u^2(d_H) + u^2(\bar{b})) + \frac{(d_H^2 - 2d_H\bar{b} + \bar{b}^2)\omega_2^2 + \tilde{C}_{Rn}(2d_H + 2\bar{b})\omega_2 + \tilde{C}_{Rn}^2}{\omega_1^2} u^2(\omega_1) + (-d_H + \bar{b})^2 u^2(\omega_2))^{-1/2} \quad (2.19)$$

$$\bar{C}_{Tn}^{\#} = \bar{C}_{Tn}^* + k_{1-\beta}(\omega_3^2(u^2(d_H) - u^2(\bar{b})) - 2\omega_3\omega_4 u^2(\bar{b}) + \omega_4^2(u^2(d_L) + u^2(\bar{b})) + \frac{(d_L^2 - 2d_L\bar{b} + \bar{b}^2)\omega_4^2 + \tilde{C}_{Tn}(2d_L + 2\bar{b})\omega_4 + \tilde{C}_{Tn}^2}{\omega_3^2} u^2(\omega_3) + (-d_L + \bar{b})^2 u^2(\omega_4))^{-1/2} \quad (2.20)$$

The detection limit can be calculated from the expressions for $\tilde{u}\tilde{C}_{Tn}$ and $\bar{C}_{Rn}^*$ pour $\bar{C}^{\#}$ or, more simply, by iterations with an approximation of $\bar{C}^{\#} = 2 \times \bar{C}^*$ in terms hand side of the following formulas. We obtained. On with $\bar{C}^{\#}$ avec $k_{1-\alpha} = k_{1-\beta} = k$:

$$\bar{C}_{Rn}^{\#} = \frac{2\bar{C}_{Rn}^* + k^2\left\{\frac{(2d_H - 2\bar{b})\omega_2 u^2(\omega_1)}{\omega_1^2}\right\}}{1 - k^2\frac{u^2(\omega_1)}{\omega_1^2}} \quad (2.21)$$

$$\bar{C}_{Tn}^{\#} = \frac{2\bar{C}_{Tn}^{*} + k^2 \left\{ \frac{(2d_L - 2\bar{b})\omega_4 u^2(\omega_3)}{\omega_3^2} \right\}}{1 - k^2 \frac{u^2(\omega_3)}{\omega_3^2}} \tag{2.22}$$

The values $\alpha = \beta = 0.05$ and thus $k_{1-\alpha} = k_{1-\beta} = 1.65$ are often chosen by default.

2.3.13 Thoron progeny concentration measurement in dwellings

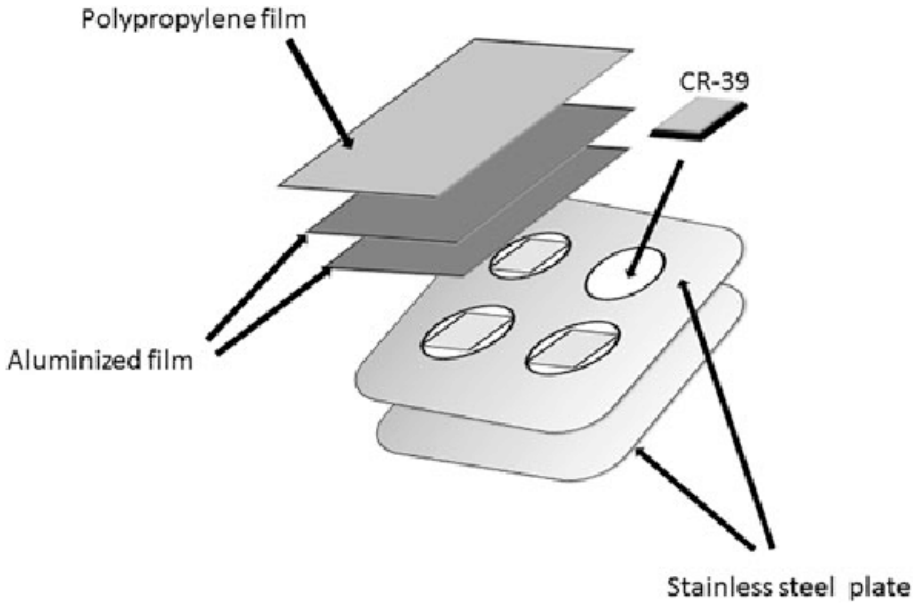

Figure 2.13: Measurement principle of thoron progeny monitor.

A total of 50 thoron progeny monitors were used in this work. These are detectors made from CR-39 at a size of 10×10 mm^2 mounted on a stainless-steel plate and covered with a thin absorbent foil. The CR-39 parts are covered with a 71 mm thick vaporized aluminium Mylar film equivalent to air. The thickness of the Mylar film allows the detection of only the 8.8 MeV alpha particles emitted by the ^{212}Po. The calibration protocol for these monitors has been well developed [99–101] Figure 2.13 shows the prototype of a thoron progeny monitor. After exposure in dwellings, the data processing follows the same procedure as for RADUET. With the trace density and the conversion factor, the concentration of thoron progeny can be obtained as equivalent equilibrium thoron concentrations (EETC). To calculate the EETC, the trace density obtained was substituted in the following equation:

$$N_{TnP} = EETC \times F_{TnP} + N_{B2} \tag{2.23}$$

Where N_{TnP} is the trace density of CR-39 in the thoron progeny detector, N_{B2} is the background trace density, and F_{TnP} is the conversion factor for the thoron, N_{B2} is the background trace density, and F_{TnP}

is a conversion factor for the Thoron progeny deposition detectors [99–101]. The conversion factor was determined based on the results of a field survey and the chemical etching condition, and it was 6.9×10^{-2} traces cm^{-2} (Bq m^{-3})$^{-1}$. The detection limit of EETC was less than 0.01 Bq m^{-3} for a measurement period of approximately six months [99].

2.4 Dose assessment

2.4.1 Absorbed dose rate at 1 meter of the ground surface

Since the respective activity concentrations of ^{226}Ra, ^{232}Th, and ^{40}K measured in soil samples are known, the absorbed dose rate in outdoor ambient air at a height of one meter above the ground was calculated using the dose rate conversion factors of :0.462 (nGy h^{-1}) (Bq kg^{-1}) $^{-1}$ pour le ^{226}Ra ; 0,604 (nGy h^{-1}) (Bq kg^{-1})$^{-1}$ pour le ^{232}Th ; 0.0417 (nGy h^{-1}) (Bq kg^{-1})$^{-1}$ pour le ^{40}K [111]. It was estimated according to the following equation:

$$D(nGyh^{-1}) = 0.462A_{Ra} + 0.604A_{Th} + 0.0417A_K \tag{2.24}$$

where A_{Ra}, A_{Th} et A_K are the activity concentrations of ^{226}Ra, ^{232}Th, and ^{40}K respectively.

2.4.2 External effective dose

The annual effective dose received by an individual adult is the amount of radiation energy absorbed per unit mass of material over a specified time. The effective dose is used to combine the doses delivered to several different tissues or organs and to obtain an estimate of the health detriment. The effective dose due to external irradiation, E($mSvy^{-1}$) was calculated using the following formula

$$E(mSvy^{-1}) = D \times F_c \times T \times [F_{occ} + (1 - F_{occ})] \times 10^{-6} \tag{2.25}$$

Where F_c = 0.7 is the conversion coefficient from absorbed dose to air to effective dose to adults, D is the absorbed dose rate for each sample analyzed, t = 8760 h is the annual outdoor residence time (in h/y) and F_{occ} = 0.6 is the occupancy coefficient [112].

2.4.3 Inhalation effective dose from outdoor ^{222}Rn

The annual inhalation dose E_{inh} (mSv) from outdoor ^{222}Rn received by the public is therefore calculated using the equation (8) [1].

$$E'_{inh}(mSvy^{-1}) = C'_{Rn} \times F_C \times F'_{occ} \times F_{eq} \times t \tag{2.26}$$

Where E'_{inh} is the inhalation dose form outdoor ^{222}Rn concentration that received by the public, F_{eq} is the equilibrium factor (F_{eq} = 0.6), F'_{occ} = 0.4 is the outdoor occupation factor per individual, and F_C is the dose conversion factor for ^{222}Rn exposure, 9 nSv (Bq h m^{-3}) $^{-1}$ [1].

2.4.4 Inhalation effective dose due to indoor ^{222}Rn, ^{220}Rn, and their progeny

The large proportion of the total inhaled dose received by the lung does not come from radon gas (^{222}Rn, ^{220}Rn and ^{219}Rn) itself. In fact, according to its characteristics and physicochemical properties as an inert and insipid gas does not react chemically with the biological tissues of the body. Its low solubility with these same tissues also makes the radiotoxicity of inhaled radon relatively insignificant compared to that of its immediate offspring. These are short-lived solid particle emitters with which it is in partial equilibrium. The equilibrium radon equivalent concentration (EEC) of a mixture of radon decay products is the activity concentration of radon in radioactive equilibrium with its short-lived progeny having the same potential energy concentration alpha [113]. The origin of the exposure is thus due to the inhalation of the alpha emitting radon decay products present in the domestic air breathe and their deposition in the respiratory tract according to their size. The energy communicated to the lung tissues during the alpha decay contributes thus mainly to the dose brought to the lung and to the induced risk of broncho-pulmonary cancer.

Exposures are estimated in terms of radon activity concentration rate (in Bq h m^{-3}) in dwellings, while in the professional mining environment in Working Levels months (**WLM**). In the case of an exposure in a dwelling for a duration of 7000 hours which would correspond approximately to the average time spent there and average equilibrium factor of F = 0.4, we end up with exposure of 227 Bq m^{-3} or **WLM**, which corresponds to the exposure of a person over a period of one month of work, i.e. 170 hours and is equivalent to 3.54×10^{-3} J h m^{-3} in the international system [114 –116].

For RADTRAK^{2}® detectors, the effective inhalation dose due to radon and its associated progeny in dwellings is given by the following equation:

$$E_{inh}(mSvy^{-1}) = A_{inh} \times e_{inh} \times F_{occ} \times F_{Rn} \times t \tag{2.27}$$

A_{inh} is the geometric mean of the radon concentration distribution;
e_{inh}= 9 nSv (Bq.h.m^3)$^{-1}$ is the inhalation dose conversion factor;
F_{occ} (0,6) is the occupancy factor inside the dwelling;
F_{Rn} (0,4) is the equilibrium factor considered (for radon);
t = 8760 (h/y) is the exposure time [112].

For RADUET detectors, the total doses due to inhalation of ^{222}Rn and its decay products (E_{Rn}), and to inhalation of ^{220}Rn and its progeny (D_{Tn}) are estimated using equations 2.28 and 2.29, and using the conversion factors for radon concentration (C_{Rn}), thoron concentration (C_{Tn}), EERC, and EETC, whose

respective values recommended by **UNSCEAR** are: 0.17; 0.11; 9 and 40 nSv Bq^{-1} h^{-1} m^3 [112].

$$E_{Rn}(mSvy^{-1}) = (0.17 + 9F_R) \times C_{Rn} \times t \times F_{occ} \times 10^{-6} \tag{2.28}$$

$$E_{Tn}(mSvy^{-1}) = (0.11 \times C_{Tn} + 40 \times EETC) \times t \times F_{occ} \times 10^{-6} \tag{2.29}$$

where 0,6 is the occupancy factor inside the dwelling; t = 8760 h (24 h $\times$ 365 j) is the time of exposure in one year (in h/y) [51, 114]. The usual occupancy factor used is F_{occ} = 0,8. However, this study was conducted in sub-Saharan Africa, specifically in western Cameroon region where the minimum temperatures rarely fall below 20^oC in the shade. Most of the people surveyed work all day in the fields, at the market, or in the open air. Other members of the public (the elderly, the retired...) who do not go to work spend more time outside the buildings, under the trees or on the terraces of the dwellings because of the heat. Therefore, certainly because of the cold, the public spends 80% of the time indoors. The time spent in a house for the case of this study is estimated at 60%; an average of 14 hours per day, attributable to heat, poverty, lack of air conditioning and lack of electricity in the area.

When the contributions of ^{222}Rn and ^{220}Rn are not taken into account, the effective doses were determined on the one hand by the traditional or indirect method using the equilibrium factor between radon gas and its direct progeny by direct measurements using the EETC directly measured from the thoron progeny monitors deployed in the different dwellings and given by following the equation:

$$E_{Rn}(mSvy^{-1}) = 9 \times C_{Rn} \times t \times F_{occ} \times 10^{-6} \tag{2.30}$$

$$D_{Tn}(mSvy^{-1}) = 40 \times EETC \times t \times F_{occ} \times 10^{-6} \tag{2.31}$$

Recent studies have shown that the contribution of ^{220}Rn to internal public exposure is not always negligible compared to radon. In some places, this contribution can be higher than that of ^{222}Rn [18, 20, 23, 25, 38]. To estimate the effective inhalation doses of ^{222}Rn, radon progeny, ^{220}Rn and thoron progeny, **UNSCEAR** proposes the following formulas respectively [112] :

$$E_{Rn}(mSvy^{-1}) = 0.17 \times C_{Rn} \times t \times F_{occ} \times 10^{-6} \tag{2.32}$$

$$E_{RnP}(mSvy^{-1}) = 9 \times C_{Rn} \times F_{Rn} \times t \times F_{occ} \times 10^{-6} \tag{2.33}$$

$$E_{Tn}(mSvy^{-1}) = 0.11 \times C_{Tn} \times t \times F_{occ} \times 10^{-6} \tag{2.34}$$

$$E_{TnP}(mSvy^{-1}) = 40 \times EETC \times t \times F_{occ} \times 10^{-6} \tag{2.35}$$

Equations 2.32 and 2.34 give the direct measurements of the inhalation effective dose of radon and thoron ^{220}Rn. Equations 2.33 and 2.35 give the indirect measurements of the inhalation effective dose from ^{222}Rn and thoron progeny. Equation 2.28 is the combination of equations 2.32 and 2.33, while equation 2.29 is the combination of equations 2.34 and 2.35. In the two cases, it is the sum of the dose of the gas and that of its associated progeny.

2.5 Risk assessment

2.5.1 Excess lifetime cancer risk (ELCR)

The ELCR is the probability that an individual will contract or develop a radiation-induced cancer during his lifetime, because of his exposure to ionizing radiation. It was estimated for this using the equation [13, 117, 118]:

$$ELRC = ELCR_{out} + E_{in} \tag{2.36}$$

$ELCR_{out}$ = E_{out}×DL×RF is the outdoor risk, $ELCR_{in}$ = E_{in}× DL×RF is the indoor risk, E_{out} and E_{in} are the indoor and outdoor effective dose, respectively, DL is the average life expectancy of 70 years, and RF is the risk factor (risk of fatal cancer per mSv). In its publication 106, **ICRP** recommends value of **RF**= 0,05 10^{-3} mSv^{-1} for induction to stochastic effects of members to the public.

2.5.2 Excess Cancer Risk (ECR) Computer Using RESRAD-ONSITE and RESRAD-BUILD Codes

Since most dwellings in the study are constructed with locally manufactured earthen or sand bricks, the of ^{40}K, ^{226}Ra and ^{232}Th concentrations in soil are input data (contaminant on source parameters) at runtime by RESRAD-ONSITE and RESRAD-BULD codes version 7.2 and 3.5 respectively.

RESRAD-ONSITE is used to assess the ECR due to these natural occurring radionuclides in soil at the bauxite bearing area of Fongo-Tongo. The site-specific of the area are listed in Table 2.2. The other parameters are used as defaults values [119]. Together all of the above parameters were considered in the evaluation of the risk factors.

RESRAD-BUILD allowed the assessment of radiation doses received by a resident living or working in a house contaminated by radioactive materials. These doses are those from the different exposure pathways (external and internal including inhalation of radon progeny inside the home). The radiological risk was estimated over the periods of 1, 10, 30, 50, 70 and 90 years of exposure. However, 85% of the dwellings

in the area are made of mud bricks, usually produced on the same site, and samples of these earth bricks were analysed to obtain the concentrations introduced as input data mentioned above. Table 2.2 presented the other input parameters.

Table 2.2: Input parameters for RESRAD codes.

RESRAD-ONSITE	
Parameters	Site-Specific Data
Site-Specific Data	25000 m^2
Cover depth	1m
Density of contaminated zone	1.8 cm^3 g^{-1}
Precipitation rate	0.4473 m y^{-1}
Wind speed	1.2 m s^{-1}
Well pump intake	8 m
Porosity	0,1
RESRAD-BULD	
Parameters	Dwellings-Specific Data
Indoor/time fraction	0,6
Deposition Velocity 0.01 m s^{-1}	
Resuspension rate	5×10^{-7} s^{-1}
Occupant location in the room Centered	
Ingestion rate	44661
Room surface area and volume	16 m^2 and 40 m^3
Breathing rate	18 m^3 d^{-1}
thickness	0
Type of source	Volume
Source geometry	Rectangular
Release air fraction	0,1
Radon diffusion rate	2×10^{-5} m s^{-1}
Number of room/Occupant	1

2.5.3 Risk due to radon inhalation: the absolute lifetime excess risk

Epidemiological studies on miners exposed to radon in underground caves and residential exposure of the public to radon have demonstrated the existence of a lung cancer risk following inhalation radon and its decay products [115, 116]. Indeed, it is the cumulative risk of an individual until a given year. The life

span usually considered is 90 years as in the different **ICRP** publications. The risk due to ^{222}Rn inhalation is generally estimated by the Lifetime Excess Absolute Risk (LEAR), and corresponds to the individual probability of death from lung cancer attributable to an exposure of 1 **WLM** (Working Level Month). This indicator is to be compared to the spontaneous probability of death from lung cancer (Life time Baseline Risk), over the same lifetime. It is expressed as the number of deaths per 10,000 person-years per WLM. For radon, the exposure scenario considered is based on a constant low-level exposure of 2 WLM per year from 18 to 64 years of age, as proposed in Publication 65 [120]. Thus, **UNSCEAR** and **ICRP** recommend the **LEAR** of $5\times10^{-4}\times\mathbf{WLM}^{-1}$ as the probability of developing lung cancer from exposure to radon and its progeny [121].

$$\mathbf{LEAR} = 5\times10^{-4}?WLM^{-1} = 7.85\times10^{-10}(F_{eq}.Bq.h.m^{-3}) \tag{2.37}$$

with **WLM**=6.37 105/(Feq.Bq.h.m^{-3}). To estimate the **LEAR** per year for the study area, the internal occupancy factor of 0.6 and the equilibrium factor of 0.4 for radon were used. The risk coefficients used to analyze the Fongo-Tongo bauxite zone case were derived from the results of epidemiological studies conducted elsewhere on populations exposed to ionizing radiation.

Conclusion

In this chapter, The study area was also presented geographically and its geology and mineralogy were also described. Material and the different methods used to measure environmental natural radioactivity have been presented. Activity concentrations of ^{226}Ra, ^{232}Th and ^{40}K were determined by *in situ* and laboratory γ spectrometry in soil samples. Dose and risk assessment parameters of external exposure were also done. The different methods of measuring the concentrations of ^{222}Rn, ^{220}Rn, and thoron progeny were also presented and the method of inhalation dose assessment for the case of internal exposure of the public in the bauxite bearing area of Fongo-Tongo is briefly described. The results obtained are presented and discussed in the following chapter.

Chapter 3

Results and Discussion

Introduction

In this chapter, we present and discuss the results obtained in this study. The activitiy concentrations of the primordial radionuclides were determined in soil samples by laboratory and *in situ* measurements, while ^{222}Rn concentrations were measured in soil and the ^{222}Rn, ^{220}Rn and thoron progeny concentrations were also measured in dwellings in the bauxite bearing area of Fongo-Tongo. The statistics of the data is summarized in figures and tables. These results and their various meanings are discussed and compared to international reference values and to results reported. Other results are reported in the appendix of this work.

3.1 ^{226}Ra, ^{232}Th and ^{40}K activity concentration in soil

The most effective approach to measure the activity concentration of ^{226}Ra, ^{232}Th, and ^{40}K in soil involves creating a geographic grid of the area and conducting measurements at each point. This method ensures a well-distributed data collection across the field, facilitating the creation of a more accurate radioactivity map of the region. However, practical field conditions often do not favor this technique. As a result, using random sampling points to cover the entire area was considered. The samples were collected using both in-situ and laboratory gamma spectrometry methods.

3.1.1 ^{226}Ra, ^{232}Th and ^{40}K activity concentrations in soil

In Fongo-Tongo, the activity concentrations of ^{226}Ra, ^{232}Th, and ^{40}K obtained through laboratory and *in situ* methods varied from 106 to 170 Bq kg^{-1} and from 93 to 201 Bq kg^{-1} for ^{226}Ra; from 119 to 295 Bq kg^{-1} and from 40 to 327 Bq kg^{-1} for ^{232}Th; and from 188 to 458 Bq kg^{-1} and from 49 to 321 Bq kg^{-1} for ^{40}K. The mean values were found to be 148$\pm$23, 212$\pm$54, and 230$\pm$28 for ^{226}Ra; and 129$\pm$16, 214$\pm$67, and 229$\pm$54 for ^{232}Th, respectively.

In Dschang, the activity concentrations of ^{226}Ra, ^{232}Th, and ^{40}K ranged from 99 to 167 Bq kg^{-1} and from 98 to 181 Bq kg^{-1} for ^{226}Ra; from 100 to 275 Bq kg^{-1} and from 139 to 309 Bq kg^{-1} for ^{232}Th; and from 198 to 297 Bq kg^{-1} and from 151 to 280 Bq kg^{-1} for ^{40}K. The mean values were calculated as 118±17, 1752±46, and 230±28 for ^{226}Ra; and 138±19, 231±35, and 237±26 for ^{232}Th, respectively.

Figure 3.6 illustrates the box-plot distributions of these concentrations obtained through laboratory (a) and *in situ* (b) measurements for each locality and for the entire study area.

According to Table 3.1, 50 of the sampling points showed concentrations higher than 151 Bq kg^{-1}, 209 Bq kg^{-1}, and 234 Bq kg^{-1} for ^{226}Ra, ^{232}Th, and ^{40}K, respectively, in laboratory measurements. Additionally, the *in situ* measurements exhibited a lognormal distribution, with the mean value represented by the geometric mean, while laboratory measurements followed a normal distribution and were represented by the arithmetic mean.

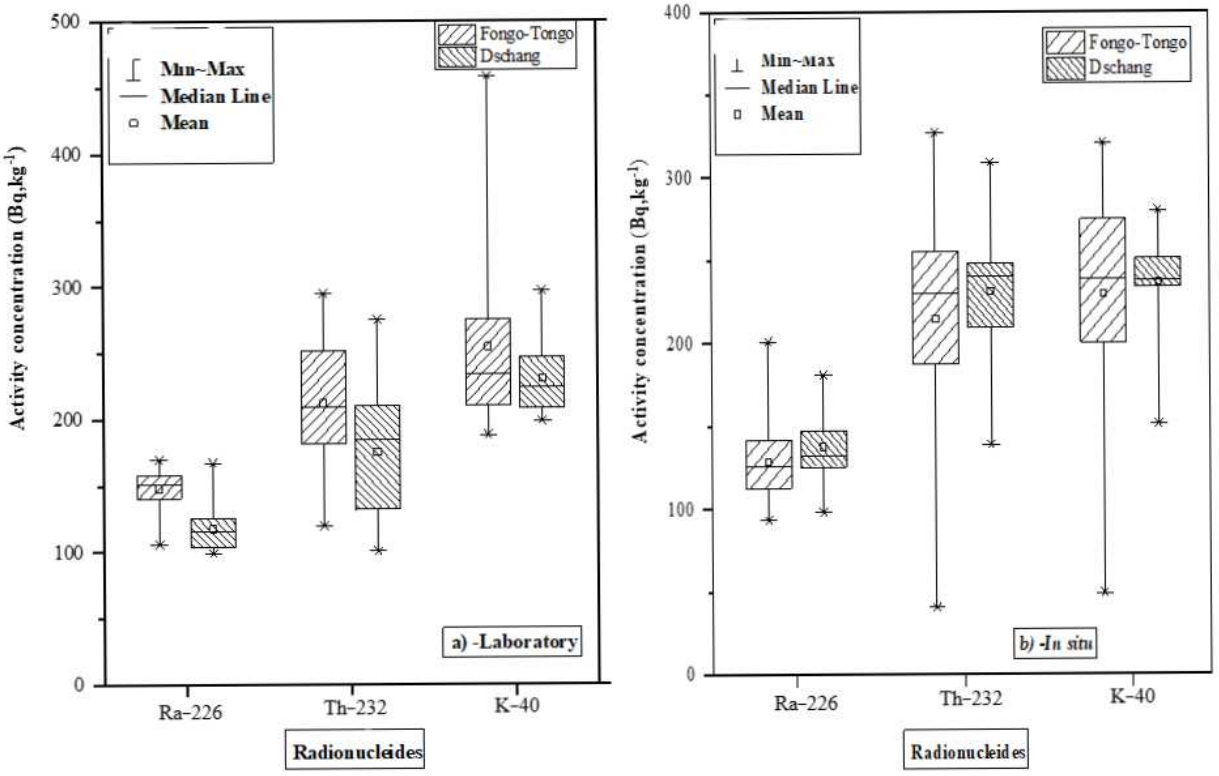

Figure 3.1: Boxplot distribution of activity concentration of ^{226}Ra, ^{232}Th, and ^{40}K obtained by laboratory **(a)** and **(b)** measurements.

Certainly, this is not a comparative study between in-situ and laboratory measurements. It is challenging to make a precise comparison between the results obtained from these two methods. In-situ measurements provide a broad overview of the accuracy of laboratory measurements. However, overall, the results from both techniques exhibit many similarities, especially in areas where both methods were applied to measure natural radioactivity.

Some differences noted in the results can be attributed to the nature of in-situ γ-spectrometry, which

offers a representation of source concentration across a wide horizontal plane, extending up to a radius of 10 m and a depth of 10 cm. In contrast, laboratory γ-spectrometry measures radioactivity in a soil sample collected from a 1 m^2 area (roughly a 70 cm radius). Furthermore, the composition of the sampled matrix (the soil) differs between the two processes. by in-situ γ-spectrometry, the sampled soil is typically compact, heterogeneous, varying in moisture content, and containing various rocks, vegetation, and debris (such as plants and minerals). On the other hand, in laboratory γ-spectrometry, the soil matrix is dried, homogeneous, free of debris, and uncompressed. It undergoes sieving to ensure that the solid particles it contains have roughly the same volume. This matrix undergoes disturbances during sampling, and the radioelements within it must achieve secular equilibrium to accurately reveal their activities. Considering the uncertainties associated with each measurement technique (in-situ and laboratory), the values of the results obtained are approximately comparable.

Table 3.1: Statistical parameters of ^{226}Ra, ^{232}Th, ^{40}K, and ^{222}Rn concentrations obtained by *in situ* and laboratory measurements for the localities of Dschang and Fongo-Tongo.

		Laboratory			*In situ*			
Locality	Parameters	^{226}Ra	^{232}Th	^{40}K	^{226}Ra	^{232}Th	^{40}K	^{222}Rn
Fongo-Tongo	Min-Max	106-170	119-295	188-458	93-201	94-327	49-321	35-202
	Median	151	209	234	126	229	239	53
	AM $\pm$ SD	148 $\pm$ 23	212 $\pm$ 54	230 $\pm$ 28	-	-	-	-
	GM(GSD)	-	-	-	129 (16)	214 (67)	229 (54)	69 (8)
Dschang	Min-Max	99-167	100-275	198-297	98-181	139-309	151?280	48-255
	Median	116	185	224	132	240	238	62
	AM $\pm$ SD	118 $\pm$ 17	175 $\pm$ 46	230 $\pm$ 28	-	-	-	-
	GM(GSD)	-	-	-	138 (19)	231 (35)	237 (26)	82 (14)

The laboratory analysis of soil samples reveals significantly elevated concentrations of ^{226}Ra and ^{232}Th. Table 3.1.1 demonstrates that the minimum and maximum values of ^{226}Ra from laboratory and in-situ measurements are respectively three and five times higher than the global average of 35 Bq kg^{-1} [1]. Similarly, for ^{232}Th, these values are two and four times higher than the global average of 45 Bq kg^{-1} [1]. These heightened concentrations of ^{226}Ra and ^{232}Th are also evident in the results obtained via in-situ γ spectrometry. The minimum values for ^{226}Ra and ^{232}Th are respectively three and two times higher than the global average, while the maximum values are six and seven times higher than the global average [1]. Moreover, the average values of ^{40}K, as well as the maximum values for both in-situ and laboratory methods, are below 420 Bq kg^{-1}, the global average value [1].

Figure 2.2 illustrates that the surveyed area encompasses a geological structure with basaltic and trachytic

granitic rock coverings [72, 122]. Activity concentrations of ^{226}Ra, ^{232}Th, and ^{40}K vary across different points for both in-situ and laboratory gamma spectrometry techniques. This variability can be attributed to the non-uniform distribution of radioactivity in soil [42]. It is noted that rocks such as syenite, granite, granulite, rhyolites, and plutonic contain high concentrations of ^{238}U, ^{232}Th, and ^{40}K [4, 5, 42]. The lower concentrations of ^{40}K can be explained by leaching and transport of potassium elements due to erosion effects, drainage, and sediment accumulation in seabeds [123, 124]. Erosion or volcanic activity-induced transfer of ores significantly alters the content and concentrations of this radionuclide in soil, with basalt showing lower concentrations [4, 5, 42]. The presence of these rocks contributes to considerable variation in the concentrations of primordial radionuclides across different sites, as shown in Figure 3.6. Additionally, the soil in Fongo-Tongo may exhibit higher compactness and moisture levels compared to that in Dschang [122, 126]. Table 3.2 highlights that primordial radionuclide activity concentrations in Cameroonian soil exceed those in some other global regions [122-125]. However, elevated ^{40}K concentrations are observed elsewhere outside of this study area as well [128, 131].

Table 3.2: Comparison of ^{226}Ra, ^{232}Th, ^{40}K, and ^{222}Rn activity concentration with other countries.

Country	^{226}Ra	^{232}Th	^{40}K	^{222}Rn	References
Jordan	57.7±5.4	18.1 ±1.4	138.1 ± 40.8		[116]
Egyp	t 134.7±24.1	131.8±16.7	11,644 ± 550		[117]
India	116.1	43.51	300.07	-	[118]
Iraq	58.44	19.38	321.76	-	[9]
	45.71	20.33	337.02		
Nigeria	64.64±28.10	110.18±46.12	1190.10±373.62		[112]
Australia	38	45	635	-	[10]
Japan	38±1	43±1	590	-	[8]
Cameroon	14±2	30±3	103±12	9±2	[119]
	-	390	850	-	[120]
	124.9	157.3	670.9	[121]	
	166.18	170.04	94.54		[13]
	118±17(138±19)	175±46 (231±35)	230±28 (237±26)	82±56	Present study
	148±23 (129±16)	21±54 (214±67)	230±28 (229±54)	69	40

3.2 ^{222}Rn, ^{220}Rn and their progeny concentration in the environment

Radon concentrations were assessed in soil near dwellings using RADTRAK^{2}® detectors and soil sampling points. The measured soil concentrations were utilized to categorize sites with high radon potential or

to pinpoint areas with potential high risk following Swedish risk classification criteria [124].

^{222}Rn concentrations within dwellings in our study were measured in two phases using different detector types. The initial phase employed RADTRAK^{2}® and RadonEye+^{2} detectors during the dry season, specifically between December and February. Subsequently, the second phase utilized RADUET detectors and thoron progeny monitors during the rainy season, particularly from July to September.

The dwellings in this study were characterized by either one front door and one window or two doors with multiple windows. Detectors were positioned 80 cm away from walls and at a height of 150 cm from the floor, suspended from the ceiling of the dwellings.

Furthermore, radon concentrations obtained within dwellings were analyzed, interpreted, and discussed in accordance with international reference values, site-specific geological and environmental parameters, and comparisons with previous studies.

3.2.1 ^{222}Rn concentration in soil

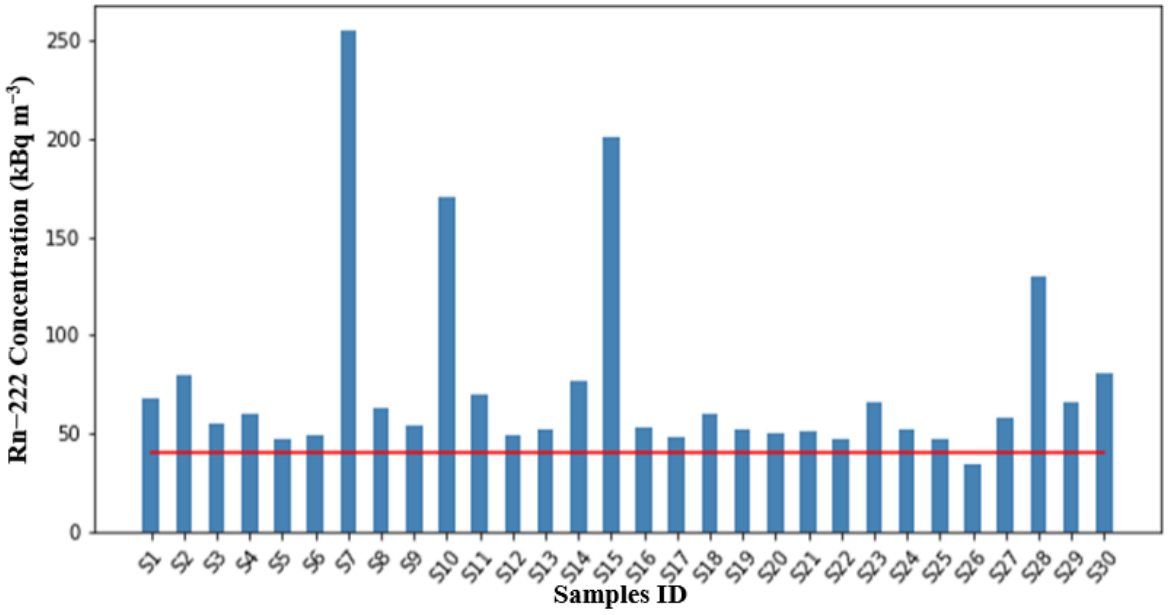

Figure 3.2: ^{222}Rn distribution in soil of the bauxite bearing area of Fongo-Tongo.

The ^{222}Rn concentrations at a depth of 1 m in soil, as presented in Table 3.3, ranged from 35 to 202 kBq m^{-3} in Fongo-Tongo, with a mean value of 69 $\pm$ 40 kBq m^{-3}. In Dschang, the concentrations ranged from 48 to 255 kBq m^{-3}, with a mean value of 82 $\pm$ 56 kBq m^{-3}. More than half of the sampled points in Dschang exhibited ^{222}Rn concentrations in soil greater than or equal to 62 kBq m^{-3}, while in Fongo-Tongo, this threshold was 53 kBq m^{-3}.

As depicted in Figure 3.2, a majority of radon concentrations in soil surpassed the 40 kBq m^{-3} threshold, denoted by the red line, which is considered the limit for high radon-exposure risk according to Swedish risk

assessment criteria [124]. The variation in ^{222}Rn concentrations across different locations may stem from differences in geological structure and the mineralogical composition of the soil [42, 123]. The geological structure, geochemical processes of the soil, and gas emanation rates in the region are influenced by soil permeability [42, 72, 74, 122, 125].

Table 3.3 indicates that the average and maximum values of ^{222}Rn in soil in Dschang exceed those in Fongo-Tongo, unlike the ^{226}Ra values obtained in these two localities. This discrepancy could be attributed to variations in soil moisture and porosity.

Table 3.3: Statistical parameters of ^{222}Rn concentration in soil at the bauxite bearing area of Fongo-Tongo and Dschang.

Locality	GM (GSD)	Median	Range
Dschang	82 (14)	62	48-255
Fongo-Tongo	69 (8)	53	35-202
Whole study area	67(18)	57,6	35-255

3.2.2 Geogenic radon potential and outdoor radon concentration

The concentrations of ^{222}Rn in soil served as a basis for evaluating radon concentrations at the Earth's surface. The data, outlined in Table 3.4, are crucial as radon diffuses from the ground into the atmosphere, where it quickly dilutes with ambient air. Subsequently, it migrates through convection into homes, where it can accumulate to significant levels and pose carcinogenic risks to the respiratory tract [7]. Therefore, to safeguard the population from ^{222}Rn exposure, it is imperative to analyze ^{222}Rn levels in all potential sources, including soil, water, food, and building materials. This comprehensive analysis is vital for devising action plans that identify areas prone to generating high indoor ^{222}Rn levels, known as ^{222}Rn risk areas.

Table 3.4 presents the assessment of geogenic ^{222}Rn potential values derived from ^{222}Rn concentrations and soil permeability, categorized as k= 10^{-11} m s^{-1}, k= 10^{-12} m s^{-1}, and k=10^{-13} m s^{-1} [105]. According to the Czech Republic's classification of regions with ^{222}Rn potential in soil, 100%, 26.7%, and 13.3% of measurement points exhibit a ^{222}Rn index with a **GRP** (geogenic radon potential) exceeding 35 for permeability values of k= 10^{-11} m s^{-1}, k= 10^{-12} m s^{-1}, and k=10^{-13} m s^{-1}, respectively. The distribution of sampling points suggests that the region can be classified as a moderate ^{222}Rn risk area, with the **GRP** increasing with soil permeability. This underscores the importance of permeability as a critical parameter in determining the mobility of ^{222}Rn in soil [103]. Indeed, high permeability in soil can lead to significant diffusion of ^{222}Rn into the atmosphere, a factor heavily influenced by the geological characteristics of the area [106, 137].

Table 3.4: Statistical parameters of exhalation rate and **GRP** for the investigated sites.

Statistical parameters	a $(Bq.m^{-3}.s)$	E $(Bq.m^{-2}.s)$	C'$(Bq.m^{-3})$	k=10^{-11}	k=10^{-12}	k=10^{-13}
AM	0,1587	0,033	75,6	75,6	37,8	25,2
SD	0,102	0,021	48,2	48,2	24,1	16,1
GM	0,1401	0,029	66,7	66,7	33,4	22,3
GSD	0,1029	0,022	48,9	48,9	24,5	16,3
Median	0,1210	0,025	57,6	57,6	28,8	19,2
Min	0,0725	0,015	35	35	17,25	11,5
Max	0,5351	0,112	255	255	127,4	84,9

3.2.3 Indoor ^{222}Rn distribution using RADTRAK^{2}® detector

Indoor ^{222}Rn levels were assessed in 50 dwellings across the study area, comprising 30 in Dschang and 20 in Fongo-Tongo. The main results are summarized in Table 3.5, revealing a range of indoor ^{222}Rn concentrations from 85 Bq m^{-3} to 410 Bq m^{-3}, with a mean value of 152 $\pm$ 26 Bq m^{-3}. Specifically, indoor ^{222}Rn levels in Dschang and Fongo-Tongo varied from 85 to 250 Bq m^{-3} and from 98 to 410 Bq m^{-3}, with mean values of 144 $\pm$ 24 and 166 $\pm$ 31 Bq m^{-3}, respectively. The study underscores that the average ^{222}Rn concentration in these regions exceeds the global average value of 30 Bq m^{-3} [1].

Table 3.5: Summary of the results of ^{222}Rn survey using RADTRAK^{2}® detectors.

Locality	GM (GSD)	Median	Range
Dschang	144 (24)	140	85-250
Fongo-Tongo	166 (31)	150	98-410
Whole study Area	152 (26)	140	85-410

GM: geometric mean, GSD: geometric standard deviation

The elevated levels of indoor ^{222}Rn can be attributed to the architectural style of these dwellings, primarily constructed with mud bricks. The emanation of ^{222}Rn from these building materials likely contributes to the increased indoor ^{222}Rn levels. Particularly, in earthen houses where walls and floors lack cement covering, high ^{222}Rn concentrations are observed. This is due to radon gas, trapped in the earth constituting the building material, diffusing easily and accumulating in poorly ventilated houses.

Moreover, the persistently cold and damp climate of the region compels inhabitants to keep their dwelling openings closed, reducing air exchange between the indoors and outdoors and further enhancing ^{222}Rn gas accumulation [140]. Additionally, most monitored dwellings lack ground waterproofing, allowing ^{222}Rn to emanate from the ground without attenuation. The substantial ^{222}Rn concentrations and variations observed among dwellings and sites are closely tied to geological structure, ventilation conditions, atmospheric and

climatic factors, architectural design, and residents' lifestyle [142].

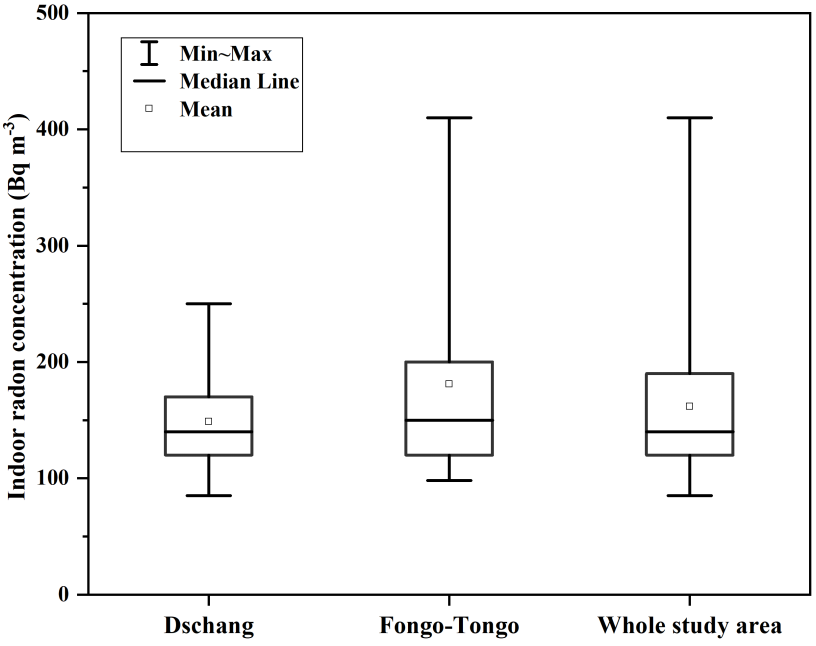

Figure 3.3: Boxplot distribution of indoor ^{222}Rn at the different site and for whole study area.

The elevated levels of indoor ^{222}Rn can be attributed to the architectural style of these dwellings, primarily constructed with mud bricks. The emanation of ^{222}Rn from these building materials likely contributes to the increased indoor ^{222}Rn levels. Particularly, in earthen houses where walls and floors lack cement covering, high ^{222}Rn concentrations are observed. This is due to radon gas, trapped in the earth constituting the building material, diffusing easily and accumulating in poorly ventilated houses.

Moreover, the persistently cold and damp climate of the region compels inhabitants to keep their dwelling openings closed, reducing air exchange between the indoors and outdoors and further enhancing ^{222}Rn gas accumulation [140]. Additionally, most monitored dwellings lack ground waterproofing, allowing ^{222}Rn to emanate from the ground without attenuation. The substantial ^{222}Rn concentrations and variations observed among dwellings and sites are closely tied to geological structure, ventilation conditions, atmospheric and climatic factors, architectural design, and residents' lifestyle [142].

Therefore, soils rich in uranium are also enriched in radium and radon. Porous and permeable soils, such as those found in the bauxite zones of Fongo-Tongo, facilitate the diffusion and migration of radon to the surface. Previous studies conducted in this area have revealed elevated concentrations of ^{226}Ra and ^{222}Rn in soil [146]. These studies also indicate a correlation between ^{226}Ra and ^{222}Rn concentrations in soil.

During the measurement period, the population was actively engaged in fieldwork daily and typically

Table 3.6: Comparison of the results of the current study with those obtained in other countries.

Country	Area	GM	Range	References
Canada	Ottawa	72 × 2	8-1525	[35]
China	-	58 × 2	12-427	[38]
Hungary	Great Hungarian Plain	166	45-609	[36]
	Kövágószölöss	-	17-1083	[37]
North Macedonia	-	114	30-535	[39]
South Africa	West	-	28-465	[40]
Cameroon	Lolodorf	89 × 2	26-976	[9]
	Lomié	58 × 24	27-300	[19]
	Southern Adamawa	102 × 21	43-270	[6]
	Fongo-Tongo	152×26	85-410	Current study

kept their homes closed, leading to the accumulation of gas indoors [16, 20, 110]. Thus, the high concentrations observed in this study can be attributed to the various geological, climatic, and anthropological factors mentioned above.

Table 3.6 compares the measured ^{222}Rn concentrations in this study with those reported in previous research. The maximum levels observed here are two to three times lower than the highest values reported in other studies [17, 147-149]. Indeed, these references cite maximum ^{222}Rn levels higher than those observed in the study areas but within the range of 400 to 600 Bq m^{-3} [17, 150, 151].

3.2.4 Indoor ^{222}Rn and ^{220}Rn distribution using RADUET detector.

Figures 3.4 and 3.5 illustrate the frequency distribution of ^{222}Rn, ^{220}Rn, radon progeny, and thoron progeny concentrations in selected dwellings within the Fongo-Tongo bauxite area. Measurements at the site revealed an asymmetric distribution, primarily due to the prevalence of low concentration values in many dwellings compared to the fewer instances of high concentrations. As a result, the extreme high values significantly impact the arithmetic mean of such a distribution. This distribution pattern was expected, given that it reflects the outcomes of short-term (spot) sampling.

As outlined in Table 3.7, ^{222}Rn concentrations measured with RADUETS varied between 31 and 123 Bq m^{-3}, with an arithmetic mean of 64 ± 24 Bq m^{-3} and a geometric mean of 60 ± Bq m^{-3}. These values fall below the 300 Bq m^{-3} reference value recommended by the **ICRP** [114] and the **IAEA** [82]. However, they are lower than the 148 Bq m^{-3} threshold recommended by the United States Environmental Protection Agency [153] and the intervention threshold of 200 Bq m^{-3} prescribed in many **EU** countries [154]. Specifically, only 12% of the 50 monitored dwellings had radon concentrations exceeding the **WHO**

recommended value of 100 Bq m^{-3}, with 88% recording concentrations below this threshold [7].

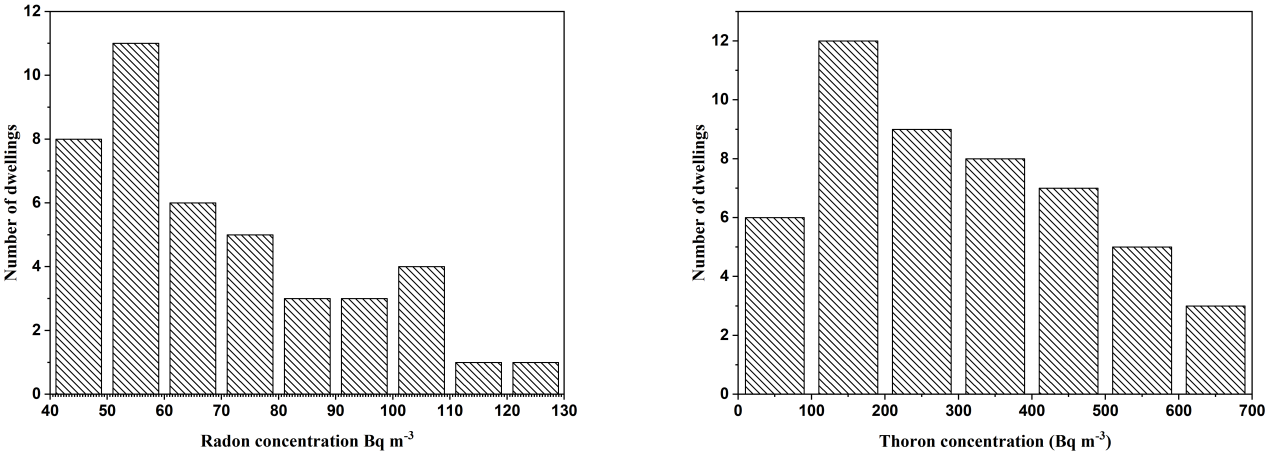

Figure 3.4: Frequency distribution of ^{222}Rn and ^{220}Rn concentrations.

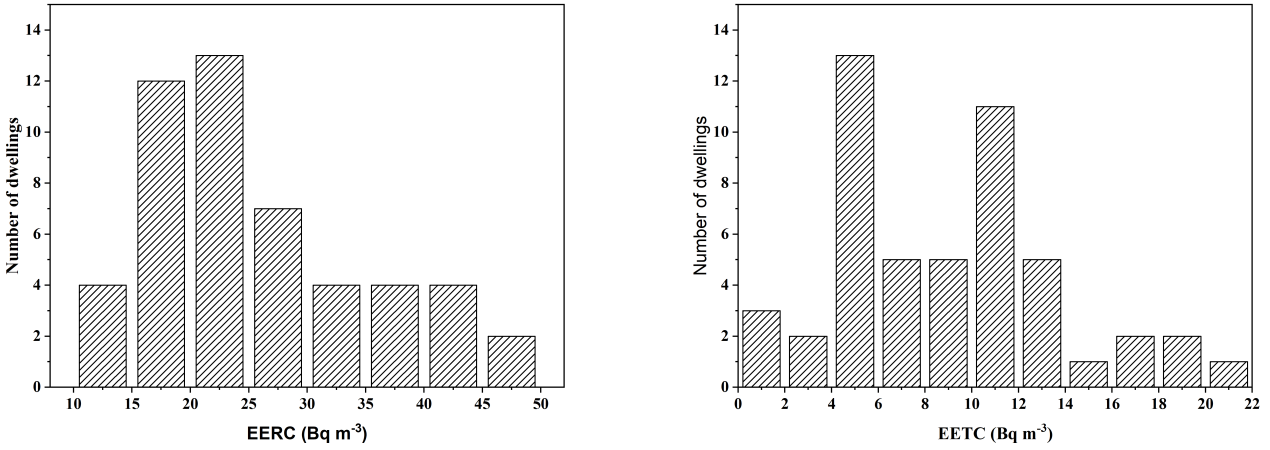

Figure 3.5: Frequency distribution of EERC and EETC.

The most effective approach to measure the activity concentration of ^{226}Ra, ^{232}Th, and ^{40}K in soil involves creating a geographic grid of the area and conducting measurements at each point. This method ensures a well-distributed data collection across the field, facilitating the creation of a more accurate radioactivity map of the region. However, practical field conditions often do not favor this technique. As a result, using random sampling points to cover the entire area was considered. The samples were collected using both in-situ and laboratory gamma spectrometry methods. In Fongo-Tongo, the ^{226}Ra, ^{232}Th, and ^{40}K activity concentrations obtained by laboratory and *in situ* methods ranged from 106 to 170 Bq kg^{-1} and from 93 to 201 Bq kg^{-1} for ^{226}Ra; from 119 to 295 Bq kg^{-1} and from 40 to 327 Bq kg^{-1} for ^{232}Th; and

from 188 to 458 Bq kg^{-1} and from 49 to 321 Bq kg^{-1} for ^{40}K which a means values of 148±23, 212 ± 54 and 230 ± 28 and 129±16, 214±67 and 229±54 respectively. In Dschang, the ^{226}Ra, ^{232}Th, and ^{40}K activity concentrations range from 99 to 167 Bq kg^{-1} and from 98 to 181 Bq kg^{-1} for ^{226}Ra, from 100 to 275 Bq kg^{-1} and from 139 to 309 Bq kg^{-1} for ^{232}Th; and from 198 to 297 Bq kg^{-1} and from 151 to 280 Bq kg^{-1} for ^{40}K. Figure 3.6 shows the box-plot distributions of these concentrations in laboratory (a) and *in situ* (b) for each locality and for the whole study area which a means values of 118±17, 1752 ±46 and 230 ± 28 and 138±19, 231±35 and 237±26 respectively According to Table 3.1, 50% of sampling points have a concentration higher than 151 Bq kg^{-1}, 209 Bq kg^{-1}, and 234 Bq kg^{-1} for ^{226}Ra, ^{232}Th and ^{40}K, respectively, in laboratory measurements. Furthermore, the *in situ* measurements follow a lognormal distribution. Thus, the mean value is represented by the geometric mean, whereas laboratory measurements follow a normal distribution and are represented by the arithmetic mean.

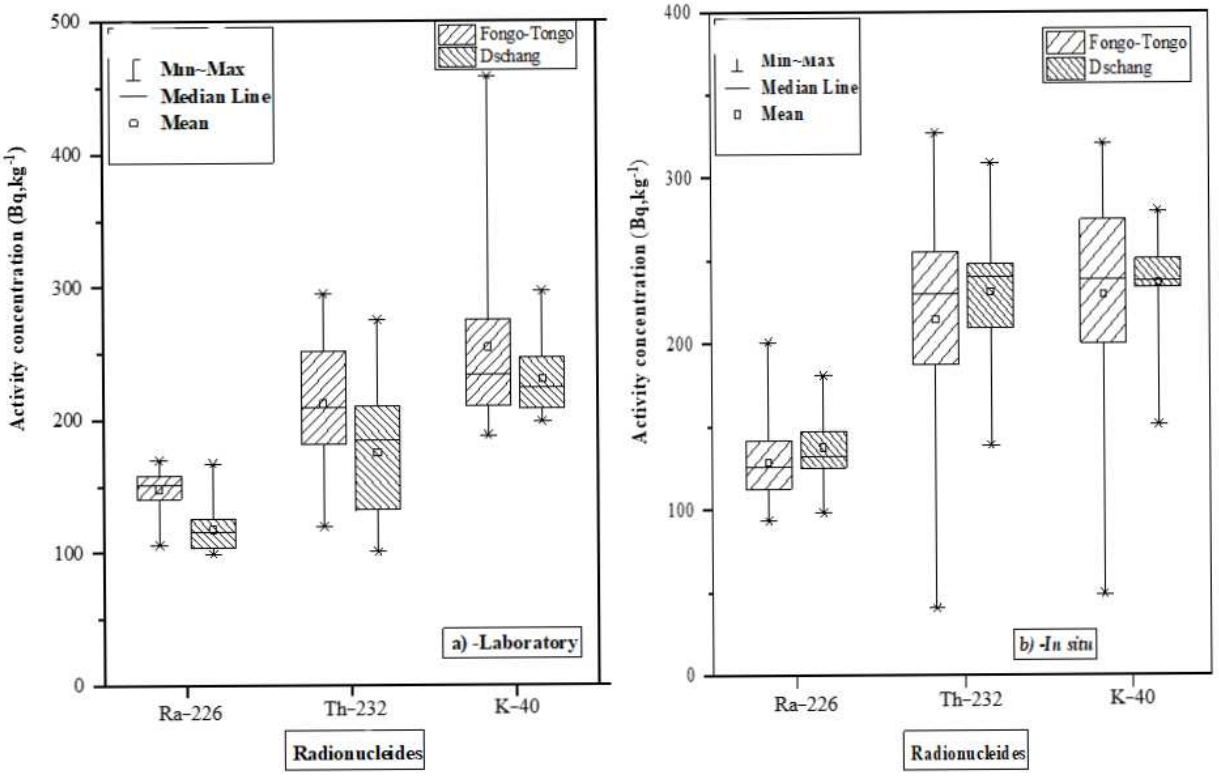

Figure 3.6: Boxplot distribution of activity concentration of ^{226}Ra, ^{232}Th, and ^{40}K obtained by laboratory **(a)** and **(b)** measurements.

In Fongo-Tongo, the activity concentrations of ^{226}Ra, ^{232}Th, and ^{40}K obtained through laboratory and *in situ* methods varied from 106 to 170 Bq kg^{-1} and from 93 to 201 Bq kg^{-1} for ^{226}Ra; from 119 to 295 Bq kg^{-1} and from 40 to 327 Bq kg^{-1} for ^{232}Th; and from 188 to 458 Bq kg^{-1} and from 49 to 321 Bq kg^{-1} for ^{40}K. The mean values were found to be 148±23, 212±54, and 230±28 for ^{226}Ra; and 129±16, 214±67, and 229±54 for ^{232}Th, respectively.

In Dschang, the activity concentrations of ^{226}Ra, ^{232}Th, and ^{40}K ranged from 99 to 167 Bq kg^{-1} and

from 98 to 181 Bq kg^{-1} for ^{226}Ra; from 100 to 275 Bq kg^{-1} and from 139 to 309 Bq kg^{-1} for ^{232}Th; and from 198 to 297 Bq kg^{-1} and from 151 to 280 Bq kg^{-1} for ^{40}K. The mean values were calculated as 118±17, 1752±46, and 230±28 for ^{226}Ra; and 138±19, 231±35, and 237±26 for ^{232}Th, respectively.

Figure 3.6 illustrates the box-plot distributions of these concentrations obtained through laboratory (a) and *in situ* (b) measurements for each locality and for the entire study area.

According to Table 3.1, 50% of the sampling points showed concentrations higher than 151 Bq kg^{-1}, 209 Bq kg^{-1}, and 234 Bq kg^{-1} for ^{226}Ra, ^{232}Th, and ^{40}K, respectively, in laboratory measurements. Additionally, the *in situ* measurements exhibited a lognormal distribution, with the mean value represented by the geometric mean, while laboratory measurements followed a normal distribution and were represented by the arithmetic mean.

Indeed, it is not a comparative study between in situ and laboratory measurements. It is very difficult to compare with a good approximation the results of these two methods. The in situ measurements simply allow us to have a general idea on the veracity of the results of the laboratory measurements. Nevertheless, the results obtained from the two techniques as a whole reveal many similarities at certain points where the two techniques for measuring natural radioactivity were practiced. Some of the differences observed in the results can be explained by the fact that in-situ γ-spectrometry gives a representation of the source concentration on a wide horizontal plane, up to 10 m in radius and 10 cm in depth. In contrast, laboratory ?-spectrometry measures radioactivity in a soil sample collected over an area of 1 m 2 (approximately 70 cm radius). Moreover, the matrix sampled (the soil) is not the same in composition in the two processes: in in-situ γ spectrometry, the sampled soil is generally compact and inhomogeneous, more or less humid, with various rocks, vegetation and debris of all kinds (plants, minerals, etc.). On the other hand, in laboratory γ-spectrometry, the soil matrix is dried, homogeneous, free of any debris and not compact. In addition, it is sieved so that the solid particles that constitute it have approximately the same volume. It is a matrix in which the radioelements it contains have undergone disturbances during sampling and must reach secular equilibrium in order to be able to reveal with the greatest precision, their different activities. If we take into account the uncertainties related to each measurement technique (in-situ, laboratory), the values of the results obtained are approximately the same.

Certainly, this is not a comparative study between in-situ and laboratory measurements. It is challenging to make a precise comparison between the results obtained from these two methods. In-situ measurements provide a broad overview of the accuracy of laboratory measurement. However, overall, the results from both techniques exhibit many similarities, especially in areas where both methods were applied to measure natural radioactivity.

Some differences noted in the results can be attributed to the nature of in-situ γ-spectrometry, which offers a representation of source concentration across a wide horizontal plane, extending up to a radius of 10 m and a depth of 10 cm. In contrast, laboratory γ-spectrometry measures radioactivity in a soil sample collected from a 1 m^2 area (roughly a 70 cm radius).

Furthermore, the composition of the sampled matrix (the soil) differs between the two processes. by in-situ γ spectrometry, the sampled soil is typically compact, heterogeneous, varying in moisture content, and containing various rocks, vegetation, and debris (such as plants and minerals). On the other hand, by laboratory γ-spectrometry, the soil matrix is dried, homogeneous, free of debris, and uncompressed. It undergoes sieving to ensure that the solid particles it contains have roughly the same volume. This matrix undergoes disturbances during sampling, and the radioelements within it must achieve secular equilibrium to accurately reveal their activities.

Soil samples analyzed in the laboratory have high concentrations of ^{226}Ra and ^{232}Th. As presented in Table 3.1.1, the minimum and maximum values of ^{226}Ra obtained in laboratory and *in situ* measurements are, respectively, three and five times higher than the world average value of 35 Bq kg^{-1} [1]. In the case of ^{232}Th, they are two and four times higher than the world average value of 45 Bq kg^{-1}, respectively [1]. These high values of ^{226}Ra and ^{232}Th activity concentrations are also observed for the results obtained by *in situ* γ spectrometry. The minimum values of ^{226}Ra and ^{232}Th are, respectively, three and two times higher than the world average value, while the maximum values are, respectively, six and seven times higher than the world average value [1]. Furthermore, the average values of ^{40}K, as well as the maximum values for *in situ* and laboratory methods, are lower than 420 Bq kg^{-1}, the world average value [1].

Figure 2.2 shows that the investigated area extends over a geological structure covered by basaltic and trachytic granitic rocks [72, 122]. ^{226}Ra, ^{232}Th, and ^{40}K activity concentrations differ from one point to another for the two techniques used: *in situ* and laboratory gamma spectrometry. This can be explained by the fact that radioactivity is not uniformly distributed in soil [42]. It is reported that ^{238}U, ^{232}Th, and ^{40}K have high concentrations in some rocks, such as syenite, granite, granulite, rhyolites, and plutonic [4, 5, 42]. The low concentrations of ^{40}K can be explained by the phenomenon of leaching and transport of potassium elements to the surface due to the effects of erosion, drainage, and an accumulation of sediments in the seabed [123, 124]. The transfer of ores by erosion or by eruptive voice can therefore considerably modify the content and concentrations of this radionuclide in soil [125]. It has low concentrations in basalt [4, 5, 42]. According to Figure 2.2, the presence of the above rocks can account for considerable variation in the concentrations of these primordial radionuclides from one site to another, as shown in Figure 3.6. In addition, the soil of Fongo-Tongo may be more compact and moister than that in Dschang [122, 126]. In addition, Table 3.2 shows that activity concentrations of the primordial radionuclides in soil in Cameroon are higher than those in some other regions of the world [122–125]. Nevertheless, ^{40}K concentrations are also high elsewhere than in the present study [128, 131].

The laboratory analysis of soil samples reveals significantly elevated concentrations of ^{226}Ra and ^{232}Th. Table 3.1.1 demonstrates that the minimum and maximum values of ^{226}Ra from laboratory and in-situ measurements are respectively three and five times higher than the global average of 35 Bq kg^{-1} [1]. Similarly, for ^{232}Th, these values are two and four times higher than the global average of 45 Bq kg^{-1} [1]. These heightened concentrations of ^{226}Ra and ^{232}Th are also evident in the results obtained via in-situ γ spectrom-

etry. The minimum values for ^{226}Ra and ^{232}Th are respectively three and two times higher than the global average, while the maximum values are six and seven times higher than the global average [1]. Moreover, the average values of ^{40}K, as well as the maximum values for both in-situ and laboratory methods, are below 420 Bq kg^{-1}, the global average value [1].

Figure 2.2 illustrates that the surveyed area encompasses a geological structure with basaltic and trachytic granitic rock coverings [72, 122]. Activity concentrations of ^{226}Ra, ^{232}Th, and ^{40}K vary across different points for both in-situ and laboratory gamma spectrometry techniques. This variability can be attributed to the non-uniform distribution of radioactivity in soil [42]. It is noted that rocks such as syenite, granite, granulite, rhyolites, and plutonic contain high concentrations of ^{238}U, ^{232}Th, and ^{40}K [4, 5, 42]. The lower concentrations of ^{40}K can be explained by leaching and transport of potassium elements due to erosion effects, drainage, and sediment accumulation in seabeds [123, 124]. Erosion or volcanic activity-induced transfer of ores significantly alters the content and concentrations of this radionuclide in soil, with basalt showing lower concentrations [4, 5, 42]. The presence of these rocks contributes to considerable variation in the concentrations of primordial radionuclides across different sites, as shown in Figure 3.6. Additionally, the soil in Fongo-Tongo may exhibit higher compactness and moisture levels compared to that in Dschang [122, 126]. Table 3.2 highlights that primordial radionuclide activity concentrations in Cameroonian soil exceed those in some other global regions [122-125]. However, elevated ^{40}K concentrations are observed elsewhere outside of this study area as well [128, 131].

Radon concentrations were assessed in soil near dwellings using RADTRAK^{2}® detectors and soil sampling points. The measured soil concentrations were utilized to categorize sites with high radon potential or to pinpoint areas with potential high risk following Swedish risk classification criteria [124]. ^{222}Rn concentrations within dwellings in our study were measured in two phases using different detector types. The initial phase employed RADTRAK^{2}® and RadonEye+^{2} detectors during the dry season, specifically between December and February. Subsequently, the second phase utilized RADUET detectors and thoron progeny monitors during the rainy season, particularly from July to September. The dwellings in this study were characterized by either one front door and one window or two doors with multiple windows. Detectors were positioned 80 cm away from walls and at a height of 150 cm from the floor, suspended from the ceiling of the dwellings.

Furthermore, radon concentrations obtained within dwellings were analyzed, interpreted, and discussed in accordance with international reference values, site-specific geological and environmental parameters, and comparisons with previous studies.

The ^{222}Rn concentrations at a depth of 1 m in soil, as presented in Table 3.3, ranged from 35 to 202 kBq m^{-3} in Fongo-Tongo, with a mean value of 69 $\pm$ 40 kBq m^{-3}. In Dschang, the concentrations ranged from 48 to 255 kBq m^{-3}, with a mean value of 82 $\pm$ 56 kBq m^{-3}. More than half of the sampled points in Dschang exhibited ^{222}Rn concentrations in soil greater than or equal to 62 kBq m^{-3}, while in Fongo-Tongo, this threshold was 53 kBq m^{-3}. As depicted in Figure 3.2, a majority of radon concentrations in soil surpassed

the 40 kBq m^{-3} threshold, denoted by the red line, which is considered the limit for high radon-exposure risk according to Swedish risk assessment criteria [124]. The variation in ^{222}Rn concentrations across different locations may stem from differences in geological structure and the mineralogical composition of the soil [42, 123]. The geological structure, geochemical processes of the soil, and gas emanation rates in the region are influenced by soil permeability [42, 72, 74, 122, 125]. Table 3.3 indicates that the average and maximum values of ^{222}Rn in soil in Dschang exceed those in Fongo-Tongo, unlike the ^{226}Ra values obtained in these two localities. This discrepancy could be attributed to variations in soil moisture and porosity.

The concentrations of ^{222}Rn in soil served as a basis for evaluating radon concentrations at the Earth's surface. The data, outlined in Table 3.4, are crucial as radon diffuses from the ground into the atmosphere, where it quickly dilutes with ambient air. Subsequently, it migrates through convection into homes, where it can accumulate to significant levels and pose carcinogenic risks to the respiratory tract [7]. Therefore, to safeguard the population from ^{222}Rn exposure, it is imperative to analyze ^{222}Rn levels in all potential sources, including soil, water, food, and building materials. This comprehensive analysis is vital for devising action plans that identify areas prone to generating high indoor ^{222}Rn levels, known as ^{222}Rn risk areas.

Table 3.4 presents the assessment of geogenic ^{222}Rn potential values derived from ^{222}Rn concentrations and soil permeability, categorized as k= 10^{-11} m s^{-1}, k= 10^{-12} m s^{-1}, and k=10^{-13} m s^{-1} [105]. According to the Czech Republic's classification of regions with ^{222}Rn potential in soil, 100%, 26.7%, and 13.3% of measurement points exhibit a ^{222}Rn index with a **GRP** (geogenic radon potential) exceeding 35 for permeability values of k= 10^{-11} m s^{-1}, k= 10^{-12} m s^{-1}, and k=10^{-13} m s^{-1}, respectively. The distribution of sampling points suggests that the region can be classified as a moderate ^{222}Rn risk area, with the **GRP** increasing with soil permeability. This underscores the importance of permeability as a critical parameter in determining the mobility of ^{222}Rn in soil [103]. Indeed, high permeability in soil can lead to significant diffusion of ^{222}Rn into the atmosphere, a factor heavily influenced by the geological characteristics of the area [106, 137].

Indoor ^{222}Rn levels were assessed in 50 dwellings across the study area, comprising 30 in Dschang and 20 in Fongo-Tongo. The main results are summarized in Table 3.5, revealing a range of indoor ^{222}Rn concentrations from 85 Bq m^{-3} to 410 Bq m^{-3}, with a mean value of 152 $\pm$ 26 Bq m^{-3}. Specifically, indoor ^{222}Rn levels in Dschang and Fongo-Tongo varied from 85 to 250 Bq m^{-3} and from 98 to 410 Bq m^{-3}, with mean values of 144 $\pm$ 24 and 166 $\pm$ 31 Bq m^{-3}, respectively. The study underscores that the average ^{222}Rn concentration in these regions exceeds the global average value of 30 Bq m^{-3} [1].

The elevated levels of indoor ^{222}Rn can be attributed to the architectural style of these dwellings, primarily constructed with mud bricks. The emanation of ^{222}Rn from these building materials likely contributes to the increased indoor ^{222}Rn levels. Particularly, in earthen houses where walls and floors lack cement covering, high ^{222}Rn concentrations are observed. This is due to radon gas, trapped in the earth constituting the building material, diffusing easily and accumulating in poorly ventilated houses.

Moreover, the persistently cold and damp climate of the region compels inhabitants to keep their dwelling

openings closed, reducing air exchange between the indoors and outdoors and further enhancing ^{222}Rn gas accumulation [140]. Additionally, most monitored dwellings lack ground waterproofing, allowing ^{222}Rn to emanate from the ground without attenuation. The substantial ^{222}Rn concentrations and variations observed among dwellings and sites are closely tied to geological structure, ventilation conditions, atmospheric and climatic factors, architectural design, and residents' lifestyle [142]. Therefore, soils rich in uranium are also enriched in radium and radon. Porous and permeable soils, such as those found in the bauxite zones of Fongo-Tongo, facilitate the diffusion and migration of radon to the surface. Previous studies conducted in this area have revealed elevated concentrations of ^{226}Ra and ^{222}Rn in soil [146]. These studies also indicate a correlation between ^{226}Ra and ^{222}Rn concentrations in soil. During the measurement period, the population was actively engaged in fieldwork daily and typically kept their homes closed, leading to the accumulation of gas indoors [16, 20, 110]. Thus, the high concentrations observed in this study can be attributed to the various geological, climatic, and anthropological factors mentioned above. Table 3.6 compares the measured ^{222}Rn concentrations in this study with those reported in previous research. The maximum levels observed here are two to three times lower than the highest values reported in other studies [17, 147-149]. Indeed, these references cite maximum ^{222}Rn levels higher than those observed in the study areas but within the range of 400 to 600 Bq m^{-3} [17, 150, 151].

Figures 3.4 and 3.5 illustrate the frequency distribution of ^{222}Rn, ^{220}Rn, radon progeny, and thoron progeny concentrations in selected dwellings within the Fongo-Tongo bauxite area. Measurements at the site revealed an asymmetric distribution, primarily due to the prevalence of low concentration values in many dwellings compared to the fewer instances of high concentrations. As a result, the extreme high values significantly impact the arithmetic mean of such a distribution. This distribution pattern was expected, given that it reflects the outcomes of short-term (spot) sampling.

As outlined in Table 3.7, ^{222}Rn concentrations measured with RADUETS varied between 31 and 123 Bq m^{-3}, with an arithmetic mean of 64 $\pm$ 24 Bq m^{-3} and a geometric mean of 60 $\pm$ Bq m^{-3}. These values fall below the 300 Bq m^{-3} reference value recommended by the **ICRP** [114] and the **IAEA** [82]. However, they are lower than the 148 Bq m^{-3} threshold recommended by the United States Environmental Protection Agency [153] and the intervention threshold of 200 Bq m^{-3} prescribed in many **EU** countries [154]. Specifically, only 12% of the 50 monitored dwellings had radon concentrations exceeding the **WHO** recommended value of 100 Bq m^{-3}, with 88% recording concentrations below this threshold [7].

Moreover, ^{220}Rn concentrations range from 36 to 688 Bq m^{-3}, with an arithmetic mean of 300 $\pm$ 180 Bq m^{-3} and a geometric mean of 242 $\pm$ 21 Bq m^{-3}. These concentrations exceed 100 Bq m^{-3} in 88% of dwellings, with 23% having concentrations greater than 300 Bq m^{-3}. However, it's important to note that there is no significant correlation between ^{222}Rn and ^{220}Rn concentrations in homes. Additionally, it should be noted that the reference level of 100 Bq m^{-3} is only applicable to ^{222}Rn; no reference value has been established yet for ^{220}Rn.

Nevertheless, more than half of the dwellings (65%) have ^{220}Rn concentrations above 100 Bq m^{-3},

which is 17 times higher than the world average value of 10 Bq m^{-3} [113]. All of these dwellings surpassed the world average value for ^{220}Rn concentration. Establishing an action level for ^{220}Rn is now of fundamental urgency.

Table 3.7: Statistical summary of ^{222}Rn, ^{220}Rn and their progeny concentrations in dwellings.

Statistical parameters	^{222}Rn	EERC	^{220}Rn	EETC
AM	64	26	300	9
SD	24	10	180	5
GM	60	24	242	8
GSD	14	2	21	2
Median	56	23	284	8
Range	31-123	12-49	36-688	1-22

EETCs were primarily determined through direct measurements using thoron progeny monitors deployed at the site. It is noteworthy that all dwellings (100%) had concentrations higher than the world average value of 0.5 Bq m^{-3} [113]. The measured results ranged from 1 to 22 Bq m^{-3}, with an arithmetic mean of 9 $\pm$ 5 Bq m^{-3} and a geometric mean of 8 $\pm$ 2 Bq m^{-3}. These mean values are approximately 18 and 16 times higher than the world mean value mentioned earlier. Although the arithmetic, geometric mean, and maximum concentration are relatively high, the maximum value does not significantly deviate from other values in the distribution.

About 50% of dwellings have EETC values higher than the median value of 8 Bq m^{-3}; 43% of dwellings recorded EETC values above 10 Bq m^{-3}, with 2% exceeding 20 Bq m^{-3}. The mean values of the EERC, estimated at 26 $\pm$ 10 Bq m^{-3} (arithmetic mean) and 24 $\pm$ 2 Bq m^{-3} (geometric mean), are almost twice as high as the world mean value of 15 Bq m^{-3} [113]. Remarkably, 92% of the houses investigated had EERC values higher than the world average value, with no house exceeding 100 Bq m^{-3}.

The sampling results in this study follow a lognormal distribution characterized by the geometric mean (GM) and geometric standard deviation (GSD). However, the scattered data points could be attributed to the considerable distance between measurement points, diverse building materials, geological variations in the building site, architectural differences, and varying lifestyles among residents. Some dwellings also had windows that were regularly closed or non-existent during the study period.

3.2.5 Daily variations of indoor ^{222}Rn concentration

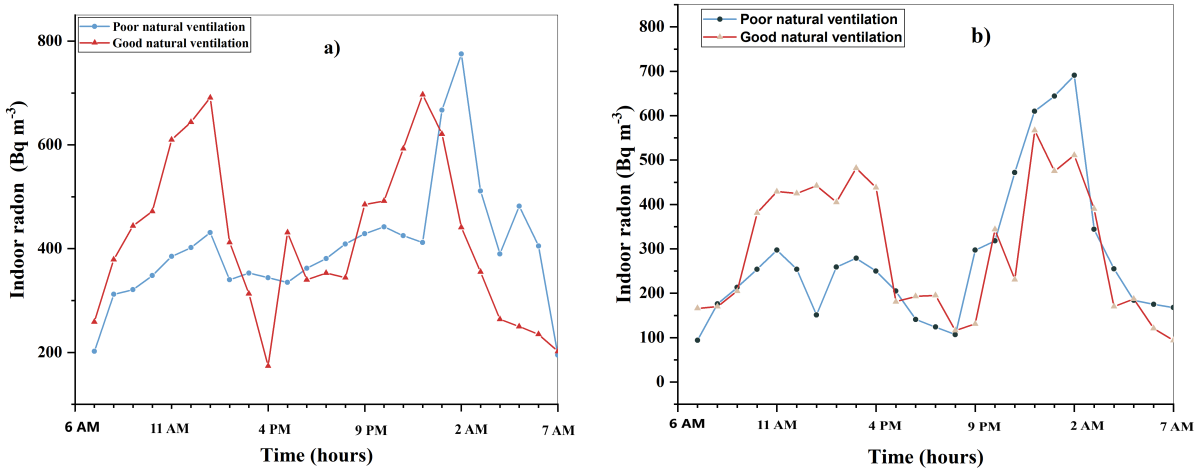

Figure 3.7: Daily dynamic variation of ^{222}Rn concentrations in some dwellings: in soil and bare ground **(a)**, in soil and concrete ground **(b)**. The graphs in red and blue represent the state of well-ventilated and poorly ventilated dwellings respectively.

It has been observed that indoor ^{222}Rn concentrations exhibit seasonal variations [155]. However, there is also evidence indicating that indoor ^{222}Rn levels fluctuate throughout the day, depending on the rate of air exchange between indoor and outdoor environments. Figure 3.7 illustrates the daily dynamic variations of indoor ^{222}Rn concentrations in various monitored dwellings within the area. These dwellings were selected based on specific construction characteristics and are represented by different colors in the figure. Interestingly, the nature of the different dwelling types appears to have little significant influence on indoor ^{222}Rn concentrations in this study, a finding consistent with previous research [23]. However, in dwellings with effective natural air circulation systems, the ^{222}Rn concentration levels notably decrease across various architectural types. These findings underscore the influence of natural ventilation systems and daily occupancy patterns on the accumulation of ^{222}Rn gas indoors originating from the soil. Nevertheless, the observed differences are likely related to the tightness of the floor, which can reduce the rate of gas emanation in certain dwellings. Regardless, variations in indoor ^{222}Rn levels were monitored at one-hour intervals over a period of approximately twenty-four hours. It was noted that indoor ^{222}Rn accumulation reached significant peaks during nighttime and even during the day when occupants were indoors with doors and windows completely closed, resulting in reduced ventilation and greater gas accumulation [6]. Figure 3.8 illustrates that indoor ^{222}Rn accumulation significantly decreases in dwellings with cemented walls and concrete floors, which effectively reduce radon exhalation from the ground surfaces of the houses.

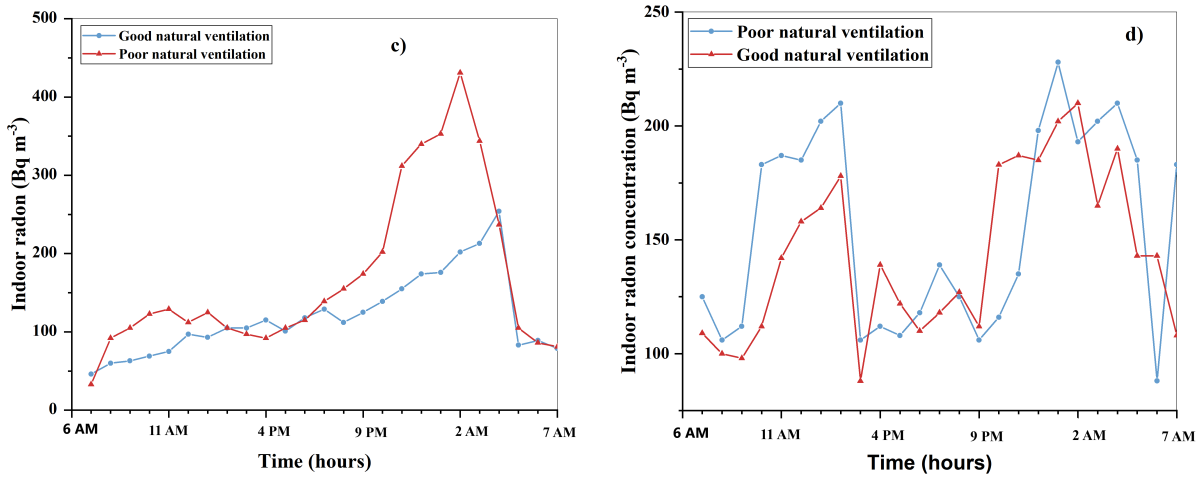

Figure 3.8: Daily dynamics variation of ^{222}Rn concentrations in some dwellings: cemented walls and bare soil **(c)**; cemented walls and concrete soil **(d)**. The graphs in red and blue represent the state of well-ventilated and poorly ventilated dwellings respectively.

3.2.6 Equilibrium factor (F_{Tn}) between ^{220}Rn and its progeny

According to **UNSCEAR**, the F_{Tn} is estimated to 0.02 [113]. Table 3.7 shows that F_{Tn} varies considerably from one house to another. The values ranged from 0.01 to 0.15 with an arithmetic mean of 0.04, and a geometric mean of 0.03; respectively 2 and 1.5 times higher than **UNSCEAR** value. The. Figure 3.9 gives the probability of F_{Tn}. This is a log normal correlation between thoron and its associated progeny. This correlation is ($R^2 = 0.5$).

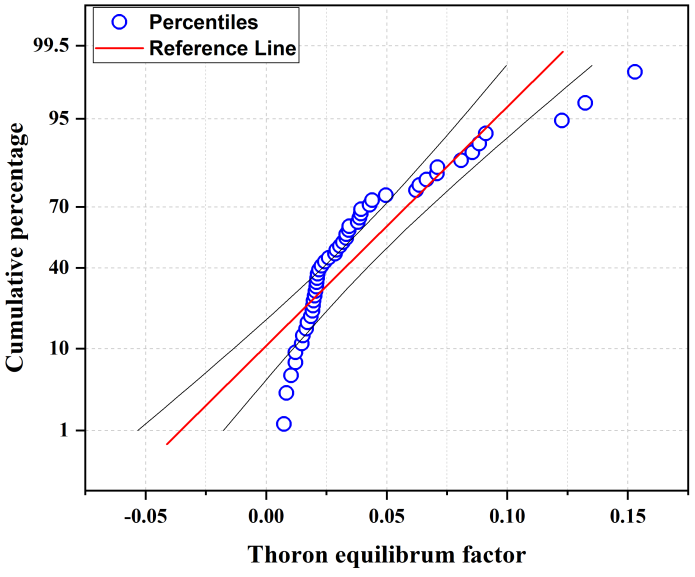

Figure 3.9: Normal probability plot of F_{Tn}. $\mu = 0.04095$ $\sigma = 0.03286$.

3.3 Seasonal variations of in indoor ^{222}Rn, ^{220}Rn and their progeny concentrations: Uncertainties on their measurements

In the current study, the maximum concentrations of ^{222}Rn and ^{220}Rn are notably elevated, significantly deviating from the rest of the distribution. Consequently, it is advisable to conduct additional measurements at these specific points to enhance the accuracy of risk assessments for residents. These high values introduce considerable uncertainty into the mean concentration estimation for the study area.

Table 3.8 illustrates the seasonal variations in radon concentrations, revealing a significant disparity between levels during different seasons. Specifically, radon levels are higher during the rainy season compared to the dry season. This phenomenon can be attributed to the cold weather during rainy periods, leading to prolonged closure of dwellings, which in turn promotes the accumulation of ^{222}Rn and occasionally results in very high concentrations.

Table 3.8: Saisnnal variation of indoor ^{222}Rn concentration in dwellings of the whole study area.

Parameters	Dry season	Rainy season	Ratio (Rainy/Dry)
AM	64	162	2.53
SD	24	26	1.08
GM	60	152	2.53
GSD	14	26	1.86
Median	56	140	2.5
Range	31-123	85-410	–

The methods and instruments used to measure ^{222}Rn, ^{220}Rn, and their progeny in this study have limitations inherent to experimental techniques. These limitations are highlighted by the observed uncertainty values in some results. The RADTRAK^{2}®, RADUET, and thoron progeny monitors are examples of solid-state nuclear track detectors (SSNTD). These detectors expose solid material samples to nuclear radiation, followed by etching and microscopic examination. The uncertainties mainly arise from the aging of the detectors and their exposure to solar radiation, heat, and humidity during measurements.

It's important to understand that direct comparisons between different types of detectors are not appropriate here. Differences in the distributions of ^{222}Rn concentrations in dwellings could be due to seasonal variations during measurements, influenced by climate fluctuations from year to year.

Furthermore, when validating with the RADUET detector in dwellings that showed concentration peaks during RADTRAK^{2} measurements, significantly higher thoron concentrations compared to radon were found. This suggests that RADTRAK^{2} detectors may be sensitive to thoron. While it would have been ideal to use the same type of detector throughout, the absence of RADTRAK detectors complicated this.

However, the RADUET detector allowed simultaneous measurement of radon and thoron, highlighting the Fongo-Tongo region as a thoron risk zone.

Moreover, fluctuations in ^{220}Rn and its progeny concentrations within a dwelling can vary over time and space, affecting calculations such as the equilibrium factor (FTn). Deploying detectors in dwellings for extended periods relies heavily on residents' cooperation to ensure reliable measurements. Mishandling of detectors by residents, such as exposure to heat or moisture, can introduce biases into the results. Additionally, uncertainties in various results can also be influenced by detector placement and specific dwelling characteristics.

The various methods and instruments utilized in this study to measure ^{222}Rn, ^{220}Rn, and their associated progeny have inherent limitations, as is common with experimental techniques. The observed uncertainty values in certain results underscore these limitations. The RADTRAK^{2}®, RADUET, and thoron progeny monitors are examples of solid-state nuclear track detectors (SSNTD). These detectors involve exposing solid material samples to nuclear radiation, followed by etching and microscopic examination. The uncertainties arise primarily from the aging effect of the detectors, direct exposure to solar radiation, heat, and humidity during measurements [156].

It's important to note that direct comparisons between different types of detectors are not suitable in this context. The differences observed in the distributions of ^{222}Rn concentrations in dwellings may stem from seasonal variations during the measurement periods. Climate fluctuations from year to year can impact the rate of radon exhalation, as discussed later.

Additionally, a validation check with the RADUET detector in dwellings that exhibited concentration peaks during RADTRAK^{2} measurements revealed significantly higher thoron concentrations compared to radon. This observation suggests that RADTRAK^{2} detectors might be sensitive to thoron. Ideally, this validation check should have been performed using the same type of detector throughout, but the absence of RADTRAK detectors hindered this process. Nonetheless, the RADUET detector enabled simultaneous measurement of radon and thoron, highlighting the Fongo-Tongo region as a thoron risk zone.

Furthermore, fluctuations in ^{220}Rn and its progeny concentrations within a dwelling can vary over time and space, leading to uncertainties that influence calculations such as the equilibrium factor (FTn). Deploying detectors in dwellings for extended periods, beyond the practitioner's direct control, relies heavily on residents' cooperation and common sense to ensure reliable measurements. Any mishandling of detectors by residents, such as scraping, exposure to heat, or moisture, in the absence of practitioners, can introduce biases into the measurement results. Apart from handling differences and laboratory treatments, uncertainties observed in various results (FTn, CTn, CRn, EETC) in this study can also be attributed to detector placement and specific dwelling characteristics.

3.4 Correlations between radionuclides activity concentrations

3.4.1 Correlation between ^{222}Rn and ^{226}Ra in Soil

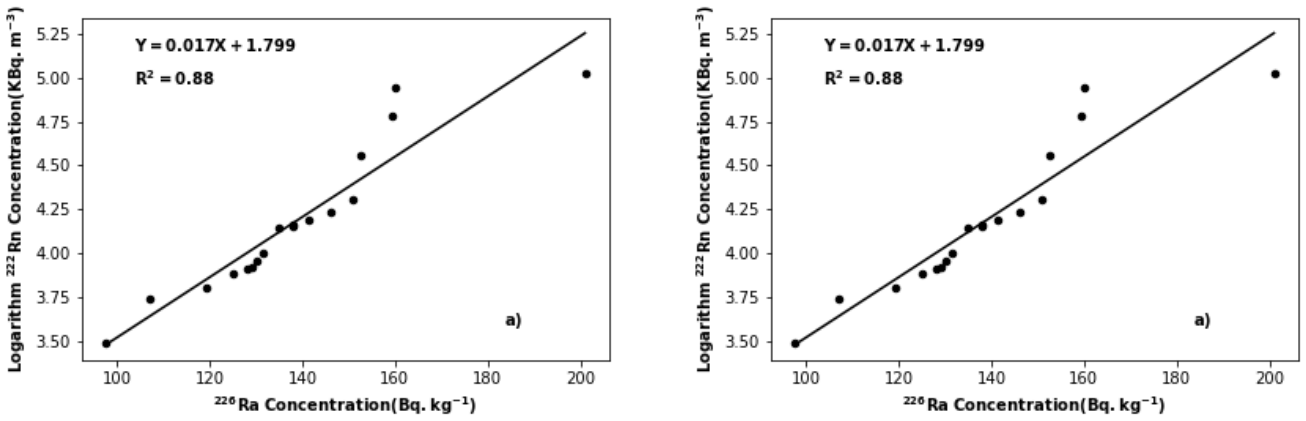

Figure 3.10: Correlation between ^{222}Rn and ^{226}Ra concentrations in soil: (a) laboratory γ-ray spectrometry and (b) *in situ* γ-ray spectrometry.

According to Figure 3.10, there is a direct correlation between ^{222}Rn concentrations in soil and the measured levels of ^{226}Ra, both at the site and in soil samples from the area. The correlation coefficients R^2 = 0.88 for the laboratory method and R^2 = 0.86 for the in situ method indicate a strong relationship between ^{222}Rn and ^{226}Ra concentrations. Similarly, the Pearson correlation coefficients of 0.92 for the laboratory and 0.90 for in situ measurements confirm this strong correlation.

In Figure 3.10-a and 3.10-b, for values ranging from 110 to 150 Bq kg^{-1} and 130 to 160 Bq kg^{-1} respectively, the residuals remain relatively constant, with a slight increase for extreme values. This dispersion of maximum values from the median is attributed to the limited number of samples, affecting the density of the scatter plot and the accuracy of regression. In essence, closer values in the datasets result in a stronger correlation coefficient and intensity, indicating a more reliable regression and a stronger correlation between the two radionuclides when standard deviation between data is minimized.

The elevated levels of ^{222}Rn concentration in soil gas at certain locations likely stem from deep-seated sources within permeable soil. This allows ^{222}Rn to easily escape from its parent, ^{226}Ra, and migrate to the soil surface. Put simply, the heightened emanation of ^{222}Rn at specific measurement points correlates closely with underlying rock types, geochemical processes, physicochemical soil properties, and the presence of ^{226}Ra in the soil. This correlation is heavily influenced by the geological structure of the area [157], a trend supported by previous studies [118, 158].

As depicted in Figure 2.2, the study area comprises diverse rock formations like granite, basalt, gneiss, and trachyte, along with deposits of bauxite ores [72, 73]. Granite, extracted from quarries in Dschang and Fongo-Tongo, likely serves as a significant source of distributed ^{226}Ra in the region, given its known high

uranium, thorium, and potassium content at elevated temperatures within these rocks [42]. Consequently, areas underlain by granitic bedrock may exhibit stronger ^{222}Rn emanation.

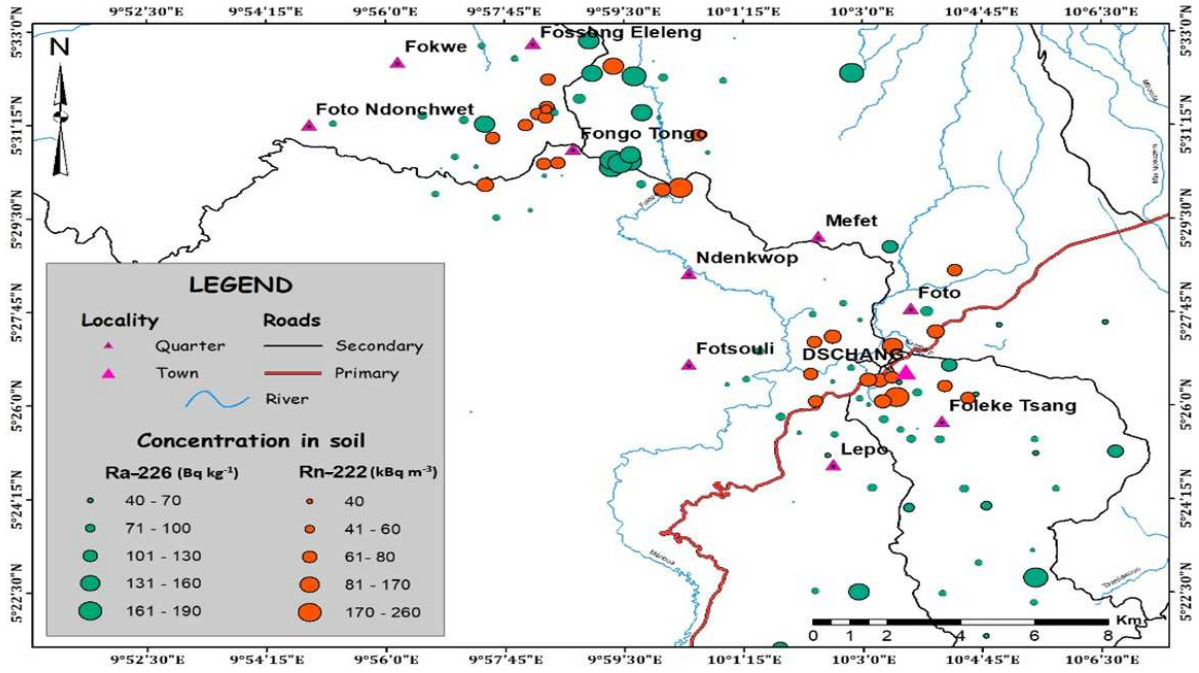

Figure 3.11: Map distribution of ^{222}Rn and ^{226}Ra concentrations in soil of the study area.

Figure 3.11 illustrates the distribution map of ^{222}Rn and ^{226}Ra activity concentrations in the study area, showcasing the increasing activity concentration of ^{226}Ra in soil with higher proximity to ^{222}Rn concentrations.

3.4.2 Study of Correlations Between ^{222}Rn Gas in Soil and ^{222}Rn in Dwellings

The correlation between ^{222}Rn concentrations in dwellings and soil gas was investigated based on dwelling architecture and natural ventilation systems. Monitored dwellings were either constructed with bare earth bricks, partially covered with cement, or entirely cemented, with varying floor types. Although ventilation parameters were not directly measured, factors allowing good air circulation, such as open windows and doors, were considered. Figures 3.12 and 3.13 display the linear regression lines and correlation coefficients for the examined cases.

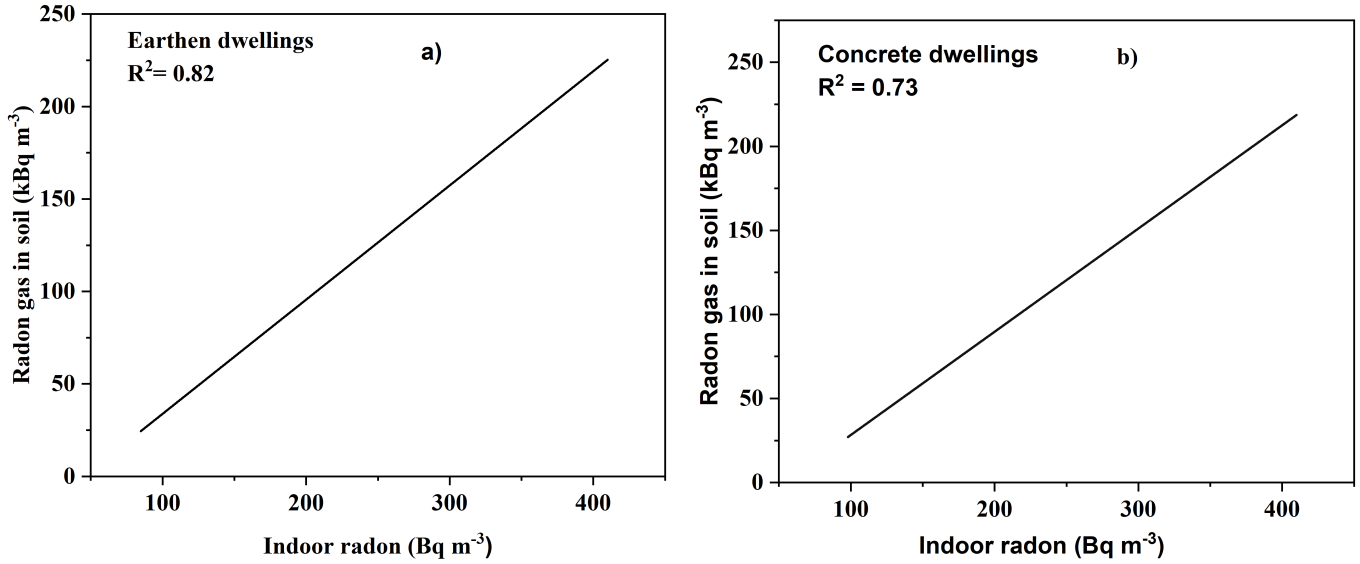

Figure 3.12: Correlation between ^{222}Rn gas in soil and its concentrations in dwellings with poor natural ventilation: earthen (a) and concrete (b).

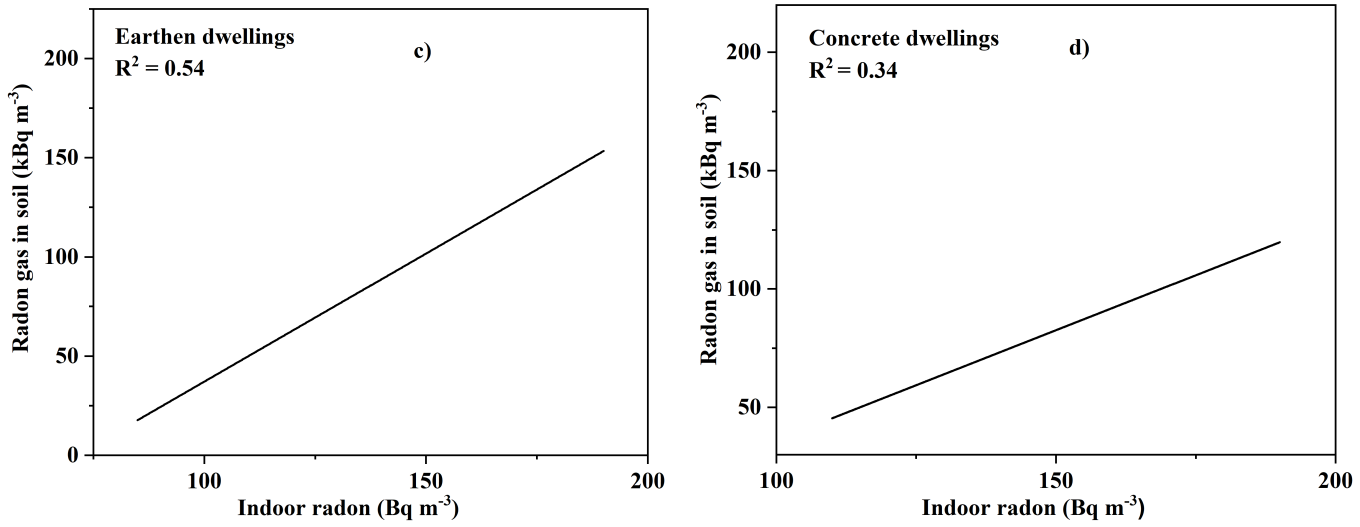

Figure 3.13: Correlation between ^{222}Rn gas in soil and its concentrations in dwellings with the best natural ventilation: earthen (c) and concrete (d).

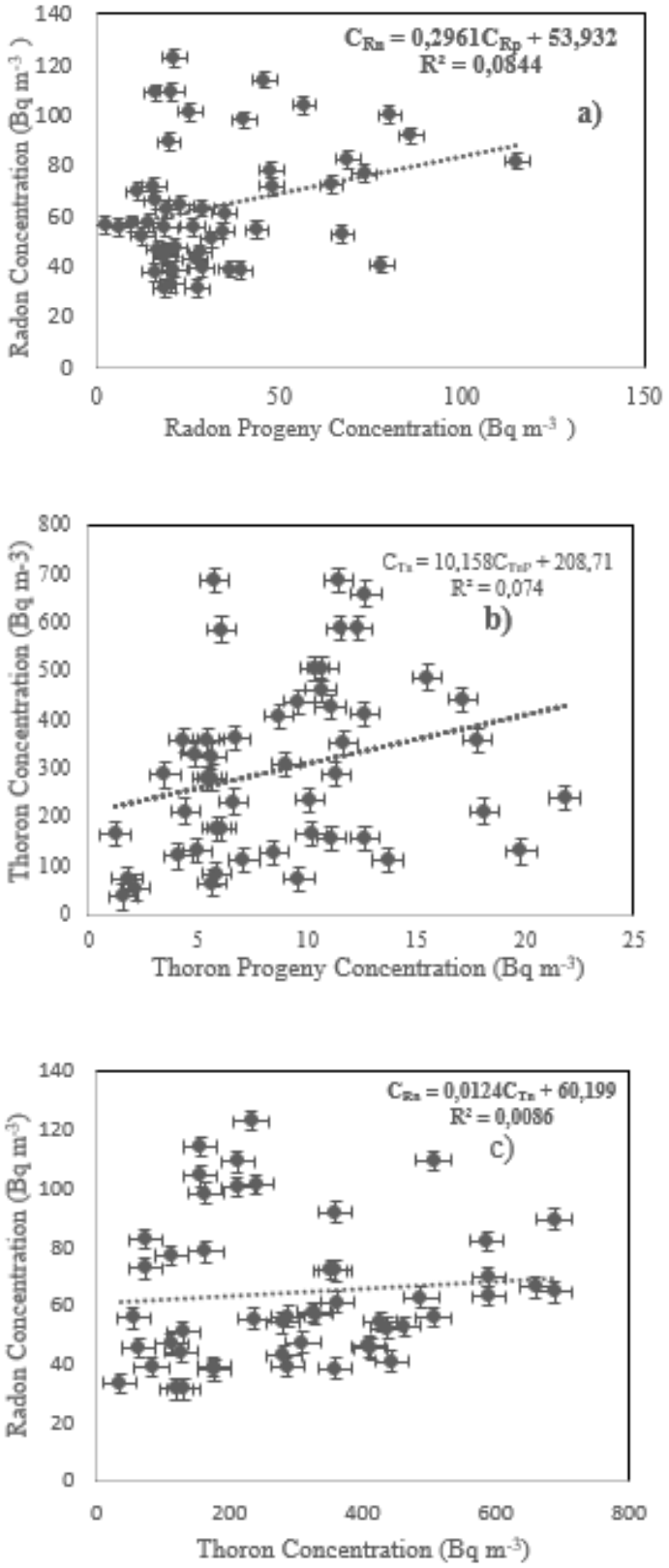

Figure 3.14: Correlation between radon and its progeny a), thoron and its progeny b) and between radon and thoron concentrations c)

Figure 3.12 depicts the correlation between ^{222}Rn gas in soil and concentrations in earthen dwellings (Figure 3.12-a) and cemented dwellings (Figure 3.12-b). The respective correlation coefficients were R^2 = 0.82 and R^2 = 0.73, indicating a stronger correlation in earthen dwellings. This robust correlation suggests that measuring ^{222}Rn gas in soil could predict concentrations in dwellings [139]. In earthen dwellings, high levels of ^{222}Rn from unpoured soil and uncemented walls are likely due to their porosity. Conversely, cemented walls and floors attenuate ^{222}Rn diffusion, resulting in a lower correlation coefficient.

Similarly, Figure 3.13 displays the correlation between ^{222}Rn gas in soil and concentrations in earthen (Figure 3.13-a) and cemented dwellings (Figure 3.13-b) with excellent natural ventilation. The correlation coefficients were R^2 = 0.54 and R^2 = 0.34, respectively, indicating a weaker correlation in cemented dwellings. This is likely due to building materials like cinder blocks and cement, which significantly reduce ^{222}Rn diffusion, leading to lower correlation coefficients.

Furthermore, Figure 3.14 shows correlations between radon, its progeny, thoron, and its progeny, as well as between radon and thoron concentrations. Weak positive correlations were observed with correlation coefficients of 0.084 (radon-radon progeny), 0.074 (thoron-thoron progeny), and 0.086 (radon-thoron concentrations). The analysis indicated that all four concentrations are independent, suggesting it's more practical to measure each concentration individually rather than using one to estimate the others.

Numerous studies have shown that high ^{222}Rn levels in dwellings can be attributed to factors such as architecture and geological parameters like rock type, soil porosity, and permeability [16, 17, 20, 151]. Soil rich in uranium or radium plays a crucial role in influencing ^{222}Rn levels indoors, while soil permeability indicates the potential for ^{222}Rn diffusion from subsurface to surface [24, 118, 159]. Therefore, poorly ventilated homes on sites with these characteristics can exhibit significantly elevated ^{222}Rn concentrations if the soil is not concreted and the walls are not cemented.

3.5 Dose assessment

3.5.1 Ambien Equivalent Dose Rate (AEDR) and Annual External Effective Dose (AEED)

To estimate the radiological impact of radiation from natural radioactivity in the area, several parameters were determined. These include the absorbed dose rate in air at one meter from the ground surface, the annual effective doses by external irradiation and inhalation, the radioactivity indices and the probability of ELCR (Excess Life time Cancer Risk) and LEAR (Lifetime Excess Absolute Risk).

The AEED obtained in the laboratory ranged from 0.58 to 1.62 mSv y^{-1}, with a mean value of 1.27 $\pm$ 0.27 mSv y^{-1}, in Fongo-Tongo; and from 0.73 to 1.46 mSv y^{-1}, with a mean value of 1.05 $\pm$ 0.17 mSv y^{-1}, in the Dschang locality. According to Table 3.9 the average values for the whole study area are above the safety limit of 1.00 mSv y^{-1} [1]. According to Table 3.10, the AEDR at one meter above ground surface

Table 3.9: Summary of the different radiological parameters obtained in laboratory.

Locality	Fongo-Tongo				Dschang						
Parameters	Min	Max	Med	AM SD	Min	Max	Med	AM	SD	Limit	
AEDR (nGy y^{-1})	130	265	211	207	37	119	238	172	170	31	1
AEED (mSv)	0.8	1.62	1.29	1.27	0.22	0.73	1.46	1.05	1.04	0.19	1
$ELCR_{in}$	1.68	3.4	2.71	2.67	0.47	1.53	3.06	2.21	2.18	0.4	
$ELCR_{out}$	1.12	2.26	1.81	1.78	0.31	1.02	2.04	1.47	1.46	0.27	
ELCR	2.59	5.66	4.52	4.44	0.78	2.55	5.11	3.69	3.64	0.66	1

ranged from 130 to 265 nGy h^{-1} and from 119 to 238 nGy h^{-1} at Fongo-Tongo and Dschang, respectively, with an average of 207 $\pm$ 37 nGy h^{-1} and 170 $\pm$ 31 nGy h^{-1} for soil samples analyzed in the laboratory. It ranged from 95 to 264 nGy h^{-1} and from 69 to 126 nGy h^{-1}, with a mean value of 198 $\pm$ 45 nGy h^{-1} and 96 $\pm$ 14 nGy h^{-1}, for the *in situ* measurement in Fongo-Tongo and Dschang, respectively. The mean values of the current studies are all above the value set of 60 nGy h^{-1} [1].

Table 3.10: Summary of the different radiological parameters obtained by *in situ.*

Locality	Fongo-Tongo					Dschang					
Parameters	Min	Max	Med	AM	SD	Min	Max	Med	AM	SD	Limit
AEDR (nGy y^{-1})	95	264	210	198	45	69	126	94	96	14	1
AEED (mSv)	0.58	1.62	1.27	1.22	0.28	0.42	0.77	0.58	0.59	0.08	1
$ELCR_{in}$	1.22	3.4	2.71	2.56	0.58	0.89	1.62	1.21	1.24	0.17	
$ELCR_{out}$	0.81	2.7	1.8	1.7	0.31	0.59	1.08	0.81	0.83	0.11	
ELCR	2.03	5.67	4.51	4.26	0.97	1.48	2.7	2.01	2.07	0.28	1

3.5.2 Inhalation Effective Dose

The inhalation effective dose was calculated at the free surface of the ground, in ambient atmospheric air and in the indoor confined air. In fact, for the case of radon gas diffused from the ground and suspended in the atmosphere, the dose was evaluated using the radon concentrations in soil. Moreover, it was estimated in two ways according to whether the concentrations were made with RADTRAK^{2}® detectors or with RADUET detectors by taking into account direct thoron progeny. On the other hand, the total inhaled dose

is estimated each time according to the measuring instrument and the inhaled dose at the free surface of the ground.

a → Inhalation dose due to ^{222}Rn

Table 3.11: ^{222}Rn inhalation effective dose to the public at the bauxite bearing areas of Dschang and Fongo-Tongo in western Cameroon: E_{in} and E_{out} are the indoor and outdoor inhalation doses respectively.

	E_{in}			E_{out}		
Parameters	GM (GSD)	Med	Range	GM (GSD)	Med	Range
Dschang	2.7 (0.4)	2.7	1.6-4.8	0.07(0.05)	0.06	0.05-0.24
Fongo-Tongo	3.1 (0.7)	2.8	1.9-7.8	0.06 (0.04)	0.05	0.03-0.19
Whole study	2.9 (0.8)	2.7	1.6-7.8	0.06 (0.05)	0.05	0.03-0.24

As presented in Table 3.11, according to RADTRAK$^{2®}$, ^{222}Rn inhalation dose in the whole study area ranges from 1.6 $\pm$ 0.5 to 7.8 $\pm$ 1.2 mSv y^{-1} with geometric mean of 2.9 $\pm$ 0.8 mSv y^{-1} Taken separately, the ^{222}Rn inhalation dose in Dschang ranges from 1.6 $\pm$ 0.5 to 4.7 $\pm$ 1.0 mSv y^{-1}, for Fongo-Tongo ranges from 1.9 $\pm$ 0.6 to 7.8 $\pm$ 1.2 mSv y^{-1} with geometric mean of 2.7 $\pm$ 0.4 mSv y^{-1} in Dschang and 3.1 $\pm$ 0.7 mSv y^{-1} in Fongo-Tongo. These average values are three to five times higher than the corresponding world average value of 1.2 mSv y^{-1} [1]. More than half of the homes investigated in this study have a dose greater than or equal to 2.7 mSv y^{-1}; a value twice as high as its world corresponding.

The outdoor ^{222}Rn inhalation dose estimated between 0.05 and 0.24 mSv y^{-1} with an average value of 0.07 mSv y^{-1} at Dschang. At Fongo-Tongo, it was estimated between 0.03 and 0.20 mSv y^{-1} with an average value of 0.06 mSv y^{-1}. These values are well below the safety limit of 0.1 mSv.y^{-1} recommended by the **WHO** and well below the **ICRP** reported reference levels of 1mSv y^{-1}. The annual effective dose associated with radon from the atmospheric surface does not pose any type of health hazard to the population and tourists in the study area [7].

According to Table 3.12, total inhalation dose due to indoor and outdoor ^{222}Rn ranged from 1.89 to 7.93 mSv y^{1-} with a mean value of 3.16 $\pm$ 0.54 mSv y^{-1} in Fongo-Tongo and from 1.65 to 4.97 mSv y^{-1} with a mean value of 2.78 $\pm$ 0.52 mSv y^{-1} in Dschang. These values are all above the recommended dose limit of 1.2 mSv.y^{-1} [1]. Figure 3.15 shows the comparison diagram of the average doses in other study areas in Cameroon [16, 18, 20, 25, 160]. However, Fongo-Tongo records inhalation dose value higher than that of Dschang and other ore bearing areas of Cameroon.

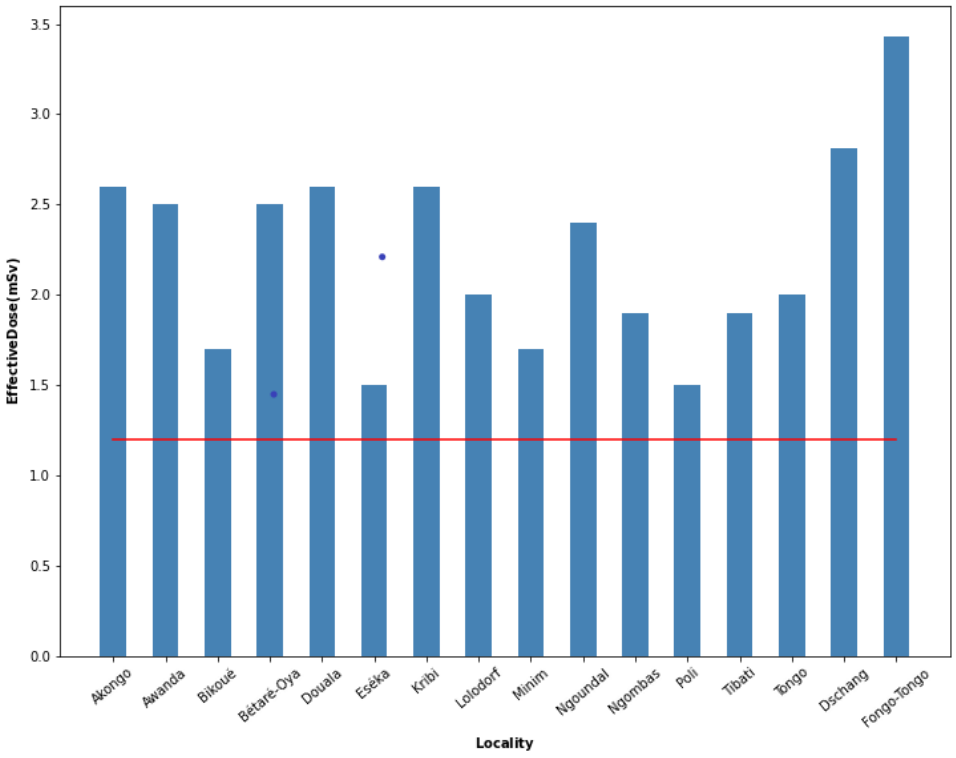

Figure 3.15: Comparative doses of the current study with dose in other mining potential areas of Cameroon.

b →Inhalation dose due to ^{222}Rn, ^{220}Rn and its progeny

Table 3.12: Total inhalation dose $E_T\,(mSv.y^{-1})$ from indoor and outdoor ^{222}Rn

Parameters	Dschang	Fongo-Tongo	Whole study area
Range	1.65-4.97	1.89-7.93	1,65-7.93
Median	2.63	2,87	2,71
GM (GSD)	2,78(0.52)	3,16(0,54)	2,90(0.88)

The annual effective dose from exposure to ^{222}Rn in the study area has been found to vary from 0.6 to 2.5 mSv mS y^{-1} with an average of 2.1± 1.1 mS y^{-1}. Similarly, the annual effective dose due to ^{220}Rn and its progeny has been found to vary from 0.4 to 4.7 mS y^{-1} with an average of 3.4±1.3 mS y^{-1}. Figure 3.16 show the distribution of inhalation dose due to ^{222}Rn, ^{220}Rn and their progeny. The mean contribution of ^{222}Rn to the total inhalation dose is 40% while that of ^{220}Rn and its progeny is 60%.

The arithmetic mean values of total inhalation dose due to ^{222}Rn, ^{220}Rn and their progeny in dwellings of the study area was found to be 3.4±1.3 mS y^{-1}. This inhalation dose received by the general public in the study area was found to be lower than the recommended value of 10 mS y^{-1} by the International Commission on Radiological Protection [161]. In additional, the contributions of ^{222}Rn and ^{220}Rn and its

progeny to the total inhalation dose range respectively between 9-36%, and 6-68% with the average values of 38% and 61% respectively.

It was observed that the highest contribution to the inhalation dose of 61% stems from ^{220}Rn and its progeny and the corresponding least contribution of 38% belongs to ^{220}Rn. Thus, ^{220}Rn itself can be neglected when assessing radiation dose. Indoor ^{222}Rn, ^{220}Rn and progeny measurements in the Bauxique bearing area of Fongo-Tongo are continuation of the work done in several regions of Cameroon, namely Doula city [25], the uranium and thorium bearing regions of Poli and Lolodorf, and the gold mining areas of Betare-Oya [162].

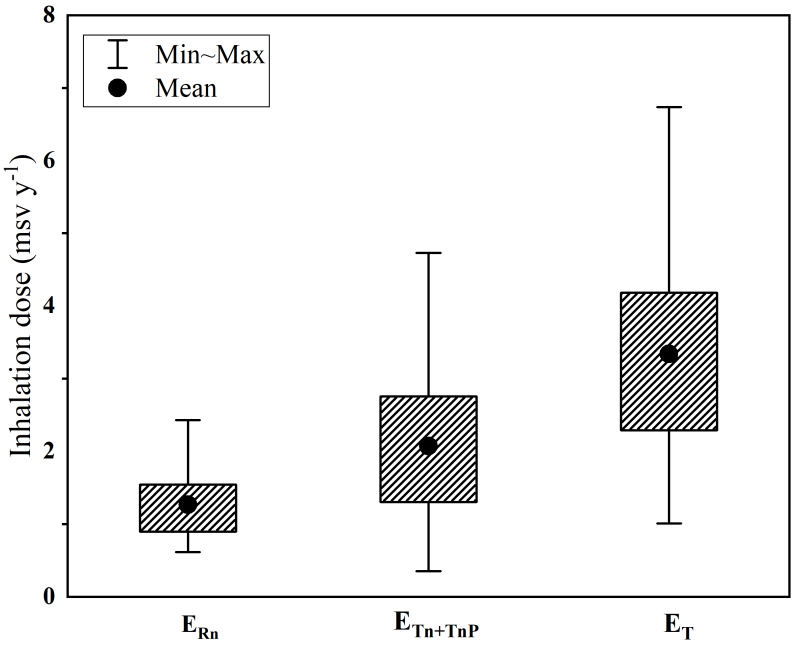

Figure 3.16: Box plot of inhalation dose of ^{222}Rn, ^{220}Rn plus its progeny and the total inhalation dose in dwellings.

The results obtained showed a significant contribution of ^{220}Rn to the total inhalation dose. It varies from 25 to 60%, 16 to 80% and from 6 to 60% in the above study areas respectively. The corresponding average values are 20, and 44% respectively. Looking at all these results we strongly believe that it is necessary for the international scientific community to define a reference value for ^{220}Rn. Table 3.13 shows the total inhalation dose of ^{222}Rn at the ground surface and of ^{222}Rn, ^{220}Rn and its progeny in dwellings of the study area.

Table 3.13: Total inhalation dose received by the general public of the Bauxique bearring area of Fongo-Tongo.

parameters	Indoor			outdoor	Total
	E_{Rn}	E_{Tn+TnP}	E_T	E_{out}	E_{in+out}
GM(GSD)	1.2 (0.4)	1.8 (0.5)	3.1 (0.8)	0.06 (0.05)	3.16 (0.7)
AM±SD	1.3×0.5	2.1×1.1	3.4×1.3	0.04×0.03	3.43×1.21
Median	1.1	2.1	3.3	0.05	3.33
Range	0.6 - 2.5	0.4 - 4.7	1 - 6.7	0.03 - 0.24	1.04 - 6.92

3.6 Influence of the equilibrium factor on the inhalation dose assessment of ^{222}Rn and ^{220}Rn

Previous studies have shown that, for a good estimation of the effective inhalation doses, ^{222}Rn and its progeny as well as ^{220}Rn and its associated progeny should be measured simultaneously at the same point. In the current work, the inhalation dose of ^{222}Rn was assessed using radon equilibrium factor of 0.4 proposed by **UNSCEAR**. While that of ^{220}Rn was determined by the experimental value of the thoron equilibrium factor of F_{Tn} = 0.03 obtained at the site by direct measurement of its progeny.

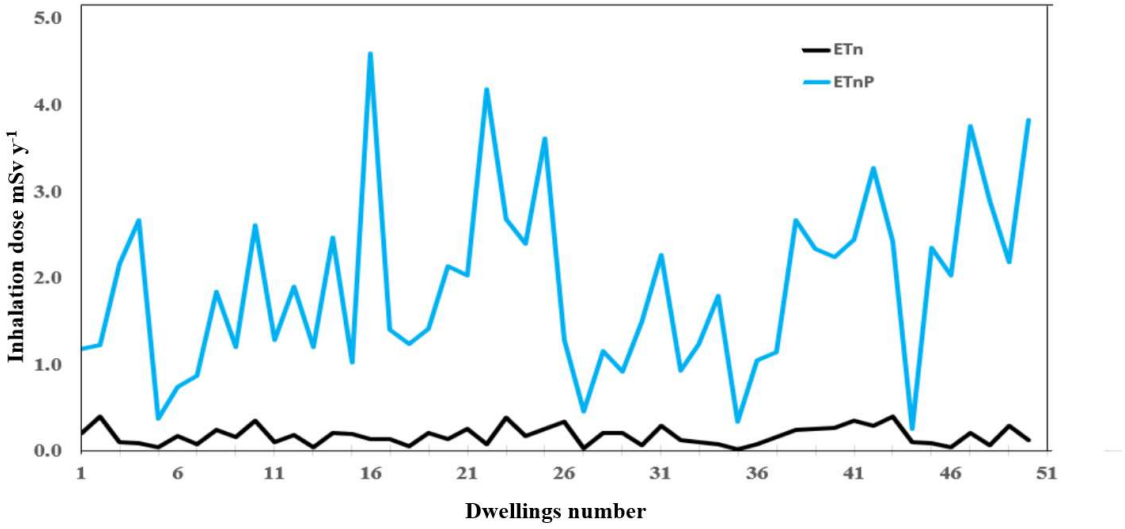

Figure 3.17: Inhalation dose due to ^{220}Rn and its progeny in the monitored dwellings of the study area.

The effective inhalation dose from ^{220}Rn and its progeny, estimated at (0.11 mSv y^{-1}), is generally negligible compared to that of ^{222}Rn and its progeny (1.15 mSv y^{-1}) in most parts of the world according to the **ICRP** [114]. However, in practice, the opposite is very often observed, as was the case in the present study where the contribution of ^{220}Rn (Tn and TnP) is almost three times that of ^{222}Rn. For the whole study

area, the contribution of ^{220}Rn and its progeny to the total effective dose varies between 6 and 70%, with an average value of 64% (Figure 3.17). Therefore, ^{220}Rn through its progeny must be taken into account in the evaluation of the dose and health risk on inhalation in indoor air.

3.7 Risk assessment

3.7.1 Excess Lifetime Cancer Risk (ELCR)

The ELCR statistical parameters values obtained by gamma spectrometry in laboratory and *in situ* are summarized in Tables 3.9 and 3.10. They ranged from 2.03×10^{-3} to 5.67×10^{-3}, with a mean value of 4.44×10^{-3}, in Fongo-Tongo; and from 1.48×10^{-3} to $5\times11\ 10^{-3}$, with a mean value of 3.64×10^{-3}, in Dschang. The mean values of ECR in Fongo-Tongo and Dschang were, respectively, 1.29 and 1.06 times higher than 0.29×10^{-3}, the **UNSCEAR** recommended limit value [1]. However, the risk values obtained could be overestimated if, in addition to the above risk, the risk due to radioactivity from building materials was taken into account, because more than 70% of the houses in the area use mainly mud bricks as building material.

3.7.2 Study of Correlations between ^{222}Rn Gas in Soil and ^{222}Rn in Dwellings

The study investigated the correlation between the concentrations of ^{222}Rn gas in dwellings and those in soil gas, considering different dwelling architectures and natural ventilation systems. The dwellings were categorized based on construction materials (earthen bricks or cement) and floor types (bare or concrete). Although ventilation parameters were not directly measured, factors such as window and door openings were considered for assessing air circulation in the dwellings.

Figure 3.12 illustrates the correlation between ^{222}Rn gas in soil and its concentrations in earthen dwellings (Figure 3.12-a) and cemented dwellings (Figure 3.12-b). The correlation coefficients were R^2 = 0.82 for earthen dwellings and R^2 = 0.73 for cemented dwellings, indicating a stronger correlation in earthen structures. This suggests that measuring ^{222}Rn gas in soil could predict concentrations in dwellings, especially in earthen constructions where the porosity of soil and walls contributes to higher levels of ^{222}Rn.

Similarly, Figure 3.13 depicts correlations in well-ventilated dwellings, showing lower correlation coefficients (R^2 = 0.54 for earthen and R^2 = 0.34 for cemented dwellings) compared to poorly ventilated ones. This difference is attributed to materials like cinder blocks, cement, and concrete that reduce ^{222}Rn diffusion in well-ventilated structures.

The analysis also explored correlations between radon, thoron, and their progeny concentrations, showing weak positive correlations (0.084 for radon-radon progeny, 0.074 for thoron-thoron progeny, and 0.086 for radon-thoron concentrations). Additionally, the study highlighted the influence of geological factors such as soil richness in uranium or radium and soil permeability on indoor radon levels.

3.7.3 Ambient Equivalent Dose Rate (AEDR) and Annual External Effective Dose (AEED)

To assess the radiological impact of natural radioactivity, parameters like absorbed dose rate in air, annual effective doses, and cancer risk were determined. Table 3.9 summarizes radiological parameters for different localities, indicating that average values exceed safety limits, particularly for annual effective doses. Further analysis in Table 3.10 shows absorbed dose rates at ground level exceeding recommended levels.

3.7.4 Inhalation Effective Dose

Inhalation effective doses were evaluated for radon and thoron gases, considering indoor and outdoor environments. Table 3.11 presents inhalation doses due to ^{222}Rn, which were notably higher in the study area compared to global averages. However, outdoor inhalation doses remained within safety limits.

Total inhalation doses, including ^{222}Rn, ^{220}Rn, and progeny, were assessed (Table 3.12), revealing values exceeding recommended limits. Figure 3.15 compares these doses with other regions in Cameroon, highlighting elevated doses in Fongo-Tongo.

3.7.5 Risk Assessment

Excess Lifetime Cancer Risk (ELCR) values were calculated and compared to recommended limits. The study found ELCR values exceeding guidelines, particularly in Fongo-Tongo and Dschang, indicating potential health risks associated with radiation exposure. However, it also noted the possibility of overestimation due to factors like building materials contributing to radioactivity.

3.7.6 Long Term ECR analysis using RESRAD-ONSITE Computer Code

As shown in Figure 3.18, the TECR calculated with RESRAD-ONSITE decreased progressively over the years, from the maximum value of 8.58×10^{-3} obtained at the dates T = 1 and T = 1 year to the value of 7.41×10^{-3} obtained at T = 100 years before decreasing significantly. This remarkable decreasing may be due to the self-absorption of building materials or to the process of radioactive decay [163].

Similarly, ^{226}Ra is the major contributor to the TECR at about 70% in the first year. This contribution decreases slightly over the years before dropping significantly after 100 years. According to Table 3.14, the maximum value of risk due to ^{226}Ra obtained at T = 10 years is 7.372×10^{-6}. The ECR due to ^{232}Th, on the other hand, is inversely proportional to that of ^{226}Ra over the period from 1 to 40 years, where it becomes practically constant, and the maximum value obtained at T = 50 years is 9.250×10^{-6}. As for ^{40}K, its contribution to the total risk remains the smallest, but it shows some slight variations before decreasing to zero. Similar results were observed in studies conducted in the cobalt?nickel region of Lomié in Eastern

Cameroon [164]. Table 3.14 summarizes the TECR for initially existent radionuclides and pathways at T = 0, 1, 10, 30, 50, and 100 years.

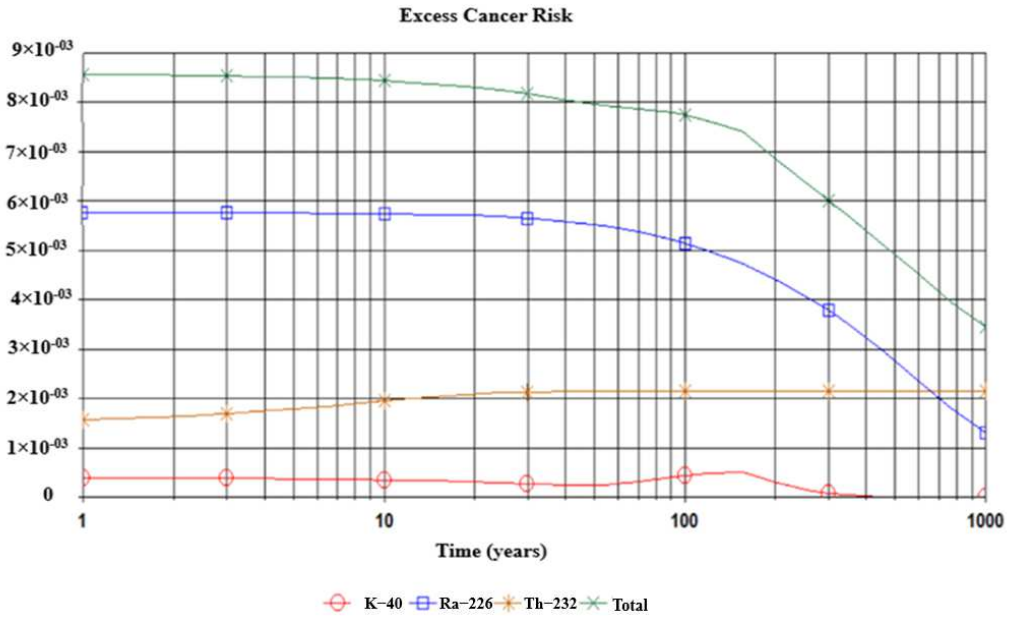

Figure 3.18: Long-term plotting of ECR for all exposure pathways and for each primordial radionuclide Compute with RESRAD-ONSITE.

Table 3.14: Total ECR for initially existent radionuclides and pathways and fraction of total risk, T(Years).

T	Ground	Inhalation	Radon	Plant	Meat	Milk	Soil	Total
0	1.74	6.32	4.89	1.56	2.24	1.44	2.22	8.58
1	1.74	6.32	4.89	1.56	2.24	1.44	2.22	8.58
3	1.73	6.32	4.87	1.55	2.18	1.42	2.22	8.54
10	1.72	6.30	4.81	1.53	2.06	1.36	2.20	8.43
30	1.69	6.27	4.67	1.49	1.76	1.24	2.17	8.17
100	1.60	6.18	4.19	1.38	.16	9.75	2.04	7.41
	$\times 10^{-3}$	$\times 10^{-6}$	$\times 10^{-3}$	$\times 10^{-6}$	$\times 10^{-3}$	$\times 10^{-4}$	$\times 10^{-5}$	$\times 10^{-3}$

3.7.7 Long Term ECR analysis using RESRAD BUILD Computer Code

RESRAD-BUILD assessed the total risk due to radioactivity from soil used in the manufacture of bricks as a building material. The results obtained for the different exposure routes and for each nuclide as a function of time are summarized in Table 3.15 The maximum value of the total excess risk obtained at T = 30 years is 5.19×10^{-2} for all the summed routes. Similarly, the value of the total excess risk for all summed

nuclides obtained at T = 30 years is 1.89×10^{-2}. However, it should be noted that the external pathway is the one that contributes the most to the total excess risk. The maximum risk value for this pathway, which is 2.33×10^{-2}, was obtained at T = 30 years. Nevertheless, the decrease observed beyond 30 years for the external route would be due to the self-absorption of building materials [56, 65, 165]. Similar results were obtained in the work carried out in the Poli uranium region [17], in the bauxite zones of Southern Adamawa [16], and in some localities of the Centre Region, Cameroon [56].

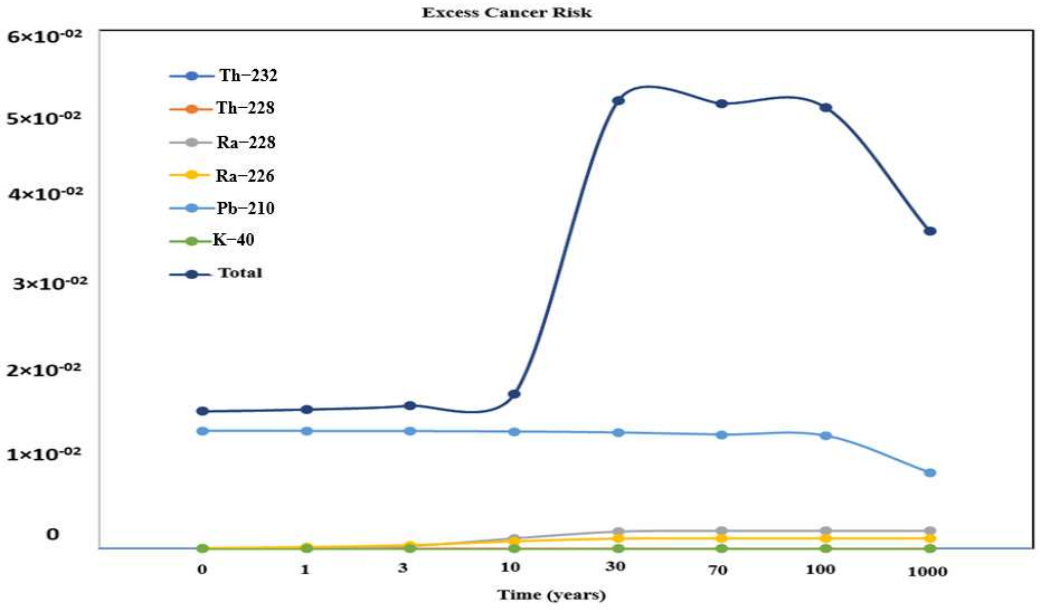

Figure 3.19: Long-term total excess risk for each nuclide Compute with RESRAD BUILD.

Table 3.15: Total risk of excess cancer for all exposure detail of risks.

Time (y)	T =0	T =1	T =3	T =10	T =30	T =70	T =100
External	1.57×10^{-2}	1.59×10^{-2}	1.63×10^{-2}	1.76×10^{-2}	2.33×10^{-2}	2.32×10^{-2}	2.30×10^{-2}
Deposition	5.15×10^{-9}	5.22×10^{-9}	5.31×10^{-9}	5.64×10^{-9}	3.68×10^{-3}	3.66×10^{-3}	3.63×10^{-3}
Immersion	4.50×10^{-11}	4.54×10^{-11}	4.65×10^{-11}	5.06×10^{-10}	3.68×10^{-3}	3.66×10^{-3}	3.63×10^{-3}
Inhalation	1.18×10^{-6}	1.23×10^{-6}	1.36×10^{-6}	1.76×10^{-6}	3.01×10^{-3}	2.99×10^{-3}	2.96×10^{-3}
Radon	2.20×10^{-4}	2.27×10^{-4}	2.49×10^{-4}	3.30×10^{-4}	4.08×10^{-3}	4.06×10^{-3}	4.03×10^{-3}
Ingestion	5.39×10^{-8}	5.88×10^{-8}	6.82×10^{-8}	8.39×10^{8}	1.89×10^{-2}	1.88×10^{-2}	1.86×10^{-2}
Total	1.59×10^{-2}	1.61×10^{-2}	1.66×10^{-2}	1.79×10^{-2}	5.19×10^{-2}	5.15×10^{-2}	5.11×10^{-2}

The results presented in Table 3.14 show that ^{226}Ra is the main contributor to the **TCR** compared to ^{232}Th and ^{40}K. The risk due to ^{226}Ra increases progressively with time until reaching an increasing threshold after 70 years. The occurrence of this radionuclide in high concentrations in building materials increases the

probability of accumulation of high indoor radon concentration [110]. Figure 3.19 represents the long-term total ECR for each radionuclide.

According to Table 3.15, the pathway that contributes most to the **TCR** is the external pathway. Like the other pathways, the risk increases until it reaches a value of 2.33×10^{-2} at T= 30 years. similarly, the total cancer risk also increases and reaches a value of 5.19×10^{-2} at the same date.

3.7.8 Specific risk from radon exposure: Lifetime Excess Absolute risk (LEAR)

The bauxite bearing area of Fongo-Tongo is not yet a mining site. The activities carried out for several years on this site reveal essentially mining exploration. For this reason, the **WLM** results are given as an indication because they do not reflect the reality of the exposure of the public living in an operating mine. In practice, this risk would be higher in these dwellings if mining activities were carried out in the area. Nevertheless, these results may be used for future work. The results in Tables 3.5 and 3.7 show increased concentrations of ^{222}Rn, ^{220}Rn and their progeny in dwellings in the study area. The **LEAR** evaluated from RADTRAK^{2}® detectors varies between 0.02 and 0.11% with a mean value of 0.04% and with RADUET detectors and thoron progeny monitors, it varies between 0.01 and 0.03% with a mean value of 0.02% for ^{222}Rn and between 0.01% and 0.19% with an average values value of 0.08% and 0.007% for thoron throughout the area; approximately 6 to 11 times higher than the world average value. These different data obtained in the present study show that the radiological risk is relatively high for the public living permanently in the studied area. Furthermore, many studies have shown a relationship between increased ^{222}Rn concentrations in dwellings, smoking (active or passive) and the risk of developing a lung cancer. It has been established that this risk is proportional to the concentration of ^{222}Rn in the inhaled air and the time of exposure [166, 167, 168]. Over a lifetime, this risk increases linearly with ^{222}Rn exposure by about 16% per 100 Bq m^{-3} [158, 169].

The results of many experimental studies carried out on animals; epidemiological studies carried out in an occupational setting among uranium miners as well as on the general public have shown that prolonged exposure to ^{222}Rn can induce lung cancer. Reports published in 2011 by the National Cancer Institute reveal that the risk incurred by an individual living in a dwelling with radon concentrations between 200 and 400 Bq m^{-3} is close to that of a non-smoker living in a passive smoking atmosphere [158]. A similar study in France showed that 5% to 12% of lung cancer cases in a year are attributable to domestic radon [167, 170, 171]. Darby *et al.* showed that if one considers the absolute risk of lung cancer at age 75 years for different concentrations of ^{222}Rn in the dwelling of 0, 100 and 400 Bq m^{-3}, this estimated risk is respectively about 0.4%, 0.5% and 0.7% for a person who has never smoked, and is nearly 25 times higher (10%, 12% and 16%) for a smoker [172].

As presented in Table 3.16, 4% of dwellings exceeded ^{222}Rn concentrations of 200 Bq m^{-3}. As for ^{220}Rn, 17% of the houses have concentrations higher than 300 Bq m^{-3}, while 35% of the houses exceed

concentrations of 200 Bq m^{-3} in thoron progeny. Comparing the results of the present work with the above information, it is clear that the public living permanently in the study area is significantly exposed to ^{222}Rn, ^{220}Rn and their associated progeny. When combined with the exposure to smoking of the residents of some houses in the various sites, the risk of developing lung cancer is found to be very high for many of the members of the public involved in the present study.

Therefore, radiation protection measures must be implemented to reduce this risk. In view of the different results above, it appears that the risk indices related to the inhalation of ^{222}Rn, ^{220}Rn and their progeny in dwellings are relatively all high. From the point of view of radiation protection, the low level of a risk index does not imply a lack of danger because any dose of ionizing radiation has a capacity to harm health. Everything depends on the reaction of the body to whatever dose it is subjected to Determination of depleted uranium in environmental samples by gamma-spectroscopic techniques.

Table 3.16: Excess lifetime risk parameter for ^{222}Rn and ^{220}Rn exposure in the study area for different types of detectors.

		LEAR(%)				
Detector	Isotopes	AM	SD	GM	Med	Range
RADTRAK$^{2®}$	^{222}Rn	0.04	0.02	0.04	0.04	0.02-0.11
RADUET	^{222}Rn	0.02	0.01	0.02	0.02	0.01-0.03
	^{220}Rn	0.08	0.05	0.07	0.08	0.01-0.19
	^{220}Rn+^{220}Rn	0.1	0.05	0.09	0.09	0.02-0.21

The various data obtained in Table 3.16 show that the radiological risk is quite high for the public living permanently in the current study area. Several studies have shown a relationship between increased radon concentrations in a dwelling, smoking (active or passive), and the risk of developing radiation-induced lung cancer. It has been established that this risk is proportional to the concentration of radon in the air breathed and the duration of exposure (Darby *et al.* 2005). By comparing the results of the present work with the above-mentioned information, it is evident that members of the public living permanently in bauxite bearing area exposed to radon. Combined with the smoking exposure of the inhabitants of some of the dwellings in the various sites, the risk of developing lung cancer is high for many of the members of the public involved in this study. Therefore, radiation protection measures must be put in place to reduce this risk.

Conclusion

Radioactivity measurements due to primordial radionuclides at Dschang and Fongo-Tongo show high concentrations of ^{226}Ra and ^{232}Th at some points, while ^{40}K concentrations were below the reference values prescribed by international organizations. Similarly, the concentrations of ^{222}Rn in soil were above the

safety limit defined by the Swedish risk classification criterion at most of the measurement points. As for the internal irradiation, the results of measurements obtained show important concentrations of ^{222}Rn and ^{220}Rn in the majority of the dwellings. Indeed, ^{222}Rn and ^{220}Rn concentrations in the dwellings were higher than the corresponding world average values. Nevertheless, it was shown that they varied from one dwelling to another according to some specific parameters linked to the architecture and its usage and also according to the seasons. For their relatively short-lived ^{220}Rn progeny, the concentrations are high wherever measurements have been made. However, the average effective doses and the different risk indices related to the soil for the whole study area do not reveal a danger for the population in general. From these data, it appears that the public living in the present study area is exposed to ionizing radiation from the primordial radionuclides, ^{222}Rn and ^{220}Rn. This exposure certainly originates from a combination of factors related to the geology, geochemistry, mineralogy, geography and anthropology of the area. Therefore, the rules of radiation protection must be observed in order to reduce this risk. Indeed, the information on the Bauxite ore is mentioned in the "study area" section. Some additional information has been added to the revised manuscript. Nevertheless, the presence of bauxite ores cannot be used to justify hight ^{226}Ra and ^{232}Th concentration in soil or radon levels in the soil and inside the houses. Indeed, the elements that influence radon concentrations in soil and in dwellings are well known. They are among others the permeability, the porosity, the geology of the soil on the one hand, the climate, the type of architecture, the ventilation, the use of these dwellings or the way of life of the populations on the other hand. Moreover, the choice of the term Bauxite in the title of the manuscript just refers to the geological and mineralogical situation of the region which abounds considerably of this mineral.

General Conclusion

The study investigated correlations between ^{226}Ra and ^{222}Rn concentrations in soil, and between ^{222}Rn in soil and indoor air. It also evaluated the effective dose of internal radiation and radiological parameters like AEED and ELCR to assess population exposure levels. Concentrations of ^{226}Ra, ^{232}Th, and ^{40}K in soil were determined using in situ and laboratory γ-spectrometry methods. ^{222}Rn in soil was measured with the Markus 10 detector, while ^{222}Rn, ^{220}Rn, and progeny concentrations were measured in dwellings using RADTRAK^{2}®, RADUET, and thoron progeny monitors. RadonEye+^{2} detectors were used to monitor daily variations in ^{222}Rn levels in selected dwellings in the bauxite area of Fongo-Tongo. The study area exhibits elevated concentrations of radium-226 and thorium-232, in line with the geological composition of its bedrock, with average concentrations surpassing the values delineated by UNSCEAR.

Approximately 6% of residences recorded radon concentrations exceeding 300 Bq m-3, the limit recommended by UNSCEAR, while roughly 12% registered thoron concentrations surpassing 500 Bq m^{-3}, the limit proposed by Cameroon. Fongo-Tongo, alongside the Ngaoundéré area, stands out globally for its high thoron concentrations, drawing attention from the international community to the associated risks.

^{222}Rn concentrations in soil ranged from 35 to 255 kBq m^{-3}, with mean values of 67 (18) kBq m^{-3} for the study area, 69$\pm$18 kBq m^{-3} at Fongo-Tongo, and 82$\pm$34 kBq m^{-3} at Dschang. The mean concentrations of ^{226}Ra, ^{232}Th, and ^{40}K in soil were similar for both in situ and laboratory methods. Compared to global data, concentrations of ^{226}Ra and ^{232}Th were relatively high, while ^{40}K was relatively low, consistent with bauxite ore deposits.

Indoor ^{222}Rn concentrations ranged from 85 to 410 Bq m^{-3} with a geometric mean of 152 (26) Bq m^{-3}, varying based on ventilation and building materials. The majority of measurement points exceeded regulatory limits, highlighting the need for expanded radon and thoron measurements across Cameroon.

The study also revealed significant variations in ^{222}Rn concentrations in soil across the area. Dwellings constructed with dense materials like cement and concrete showed lower ^{222}Rn concentrations and inhalation dose due to limited diffusion of ^{222}Rn.

Strong correlations were found between ^{222}Rn and ^{226}Ra concentrations in soil using two methods (R^2= 0.86 *in situ* and R^2= 0.88 Laboratory). For residences with inadequate natural ventilation, significant correlations were observed among dwellings constructed from earth and cement, respectively.

However, with improved ventilation conditions, these correlations notably decrease, transitioning to

medium and low levels, respectively. Good natural ventilation reduced ^{222}Rn levels further, especially in homes with well-positioned windows and doors facilitating air circulation. Earthen or brick dwellings, with or without good natural ventilation, showed stronger correlations between ^{222}Rn in soil and indoor air.

From an architectural standpoint, homes constructed from cement or concrete exhibit lower radon concentrations compared to those built from earth. Effective ventilation of residences emerges as a crucial strategy for mitigating domestic radon gas accumulation.

The correlation between radium and radon is contingent upon various environmental factors, architectural attributes, and the efficacy of the home's ventilation system.

Future work includes To enhance this work, integrate a greater number of dwellings in the studied area and expand to other localities in Cameroon. Measure radon in water and assess the dose from ingestion of radionuclides through food and drinking water. Conduct a complete study of natural radioactivity in the study area, considering soil contamination and transfer to biota.

Appendix

Appendix I: Additional Material and Methods

Ambient dose rate at one meter above ground level on site

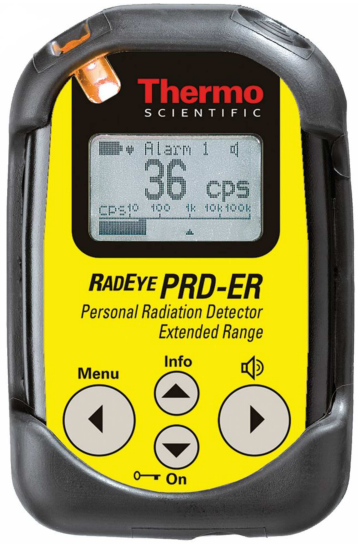

Figure 3.20: Thermo Scientific RadEye^{TM} PRD detector.

The absorbed dose rate is the amount of energy released by ionizing radiation into matter per unit of mass and per unit of time. It is expressed in Gray per second (Gy/s) or in joules per kilogram per second (j/kg/s) in the international system, but is also commonly used in nano Gray per hour (nGy/h). The contribution of natural radionuclides to the absorbed dose rate in air depends on the activity concentration of the radioelements ^{236}Ra, ^{232}Th and ^{40}K. The ambient dose equivalent rate at one meter above the ground surface, was measured inside and outside of homes using a handheld radiation dose rate meter (RadEye PRD-ER). The Thermo Scientific RadEye^{TM} PRD personal radiation detector can detect and locate sources of radiation generated by man-made devices such as nuclear weapons, improvised nuclear devices (INDs), or radiological dispersal devices (RDDs) [173]. It is a very sensitive gamma ray and dose level measurement tool. Used to detect and locate orphan sources or problematic naturally occurring radioactive material sources in scrap

yards, borders and other public places. Designed in accordance with ANSI^{TM} 42.33/1, 42.32 and IEC 62401 standards, its features include.

External effective Dose

The effective dose is given by the equation

$$E_{ext}(mSv.y^{-1}) = [(1 - F_{occ}.H_{out} + F_{occ}.H_{in}] \times t \tag{3.1}$$

Where E_{ext} (mSv.y^{-1} is the annual effective dose H_{out} and H_{in} are the average absorbed dose rates in air at 1 m from the ground (in nGy/h) outside and inside the dwellings, respectively, and t = 8760 h (24 h $\times$ 365 d) is the exposure duration and F_{occ} is the occupancy factor considering that an individual spends 40% of his or her time outside of the dwellings and 60% inside.

External and Internal risk index

The localities where this study was carried out mainly use locally manufactured mud bricks as building materials. In order to ensure that the external dose due to natural gamma radiation inside the houses from this material does not exceed the range of internationally recommended values, the external risk indices H_{out} and H_{in} were evaluated. The external hazard index was introduced to limit radiation exposure in the samples to permissible dose equivalent limit of 1.00 mSv y^{-1} and it is assessed by the equation [1, 14, 117] :

The effective dose is given by the equation

$$H_{out} = \frac{A_{Ra}}{370} + \frac{A_{Th}}{259} + \frac{A_K}{4810} \leq 1 \tag{3.2}$$

The external hazard index must not exceed the limit of unity for the radiological risk to be insignificant. The maximum value of H_{out}= equal to unity corresponds to the upper limit of 370.00 Bq.kg^{-1} of ^{226}Ra [1, 117, 175]. Furthermore, the deposition period of ^{222}Rn progeny in the pulmonary is also very dangerous [25, 118]. In order to take this threat into account and reach the normal limit of 185 Bq.kg^{-1}, the permissible value for ^{226}Ra is reduced by half to reach the limit of the unit. It is evaluated following equation [131, 175]:

The effective dose is given by the equation

$$H_{in} = \frac{A_{Ra}}{185} + \frac{A_{Th}}{259} + \frac{A_K}{4810} \leq 1 \tag{3.3}$$

The H_{out} and H_{in} risk indices must be less than 1 mSv y^{-1}, the unit of annual effective dose from radioactivity in building materials.

Radiation Hazard Index

The radioactivity level index has been evaluated in order to estimate the level of dangerousness of natural primordial radionuclides in a human body exposed to gamma radiation from these radionuclides in soil. It

is generally used under the name (radioactivity level index) and is noted Iγ . It is a very important parameter for the quality, control and monitoring of the external effective dose due to gamma radiation accumulated in the body. It was obtained by the following equation [118, 125] :

$$I_\gamma = \frac{A_{Ra}}{300} + \frac{A_{Th}}{200} + \frac{A_K}{300} \leq 1 \tag{3.4}$$

It is the index of nuclear energy level for external radiation due to specific activity of different natural radionuclides in a sample [176]. Its permissible limit is Iγ =1 and corresponds to 0.3 mSv y^{-1}. It is used to evaluate gamma radiation risk level associated with naturally occurring radionuclides. The excess alpha radiation following radon inhalation from building materials is determined using equation [127, 128] :

$$I_\alpha = \frac{A_{Ra}}{200} \leq 1 \tag{3.5}$$

The upper limit of Iα is unity, because a building material with a ^{226}Ra concentration of less than 200 Bq kg^{-1} cannot cause a minimum radon concentration greater than 200 Bq m^{-3}.

Presentation of the RESRAD code family

The RESRAD family codes is being developed by Argonne National Laboratory to analyze potential radiation exposures to humans and biota from environmental contamination of residual radioactive materials. The codes use pathway analysis to assess radiation exposure and associated risks, and to derive clean-up criteria or allowable limits for radionuclide concentrations in the contaminated area.

- RESRAD ON-SITE: To assess the radiation exposure of a human receptor located above soils contaminated by radioactive materials.
- RESRAD OFF-SITE: To assess radiation exposures to a human receptor located above or at a distance from soils contaminated with radioactive materials.
- RESRAD-BLUID: To assess radiation exposures to a human receptor in a contaminated building or in a building housing contaminated furniture or equipment.
- RESRAD-RDD: To assess human radiation exposures during the early, intermediate, or late phase of the response to a radiological dispersal device (RDD) incident
- RESRAD -BIOTA For assessing radiation exposures to non-human biota, including flora and fauna, in a terrestrial or aquatic ecosystem.

Other codes namely :

- RESRAD RECYCLE

- RESRAD BASELINE
- RESRAD CHEM
- RESRAD ECORISK content

Descriptin of the RESRAD ONSITE code

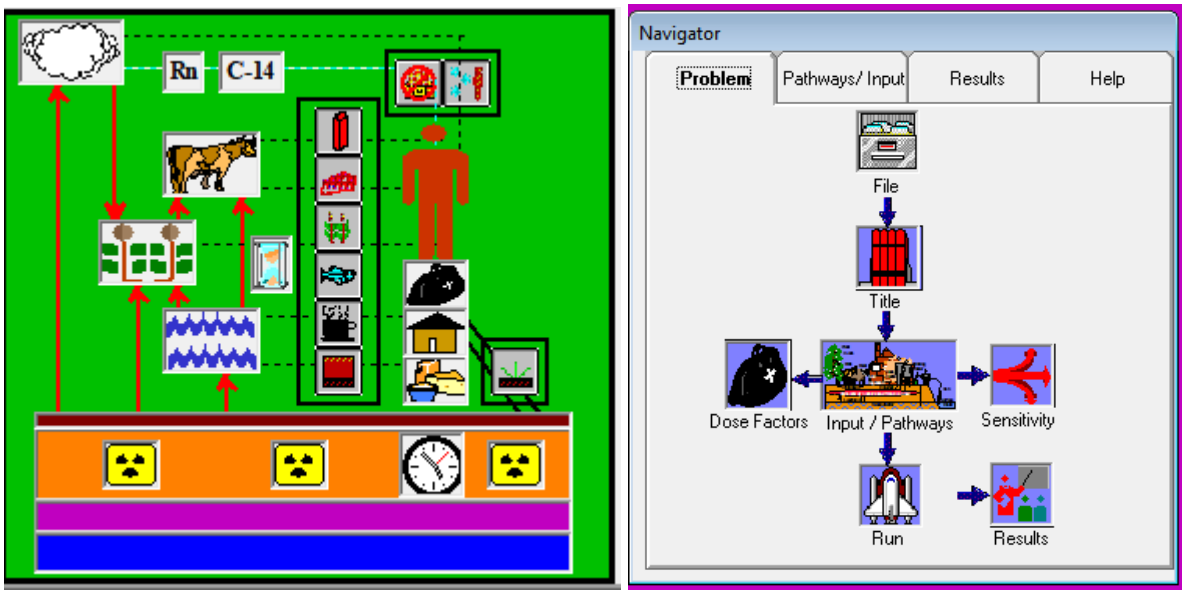

Figure 3.21: Physical Interface of RESRAD-ONSITE Code sofware problemes and solluion

The calculation of dose and cancer risk by the RESRAD-ONSITE code is scenario-based, using user-specified parameter values. Nine exposure pathways are provided, which can be selected or deleted to reflect the land use scenario and receptors considered. These nine exposure pathways are: (1) direct external radiation from radionuclides in soil, (2) inhalation of airborne radionuclides resuspended or volatilizing (H-3 and C-14) from soil, (3) incidental ingestion of soil, (4) ingestion of plant foods grown in contaminated soil and irrigated with contaminated water, (5) ingestion of meat and (6) ingestion of milk produced by livestock fed contaminated forage and water, (7) ingestion of drinking water from a well or pond adjacent to the contaminated area, (8) ingestion of aquatic food from the pond, and (9) inhalation of radon emitted from the contaminated soil. Input information needed for the calculation includes the characteristics of the contamination, properties of the surface, subsurface, and saturated soil strata, site-specific meteorological, hydraulic, and hydrogeological data, and the exposure profile of the receive.

RESRAD-ONSITE modelling accounts for radiological decay and growth as well as transport, distribution, and dilution in the environment, governed by the principle of conservation of mass over time. Essentially all input parameters used for the calculation can be specified by the user; therefore, the user can

control the level of conservatism of each calculation, and apply the RESRAD-ONSITE code for screening, site-specific screening, or site-specific assessment purposes.

Description of the RESRAD BLUID code

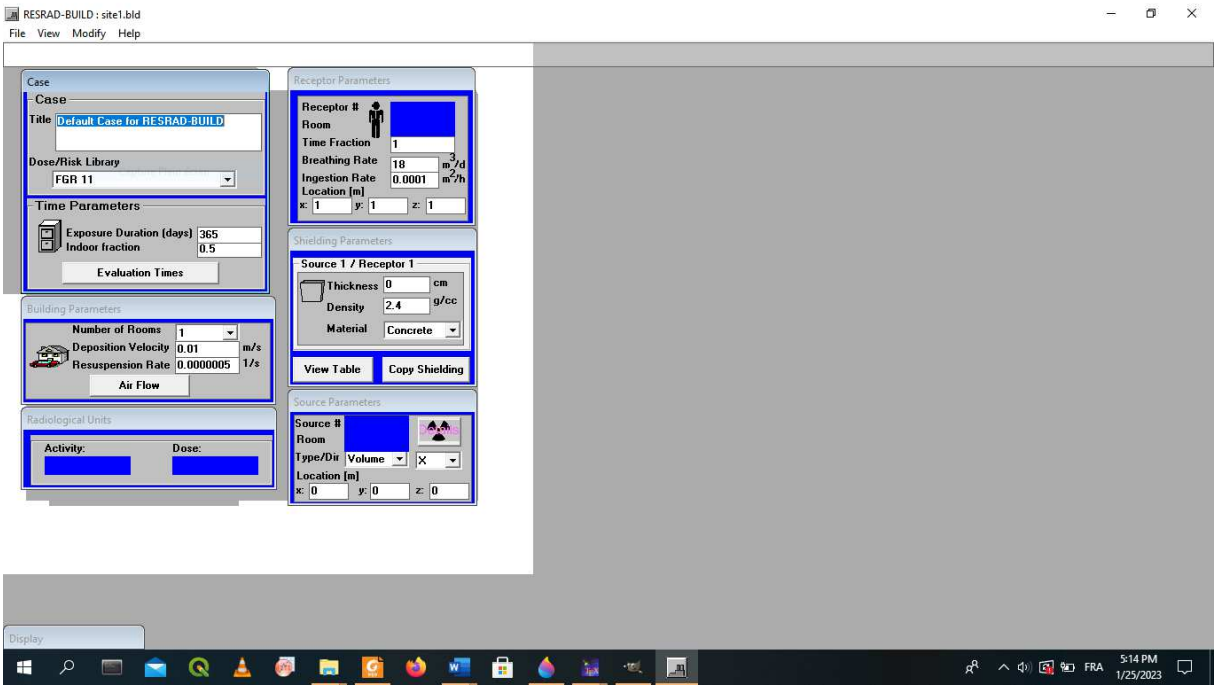

Figure 3.22: Physical sofware Interface of RESRAD-BUILD Code

The exposures analyzed for a receptor are considered to result from direct external radiation (from contaminant sources and submersion in contaminated air), inhalation of airborne contaminated dust particles, inhalation of radon, and accidental ingestion of contaminated dust particles. The building under consideration may consist of up to three rooms, with air exchange between the rooms and the outside environment. Up to 10 radiation sources and 10 receptors can be specified in a single calculation. Radiation sources and receivers can be located in any room, with specified coordinates and characteristics such as fraction of time in the room, breathing and accidental ingestion rate for receivers and orientation, shape, dimensions and erosion rate for contamination sources. Contamination sources may have point, linear, planar, or volume geometry and may be on the surface or inside the building, equipment, or furniture. Radiation shielding between receivers and contamination sources can be specified and is accounted for in the external dose calculation. Users select appropriate values of input parameters to simulate a building occupancy scenario (e.g., residential and office use) or catering scenario

Appendix II: Additional Results

Ambient dose rate at one meter above ground level on site

Table 3.17: Statistical summary of indoor and outdoor ambient dose rates and external effctive dose at the bauxite bearing areas of Dschang and Fongo-Tongo, West Region of Cameroon.

Locality	Statistical parameters	Indoor ($?Sv.h^{-1}$)	Outdoor ($?Sv.h^{-1}$)	Eext ($mSv.y^{-1}$)
Dschang	Range	0.05-0.08	0.04-0.10	0.40-0.77
	Median	0.06	0.06	0.52
	AM±SD	0.06±0.01	0.06±0.01	0.53±0.08
	GM(GSD)	0.06(0.01)	0.06(0.01)	0.52(0.08)
Fongo-Tongo	Range	0.06-0.14	0.05-0.24	0.4-1.52
	Median	0.08	0.08	0.46
	AM±SD	0.09±0.02	0.09±0.04	0.77±0.23
	GM(GSD)	0.08(0.02)	0.08(0.04)	0.74(0.24)
Whole study	Range	0.05-014	0.04-024	0.4-1.52
	Median	0.07	0.06	0.58
	AM±SD	0.07±0.02	0.07±0.03	0.63±0.20
	GM(GSD)	0.07(0.02)	0.07(0.03)	0.6(0.2)

External Hazard Index

The obtained values of H_{ext} are presented in Tables 3.18 and 3.19. The average values are 1.48 at Fongo-Tongo and 1.32 at Dschang. H_{ext} values are greater than unity, and therefore, it can be recommended to the populations of those sites to use earth as a building construction material, except in some places where the level of natural radioactivity is relatively high.

Internal Hazard Index

The statistical parameters from H_{in} are summarized in Tables 3.18 and 3.19. The maximum values of H_{in} are 2.81 and 2.04, with an average value of 1.88 and 1.68, in Fongo-Tongo and Dschang, respectively. H_{in} values are also greater than unity [1]. Nevertheless, to avoid excessive internal exposure to ^{222}Rn in these localities, the use of earth can be recommended as a building material, provided that there is good ventilation and air circulation in the rooms of the dwelling. Table 3.19 Summary of the different radiological parameters obtained in laboratory.

Table 3.18: Summary H_{in}, H_{out} $I\alpha$, I_γ obtained by *in situ*.

Locality	Fongo-Tongo					Dschang					
Parameters	Min	Max	Med	AM	SD	Min	Max	Med	AM	SD	Limit
H_{in}	0.9	2.01	1.65	1.57	0.32	1.25	2.04	1.68	1.68	0.19	1
H_{out}	0.56	1.64	1.3	1.22	0.29	0.92	1.64	1.32	1.31	0.16	1
I_α	0.47	1.01	0.63	0.64	0.11	0.49	0.9	0.66	0.69	0.09	1
I_γ	0.72	2.12	1.67	1.58	0.37	1.19	2.12	1.7	1.69	0.21	1

Table 3.19: Summary H_{in}, H_{out} $I\alpha$, I_γ obtained by laboratory.

Locality	Fongo-Tongo					Dschang					
Parameters	Min	Max	Med	AM	SD	Min	Max	Med	AM	SD	Limit
H_{in}	1.36	2.81	1.82	1.88	0.37	1.36	1.92	1.57	1.6	0.15	1
H_{out}	1.07	2.35	1.41	1.48	0.33	1.29	1.58	1.29	1.29	1.02	1
$I\alpha$	0.53	0.85	0.76	0.74	0.08	0.49	0.84	0.58	0.59	0.09	1
I_γ	1.02	2.11	1.66	1.64	0.3	0.93	1.9	1.36	1.34	0.25	1

Radiation Hazard Index

Gamma radiation Index, I_γ

The results obtained give maximum values of I_γ equal to 2.12 and 2.67 at Fongo-Tongo and equal to 2.12 and 1.90 at Dschang for in situ and laboratory measurements, respectively, which are significantly greater than or equal to 2 to 2.7 times the maximum permissible value [1]. Similarly, the mean values of 1.69 and 1.34 at Dschang and 1.58 and 1.64 at Fongo-Tongo are also above the recommended limit.

Thus, the land in the region could be exempted from all types of restrictions with respect to radiological risks, except at certain locations where I_γ is very high.

Alpha Radiation Index, I_α

The average values of I_α are reported in Table 3.18 and 3.19 and are below the reference limit value of unity for both study sites. Therefore, the soil bricks made at the study sites can be used as a building material in these two localities without exposing the inhabitant to a major risk of induction of lung cancer, because the I_α is below the safety limit recommended by **UNSCEAR**.

Bibliography

[1] UNSCEAR, Sources and effects of ionizing radiation, United Nations Scientific Committee on the Effects of Atomic Radiation, UNSCEAR 2000 report to the General Assembly, with scientific annexes, Vienna, Austria 2000: United Nations, 2000.

[2] Saïdou, Mesure de la radioactivité naturelle environnementale par spectrométries α et γ et calcul de la dose au public : application a la région uranifère de poli, Thesis, 2008.

[3] J. Barbarand *et al*., Géologie et Chimie de l'Uranium Programme et volume des résumés, 2011.

[4] A. Holmes, Petrogenesis of katungite and its associates, American Mineralogist, vol. 35, no. 9?10. pp. 772-792, 1950.

[5] J. G. P. Bariand, F. Cesbron, métamorphiques et leurs produits d'altération , par P . Bariand , F ., Bulletin de Minéralogie et de Cristallographie, vol. 2, no. 102-104, p. 356, 1978.

[6] R. Maximilien, M. C. Robe, and M. Archimbaud, Etude du transfert du radon 222 à l'intérieur des habitations, Radioprotection, vol. 20, no. 1, pp. 45-60, 1985. doi: 10.1051/radiopro/19852001045.

[7] WHO, World Health Organization Regional Office for Europe SELECTED POLLUTANTS, Denmark, 2010. [Online]. Available: www.euro.who.int. (accessed on 28 September 2022)

[8] N. M. Hassan *et al*., Assessment of the natural radioactivity using two techniques for the measurement of radionuclide concentration in building materials used in Japan, Journal of Radioanalytical and Nuclear Chemistry, vol. 283, no. 1, pp. 15-21, 2010, doi: 10.1007/s10967-009-0050-6.

[9] R. S. Mohammed and R. S. Ahmed, Estimation of excess lifetime cancer risk and radiation hazard indices in southern Iraq, Environmental Earth Sciences, vol. 76, no. 7, pp. 1?9, 2017, doi: 10.1007/s12665-017-6616-7.

[10] R. Trevisi, F. Leonardi, S. Risica, and C. Nuccetelli, Updated database on natural radioactivity in building materials in Europe, Journal of Environmental Radioactivity, vol. 187, no. January, pp. 90-105, 2018, doi: 10.1016/j.jenvrad.2018.01.024.

[11] P. Ele Abiama, S. Tokonami, and E. Abiama Patrice, Natural Radiation Survey in the Uranium and Thorium Bearing Regions of Cameroon, Radiation protection and dosimetry, 2016.

[12] D. Takoukam Soh, Saïdou, M. Hosoda, J.E. Ndjana Nkoulou II, N. Akata, O. Bouba and S. Tokonami, Natural radioactivity measurements and external dose estimation by car-borne survey in Douala city, Cameroon, Radioprotection, vol. 53, no. 4, pp. 255-263, Oct. 2018, doi: 10.1051/radiopro/2018032.

[13] B. C. Yimele, H. P. F. Ekobena, E. J. M. Nguelem, M. M. Ndontchueng, G. H. Ben-Bolie, and P. O. Ateba, Radiation hazard of naturally occurring soil in FONGO TONGO-Cameroon, Arabian Journal of Geosciences, vol. 12, no. 7, Apr. 2019, doi: 10.1007/s12517-019-4410-4.

[14] M. Ndontchueng, E. J. M. Nguelem1,2, O. Motapon2, R. L. Njinga1, A. Simo1, J. C. S. Guembou2 and B. Yimele, Radiological Hazards in Soil from the Bauxite Deposits Sites in Dschang Region of Cameroon, British Journal of Applied Science & Technology, vol. 5, no. 4, pp. 342-352, Jan. 2015, doi: 10.9734/bjast/2015/13352.

[15] S. Bachirou, Saïdou , N. N. Joseph Emmanuel, H. Flix, and K. N. Moïse Godfroy, Natural radiation exposure and radiological hazard analysis in a radon-prone area of the adamawa region, cameroon, Radiation Protection Dosimetry, vol. 198, no. 1-2, pp. 74?85, 2022, doi: 10.1093/rpd/ncab183.

[16] Saïdou, O. B. Modibo, N. N. I. J. Emmanuel, O. German, K. N. Michaux, and H. Y. Abba, Indoor radon measurements using radon track detectors and electret ionization chambers in the bauxite-bearing areas of Southern Adamawa, Cameroon, International Journal of Environmental Research and Public Health, vol. 17, no. 18, pp. 1-12, Sep. 2020, doi: 10.3390/ijerph17186776.

[17] Saïdou, Tokonami Shinji, Masahiro Hosoda, Tchuente Siaka Yvette Flore, Ndjana Nkoulou Joseph Emmanuel II, Akata Naofumi, Oumar Bobbo Modibo, Penaye Joseph, Natural radiation exposure to the public in the uranium bearing region of Poli, Cameroon: From radioactivity measurements to external and inhalation dose assessment, Journal of Geochemical Exploration, vol. 205, Oct. 2019, doi: 10.1016/j.gexplo.2019.106350.

[18] J. E. Ndjana Nkoulou, Louis Ngoa Engola, Saïdou, Masahiro Hosoda, Daniel Bongue, Takahito Suzuki, Hiromi Kudo, Moïse Godfroy Kwato Njock and Shinji Tokonami, Simultaneous indoor radon, thoron and thoron progeny measurements in betare-oya gold mining

areas, eastern cameroon, Radiation Protection Dosimetry, vol. 185, no. 3, pp. 391-401, Dec. 2019, doi: 10.1093/rpd/ncz026.

[19] F. Paquet, M. R. Bailey, M. R. Leggett, J. Lipsztein, J. Marsh, T. P. Fell, ICRP Publication 137: Occupational Intakes of Radionuclides: Part 3, Annals of the ICRP, vol. 46, no. 34, pp. 1-486, Dec. 2017, doi: 10.1177/0146645317734963.

[20] G. S. Bineng, Saïdou1, Shinji Tokonami, Masahiro Hosoda, Yvette Flore Tchuente Siaka2 , Hamadou Issa1 , Takahito Suzuki, Hiromi Kudo and Oumarou Bouba, The Importance of Direct Progeny Measurements for Correct Estimation of Effective Dose Due to Radon and Thoron, Frontiers in Public Health, vol. 8, Feb. 2020, doi: 10.3389/fpubh.2020.00017.

[21] M. Kaur and A. Kumar, Dose assessment from exposure to radon , thoron and their progeny concentrations in the dwellings of sub-mountainous region of Jammu & Kashmir , India, Journal of Radioanalytical and Nuclear Chemistry, 2017, doi: 10.1007/s10967-017-5632-0.

[22] Saïdou, S. Tokonami, M. Janik, B. G. Samuel, Abdourahimi, and N. N. Joseph Emmanuel, Radon-thoron discriminative measurements in the high natural radiation areas of southwestern Cameroon, Journal of Environmental Radioactivity, vol. 150, pp. 242-246, Dec. 2015, doi: 10.1016/j.jenvrad.2015.09.006.

[23] Saïdou, P. Ele Abiama, and S. Tokonami, Comparative study of natural radiation exposure to the public in three uranium and oil regions of Cameroon, Radioprotection, vol. 50, no. 4, pp. 265?271, Oct. 2015, doi: 10.1051/radiopro/2015017.

[24] H. Nuhu *et al*., Soil gas radon and soil permeability assessment: Mapping radon risk areas in Perak State, Malaysia, PLoS ONE, vol. 16, no. 7 July, pp. 1-17, 2021, doi: 10.1371/journal.pone.0254099.

[25] Takoukam Soh, Saïdou, Shinji Tokonami, Masahiro Hosoda, Takahito Suzuki, Hiromi Kudo and Oumarou Bouba, Simultaneous measurements of indoor radon and thoron and inhalation dose assessment in Douala City, Cameroon, Isotopes in Environmental and Health Studies, vol. 55, no. 5, pp. 499-510, 2019, doi: 10.1080/10256016.2019.1649258.

[26] J. Charuau, V.Labed , M. C. Robé, J. C.Thévenin and G. Tymen, Le radon 222 et ses descendants à vie courte dans l'environnement atmosphérique : origine et méthodes de mesure. Fiche CIRP, Radioprot. 31,371-388 (1996).

[27] The United Nations Scientific Committee on the Effects of Atomic Radiation. UNSCEAR 2000 Report, Vol. I : sources and effects of ionizing radiation. United Nations, New York (2000).

[28] M. Fulop, P. Ragan, S. Krnac, in situ spectrometry of ^{137}Cs in soil by an unfolding method,Journal of Radiological Analyt. and Nucl. Chem. 209, 373-380 (1996).

[29] The International Commission on Radiation Units and measurements, ICRU Report 53, Gamma-ray spectrometry in the environment, Sèvres France (1994).

[30] H. Matsuda, S. Minato and V. Pasquale, Evaluation of accuracy of response matrix method for environmental gamma ray analysis, Radioisot. 51, 42-50 (2002).

[31] K. Lai, S. Hu, K. Kodairi, S. Minato, A car-borne survey of terrestrial gamma-ray dose rates in Brunei Darussalam, Radioisotopes 45, 696-699 (1996).

[32] S. Turhan, I.H. Arikan, F. Oguz, T. Azdemir, B. Yuce, A. Varinlioglu, A. Kose, C arborne survey of natural background gamma dose rate in ¸Canakkale Region, Turkey, Radiat. Prot. Dosim. 148, 45-50, (2012).

[33] M. Hosoda, S. Tokonami, A. Sorimachi, S. Monzen, M. Osanai, M. Yamada, I. Kashiwakura, S. Akiba, The time variation of dose rate artificially increased by the Fukushima nuclear crisis, Sci. Reports 1, 87-98 (2011).

[34] K. Inoue, M. Arai, M. Fujisawa, K. Saito, M. Fukushi, Detailed Distribution Map of Absorbed Dose Rate in Air in Tokatsu Area of Chiba Prefecture, Japan, Constructed by Car-Borne Survey 4 Years after the Fukushima Daiichi Nuclear Power Plant Accident, PLoS ONE 12,1-13 (2017).

[35] Canberra, GENIE 2000-Logiciel de spectrométrie gamma, version 3.2.

[36] The International Atomic Energy Agency, IAEA (ENV94084-200g) by Analytic Inc, Atlanta, GA, USA.

[37] M. Hosoda, Shinji Tokonami, Yasutaka Omori, Sarata Kumar Sahoo, Suminori Akiba, Atsuyuki Sorimachi, Tetsuo Ishikawa, Raghu Ram Nair, Padmavathy Amma Jayalekshmi, Paul Sebastian, Kazuki Iwaoka, Naofumi Akata, Hiromi Kudo, Estimation of external dose by car-borne survey in Kerala, India, PLoS ONE, vol. 10, no. 4, Apr. 2015. doi: 10.1371/journal.pone.0124433.

[38] Y. Omori, Shinji Tokonami, Sarata Kumar Sahoo, Tetsuo Ishikawa, Atsuyuki Sorimachi, Masahiro Hosoda, Hiromi Kudo, Chanis Pornnumpa, Raghu Ram K Nair, Padmavaty Amma Jayalekshmi, Paul Sebastian and Suminori Akiba, Journal of Radiological Protection, vol. 37, no. 1, pp. 111-126, 2017, doi: 10.1088/1361-6498/37/1/111.

[39] J. Humblet, Physique Nucléaire, Nuclear Physics, vol. 28, no. 1. p. 6-91, 1961, doi: 10.1016/0029-5582(61)91107-5.

[40] F. Leplingard *et al*., FWM-Assisted Raman Laser for Second-Order Raman Pumping, Optics InfoBase Conference Papers. pp. 431-432,2003.

[41] N. Takigawa and K. Washiyama, Fundamentals of nuclear physics. 2017.

[42] H. Curien, La radioactivité des roches , par R . Coppens , Collection «?Que sais- je?» n ° 741 , 1957, Presses Universitaires de France, Paris, vol. 1, 1957.

[43] M. E. Denaeyer, Les syénites métasomatiques du massif de Kirumba?: Contribution à la lithogenèse des volcans du Kivu (Congo Belge), Mémoires, Académie des Sciences Coloniales, vol. 9, no. 1, p. 2-38, 1959.

[44] Pierre Curie, Marie Curie et Gustave Bémont, « Sur une nouvelle substance fortement radioactive, contenue dans la pechblende », Comptes Rendus, vol. 127-1898

[45] David R. Lide, CRC Handbook of Chemistry and Physics, CRC, 2009, 89e éd., p. 10-203

[46] G Wlérick, F Prégermain, Étude des propriétés physiques des couches minces photosensibles de sulfure de cadmium J. Phys. Radium, 1954

[47] D. R. Lide, CRC Handbook of Chemistry and Physics, Boca Raton (FL), CRC Press, 2004, 84e éd., 2616 p. (ISBN 978-0-8493-0484-2).

[48] Hammond, C. R. "Radium" in Haynes, William M., ed. (2011). CRC Handbook of Chemistry and Physics (92nd ed.). Boca Raton, FL: CRC Press. (ISBN 1439855110).

[49] W. B. Li, J. Tschiersch, U. Oeh, and C. Hoeschen, Lung Dosimetry of Inhaled Thoron Decay Products, 2014.

[50] D. U. Matériau, Etude de l'émanation du radon à partir de résidus miniers de traitement de minerais d'uranium, thèse, 1997.

[51] G. Tymen and D. Laurier, État des connaissances actuelles sur l'évaluation du risque sanitaire lié au radon Current state of knowledge about radon health risk assessment, no. 1, pp. 1-17, 2013.

[52] H. Métivier, Radioprotection et ingénierie nucléaire,EDP Sciences, 2006.

[53] The 2007 Recommendations of the International Commission on Radiological Protection, ICRP publication 103, Annals of the ICRP, vol. 37, no. 2?4, pp. 1-332, 2007, doi: 10.1016/j.icrp.2007.10.003.

[54] Cours de radioprotection, Edition septembre [Online]. Available: http://www.chuv.ch/ira. (accessed on 13 january 2023), 2014.

[55] M. R. Kibler, J. Poizat, M. R. Kibler, and J. P. La, La Physique pour la Santé: du diagnostic à la thérapie, To cite this version: HAL Id: hal-00001383 La Physique pour la Santé: du diagnostic à la thérapie, 2006.

[56] J. E. Ndjana Nkoulou, A. Manga, Saïdou, O. German, C. Sainz-Fernandez, and M. G. Kwato Njock, Natural radioactivity in building materials, indoor radon measurements, and assessment of the associated risk indicators in some localities of the Centre Region, Cameroon, Environmental Science and Pollution Research, 2022, doi: 10.1007/s11356-022-19781-z.

[57] M. Ngachin, M. Garavaglia, C. Giovani, M. G. Kwato Njock, and A. Nourreddine, Assessment of natural radioactivity and associated radiation hazards in some Cameroonian building materials, Radiation Measurements, vol. 42, no. 1, pp. 61-67, 2007, doi: 10.1016/j.radmeas.2006.07.007.

[58] A. Suhono, Sustainable Development (Sustainable Development) in Changes to the Global Environment, no. July, pp. 1-26, 2004.

[59] S. Mvondo, G. H. Ben-Bolie, J. M. E. a. Ema'a, P. O. Ateba, P. Ele abiama, and J. F. B. Ateba, Study of soil-fern transfer of naturally occurring alpha emitting radionuclides in the Southern Region of Cameroon, Journal of Environmental Radioactivity, vol. 180, no. October, pp. 114-119, 2017, doi: 10.1016/j.jenvrad.2017.10.007.

[60] S. Mvondo, J. F. Beyala Ateba, G. H. Ben-Bolie, P. Owono Ateba, A. Simo, and H. F. Ekobena, Dose estimates to the public due to 210 Po ingestion via cocoa powder from Lolodorf high background radiation area Cameroon, Radioprotection, vol. 53, no. 3, pp. 193-198, 2018, doi: 10.1051/radiopro/2018022.

[61] P. Ele Abiama, P. Owono Ateba, G. H. Ben-Bolie, F. H. P. Ekobena, and T. El Khoukhi, High background radiation investigated by gamma spectrometry of the soil in the southwestern region of Cameroon, Journal of Environmental Radioactivity, vol. 101, no. 9, pp. 739-743, 2010, doi: 10.1016/j.jenvrad.2010.04.017.

[62] Jean Félix BEYALA ATEBA *et al.*, Determination of Uranium in Rocks and Soils of South Cameroon by γ-ray Spectrometry, RADIOISOTOPES, 2011.

[63] Saïdou,,F. O. Bochud, S. Baechler, K. N. Moïse, N. Merlin, and P. Froidevaux, Natural radioactivity measurements and dose calculations to the public: Case of the uranium-bearing

region of Poli in Cameroon, Radiation Measurements, vol. 46, no. 2, pp. 254-260, Feb. 2011, doi: 10.1016/j.radmeas.2010.11.009.

[64] D. Guy Blanchard, N. Engola Louis, N. I. Nkoulou Joseph Emmanuel, T. Siaka Yvette Flore, B. Daniel, and K. Njock Moïse Godfroy, NORM measurements and radiological hazard assessment in the gold mining areas of Eastern Cameroon, Radiation Environment and Medicine, vol. 6, no. 1, pp. 22-28, 2017.

[65] S. Bachirou, I. I. Joseph, E. Ndjana, F. Haman, M. Godfroy, and K. Njock, Natural Radiation expeosure and radiological hazard analysis in radon-prone area of the Adamawa region, Cameroon, NATURAL RADIATION EXPOSURE AND RADIOLOGICAL HAZARD ANALYSIS IN A RADON-PRONE AREA OF THE ADAMAWA REGION , CAMEROON, pp. 1-12, 2022.

[66] A. Richard, K. François, B. G. Samuel, N. Ayoba, T. S. S. Didier, and Saïdou, Contribution of ^{40}K arising from agropastoral activities to the total effective dose by plant ingestion in the Far-North, Cameroon, AIMS Environmental Science, vol. 9, no. 4, pp. 444-460, 2022, doi: 10.3934/environsci.2022027.

[67] K. François, A. Richard, B. G. Samuel, N. Ayoba, H. Y. Abba, and B. G. Hubert, Assessment of Natural Radiation Exposure Due to ^{222}Rn and External Radiation Sources: Case of the Far North , Cameroon, no. May, pp. 1-13, 2022, doi: 10.1097/HP.0000000000001609.

[68] Sadjo, Takoukam Soh Didier, H. Yerima Abba, V. Valentin, Saïdou, and M. Alidou, Soil gas radon, indoor radon and its diurnal variation in the northern region of Cameroon, Isotopes in Environmental and Health Studies, vol. 0, no. 0, pp. 1-18, 2022, doi: 10.1080/10256016.2022.2102617.

[69] S. Mbida Mbembe *et al*., Indoor radon, external dose rate and assessment of lung cancer risk in dwellings: the case of Ebolowa town, Southern Cameroon, International Journal of Environmental Analytical Chemistry, vol. 00, no. 00, pp. 1-17, 2021, doi: 10.1080/03067319.2021.1946684.

[70] P. L. Kenfack, P. Tematio, M. Kwekam, G. Ngueutchoua, and P. R. Njike, Evidence of a Miocene volcano-sedimentary lithostratigraphic sequence at Ngwa (Dschang Region, West Cameroon): Preliminary analyses and geodynamic interpretation, Journal of Petroleum Technology and Alternative Fuels, 2011.

[71] P. E. Tedonkeng *et al*., Rainfall Variability along the Southern Flank of the Bambouto Mountain (West-Cameroon), Journal of the Cameroon academy of sciences, 2008.Vol. 8 N o.1, 2008.

[72] F. Nguimatsia Dongmo *et al*., Geochemical, mineralogical and macroscopic facies of the Fongo-Tongo bauxite deposit western Cameroon, Applied Earth Science, Transactions of the Institute of Mining and Metallurgy, vol. 130, no. 1, pp. 23-41, 2021, doi: 10.1080/25726838.2020.1861916.

[73] F. Dongmo, R. Yongue, A. Bolarinwa, R. Ngatcha, C. Fuanya, and M. A. Kamga, Contribution to the Study of Bauxites Formation in the Fongo-Tongo (Western Cameroon) Sites, no. January. Springer International Publishing, 2019.

[74] U. C. Tchamba , R.Yongue, Caractérisation de la bauxite de HaléoDanielle (MinimMartap, Cameroun) en vue de son utilisation industrielle dans les matériaux à haute teneur en alumine, Sil.Ind, vol. 73, p. Nr 5-6, 2008.

[75] A. Sylvain *et al*., Mineralogical and Geotechnical Characteristics of the Loose Weathered Trachytes of Fongo-Tongo (West-Cameroon), 2014.

[76] SARAD GmbH. Nuc Scout, Portable Gamma Identifier?Quantifier?Dose Rate Meter. 2018. Available online: www.sarad.de/ info@sarad.de (accessed on 8 September 2022)

[77] ARAD GmbH. Manual Software dVISION. Wiesbadener Straße 10 D-01159 Dresden Germany. 2015. Available online: https: //www.sarad.de/cms/media/docs/handbuch/Manual_dVISION_EN_16-10-15.pdf (accessed on 8 September 2022).

[78] SARAD GmbH. Manual Software dCONFIG. Wiesbadener Straße 10 D-01159 Dresden DEUTSCHLAND. 2009. Available online: http://www.sarad.de/cms/media/docs/handbuch/Manual_dCONFIG_EN_21-12-12.pdf (accessed on 8 September 2022).

[79] Saïdou, F. Bochud, J. P. Laedermann, M. G. Kwato Njock, and P. Froidevaux, A comparison of alpha and gamma spectrometry for environmental natural radioactivity surveys, Applied Radiation and Isotopes, vol. 66, no. 2, pp. 215-222, Feb. 2008, doi: 10.1016/j.apradiso.2007.07.034.

[80] H. MATSUDA, S. MINATO, and V. PASQUALE, Evaluation of Accuracy of Response Matrix Method for Environmental Gamma Ray Analysis, Radioisotopes, vol. 51, no. 1, pp. 42-50, 2002, doi: 10.3769/radioisotopes.51.42.

[81] D. Lide, Limits for Qualitative Detection and Quantitative Determination, A Century of Excellence in MEASUREMENTS STANDARDS and TECHNOLOGY, pp. 164-166, 2018, doi: 10.1201/9781351069397-46.

[82] IAEA, http://www ns.iaea.org/standards/, p. 370, 1996.

[83] AIEA, Gamma-ray and X-ray spectrometry with semiconductor detectors International Nuclear Information SystemI, 1988 Nuclear, 50 + years of INIS,

[84] Saïdou, F. Bochud, J. P. Laedermann, T. Buchillier, K. Njock Moïse, and P. Froidevaux, Calibration of an HPGe detector and self-attenuation correction for 210Pb: Verification by alpha spectrometry of 210Po in environmental samples, Nuclear Instruments and Methods in Physics Research, Section A: Accelerators, Spectrometers, Detectors and Associated Equipment, vol. 578, no. 3, pp. 515-522, Aug. 2007, doi: 10.1016/j.nima.2007.06.002.

[85] E. Gasser, Spectrométrie gamma au laboratoire et in situ: développements et applications environnementales, p. 4, 2014.

[86] M. García-Talavera, J. P. Laedermann, M. Décombaz, M. J. Daza, and B. Quintana, Coincidence summing corrections for the natural decay series in γ-ray spectrometry, Applied Radiation and Isotopes, vol. 54, no. 5, pp. 769-776, 2001, doi: 10.1016/S0969-8043(00)00318-3.

[87] ISO 18589-7 2013(en), Measurement of radioactivity in the environment Soil Part 7 In situ measurement of gamma-emitting radionuclides.

[88] Q. Shi, J. Zhang, Y. Chang, and S. Qian, Comparison between summing-up algorithms to determine areas of small peaks on high baselines, Nuclear Instruments and Methods in Physics Research, Section A: Accelerators, Spectrometers, Detectors and Associated Equipment, vol. 555, no. 1-2, pp. 220-224, 2005, doi: 10.1016/j.nima.2005.09.013.

[89] J.F. Bottollier-Depois S. Charmasson, L. Foulquier, P. Germain, D. Klein, J. Levrard, P. Livolsi, J. Lochard, J. Lombard, M. Masson, H. Maubert, H. Métivier, A. Rannou, V. Tort. J.Y. Pipaud (conception), R. Poulard (dessin), M. Beugin (mise en couleur et mise en page) CLAIR-SOLEIL NEW imprimerie ? Aubagne Repères, La radioactivité en 10 épisodes, Société Francaise de Radioprotection 2019.

[90] G. K. Skinner, Practical gamma-ray spectrometry, vol. 52, no. 3. Wiley, 1996.

[91] T. Vidmar and M. Korun, Calculation of LS-curves for coincidence summing corrections in gamma ray spectrometry, Nuclear Instruments and Methods in Physics Research, Section A: Accelerators, Spectrometers, Detectors and Associated Equipment, vol. 556, no. 2, pp. 543-546, 2006, doi: 10.1016/j.nima.2005.11.052.

[92] T. Standard, INTERNATIONALE iTeh STANDARD Partie 1: PREVIEW Applications élémentaires iTeh STANDARD PREVIEW,vol 2. 2019.

[93] F. Panza, Développement de la spectrométrie gamma in situ pour la cartographie de site, p. 221, Thesis, 2012. [Online]. Available: https://www.irsn.fr/FR/Larecherche/Formation recherche/Theses/Theses-soutenues/DEI/Documents/2012-These-Panza.pdf.(accessed Oct 17, 2022)

[94] Gammadata. User's Guide MARKUS 10 The Instrument for Determining the Radon Content in soil; Gammadata: Uppsala, Sweden, 2019.

[95] ISO 11665-4, ISO 11665-4 2021(en), Measurement of radioactivity in the environment Air: radon-222, Part 4: Integrated measurement method for determining average activity concentration using passive sampling and delayed analysis. 2021.

[96] R. FTLab, RadonEye Plus2 (BLE & Wi-Fi) [Online http://radonftlab.com/radon-sensor-product /radon-detector/new-rd200p-radon-detector, Vol. 2, pp. 2-5, 020 (accessed Oct 3, 2022).

[97] Y. Omori, M. Janik, A. Sorimachi, T. Ishikawa, and S. Tokonami, Effects of air exchange property of passive-type radon-thoron discriminative detectors on performance of radon and thoron measurements, Radiation Protection Dosimetry, vol. 152, no.

[98] T. ZHUO, Weihai; Iida, Estimation of Thoron Progeny Concentrations in Dwellings with Their Deposition Rate Measurements., Japanese Journal of Health Physics, vol. 35, no. 3, pp. 365?370, 2000 , doi: 10.5453/jhps.35.365.

[99] ISO 16641, International Organisation for Standardisation, Measurement of radioactivity in the environment Air Radon 220 Integrated measurement methods for the determination of the average activity concentration using passive solid state nuclear track detect, Geneva 2014. Available Online: http://www.iso.org/iso/catalogue_detail.htm?csnumber=57347.(accessed jan 3, 2022)

[100] Y. Mayya *et al*, Deposition based passive monitors for assigning radon, thoron inhalation doses for epidemiological studies, Radiation Protection Dosimetry, 2012.

[101] A. Sorimachi, S. Tokonami, C. Kranrod, and T. Ishikawa, Preliminary experiments using a passive detector for measuring indoor 220Rn progeny concentrations with an aerosol chamber, Health Physics, vol. 108, no. 6, pp. 597?606, Jun. 2015, doi: 10.1097/HP.0000000000000284.

[102] J. Kemski, R. Klingel, A. Siehl, and M. Valdivia-Manchego, From radon hazard to risk prediction-based on geological maps, soil gas and indoor measurements in Germany, Environmental Geology, vol. 56, no. 7, pp. 1269-1279, 2009, doi: 10.1007/s00254-008-1226-z.

[103] Neznal and M. Neznal, Permeability as an important parameter for radon risk classification of foundation soils, Annals of Geophysics, vol. 48, no. 1, 2009, doi: 10.4401/ag-3192.

[104] M. Neznal and M. Neznal, Analysis of problems and failures in the measurement of soil-gas radon concentration, Radiation Protection Dosimetry, vol. 160, no. 1?3, pp. 214?216, 2014, doi: 10.1093/rpd/ncu088.

[105] Y. Muhsin Zayir Al-bakhat, Measurement of Radon Activity in Soil Gas and the Geogenic Radon Potential Mapping Using RAD7 at Al-Tuwaitha Nuclear Site and the Surrounding Areas, Radiation Science and Technology, vol. 3, no. 3, p. 29, 2017, doi: 10.11648/j.rst.20170303.13.

[106] E. Lara,Z. Rocha, T. O. Santos, F. J. Rios, and A. H. Oliveira, Soil features and indoor radon concentration prediction: Radon in soil gas, pedology, permeability and ^{226}Ra content, Radiation Protection Dosimetry, vol. 167, no. 1-3, pp. 126-129, 2015, doi: 10.1093/rpd/ncv228.

[107] Y. Prasad, G. Prasad, G. S. Gusain, V. M. Choubey, and R. C. Ramola, Radon exhalation rate from soil samples of South Kumaun Lesser Himalayas, India, Radiation Measurements, vol. 43, no. SUPPL.1, pp. 369-374, 2008, doi: 10.1016/j.radmeas.2008.04.056.

[108] F. S. Erees, G. Yener, M. Salk, and Ö. Özbal, Measurements of radon content in soil gas and in the thermal waters in Western Turkey, Radiation Measurements, vol. 41, no. 3, pp. 354-361, 2006, doi: 10.1016/j.radmeas.2005.06.030.

[109] M. Karthik Kumar, N. Nagaiah, G. Mathews, and M. Ambika, Assessment of annual effective dose due to outdoor radon activity in the environment of Bengaluru, Radiation Protection and Environment, vol. 41, no. 3, p. 115, 2018, doi: 10.4103/rpe.rpe_40_18.

[110] Gondji *et al.*, Radon Risk Assessment and Correlation Study of Indoor Radon , Radium 226 , and Radon in Soil at the Cobalt-Nickel Bearing Area of Lomié , Eastern Cameroon, Water, Air, & Soil Pollution, pp. 1-16, 2022, doi: 10.1007/s11270-022-05666-x.

[111] UNSCEAR, Sources and Effects of Ionizing Radiation. Official Records of the General Assembly UNSCEAR 2000 Report to the General Assembly, with Scientific Annexes. ANNEX A Dose Assessment Methodologies, vol. I. United Nations, 2000.

[112] United Nations, Scientific Committee on the Effects of Atomic Radiation., Sources and effects of ionizing radiation?: United Nations Scientific Committee on the Effects of Atomic Radiation: UNSCEAR 2000 report to the General Assembly, with scientific annexes. United Nations, 2000.

[113] U. Nations, S. Committee, A. Radiation, G. Assembly, and S. Annexes, SOURCES AND EFFECTS United Nations Scientific Committee on the Effects of Atomic Radiation, vol. I. 2008.

[114] M. Tirmarche, J. D. Harrison, D. Laurier, F. Paquet, E. Blanchardon, and J. W. Marsh, Part 1: Lung Cancer Risk from Radon and Progeny, Annals of the ICRP, vol. 40, no. 1, p. 11, Feb. 2010, doi: 10.1016/j.icrp.2011.08.011.

[115] S. Kumar, S. Singh, B. S. Bajwa, B. Singh, A. D. Sabharwal, and K. P. Eappen, Indoor inhalation dose estimates due to radon and thoron in some areas of South-Western Punjab, India, Radiation Protection Dosimetry, vol. 151, no. 1, pp. 112-116, 2012, doi: 10.1093/rpd/ncr461.

[116] E. Blanchardon, D. Laurier, F. Paquet, J. F. Lecomte, and M. Tirmarche, Dosimétrie du radon: les points de vue de l'UNSCEAR et de la CIPR sont-ils contradictoires, Radioprotection, vol. 44, no. 2, pp. 207-216, 2009, doi: 10.1051/radiopro/2009007.

[117] R. S. Mohammed and R. S. Ahmed, Estimation of excess lifetime cancer risk and radiation hazard indices in southern Iraq, Environmental Earth Sciences, vol. 76, no. 7, 2017, doi: 10.1007/s12665-017-6616-7.

[118] P. Pisapak, N. Todorovic, and T. Bhongsuwan, Correlation between radon and radium concentrations in soil and estimation of natural radiation hazards in Namom district, Songkhla province (Southern Thailand), Environmental Earth Sciences, vol. 76, no. 4, pp. 1-11, 2017, doi: 10.1007/s12665-017-6439-6.

[119] C. Yu et al., User's manual for RESRAD version 6, Environmental Assessment Division, ANL, p. 458, 2001,Online. Available: http://resrad.evs.anl.gov/docs/resrad6.pdf.

[120] M. Tirmarche, J. D. Harrison, D. Laurier, F. Paquet, E. Blanchardon, and J. W. Marsh, ««Prev Next»» Lung Cancer Risk from Radon and Progeny and Statement on Radon. Available Online: http://www.icrp.org/publication.asp?id= ICRP Publication 115.

[121] Annals o f the ICRP, 2015, Available Online: http://ani.sagepub.com/.

[122] B. Hiéronymus, Etude minéralogique et géochimique des formations bauxitiques de l'Ouest du Cameroun, pp. 97-112, ORSTOM, sér Géol 1973.

[123] I. N. Waterways, Sediments and pollution General Considerations, no. October 1982, p. 33, IAEA: Vienna, Austria, p. 33, 1984.

[124] D. T. Esan *et al*., Determination of Residential Soil Gas Radon Risk Indices Over the Lithological Units of a Southwestern Nigeria University, Scientific Reports, pp. 1-10, 2020, doi: 10.1038/s41598-020-64217-8.

[125] M. M. Orosun, M. R. Usikalu, K. J. Oyewumi, and J. A. Achuka, Radioactivity levels and transfer factor for granite mining field in Asa, North-central Nigeria, Heliyon, vol. 6, no. 6, p. e04240, 2020, doi: 10.1016/j.heliyon.2020.e04240.

[126] P. L. Kenfack P. Tematio, M. Kwekam, G. Ngueutchoua, and P. R. Njike, Evidence of a Miocene volcano-sedimentary lithostratigraphic sequence at Ngwa (Dschang Region, West Cameroon): Preliminary analyses and geodynamic interpretation, Journal of Petroleum Technology and Alternative Fuels, vol. 2, no. 3, pp. 25-34, 2011, . Availabl Onlinee: http://www.academicjournals.org/JPTAF, (accessed Sep 23, 2022).

[127] K. Aladeniyi, C. Olowookere, and B. B. Oladele, Measurement of natural radioactivity and radiological hazard evaluation in soil samples collected from Owo, Ondo State, Nigeria, Journal of Radiation Research and Applied Sciences, vol. 12, no. 1, pp. 200-209, 2019, doi: 10.1080/16878507.2019.1593675.

[128] D. A. E. Darwish, K. T. M. Abul-Nasr, and A. M. El-Khayatt, The assessment of natural radioactivity and its associated radiological hazards and dose parameters in granite samples from South Sinai, Egypt, Journal of Radiation Research and Applied Sciences, vol. 8, no. 1, pp. 17-25, 2015, doi: 10.1016/j.jrras.2014.10.003.

[129] B. Merdanolu and N. Altinsoy, Radioactivity concentrations and dose assessment for soil samples from Kestanbol granite area, Turkey, Radiation Protection Dosimetry, vol. 121, no. 4, pp. 399-405, 2006, doi: 10.1093/rpd/ncl055.

[130] J. Sannappa, C. Ningappa, and K. N. P. Narasimha, Natural radioactivity levels in granite regions of Karnataka State, Indian Journal of Pure and Applied Physics, vol. 48, no. 11, pp. 817-819, 2010.

[131] H. Saleh and M. Abu Shayeb, Natural radioactivity distribution of southern part of Jordan (Ma'an) Soil, Annals of Nuclear Energy, vol. 65, no. March, pp. 184-189, 2014 doi: 10.1016/j.anucene.2013.10.042.

[132] W. Boukhenfouf and A. Boucenna, The radioactivity measurements in soils and fertilizers using gamma spectrometry technique, Journal of Environmental Radioactivity, vol. 102, no. 4, pp. 336-339, 2011, doi: 10.1016/j.jenvrad.2011.01.006.

[133] Y. Raghu, R. Ravisankar, A. Chandrasekaran, P. Vijayagopal, and B. Venkatraman, Assessment of natural radioactivity and radiological hazards in building materials used in the Tiruvannamalai District, Tamilnadu, India, using a statistical approach, Journal of Taibah University for Science, vol. 11, no. 4, pp. 523-533, Jul.2017 doi: 10.1016/j.jtusci.2015.08.004.

[134] M. Ngachin, M. Garavaglia, C. Giovani, M. G. Kwato Njock, and A. Nourreddine, Radioactivity level and soil radon measurement of a volcanic area in Cameroon, Journal of Environmental Radioactivity, vol. 99, no. 7, pp. 1056?1060, 2008, doi: 10.1016/j.jenvrad.2007.12.022.

[135] E. J. Mekongtso Nguelem, M. Moyo Ndontchueng, and O. Motapon, Determination of 226Ra, 232Th, 40K, 235U and 238U activity concentration and public dose assessment in soil samples from bauxite core deposits in Western Cameroon, SpringerPlus, vol. 5, no. 1, Dec. 2016, doi: 10.1186/s40064-016-2895-9.

[136] E. J. M. Nguelem, M. M. Ndontchueng, O. Motapon, E. O. Darko, and A. Simo, Determination of 226Ra, 232Th, 40K and 235U in soil samples from bauxite core deposits in western Cameroon, Radioprotection, vol. 51, no. 3, pp. 199-205, Jul. 2016, doi: 10.1051/radiopro/2016029.

[137] H. U. Johner and H. Surbeck, Soil gas measurements below foundation depth improve indoor radon prediction, Science of the Total Environment, vol. 272, no. 1-3, pp. 337-341, 2001, doi: 10.1016/S0048-9697(01)00712-4.

[138] H. Friedmann *et al*., Indoor radon, geogenic radon surrogates and geology Investigations on their correlation, Journal of Environmental Radioactivity, vol. 166, pp. 382-389, 2017, doi: 10.1016/j.jenvrad.2016.04.028.

[139] J. Chen and K. L. Ford, A study on the correlation between soil radon potential and average indoor radon potential in Canadian cities, Journal of Environmental Radioactivity, vol. 166, pp. 152-156, 2017, doi: 10.1016/j.jenvrad.2016.01.018.

[140] D. Xie, M. Liao, and K. J. Kearfott, Influence of Environmental Factors on Indoor Radon Concentration Levels in the Basement and Ground Floor of a Building - A Case Study, 2015.

[141] I. Yarmoshenko *et al*., Variance of indoor radon concentration: Major influencing factors, Science of the Total Environment, vol. 541, pp. 155-160, Jan. 2016, doi: 10.1016/j.scitotenv.2015.09.077.

[142] V. M. Ramola, Correlation between geology and radon levels in groundwater , soil and indoor air in Bhilangana Valley , Garhwal Himalaya , India, vol. 32, no. November, pp. 258-262, 1997.

[143] P. S. Tsopjio Jiomeneck, P. Tematio, M. A. Wilson, and M. Yemefack, Andosolization of Soils on a Strombolian Cone at Mount Bambouto, Cameroon, Open Journal of Soil Science, vol. 01, no. 03, pp. 97-105, 2011, doi: 10.4236/ojss.2011.13013.

[144] P. Tematio *et al.*, Soils and their distribution on Bambouto volcanic mountain, West Cameroon highland, Central Africa, Journal of African Earth Sciences, vol. 39, no. 3-5, pp. 447-457, 2004, doi: 10.1016/j.jafrearsci.2004.07.020.

[145] Curien, H. La Radioactivit é des Roches, par R. Coppens, Collection « Que Sais-Je ? » N0 741,Presses Universitaires de France: Paris, France; Volume 1. 1957.

[146] B. Djeufack, G. S. Bineng, O. B. Modibo, J. Emmanuel, and N. Nkoulou, Correlation between Ground 222 Rn and 226 Ra and Long-Term Risk Assessment at the at the Bauxite Bearing Area of Fongo-Tongo , Western Cameroon, pp. 387-404, 2022.

[147] J. Chen, S. Tokonami, A. Sorimachi, H. Takahashi, and R. Falcomer, Preliminary results of simultaneous radon and thoron tests in Ottawa, Radiation Protection Dosimetry, vol. 130, no. 2, pp. 253-256, 2008, doi: 10.1093/rpd/ncm503.

[148] Z. Szabó *et al.*, Radon and thoron levels, their spatial and seasonal variations in adobe dwellings - a case study at the great Hungarian plain, Isotopes in Environmental and Health Studies, vol. 50, no. 2, pp. 211-225, 2014, doi: 10.1080/10256016.2014.862533.

[149] S. Zora *et al.*, Field experience with soil gas mapping using Japanese passive radon/thoron discriminative detectors for comparing high and low radiation areas in Serbia (Balkan region), Journal of Radiation Research, vol. 50, no. 4, pp. 355?361, 2009, doi: 10.1269/jrr.08098.

[150] B. Shang, B. Chen, Y. Gao, Y. Wang, H. Cui, and Z. Li, Thoron levels in traditional Chinese residential dwellings, Radiation and Environmental Biophysics, vol. 44, no. 3, pp. 193-199, Dec. 2005, doi: 10.1007/s00411-005-0020-5.

[151] Z. Stojanovska *et al.*, Prediction of long-term indoor radon concentration based on short-term measurements, Nuclear Technology and Radiation Protection, vol. 32, no. 1, pp. 77-84, 2017, doi: 10.2298/NTRP1701077S.

[152] R. Lindsay, R. T. Newman, and W. J. Speelman, A study of airborne radon levels in Paarl houses (South Africa) and associated source terms, using electret ion chambers and gamma-ray spectrometry, Applied Radiation and Isotopes, vol. 66, no. 11, pp. 1611?1614, Nov. 2008, doi: 10.1016/j.apradiso.2008.01.022.

[153] N. Primary, D. Water, and P. Rule, 40 CFR Parts 141 and 142 National Primary Drinking Water Regulations; Radionuclides; Notice of Data Availability; Proposed Rule, pp. 1-54, 2000.

[154] G. Dubois, An overview of radon surveys in Europe. European Communities, 2005.

[155] I. Malmonge Martin, Global journal of engineering science and researches radon gas intensity variation from april to july 2018 in são josé dos campos, brazil region, vol. 5, no. 8, 2018, doi: 10.5281/zenodo.1342502.

[156] K. Kojo and P. Kurttio, Indoor radon measurements in finnish daycare centers and schools-enforcement of the radiation act, International Journal of Environmental Research and Public Health, vol. 17, no. 8, Apr. 2020, doi: 10.3390/ijerph17082877.

[157] P. T. Huynh Nguyen, V. T. Nguyen, N. B. Vu, V. D. Nguyen, and H. Le Cong, Soil radon gas in some soil types in the rainy season in Ho Chi Minh City, Vietnam, Journal of Environmental Radioactivity, vol. 193?194, no. August, pp. 27?35, 2018, doi: 10.1016/j.jenvrad.2018.08.017.

[158] H. A. Yalim, I. Akkurt, F. B. Ozdemir, R. Unal, A. Sandikcioglu, and A. Akkurt, The measurement of radon and radium concentrations in well water in the Afyonkarahisar area of Turkey, Indoor and Built Environment, vol. 16, no. 1, pp. 77-81, 2007, doi: 10.1177/1420326X06074731.

[159] S. M. Farid, Indoor radon in dwellings of Jeddah city, Saudi Arabia and its correlations with the radium and radon exhalation rates from soil, Indoor and Built Environment, vol. 25, no. 1, pp. 269-278, 2016, doi: 10.1177/1420326X14536749.

[160] Saïdou, Abdourahimi, Y. F. Tchuente Siaka, and M. G. Kwato Njock, Natural radiation exposure to the public in the oil-bearing Bakassi Peninsula, Cameroon, Radioprotection, vol. 50, no. 1, pp. 35-41, Jan. 2015, doi: 10.1051/radiopro/2014025.

[161] W. E. Bolch, N. Petoussi-Henss, F. Paquet, and J. Harrison, ICRP dose coefficients: computational development and current status, 2016.

[162] Saïdou, Tokonami, S. and Elé Abiama, P. Natural radiation survey in the uranium and thorium bearing regions ofCameroon. Radiat. Environ. Med. 5(1), 53-58 2016.

[163] N. P. Petropoulos, M. J. Anagnostakis, and S. E. Simopoulos, Photon attenuation, natural radioactivity content and radon exhalation rate of building materials, Journal of Environmental Radioactivity, vol. 61, no. 3, pp. 257?269, 2002, doi: 10.1016/S0265-931X(01)00132-1.

[164] S. Gondji, Saïdou, O. Bobbo Modibo, D. Lepoire, and S. Tokonami, Risk Assessment of Exposure to Natural Radiation in Soil Using RESRAD-ONSITE and RESRAD-BIOTA in the Cobalt-Nickel Bearing Areas of Lomié in Eastern Cameroon, Radiation, vol. 2, no. 2, pp. 177-192, 2022, doi: 10.3390/radiation2020013.

[165] S. Risica, C. Bolzan, and C. Nuccetelli, Radioactivity in building materials: room model analysis and experimental methods, Science of the Total Environment, vol. 272, no. 1-3, pp. 119-126, 2001, doi: 10.1016/S0048-9697(01)00675-1.

[166] O. Baykara, M. Doru, M. Inceöz, and E. Aksoy, Measurements of radon emanation from soil samples in triple-junction of North and East Anatolian active faults systems in Turkey, Radiation Measurements, vol. 39, no. 2, pp. 209-212, 2005, doi: 10.1016/j.radmeas.2004.04.011.

[167] H. Baysson *et al.*, Exposition domestique au radon et risque de cancer du poumon,? Revue des Maladies Respiratoires, vol. 22, no. 4, pp. 587?594,2005, doi: 10.1016/s0761-8425(05)85611-6.

[168] I. Baldi *et al.*, Cancer et environnement: expertise collective - Hémopathies malignes, 2017, Available Online: https://hal-lara.archives-ouvertes.fr/hal-01570675. (accessed on 28 December 2022).

[169] R. Corrigan, Lung Cancer Risks to Canadians from Residential Radon Exposure, Thesis, 2017.

[170] Organisation mondiale de la Santé, Radon et cancer, Aide-mémoire no. 291, 2009.

[171] H. Zeeb and Z. Carr, Bulletin épidémiologique hebdomadaire Numéro thématique - Impact sanitaire du radon domestique: de la connaissance à l'action, Special issue - Health impact of radon: from knowledge to action Radon and lung cancer: call for public health policy, 2007.

[172] S. Darby Darby S, Hill D, Deo H, Auvinen A, Barros-Dios JM, Baysson H, Bochicchio F, Falk R, Farchi S, Figueiras A, Hakama M, Heid I, Hunter N, Kreienbrock L, Kreuzer M, Lagarde F, Mäkeläinen I, Muirhead C, Oberaigner W, Pershagen G, Ruosteenoja E, Schaffrath Rosario A, Tirmarche M, Tomá?ek L, Whitley E, Wichmann H-E, Doll R, Residential radon and lung cancer?detailed results of a collaborative analysis of individual data on 7148

persons with lung cancer and 14 208 persons without lung cancer from 13 epidemiologic studies in Europe, Scand J Work Environ Health, vol. 32, no. suppl 1, pp. 1-84, 2006.

[173] Handheld Detection for Any Scenario RadEye Selection Guide RadEye Product Family, 2012.

[174] UNSCEAR, Nations Scientific Committee on the Effects of Atomic Radiation, SOURCES AND EFFECTS OF IONIZING RADIATION United Nations Scientific Committee on the Effects of Atomic Radiation UNSCEAR 2000 Report to the General Assembly, with Scientific Annexes VOLUME II: SOURCES UNITED NATIONS, 2000.

[175] S. Penabei, D. Bongue1, P. Maleka, T. Dlamini, Saïdou, C.J. Guembou Shouop, Y.I. Halawlaw, A. Ngwa Ebongue6 and M.G. Kwato Njock, Assessment of natural radioactivity levels and the associated radiological hazards in some building materials from Mayo-Kebbi region, Chad, Radioprotection,vol. 53, no. 4, pp. 265-278, 2018, doi: 10.1051/radiopro/2018030.

[176] European Commission, Report on radiological protection principles concerning the natural radioactivity of building materials, radiation protection No. 112. Directorate-General Environment, Nuclear Safety and Civil Protection, 1999.

List of publications

- **1.** **Léonard Boris Djeufack**, Laurelle Tsafack Kendjou, Guillaume Samuel Bineng, Oumar Bobbo Modibo, Hamadou Yerima Abba, Saïdou and Mikhail Zhukovsky, "*Study of correlation between radon (^{222}Rn) gas in soil and indoor radon with dose assessment in the bauxite bearing area of Fongo-Tongo, Western Cameroon*" International Journal of Environmental Analytical Chemistry, 131 20 (*Dec*.2022), https://doi.org/10.1080/03067319.2022.2154662.

- **2.** **Léonard Boris Djeufack**, Guillaume Samuel Bineng, Oumar Bobbo Modib, Joseph Emmanuel Ndjana Nkoulou and Saïdou , "*Correlation between Ground ^{222}Rn and ^{226}Ra and Long-Term Risk Assessment at the at the Bauxite Bearing Area of Fongo-Tongo, Western Cameroon*" Radiation 2022, 2, 387-404. https://doi.org/10.3390/radiation2040029.

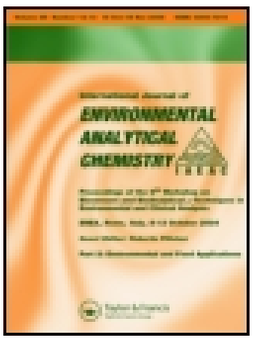

International Journal of Environmental Analytical Chemistry

ISSN: (Print) (Online) Journal homepage: https://www.tandfonline.com/loi/geac20

Study of correlation between radon (^{222}Rn) gas in soil and indoor radon with dose assessment in the bauxite bearing area of Fongo-Tongo, Western Cameroon

Léonard Boris Djeufack, Laurelle Tsafack Kendjou, Guillaume Samuel Bineng, Oumar Bobbo Modibo, Hamadou Yerima Abba, Saïdou & Mikhail Zhukovsky

To cite this article: Léonard Boris Djeufack, Laurelle Tsafack Kendjou, Guillaume Samuel Bineng, Oumar Bobbo Modibo, Hamadou Yerima Abba, Saïdou & Mikhail Zhukovsky (2022): Study of correlation between radon (^{222}Rn) gas in soil and indoor radon with dose assessment in the bauxite bearing area of Fongo-Tongo, Western Cameroon, International Journal of Environmental Analytical Chemistry, DOI: 10.1080/03067319.2022.2154662

To link to this article: https://doi.org/10.1080/03067319.2022.2154662

Published online: 20 Dec 2022.

INTERNATIONAL JOURNAL OF ENVIRONMENTAL ANALYTICAL CHEMISTRY
https://doi.org/10.1080/03067319.2022.2154662

Study of correlation between radon (^{222}Rn) gas in soil and indoor radon with dose assessment in the bauxite bearing area of Fongo-Tongo, Western Cameroon

Léonard Boris Djeufack[a,b], Laurelle Tsafack Kendjou[a], Guillaume Samuel Bineng[a,b], Oumar Bobbo Modibo[b], Hamadou Yerima Abba[a,b], Saïdou[b] and Mikhail Zhukovsky[c]

[a]Nuclear Physics Laboratory, Faculty of Science, University of Yaoundé I, Yaoundé, Cameroon; [b]Research Centre for Nuclear Science and Technology, Institute of Geological and Mining Research, Yaoundé, Cameroon; [c]Institute of industrial Ecology, Ural Branch of the Russian Academy of Sciences, Yekaterinburg, Russia

ABSTRACT

The aim of the current work is to study the correlation between ^{222}Rn gas in soil and indoor ^{222}Rn concentrations. Markus 10 and RADTRAK detectors were used to measure ^{222}Rn concentrations at 1 m depth in soil 30 points and 50 dwellings respectively. These concentrations varied from 35 kBq m^{-3} to 255 kBq m^{-3} with a geometric mean of 67 (18) kBq m^{-3}, and from 85 Bq m^{-3} to 410 Bq m^{-3}, with a geometric mean of 152 (26) Bq m^{-3} respectively in the soil gas and dwellings. In additional, 99% of the measurement points had concentrations higher than the limit value of 40 kBq m^{-3} according to the Swedish criterion for risk levels; 94% of the houses had radon concentrations higher than 100 Bq m^{-3}, the reference value of the World Health Organization (WHO). When there was not a good air flow between the outside and the inside of the dwelling, the correlation coefficients were $R^2 = 0.82$ and $R^2 = 0.73$ respectively for the earthen and concrete dwellings. Under the best natural ventilation conditions, these correlation coefficients decrease significantly. Their values were $R^2 = 0.54$ and $R^2 = 0.34$ respectively for the earthen and concrete dwellings. Furthermore, a RadonEye +2 detector revealed a daily ^{222}Rn accumulation reaching values of 800 Bq m^{-3} in some dwellings when all doors and windows were closed. Architecturally, dwellings built with sealed materials such as cement and concrete, whose do not facilitate ^{222}Rn diffusion and transport, have lower ^{222}Rn concentrations and effective dose than others These results show that ^{222}Rn gas in soil and in confined air in dwellings are strongly correlated.

ARTICLE HISTORY
Received 18 October 2022
Accepted 28 November 2022

KEYWORDS
Markus 10; RADTRAK2®; RadonEye+2; radon; correlation; inhalation dose

1. Introduction

Humans are naturally and permanently irradiated. There are two different sources of ionizing radiation: one source from stars in outer space known as cosmic radiation, and another source from the earth known as terrestrial radiation. The latter is created by the various radioelements present in the earth's crust [1]. Exposure to the crust sources

CONTACT Saïdou saidous2002@yahoo.fr; ous.saidou@gmail.com

depends on the soil geology. For the rich minerals ores areas, the various activities related to the ore exploration and exploitation at these sites may lead to high risks of exposure to naturally occurring radioactive materials (NORM) Uranium-238 (^{238}U) series Thorium-232 (^{232}Th) series, and Potassium-40 (^{40}K) series. ^{222}Rn belongs to the ^{238}U series and contributes to about a half of the human exposure from all-natural radiation sources combined [2]. ^{222}Rn is a natural radioactive gas. It diffuses from the rock to the atmosphere through pores and cracks and can accumulate in confined spaces in homes [2]. Its high levels in dwellings are a public health problem. ^{222}Rn is ricognized as a lung carcinogen after tobacco [3].

Current knowledge about the risk of public exposure to ^{222}Rn, thoron and their associated progeny is based on a sufficiently small sample size. This is justified by the fact that ^{222}Rn measurements require the mobilizationof a lot of material, financial and human resources. Even when financial and material resources are available, access to a dwelling to make a measurement or a series of measurements of the above radionuclides is not obvious because of the public's reluctance or even ignorance of the health importance of these measurements. Most of the general public is unaware of the consequences of long-term exposure to ^{222}Rn. In view of the many difficulties mentioned above, it is therefore important to find an alternative solution to make a correct estimation of the health risk induced by this exposure to ^{222}Rn in a house or a locality without necessarily going through field measurements. Hence the study of the correlation that exists between ^{222}Rn gas in soil and its concentrations in dwellings. Indeed, knowledge of the geological structure and mineralogical composition of a soil, the climatic conditions, the type of architecture of the houses, the way these houses are used or the lifestyle of the inhabitants of a locality can provide an excellent prediction of the ^{222}Rn exposure risks of the people living there permanently.

Many studies conducted around the world and at the uranium and thorium bearing areas in particular have revealed high levels of natural radioactivity in the environment. This radioactivity due to ^{238}U and ^{232}Th varied from site to site. Similarly, ^{222}Rn concentrations measured in soil gas varied from one region to another depending on some parameters such as the depth of the measurement point, the geological structure of the bedrock, the porosity and permeability of the soil [4,5]. Some of these studies even confirmed that beyond soil porosity and permeability, ^{222}Rn migration from the soil to the atmospheric surface and its accumulation in dwellings were closely related to the climatic parameters of the region [4,6–9]. In the literature, it has also been shown that concentrations of ^{222}Rn, thoron and their associated progeny can be high within a dwelling and even in a region [10,11]. Several studies in Cameroon and elsewhere have also found high levels of ^{222}Rn in some houses. They have shown that these high ^{222}Rn, ^{220}Rn and its progeny accumulations are mainly due to the type of architecture of these houses, the geological structure of the soil and its mineralogical composition [6,9,12].

In the current work, the objective was to study of correlation between ^{222}Rn gas in soil and its concentrations in the confined air of some dwellings. To achieve this, the RADTRAK2® and RadonEye +2 detectors were deployed in dwellings in the bauxite bearing area of Fongo-Tongo to measure ^{222}Rn concentrations, and to observe its daily dynamic variations respectively. Furthermore, the Markus 10 detector was used to measure ^{222}Rn in soil. Finally, the correlation coefficients were estimated according to the type of architecture of the dwellings. The external effective dose and the inhalation dose due to ^{222}Rn were also assessed.

2. Materials and methods

2.1. Study areas

The study areas presented in Figure 1 made with the ArcMAP module of ArcGIS software version 10.5. are located in the Menoua subdivision, Western Region of Cameroon. Dschang and Fongo-Tongo constituting the urban core of the area. Fongo-Tongo is known to have a large bauxite ore deposit, which has been investigated by the French Geological and Mining Research Bureau (FGMRB) since 1950 [13].

The average altitude of the areas is approximately 1600 m. The area is located on the south-western slopes of the Bamboutos Mountains, and is dominated by low plateaus that are strongly dissected by small, sometimes swampy valley [14]. The climate is sub-equatorial Cameroonian generally humid and strongly influenced by altitude. Over the year, the average temperature of the area is 22.5°C and the average rainfall is 1364.4 mm. The vegetation is strongly influenced by anthropogenic activities and cultivated crops [14]. The area is characterized by several volcanic activities and volcanic products of various facies basalts, trachyte's, phonolites, rhyolites and ignimbrites [15]. The soils are composed of the granite and orthogenetic basement formations, hence the name granite-gneiss complex [13,16]. The bauxite ore deposits in this area are developed exclusively from aphyric or porphyry mid-oscine basalts. The average chemical composition of these basalts is as follows: 15.9% Al_2O_3, 13.5% FeO_3 and 44.6% SiO_2 [17].

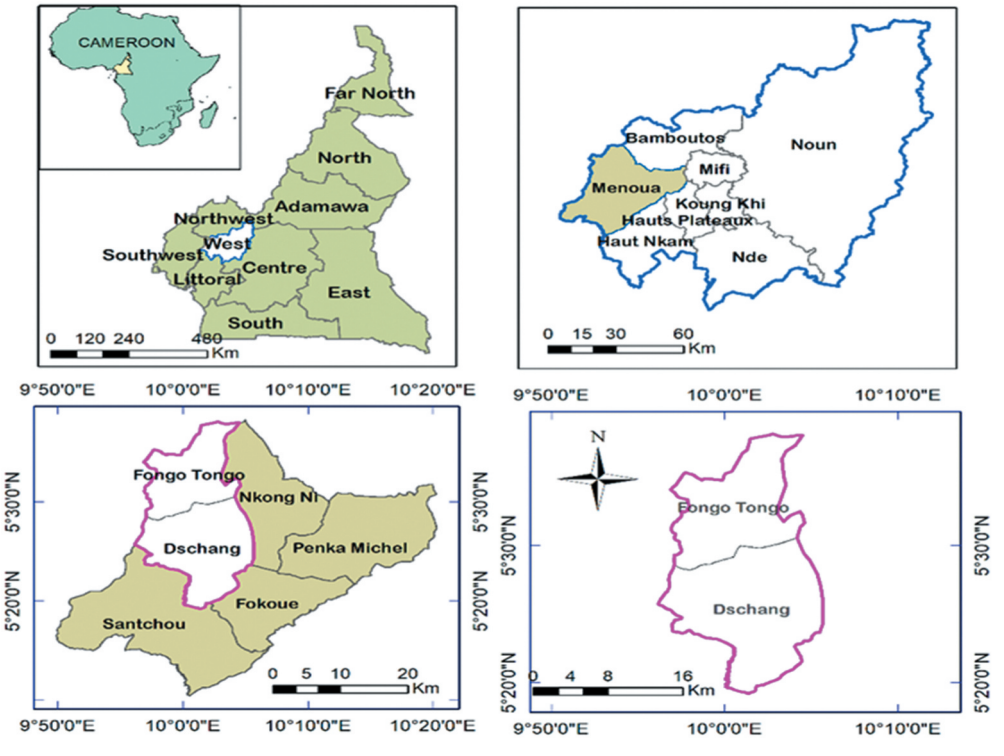

Figure 1. Location of the study areas.

2.2. Characteristics of the dwellings in the study area

The dwellings monitored were built either of earth bricks and cement. Cement dwellings were those with concrete floors and walls built of earth or earth bricks covered with cement, or simply cinder blocks. These dwellings had large openings so that they were well ventilated. Nevertheless, some of these dwellings kept their openings generally closed. In this area, farming and livestock raising are the main activities of the population. However, the houses remain closed for most of the time during some hours of the morning when these occupants go to their various activities and will be covered only at their return. Nevertheless, because of the wet and cold climate prevailing in this locality, the great majority of these dwellings use the main room as a bunkhouse, kitchen and attic with a ceiling made of bamboo to warm up and dry the various products of their crops.

In additional, the measurements with the instruments were made during the dry season precisely between December and February. In this study, the dwellings had one front door and one window or two doors and several windows. The detectors were deployed 80 cm from the walls and at a height of 150 cm from the floor surface, hanging from a string from the ceiling of the dwellings.

2.3. Indoor ^{222}Rn measurements

2.3.1. ^{222}Rn measurements using passive RADTRAK2® detector

Indoor ^{222}Rn measurements were performed using a CR-39 closed alpha track detector, commercially called RADTRAK2®. Thirty detectors were deployed in Dschang and 20 in Fongo-Tongo, for three months exposure period. After the exposure, detectors were returned for analysis to RADONOVA laboratory in Uppsala, Sweden. The measurement were performed according to the standard ISO11665–4 [18]. More details on the detector characteristics are reported by a previous study [6,19]. However, the arithmetic mean of the ^{222}Rn concentration measured is given by the Equation (1).

$$\begin{cases} \bar{C} = \left(n_g - \bar{n}_s\right)\frac{1}{t.S_{SSNTD}.F_c} = \left(n_g - \bar{n}_s\right).\omega \\ \omega = \frac{1}{t.S_{SSNTD}.F_c} \end{cases} \tag{1}$$

is are the number of track recorded on the CR-39 after the exposure, $\bar{n}_s$ the average number of track due to the background radiation is given by the manufacturer t, the sampling time, F_c the calibration factor, ω the correction factor related to the calibration factor, and S_{SSNTD}, sampling time, and the detector area used for counting the number of traces etched in cm^{-2} respectively.

The standard uncertainty u(c) of ^{222}Rn concentration measurement C is given as the Equation (2).

$$\begin{cases} u(\bar{c}) = \sqrt{\left(n_g - \frac{\bar{n}_b}{n}\right)^2 + \bar{c}^2 u_{rel}^2(\omega)} \\ u_{rel}^2(\omega) = u_{rel}^2(F_C) + u_{rel}^2(S) \end{cases} \tag{2}$$

where u_{rel} represented the relative standard uncertainty, the uncertainty in the sampling time is not considered and is therefore considered negligible.

2.3.2. ^{222}Rn variation measurements using RadonEye +2 detector

The detector can connect the data anytime, anywhere, by smartphone or computer connected to the Internet. Indoor radon concentration is well known as one of the main causes of lung cancer in the human body. ^{222}Rn is a gas that circulates in the air, so it must be monitored in real time. In addition, indoor ^{222}Rn concentrations vary with the seasons, day and night. As show in Figure 2 he RadonEye2+ monitors the radon level inside your home quickly and accurately.

The RadonEye +2 is an active detector for indoor ^{222}Rn measurement, based on the ionization principle. It measures 222Rn levels quickly and with an accuracy lower than ±10% (min. error <±0.5pCi L^{-1}. The recorded data are automatically updated after every 10 minutes and the recording is done after every one hour of measurement for a maximum duration of one year. The detector operates in the range of: 10°C ~ 40°C (50°F ~ 100°F), RH < 80%; and in the range: 0.2 ~ 255 pCi/L (7 ~ 9,435 Bq m^{-3}). On a 0.96-inch screen, you can see the result or progress of the measurement displayed in real time [20].

2.4. ^{222}Rn measurements in soil using Markus 10

^{222}Rn gas in soil were measured at different locations with Markus 10 version 1.4. This instrument was developed by Radanova laboratories to measure the volumic activity of

Figure 2. Real-Time radon detector RadonEyes+2.

^{222}Rn in soil. It has a mass of about 3 kg, with an energy resolution of less than 16 keV (α). It is an Ortec Ultra Silicon detector with the volum of $220 \times 122 \times 80\ cm^3$, with a pumping capacity of $1.8\ l\ min^{-1}$ for a duration of 30 seconds, under a limiting pressure of 0.96 bar. The duration of a measurement is typically 12 minutes, its battery has a capacity of about 70 measurements before being fully recharged for 8 hours [21].

The depth of the sampling point is determined by the length of the probe inserted into the ground, taking into account the location of the sampling points on the probe handle as a reference point. When the probe is buried in the soil, the instrument is mounted on the water seal and turned on by pressing the start button. After it is turned on, the measurement is done in two steps. The first step is to pump the gas from the soil into the measuring chamber. When the gas pumping phase stops. The measuring chamber is automatically actuated and the display starts to flash. An electric field is instantly created. It directs the radioactive ^{222}Rn progeny, electrically charged, to the detector. The detector records the alpha radiation from the ^{222}Rn progeny. The electric pulses delivered by the sensor are amplified then filtered in the analysis channel which allows only the counting of the pulses corresponding to the energy resulting from polonium 218. This filtering principle makes it possible to ignore the pulses coming from polonium 214, which are slower to occur and which can create a latent measurement background in the chamber. The device then counts the pulses and the result is displayed on the screen. These results are expressed in $kBq.m^{-3}$ of ^{222}Rn gas activity. The display flashes during the measurement phase. It stabilize to signal the measurement. More details on the principle of the measurement are reported in the manual guide and the previous work [19,21]. The measurement was performed following the standard ISO [22].

2.5. Geogenic radon potential (GRP)

Geogenic ^{222}Rn potential (GRP) is the parameter that quantifies the rate of ^{222}Rn escaped from the adjacent geological formation to the atmosphere. It is an indicator of the potential of the soil to be a source of indoor ^{222}Rn [23]. Considering the soil of the area as highly permeable (of the order of 10^{-11}, $10^{-12}$and 10^{-13}), geogenic ^{222}Rn potential was assessed based on the formula proposed by Neznal, defined in Equation (3) [24–26].

$$GRP = \frac{C_{Rn}}{-\log_{10}k - 10} \tag{3}$$

where C_{Rn} ($kBq\ m^{-3}$) is the concentration of ^{222}Rn gas in soil and k (m^2) is the permeability. High average geogenic ^{222}Rn potential values imply a greater potential for ^{222}Rn migration into the soil [27]. ^{222}Rn-prone areas are generally classified using the ^{222}Rn index (RI) based on geogenic ^{222}Rn potential values. Many years of extensive research in the Czech Republic have classified ^{222}Rn prone areas into three categories based on geogenic ^{222}Rn potential values: low RI (GRP <10), medium RI (10 < GRP <35) and high RI (GRP >35) [25].

2.6. Doses assessments

2.6.1. Ambient dose equivalent rates measurements and external effective dose assessment

The absorbed dose rate measured about one meter above the ground surface, was carried out by the personal radiation detector (RadEye PRD-ER). It has a highly sensitive NaI(Tl) scintillation detector with a miniature photomultiplier for gamma radiation measurement [28]. The external effective dose is obtained by applying the Equation (4).

$$E_{ext}\left(mSv.y^{-1}\right) = [(1 - F_{occ}).H_{out} + F_{occ}.H_{int}] \times t \tag{4}$$

where F_{occ} is the occupancy factor, H_{out} and H_{int} are the arithmetic mean of ambient and indoor equivalent dose rates and obtained by the Equation (5);

$$\begin{aligned} H_{out} &= D_{out} \times F_C \\ H_{in} &= D_{in} \times F_C \end{aligned} \tag{5}$$

where D_{out} and D_{in} are respectively the Dose rates outside and inside the dwellings and F_c the conversion factor.

2.6.2. Inhalation effective dose from indoor ^{222}Rn

The inhalation dose from indoor ^{222}Rn is given by the Equation (6).

$$E_{inh} = A_{inh} \times e_{inh} \times F_{occ} \times F_{eq} \times t \tag{6}$$

Where A_{inh}, e_{inh}, F_{occ}, F_{eq} and t are respectively the geometric mean of the ^{222}Rn concentration; the inhalation dose conversion factor of 9 nSv $(Bq.h.m^{-3})^{-1}$; the occupancy factor of 60%, the equilibrium factor of $F_{eq} = 0.4$ representing the default value and the time corresponds to one year expressed in hours [1].

The equilibrium factor (F_{eq}) determines the level of radioactive equilibrium between ^{222}Rn, and its decay products and it is used when the equivalent equilibrium concentration (EEC) of ^{222}Rn decay products is not directly measured. The occupancy factor (F_{occ}) is estimated at 60%, or 14 hours per day according to the lifestyle in tropical area.

2.6.3. Inhalation dose from outdoor ^{222}Rn concentration

Estimation of ^{222}Rn in soil gases and in the atmosphere has been proposed as a tool for many research purposes such as uranium exploration, earthquake prediction, groundwater transport and geothermal resource assessment [29]. If the soil is sufficiently porous, diffusion proceeds as if the soil were absent. From production to exhalation into the atmosphere [30], ^{222}Rn concentration C'_{Rn} (Bq m^{-3}) in air near the ground surface is estimated by the Equation (7) [19,31]:

$$C'_{Rn} = C_{sg}\sqrt{\frac{d}{D}} \tag{7}$$

Where C_{sg} is ^{222}Rn concentration gas in soil in kBq m^{-3}, d is the exhalation diffusion constant (= 0.05 cm^2 s^{-1}) and D is the diffusion coefficient (5×104 cm^2 s^{-1}).

The annual inhalation dose E_{inh} (mSv) from outdoor ^{222}Rn received by the public is therefore calculated using the Equation (8) [1].

$$E'_{inh} = C'_{Rn} \times F_{occ} \times F_{eq} \times F_C \times t \quad (8)$$

Where E'_{inh} is the inhalation dose form outdoor ^{222}Rn concentration that received by the public, F_{eq} is the equilibrium factor ($F_{eq} = 0.6$), $F_{occ} = 0.4$ is the outdoor occupation factor per individual, and F_C is the dose conversion factor for ^{222}Rn exposure 9 nSv (Bq h m^{-3}) $^{-1}$ [1].

3. Results and discussion

3.1. ^{222}Rn concentration distribution using RADTRAK2® detector

Indoor ^{222}Rn were determined in 50 dwellings monitored in the area, 30 in Dschang and 20 in Fongo-Tongo. Table 1 summarises the main results observed. It shows that, indoor ^{222}Rn ranges from 85 Bq m^{-3} to 410 Bq m^{-3} with a mean value of 152 ± 26 Bq m^{-3}. indoor ^{222}Rn in Dschang and Fongo-Tongo ranged from 85 to 250 Bq m^{-3} and from 98 to 410 Bq m^{-3} , with a value mean of 144 ± 24 and 166 ± 31 Bq m^{-3} respectively. The study shows that the average ^{222}Rn concentration in these regions is higher than the world average values of 30 Bq m^{-3} [1].

This high ^{222}Rn level can be justified by the type of architecture of these dwellings, which are mostly built with mud bricks. The ^{222}Rn exhalating from these building materials would probably contribute to the increase of the indoor ^{222}Rn level. These high ^{222}Rn concentrations in earthen houses when the walls and the floor are not covered with cement can be justified by the fact that: the radon gas, permanently trapped in the earth which constitutes the building material, diffuses easily and escapes to concentrate inside the poorly ventilated houses. In addition, the persistent cold and damp conditions of the region's climate force the inhabitants to keep the openings of their dwellings permanently closed [32]. This reduces the exchange of air between the outdoor and indoor of their homes and therefore further promotes the accumulation of ^{222}Rn gas [33]. As well as the lack of waterproofing of the ground for the majority of the monitored dwellings are not less. In fact, the bare floor of these dwellings does not attenuate the rate of exhalation of ^{222}Rn following its emanation in the ground. The high concentrations of ^{222}Rn and the variation observed from one monitored dwellings to another and from one site to another are closely related to the geological structure of the area, the ventilation parameters, the atmospheric and climatic constraints, the architecture and the lifestyle of the people living in those houses [34].

According to Figure 3, 6 % of the monitored dwellings had ^{222}Rn concentration above the reference value of 100 Bq m^{-3} recommended by the World Health Organization [3]. The large number of houses had ^{222}Rn concentration between 100 and 200 Bq m^{-3}. Similarly, 6% dwellings had indoor ^{222}Rn above 200 Bq m^{-3}. And another 6% of these

Table 1. Summary of the results of ^{222}Rn survey using RADTRAK2® detectors.

	^{222}Rn Concentration (Bq m^{-3})		
Locality	GM (GSD)	Median	Range
Dschang	144 (24)	140	85-250
Fongo-Tongo	166 (31)	150	98-410
Whole study Area	152 (26)	140	85-410

GM: geometric mean, GSD: geometric standard deviation.

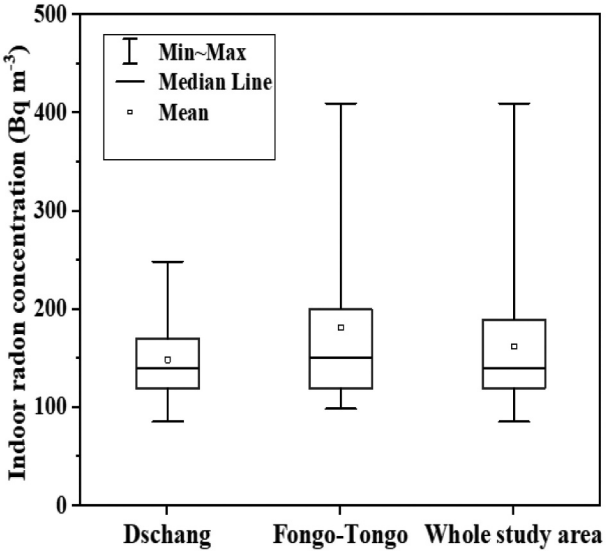

Figure 3. Boxplot distribution of indoor ^{222}Rn at the different site and the whole study area.

monitored dwellings have a ^{222}Rn concentration higher than 300 Bq m^{-3}. Figure 3 shows the Boxplot distribution of the monitored areas and the whole study area.

Furthermore, the soils in this area are of the andic, ferrallitic, trachytic, granitic and basaltic type with a matrix that rests on an extensive and thick loose mantle developed on trachyte that generally forms a differentiated geological profile. In addition, they present a porous and permeable structure [14,35,36]. In the literature, it is shown that some types of rocks such as granite and basalt can have high uranium contents [9,37]. Similarly, there is a good correlation between the climate, the architecture, the mineralogical and geological structure of the soil of an area, the way of life of the populations and the concentrations of radon in the dwellings [9]. Therefore, a soil rich in uranium is also rich in radium and radon. Porous and permeable soils such as those in the bauxite zones of Fongo-Tongo also facilitate the diffusion and migration of radon to the free surface. Some studies conducted in the present study area have revealed elevated concentrations of radium-226 and radon-222 in the soil [38]. In addition, these studies have shown that there is a correlation between radium-226 and radon-222 concentrations in soil. During the measurement period, the population was working in the fields on a daily basis and generally kept their homes closed. This favours an accumulation of gas inside the houses [6,9,19]. Thus, the high concentrations obtained in the present study can be justified by the different geological, climatic and anthropological elements presented above.

Table 2 compares ^{222}Rn concentration measured in the current study to those reported in previous works. These levels can reach maximum values two to three times the maximum value obtained in this study [7,39–41]. Indeed, references report higher maximum ^{222}Rn levels than those of the areas we studied, but they are substantially in the range of 400 to 600 Bq m^{-3} [7,42,43].

Table 2. Comparison of the results of the current study with those obtained in other countries.

		^{222}Rn concentration (Bq m^{-3})		
Country	Area	GM	Range	References
Canada	Ottawa	72 ± 2	8-1525	[39]
China		58 ± 2	12-427	[42]
Hungary	Great Hungarian Plain	166	45-609	[40]
	Kövágószölös		17-1083	[41]
North Macedonia		114	30-535	[43]
South Africa	West	-	28-465	[44]
Cameroon	Lolodorf	89 ± 2	26-976	[9]
	Lomié	58 ± 24	27-300	[19]
	Southern Adamawa	102 ± 21	43–270	[6]
	Fongo-Tongo	152 ± 26	85-410	Current study

GM: geometric mean.

3.2. Indoor ^{222}Rn variation by RadonEye +2

It has been shown that indoor ^{222}Rn varies with the seasons [45]. However, it has also been shown that the indoor ^{222}Rn concentration varies throughout the day depending on the rate of air exchange between indoor and outdoor environments. Figure 4 shows daily dynamic variation of indoor ^{222}Rn in the different monitored dwellings of the area. These are chosen according to specific construction characteristics observed and are represented by different colours. The nature of the different dwelling types has little significant influence on indoor ^{222}Rn in this case, although other studies report almost the same finding [46]. However, in the case of dwellings with good natural air circulation, the ^{222}Rn concentration level decreases considerably for these different types of architecture. These results show that the accumulation of ^{222}Rn gas in the home from the soil is clearly influenced by the natural ventilation system and the daily occupancy patterns of the home.

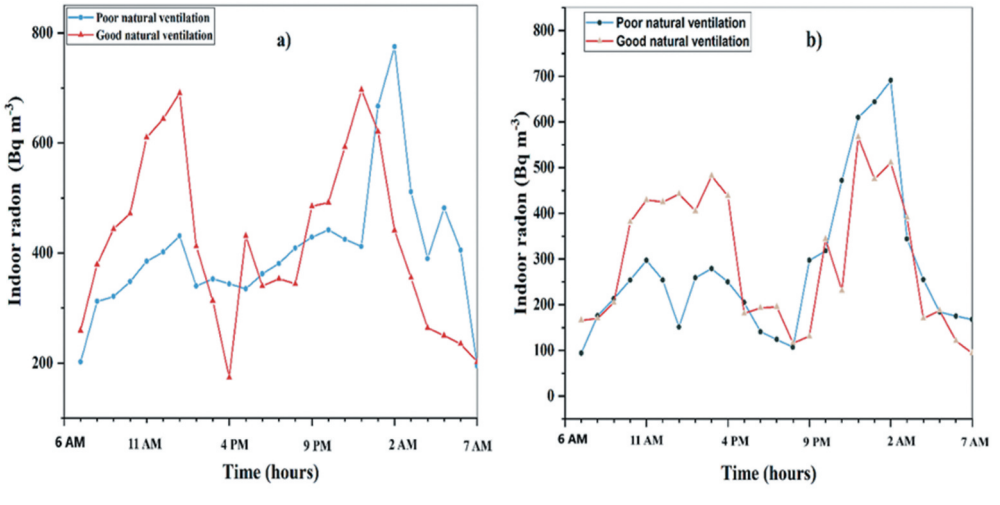

Figure 4. Daily dynamic variation of ^{222}Rn concentrations in some dwellings: in soil and bare ground (a) in soil and concrete ground (b) the graphs in red and blue represent the state of well-ventilated and poorly ventilated dwellings respectively.

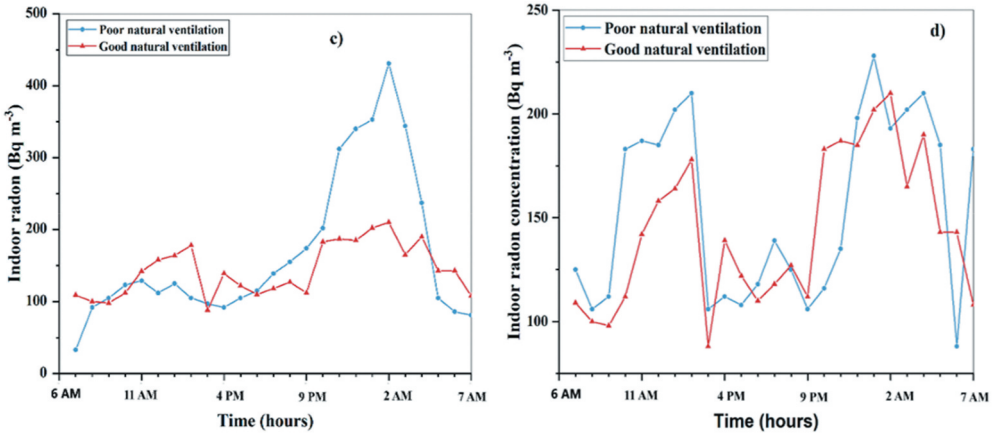

Figure 5. Daily dynamics variation of ^{222}Rn concentrations in some dwellings: cemented walls and bare soil (c); cemented walls and concrete soil (d). The graphs in red and blue represent the state of well-ventilated and poorly ventilated dwellings respectively.

Nevertheless, the observed difference would probably be related to tightness of floor, which would however reduce the gas rate emanation in some dwellings. In all cases, we observe variations of ^{222}Rn level taken at intervals of one hour each for about twenty-four hours. We then observe that indoor ^{222}Rn accumulation reaches considerable peaks during the night and even during the day when the occupants go about their business while the openings (doors and windows) of the house are totally closed, decreasing the ventilation of house and thus favouring a greater accumulation of gas [2].

Figure 5 shows that indoor radon accumulation decreases considerably when the dwellings are made which the cemented walls and concrete soil. Theses reduce radon exhalation to the ground surfaces of the houses.

3.3. ^{222}Rn concentration in soil

^{222}Rn concentrations at 1 m thickness in soil, presented in Table 3, ranged from 35 to 202 kBq m^{-3} with a mean value of 69 ± 8 kBq m^{-3} in Fongo-Tongo and from 48 to 255 kBq m^{-3} with a mean value of 82 ± 14 kBq m^{-3} in Dschang. Table 3 shows that more than half of the sampled points have ^{222}Rn concentrations greater than or equal to 62 kBq m^{-3} in Dschang and 69 kBq m^{-3} in Fongo-Tongo. These values are high according to the Swedish risk assessment criteria [47].

The difference between ^{222}Rn gas in soil from one location to another may be due to geological and mineralogical constitution of the soil of the area [48]. furthermore, variation of ^{222}Rn gases in soil from one point or one site to another can also be justified by the diversity of underlying rocks [49]. That is, to geological constitution, geochemical process in soil, to porosity and to emanation rate gas of the area [25,43,50]

Table 3. Statistical parameters of ^{222}Rn concentration in soil at the bauxite bearing area of Fongo-Tongo and Dschang.

	^{222}Rn in soil (kBq m^{-3})		
Locality	GM (GSD)	Median	Range
Dschang	82 (14)	62	48-255
Fongo-Tongo	69 (8)	53	35-202
Whole study area	67(18)	57,6	35-255

Table 4. Statistical parameters of exhalation rate and geogenic ^{222}Rn potential for the investigated sites.

				Geogenic ^{222Rn} Potential		
Statistical parameters	a (Bq m^{-3} s)	E (Bq.m^{-2}. s)	C′ (Bq m^{-3})	k=10^{-11}	k=10^{-12}	k=10^{-13}
AM	0,1587	0,033	75,6	75,6	37,8	25,2
SD	0,1012	0,021	48,2	48,2	24,1	16,1
GM	0,1401	0,029	66,7	66,7	33,4	22,3
GSD	0,1029	0,022	48,9	48,9	24,5	16,3
Median	0,1210	0,025	57,6	57,6	28,8	19,2
Min	0,0725	0,015	35	35	17,25	11,5
Max	0,5351	0,112	255	255	127,4	84,9

a: Production rate, E: Exhalation rate, C′: ^{222}Rn emanation

3.4. Geogenic radon potential (GRP)

To protect population from ^{222}Rn exposure, it is necessary to analyse ^{222}Rn in all sources (soil, water, food, building materials...), so that action plan take into account the identification of areas prone to generate high levels of indoor ^{222}Rn. That is, ^{222}Rn risk areas.

Table 4 shows the geogenic ^{222}Rn potential values have been assessed from the ^{222}Rn concentration and the permeability in the soil in the order of $k = 10^{-11}$ ms^{-1}, $k = 10^{-12}$ ms^{-1} and $k = 10^{-13}$ ms^{-1} [24]. According to the Czech Republic classification to regions with ^{222}Rn potential in soil, 100%, 26.7% and 13.3% of the measurement points have a ^{222}Rn index with a GRP greater than 35 for permeability values of $k = 10^{-11}$ ms^{-1}, $k = 10^{-12}$ ms^{-1} and $k = 10^{-13}$ ms^{-1} respectively. The various sampling points allow the region to be classified as a moderate ^{222}Rn risk area. It shows that, the GRP increases with soil permeability. This permeability is therefore a fundamental parameter to determine the mobility of ^{222}Rn in the soil [25]. Indeed, the presence of a soil with high permeability can imply a strong diffusion of ^{222}Rn to the atmosphere and can be strongly influenced by the geological characteristics of the area [27,51].

However, for geogenic reasons, such as the radium or uranium content of the rock, the permeability of the rock, and also faults related to ^{222}Rn mobility, the GRP indicates a probability of accumulation of ^{222}Rn concentrations in dwellings depending on its type of architecture and its usage. Classification using the ^{222}Rn index (RI) based on the values of geogenic ^{222}Rn potential allows us to appreciate the correlation between ^{222}Rn concentrations in the soil and those in homes [25]. Studies have shown that there is a relationship between ^{222}Rn concentration in soil gas and the underlying geology [52,53].

3.5. Correlation between ^{222}Rn gas in soil and ^{222}Rn in dwellings

The correlation between ^{222}Rn concentrations in dwellings and ^{222}Rn concentrations in soil gas was studied according to the type of dwelling architecture and its natural ventilation system. The monitored dwellings were made of bare earth bricks, or covered with cement for some and exclusively with cement for others. Similarly, the floors of these dwellings were either bare or covered with concrete. The ventilation parameters were not measured. Nevertheless, the openings (windows and doors) that allow a good air circulation in a dwelling have been taken into account. Figures 4 and Figure 5 show the different linear regression lines and the correlation coefficients obtained for the cases investigated.

Figure 6 shows the correlation between ^{222}Rn gas in soil and its concentrations in earthen dwellings (Figure 6(a)) on the one hand, and between ^{222}Rn in soil and its concentrations in cemented dwellings (Figure 6(b)) on the other hand. Their correlation coefficients were respectively estimated at $R^2 = 0.82$ and $R^2 = 0.73$; this correlation is stronger in the case of earthen dwellings. This strong correlation indicated that, measuring ^{222}Rn gas in soil may be an alternative to predict ^{222}Rn concentrations in dwellings [53]. In fact, in the dwellings, ^{222}Rn from unpoured (or concreted) soil and uncemented earthen (or earthen brick) walls are found at high levels. This is certainly due to the porosity of the soil and walls. In contrast, when the walls are cemented and the floor is poured (concrete or tiled), ^{222}Rn diffusion is considerably attenuated; this is due to the compactness of the cement and the concrete. Hence a correlation coefficient lower than the first.

Similarly, Figure 7 shows the correlation between ^{222}Rn gas in soil and its concentrations in earthen dwellings (Figure 7(a)) and, that between ^{222}Rn in soil and its concentrations in cemented dwellings (Figure 7(b)). Furthermore, the dwellings in the two cases above are very well ventilated. Their correlation coefficients were respectively assessed at $R^2 = 0.54$ and $R^2 = 0.34$; this correlation is lower in the case of the cemented dwellings. This is certainly due to the cinder blocks, the cement covering the earthen walls and bricks, and the concrete on the floor. Indeed, these types of building materials (cinder block, cement and concrete) considerably reduce the diffusion of indoor ^{222}Rn.

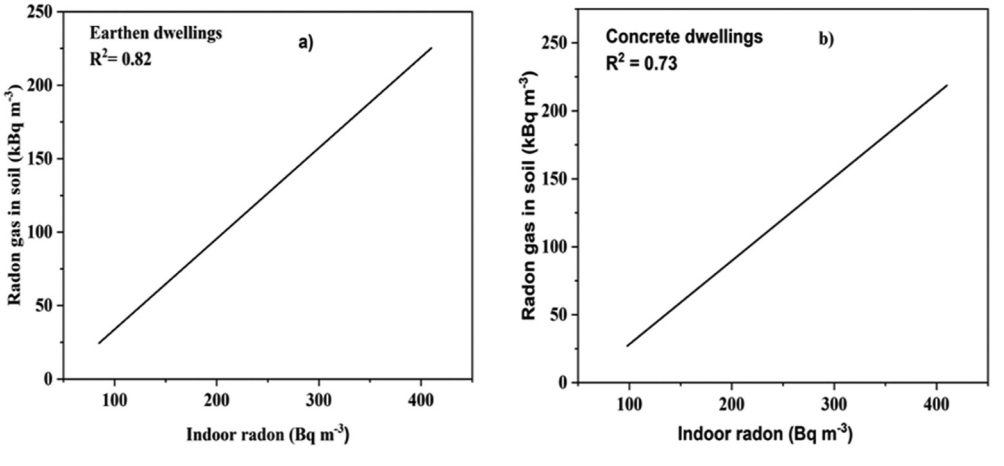

Figure 6. Correlation between ^{222}Rn gas in soil and these concentrations in dwellings with poor natural ventilation: earthen (a) and concrete (b).

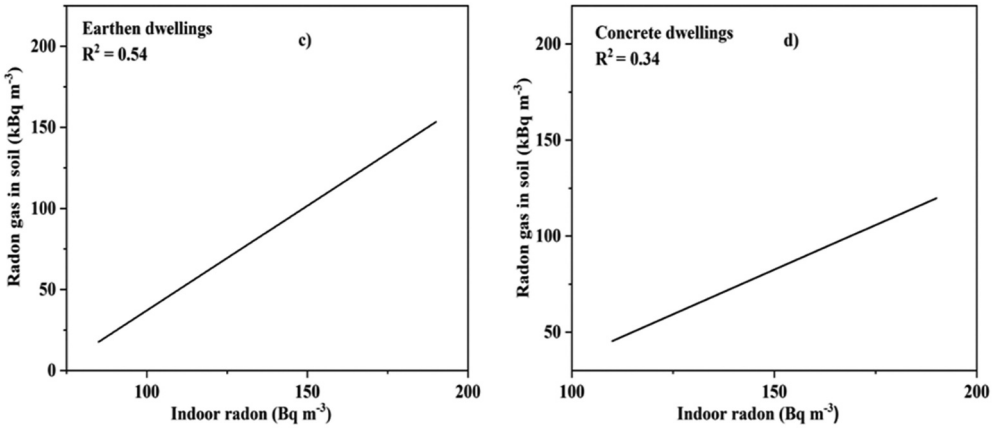

Figure 7. Correlation between ^{222}Rn gas in soil and its concentrations in dwellings with the best natural ventilation: earthen (c) and concrete (d).

Compared to the values presented in Figure 6 above-mentioned, the correlation coefficients in Figure 7 are generally lower. In fact, under the best natural ventilation, ^{222}Rn gas in home is largely carried by the wind from inside the house to the outside. The proportion of ^{222}Rn in this type of dwellings after exhalation from its matrix and by transport in the air, is found at low levels of concentration. This considerably reduces the correlation coefficient between ^{222}Rn concentrations in soil gas and those in these dwellings.

Many studies carried out elsewhere have shown that high ^{222}Rn in dwelling can be justified by its architecture and some geologic parameters such as rock type, soil porosity and permeability [6,7,9,43]. This means that uranium or radium rich soil is a very important parameter that can influence ^{222}Rn levels in a home. Similarly, soil permeability is a good indicator of the potential for ^{222}Rn diffusion from the subsurface to the free surface of the earth [4,54,55]. Thus, a poorly ventilated home built on a site with the above characteristics will have very high ^{222}Rn concentrations if its soil is not concreted and its walls cemented.

3.6. Equivalent dose rate and external effective dose

Figure 8 presents the scatter plot between ambient dose equivalent rate and ^{222}Rn concentration in dwellings in the study area. The Pearson correlation coefficient less than 3% was obtained, and it shows that ambient dose equivalent rate is independent of ^{222}Rn gas concentration in the study areas. Furthermore, the ambient dose equivalent rate values measured were in the range of the Country's background. The maximum value of the ambient dose equivalent rate measured was 0.14 μSv h^{-1} is obtained for a value of ^{222}Rn gas concentration of 100 Bq m^{-3} which is less than 166 ± 31 the average value of indoor ^{222}Rn distribution in the study areas.

According to Table 5, indoor and outdoor ambient dose equivalent rates range from 0.05 to 0.14 μSv h^{-1} and from 0.04 to 0.24 μSv h^{-1} respectively with a geometric mean of 0.07 ± 0.03 μSv h^{-1}. External effective dose ranges from 0.4 to 1.52 μSv h^{-1} with geometric mean of 0.60 ± 0.20 μSv h^{-1} for the study areas. The annual effective dose from external radiation ranges from 0.40 to 0.77 mSvy^{-1} Dschang and from 0.46 to 1.52 mSv y^{-1} in

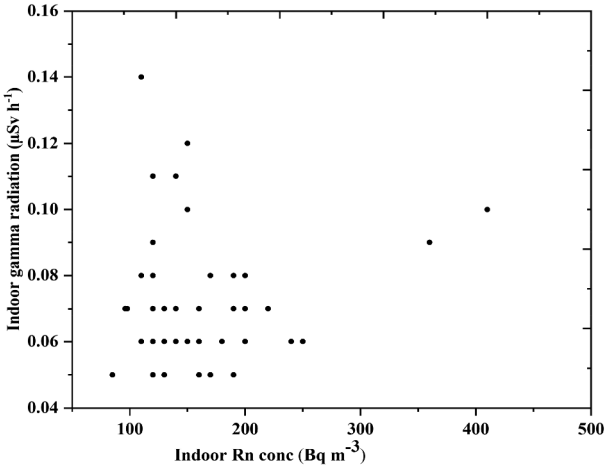

Figure 8. Scatter plot between ambient equivalent dose rate and ^{222}Rn in the dwellings of the at the bauxite bearing areas of Dschang and Fongo-Tongo, Western Cameroon.

Table 5. Statistical summary of indoor and outdoor ambient dose rates and external effective dose at the bauxite bearing areas of Dschang and Fongo-Tongo, West Region of Cameroon.

Locality	Statistical parameters	Indoor (μSv.h^{-1})	Outdoor (μSv.h^{-1})	E_{ext} (mSv.y^{-1})
Dschang	Range	0.05–0.08	0.04–0.10	0.40–0.77
	Median	0.06	0.06	0.52
	AM ± SD	0.06 ± 0.01	0.06 ± 0.01	0.53 ± 0.08
	GM(GSD)	0.06(0.01)	0.06(0.01)	0.52(0.08)
Fongo-Tongo	Range	0.06–0.14	0.05–0.24	0.4–1.52
	Median	0.08	0.08	0.46
	AM ± SD	0.09 ± 0.02	0.09 ± 0.04	0.77 ± 0.23
	GM(GSD)	0.08(0.02)	0.08(0.04)	0.74(0.24)
Whole study	Range	0.05-014	0.04-024	0.4–1.52
	Median	0.07	0.06	0.58
	AM ± SD	0.07 ± 0.02	0.07 ± 0.03	0.63 ± 0.20
	GM(GSD)	0.07(0.02)	0.07(0.03)	0.6(0.2)

AM: Arithmetic Mean, SD Standard Deviation, GM: Geometric Mean, GSD: Geometric Standard Deviation

Fongo-Tongo with a geometric mean of 0.52 ± 0.08 mSv y^{-1} for Dschang, and 0.74 ± 0.24 mSv y^{-1} for Fongo-Tongo. These values are higher than the world average values of 0.5 mSv y^{-1} for the exposure to the terrestrial radiation [1]. However, exposure to external radiation sources in the region is not critical.

3.7. Inhalation doses due to ^{222}Rn

As presented in Table 6, ^{222}Rn inhalation dose in the whole study area ranges from 1.6 ± 0.5 to 7.8 ± 1.2 mSv y^{-1}with geometric mean of 2.9 ± 0.8 mSv y^{-1} Taken separately, the ^{222}Rn inhalation dose in Dschang ranges from 1.6 ± 0.5 to 4.7 ± 1.0 mSv y^{-1}, for Fongo-Tongo ranges from 1.9 ± 0.6 to 7.8 ± 1.2 mSv y^{-1} with geometric mean of 2.7 ± 0.4 mSv y^{-1} in Dschang and 3.1 ± 0.7 mSv y^{-1} in Fongo-Tongo. These average values are three to five times higher than the corresponding world average value of 1.2 mSv y^{-1} [1]. More than half of the homes

Table 6. ^{222}Rn inhalation effective dose to the public at the bauxite bearing areas of Dschang and Fongo-Tongo in Western Cameroon: E_{int} and E_{out} are the indoor and outdoor inhalation doses respectively.

	Inhalation dose E (mSv y^{-1})					
	E_{in}			E_{out}		
Parameters	GM (GSD)	Med	Range	GM (GSD)	Med	Range
Dschang	2.7 (0.4)	2.7	1.6–4.8	0.07 (0.05)	0.06	0.05–0.24
Fongo-Tongo	3.1 (0.7)	2.8	1.9–7.8	0.06 (0.04)	0.05	0.03–0.19
Whole study	2.9 (0.8)	2.7	1.6–7.8	0.06 (0.05)	0.05	0.03–0.24

Table 7. Total inhalation dose due to indoor and outdoor ^{222}Rn at the bauxite bearing areas of Dschang and Fongo-Tongo.

Total inhalation dose E_T (mSv y^{-1})			
Parameters	Dschang	Fongo-Tongo	Whole study area
Range	1.65–4.97	1.89–7.93	1,65–7.93
Median	2.63	2,87	2,71
GM (GSD)	2,78 (0.52)	3,16 (0,54)	2,90 (0.88)

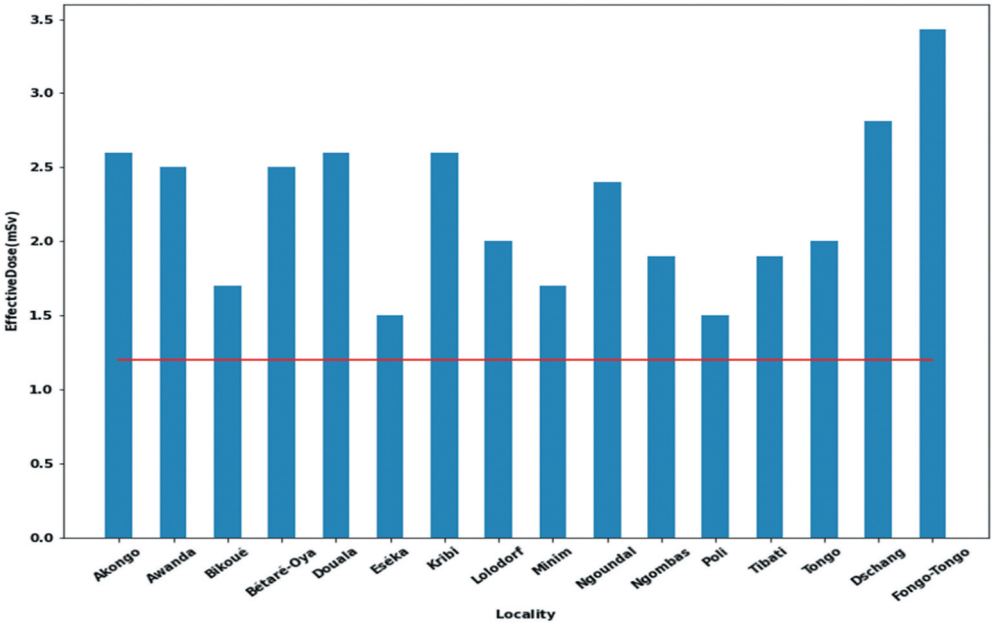

Figure 9. Comparative doses of the current study with dose in other mining potential areas of Cameroon.

investigated in this study have a dose greater than or equal to 2.7 mSv y^{-1}; a value twice as high as its world corresponding.

The outdoor ^{222}Rn inhalation dose estimated between 0.05 and 0.24 mSv y^{-1} with an average value of 0.07 mSv y^{-1} at Dschang. At Fongo-Tongo, it was estimated between 0.03 and 0.20 mSv y^{-1} with an average value of 0.06 mSv y^{-1}. These values are well below

the safety limit of 0.1 mSv.y^{-1} recommended by the WHO and well below the ICRP reported reference levels of 1mSv.y^{-1}. The annual effective dose associated with radon from the atmospheric surface does not pose any type of health hazard to the population and tourists in the study area [3].

According to Table 7, total inhalation dose due to indoor and outdoor ^{222}Rn ranged from 1.89 to 7.93 mSv y^{-1} with a mean value of 3.16 ± 0.54 mSv y^{-1} in Fongo-Tongo and from 1.65–4.97 mSv y^{-1} with a mean value of 2.78 ± 0.52 mSv y^{-1} in Dschang. These values are all above the recommended dose limit of 1.2 mSv.y^{-1} [1].

Figure 9 shows the comparison diagram of the average doses in other study areas in Cameroon [6,8,9,56,57]. However, Fongo-Tongo records inhalation dose value higher than that of Dschang and other ore bearing areas of Cameroon.

4. Conclusion

Exposure to natural radioactivity and radon ($_{86}$Rn) in particular with its progeny is a public health problem. The challenge is often to protect against the harmful effects of this radioactivity. This protection begins with radiological monitoring in the environment. The radioactive source responsible for the exposure must be identified. The deployment of detection and measurement equipment is often not easy in the field because of the reluctance of some members of the public. They remain suspicious of strangers and their equipment. Moreover, access to the equipment and the descent on the field of study sometimes require the mobilization of many logistic, financial and human means. In the particular case of indoor ($_{86}$Rn) monitoring and its associated progeny, the lack of awareness and ignorance of the public on their carcinogenic effects makes the deployment of the various detectors in the dwellings even more difficult. A radon hazard prediction technique such as the one proposed in this study can therefore be an effective way to overcome the above-mentioned difficulties. It is based on the existing climatic, geological, mineralogical and anthropological characteristics of a locality. The current study carried out in the bauxite bearing areas of Fongo-Tongo, it investigated the correlation between ^{222}Rn in the soil and its concentrations in the confined air of dwellings. In addition, the effective dose from internal radiation was evaluated. The Markus 10 and RADTRAK detectors were used to measure ^{222}Rn concentrations in soil and in dwellings, respectively. The results obtained show that the soil gas in the current study is very rich in ^{222}Rn in some places. Architecturally, dwellings built with sealed materials such as cement and concrete, whose do not facilitate ^{222}Rn diffusion and transport, have lower ^{222}Rn concentrations and inhalation effective dose than others. These concentrations are even lower in dwellings with many doors and windows regularly opened and well positioned in relation to the wind movement so that the air coming from outside can permanently expel the air highly concentrated in ^{222}Rn present inside. Therefore there is a good correlation between ^{222}Rn in the soil gas and ^{222}Rn concentrations in the confined air of a house. The coefficient of this correlation varies considerably with the geological and mineralogical constitution of the soil, the building material, the air circulation conditions between the outside and the inside of the dwelling and the way it is used.

Acknowledgement

We also extend our acknowledgments to Dr Zora S. Žunić from the Institut of Nuclear Sciences Vinca of Belgrade, Serbia for reading the manuscript.

Author contributions

All authors contributed to the study. Conceptualization [Léonard Boris Djeufack], [Saïdou], [Mikhail Zhukvosky] Material preparation, data collection and analysis were performed by [Léonard Boris Djeufack], [Laurelle Tsafack Kendjou] and [Yerima Hamadou Abba]. The first draft of the manuscript was written by [Léonard Boris Djeufack]; [Guillaume Samuel Bineng] and [Oumar Bobbo Modibo] all authors commented on previous versions of the manuscript. All authors read and approved the final manuscript.

Disclosure statement

No potential conflict of interest was reported by the author(s).

Funding

This work was supported by the International Atomic Energy Agency (IAEA) within the framework of the Technical Cooperation (TC) Project CMR9009 titled "Establishing a national ^{222}Rn plan for controlling public exposure due to ^{222}Rn indoors". The Government of Cameroon supported field works through the Public Investment Budget 2020 and 2021 of the Ministry of Scientific Research and Innovation.

ORCID

Léonard Boris Djeufack http://orcid.org/0000-0002-2966-8851
Saïdou http://orcid.org/0000-0001-7427-0239
Mikhail Zhukovsky http://orcid.org/0000-0002-5729-6530

Data availability statement

The authors confirm that the data supporting the findings of this study are available within the article.

References

[1] UNSCEAR, *Sources and Effects of Ionizing Radiation : United Nations Scientific Committee on the Effects of Atomic Radiation : UNSCEAR 2000 Report to the General Assembly, with Scientific Annexes*, (United Nations, Vienna, Austria), 2000.
[2] R. Maximilien, M.C. Robe and M. Archimbaud, Radioprotection. **20** (1), 45–60 (1985). doi:10.1051/radiopro/19852001045.
[3] WHO, World Health Organization Regional Office for Europe Selected Pollutants, Denmark, (2010). [Online]. www.euro.who.int
[4] H. Nuhu, S. Hashim, M.A. Saleh, M.S.M. Sanusi, A.H. Alomari, M.H. Jamal, R.A. Abdullah and S. A. Hassan, PLoS ONE. **16** (7), 1–17 (July 2021). doi:10.1371/journal.pone.0254099.
[5] K.F. Ubeid and K.A. Ramadan, Pol. J. Soil Sci. **53** (1), 55–72 (2020). doi:10.17951/pjss/2020.53.1.55.

[6] O.B.M. Saïdou, N.N.I.J. Emmanuel, O. German, K.N. Michaux and H.Y. Abba, Int. J. Environ. Res. Public. Health. **17** (18), 1–12 (Sep 2020). doi:10.3390/ijerph17186776.
[7] Saïdou, T. Shinji, M. Hosoda, T.S. Flore, N.N. Emmanuel II, A. Naofumi, O.B. Modibo and P. Joseph, J. Geochem. Explor. **205**, (Oct 2019). doi:10.1016/j.gexplo.2019.106350.
[8] T.S.S. Didier, Saïdou, S. Tokonami, M. Hosoda, T. Suzuki, H. Kudo and O. Bouba, Isotopes. Environ. Health Stud. **55** (5), 499–510 (2019). doi:10.1080/10256016.2019.1649258.
[9] G.S. Bineng, S. Tokonami, M. Hosoda, Y.F.T. Siaka, H. Issa, T. Suzuki, H. Kudo and O. Bouba, Front. Public Health. **8**, (Feb 2020). doi:10.3389/fpubh.2020.00017.
[10] M. Hosoda, S. Tokonami, Y. Omori, S.K. Sahoo, S. Akiba, A. Sorimachi, T. Ishikawa, R.R. Nair, P. A. Jayalekshmi, P. Sebastian and K. Iwaoka, Plos One. **10** (4), 0124433 (Apr 2015). doi:10.1371/journal.pone.0124433.
[11] Y. Omori, S. Tokonami, S.K. Sahoo, T. Ishikawa, A. Sorimachi, M. Hosoda, H. Kudo, C. Pornnumpa, R.R. Nair, P.A. Jayalekshmi and P. Sebastian, J. Radiol. Prot. **37** (1), 111–126 (2017). doi:10.1088/1361-6498/37/1/111.
[12] M. Kaur and A. Kumar, J. Radioanal. Nucl. Chem. **315** (1), 75 (2017). doi:10.1007/s10967-017-5632-0.
[13] F.W. Nguimatsia Dongmo, R. Yongue Fouateu, R.F. Donald Ntouala, Y.B. Lemdjou, D. Chirstophe Ledoux and A.T. Bolarinwa, Appl. Earth Sci. Trans. Inst. Min. Metall. **130** (1), 23–41 (2021). doi:10.1080/25726838.2020.1861916.
[14] P.L. Kenfack, P. Tematio, M. Kwekam, G. Ngueutchoua and P.R. Njike, *Evidence of a Miocene Volcano-Sedimentary Lithostratigraphic Sequence at Ngwa (Dschang Region, West Cameroon): Preliminary Analyses and Geodynamic Interpretation*, 2011. [Online]. http://www.academicjournals.org/JPTAF (accessed Sep 23, 2022).
[15] P.E. Tedonkeng, Rainfall Variability Along the Southern Flank of the Bambouto Mountain (West-Cameroon), 2008.
[16] F.W.N. Dongmo, R.F. Yongue, A.T. Bolarinwa, R.B. Ngatcha, C. Fuanya and M.A. Kamga, *Contribution to the Study of Bauxites' Formation in the Fongo-Tongo (Western Cameroon) Sites* (Switzerland: Springer International Publishing), pp. 241–244 , 2019.
[17] A. Sylvain, W.H. Tchungouelieu, F. Ngapgue, V. Katte and V.K. Beyala, Mineralogical and Geotechnical Characteristics of the Loose Weathered Trachytes of Fongo-Tongo (West-Cameroon), 2014. [Online]. https://www.researchgate.net/publication/316715585 (accessed Sep 12, 2022).
[18] ISO 11665-4, Measurement of Radioactivity in the Environment— Air: Radon-222 — Part 4: Integrated Measurement Method for Determining Average Activity Concentration Using Passive Sampling and Delayed Analysis, 2021, https://www.iso.org/obp/ui/#iso:std:iso:11665:-4:ed-3:v1:en. (accessed Oct 3, 2022).
[19] Dieu Souffit G, M.J. Valdes, O.B. Modibo, TS. Flore, B.A.J. Félix and S. Tokonami, Water Air Soil Pollut. 1–16 (2022). doi:10.1007/s11270-022-05666-x.
[20] R. FTLab, RadonEye Plus2 (BLE & Wi-Fi) [Online] http://radonftlab.com/radon-sensor-product/radon-detector/new-rd200p-radon-detector/ Vol. 2, pp. 2–5, 2020 (accessed Oct 3, 2022).
[21] Gammadata, *User's Guide MARKUS 10 the Instrument for Determining the Radon Content in the Soil*, *Gammadata* (Gamnet, Uppsala, Sweden, 2019).
[22] ISO 11665-4, ISO 11665-11. Draft. Measurement of Radioactivity in the Environment. Air: Radon-222. Part 11: Test Method for Soil Gas with Sampling at Depth, International Organization for Standardization, 26 (2014). [Online]. https://standards.iteh.ai/catalog/standards/cen/f0e49bc5-ba47-4725-a91a-269a995d29bf/en-iso-11665-11-2019
[23] J. Kemski, R. Klingel, A. Siehl and M. Valdivia-Manchego, Environ. Geol. **56** (7), 1269–1279 (2009). doi:10.1007/s00254-008-1226-z.
[24] Y. Muhsin Zayir Al-Bakhat, Radiat. Sci. Technol. **3**(3), 29 (2017). doi:10.11648/j.rst.20170303.13.
[25] M. Neznal, Ann. Geophys. **48** (1), (2009). doi: 10.4401/ag-3192.
[26] M. Neznal and M. Neznal, Radiat. Prot. Dosimetry **160** (1–3), 214–216 (2014). doi:10.1093/rpd/ncu088.
[27] E. Lara, Z. Rocha, T.O. Santos, F.J. Rios and A.H. Oliveira, Radiat. Prot. Dosimetry **167** (1–3), 126–129 (2015). doi:10.1093/rpd/ncv228.

[28] RadEye Selection Guide, Handheld Detection for Any Scenario RadEye Selection Guide RadEye Product Family, 2012.
[29] Y. Prasad, G. Prasad, G.S. Gusain, V.M. Choubey and R.C. Ramola, Radiat. Meas. **43** (SUPPL.1), 369–374 (2008). doi:10.1016/j.radmeas.2008.04.056.
[30] F.S. Erees, G. Yener, M. Salk and Ö. Özbal, Radiat. Meas. **41** (3), 354–361 (2006). doi:10.1016/j.radmeas.2005.06.030.
[31] M. Karthik Kumar, N. Nagaiah, G. Mathews and M. Ambika, Radiat. Prot. Environ. **41** (3), 115 (2018). doi:10.4103/rpe.rpe_40_18.
[32] D. Xie, M. Liao and K.J. Kearfott, Influence of Environmental Factors on Indoor Radon Concentration Levels in the Basement and Ground Floor of a Building - A Case Study, 2015.
[33] I. Yarmoshenko, A. Vasilyev, G. Malinovsky, P. Bossew, Z.S. Žunić, A. Onischenko and M. Zhukovsky, Sci. Total Environ. **541**, 155–160 (Jan 2016). doi:10.1016/j.scitotenv.2015.09.077.
[34] V.M.C.R.C. Ramola. Environmental Geology. **32** 258–262 (1997).
[35] P.S. Tsopjio Jiomeneck, P. Tematio, M.A. Wilson and M. Yemefack, Open J. Soil Sci. **1** (3), 97–105 (2011). doi:10.4236/ojss.2011.13013.
[36] P. Tematio, L. Kengni, D. Bitom, M. Hodson, J.C. Fopoussi, O. Leumbe, H.G. Mpakam and D. Tsozué, J. Afr. Earth Sci. **39** (3–5), 447–457 (2004). doi:10.1016/j.jafrearsci.2004.07.020.
[37] Que sais-je N° 741 La radioactivité des roches by Coppens René bon Couverture souple (1957) Le-Livre.
[38] B. Djeufack, G.S. Bineng, O.B. Modibo, J. Emmanuel and N. Nkoulou, Correlation Between Ground 222 Rn and 226 Ra and Long-Term Risk Assessment at the at the Bauxite Bearing Area of Fongo-Tongo, Western Cameroon, 387–404, 2022.
[39] J. Chen, S. Tokonami, A. Sorimachi, H. Takahashi and R. Falcomer, Radiat. Prot. Dosimetry. **130** (2), 253–256 (2008). doi:10.1093/rpd/ncm503.
[40] Z. Szabó, G. Jordan, C. Szabó, Á. Horváth, Ó. Holm, G. Kocsy, I. Csige, P. Szabó and Z. Homoki, Isotopes Environ. Health Stud. **50** (2), 211–225 (2014). doi:10.1080/10256016.2014.862533.
[41] Z.S. Žunić, M. Janik, S. Tokonami, N. Veselinović, I.V. Yarmoshenko, M. Zhukovsky, T. Ishikawa, R.C. Ramola, G. Ciotoli, P. Jovanović and K. Kozak, J. Radiat. Res. **50** (4), 355–361 (2009). doi:10.1269/jrr.08098.
[42] B. Shang, B. Chen, Y. Gao, Y. Wang, H. Cui and Z. Li, Radiat. Environ. Biophys. **44** (3), 193–199 (Dec 2005) . doi:10.1007/s00411-005-0020-5.
[43] Z. Stojanovska, K. Ivanova, P. Bossew, B. Boev, Z.S. Žunić, M. Tsenova, Z. Ćurguz, P.M. Kolarž, M. Zdravkovska and M. Ristova, Nucl. Technol. Radiat. **32** (1), 77–84 (2017). doi:10.2298/NTRP1701077S.
[44] R. Lindsay, R.T. Newman and W.J. Speelman, Appl. Radiat. Isot. **66** (11), 1611–1614 (Nov 2008). doi:10.1016/j.apradiso.2008.01.022.
[45] I. Malmonge Martin, **5** (8), Radon gas intensity variation from April to July 2018 in são josé dos campos, Brazil region. Global J. Of Engg. Science And Researches. **5** (8) (2018). doi:10.5281/zenodo.1342502.
[46] P. Saïdou, E. Abiama and S. Tokonami, Radioprotection. **50** (4), 265–271 (Oct 2015). doi:10.1051/radiopro/2015017.
[47] D.T. Esan, M.K. Sridhar, R Obed, Y. Ajiboye, O. Afolabi, B. Olubodun and O.M.Oni, Sci. Rep. **10** (1), 1–10 (2020). doi:10.1038/s41598-020-64217-8.
[48] P.T. Huynh Nguyen, V.T. Nguyen, N.B. Vu, V.D. Nguyen and H. Le Cong, J. Environ. Radioact. **193–194** (August), 27–35 (2018). doi:10.1016/j.jenvrad.2018.08.017.
[49] H. Curien, Presses Universitaires de France, Paris, **1**, 126.
[50] F. Barazza, W. Gfeller, M. Palacios and C. Murith, Radiat. Prot. Dosimetry. **167** (1–3), 75–81 (Nov 2015) . doi:10.1093/rpd/ncv209.
[51] H.U. Johner and H. Surbeck, Sci. Total Environ. **272** (1–3), 337–341 (2001). doi:10.1016/S0048-9697(01)00712-4.
[52] H. Friedmann, A. Baumgartner, M. Bernreiter, J. Gräser, V. Gruber, F. Kabrt, H. Kaineder, F. J. Maringer, W. Ringer, C. Seidel and G. Wurm, J. Environ. Radioact. **166**, 382–389 (2017). doi:10.1016/j.jenvrad.2016.04.028.
[53] J. Chen and K.L. Ford, J. Environ. Radioact. **166**, 152–156 (2017). doi:10.1016/j.jenvrad.2016.01.018.

[54] S.M. Farid, Indoor. Built. Environ. **25** (1), 269–278 (2016). doi:10.1177/1420326X14536749.
[55] P. Pisapak, N. Todorovic and T. Bhongsuwan, Environ. Earth Sci. **76** (4), 1–11 (2017). doi:10.1007/s12665-017-6439-6.
[56] J.E. Ndjana Nkoulou, L.N. Engola, M. Hosoda, D. Bongue, T. Suzuki, H. Kudo, M.G. Kwato Njock and S. Tokonami, Radiat. Prot. Dosimetry. **185** (3), 391–401 (Dec 2019). doi:10.1093/rpd/ncz026.
[57] A. Saïdou, Y.F. Tchuente Siaka and M.G. Kwato Njock, Radioprotection. **50** (1), 35–41 (Jan 2015). doi:10.1051/radiopro/2014025.

radiation

MDPI

Article

Correlation between Ground ^{222}Rn and ^{226}Ra and Long-Term Risk Assessment at the at the Bauxite Bearing Area of Fongo-Tongo, Western Cameroon

Léonard Boris Djeufack [1,2], Guillaume Samuel Bineng [1], Oumar Bobbo Modibo [2], Joseph Emmanuel Ndjana Nkoulou II [2] and Saïdou [1,2,*]

[1] Nuclear Physics Laboratory, Faculty of Science, University of Yaoundé I, Yaoundé P.O. Box 812, Cameroon
[2] Research Centre for Nuclear Science and Technology, Institute of Geological and Mining Research (IRGM), Yaoundé P.O. Box 4110, Cameroon
* Correspondence: saidous2002@yahoo.fr; Tel.: +237-674-174-473

Simple Summary: This paper presents a study of radioactivity in soil that included an assessment of radiological risk parameters and long-term health risks from exposure to naturally occurring radionuclides in soil at the bauxite-bearing area of Fongo-Tongo in Western Cameroon. The radionuclides measured in the soil had concentration values above the recommended limits. However, the total long-term excess risk at the site decreased progressively over the years, and the maximum value of 8.58×10^{-3} was obtained at T = 0 years. In addition, the external pathway is the largest contributor to the total excess risk assessed inside the building. The maximum risk value for this pathway, which is 2.33×10^{-2}, was obtained at T = 30 years before decreasing sharply thereafter.

Abstract: The aim of the current work was to study natural radioactivity in soil and the correlation between ^{222}Rn and ^{226}Ra in the ground and to assess the onsite and indoor long-term excess cancer risk at the bauxite bearing area of Fongo-Tongo in Western Cameroon. ^{222}Rn was measured in the ground at a depth of one meter, using Markus 10 detector. ^{226}Ra, ^{232}Th, and ^{40}K activity concentrations were measured in soil by two techniques, in situ and laboratory gamma spectrometry. The mean values of ^{222}Rn concentrations in the ground were 69 ± 18 kBqm^{-3} for Fongo-Tongo and 82 ± 34 kBq m^{-3} for the locality of Dschang, respectively. The mean values of ^{226}Ra, ^{232}Th, and ^{40}K activity concentrations obtained with in situ gamma spectrometry were 129 ± 22, 205 ± 61, and 224 ± 39 Bq kg^{-1} for ^{226}Ra, ^{232}Th, and ^{40}K, respectively, and those obtained by laboratory gamma spectrometry were 129 ± 23, 184 ± 54, and 237 ± 44 Bq kg^{-1}, respectively. A strong correlation between ^{222}Rn and ^{226}Ra activity concentrations determined by in situ and laboratory measurements (R^2 = 0.86 and 0.88, respectively) was found. In addition, it is shown that the total excess cancer risk has a maximum value of 8.6×10^{-3} at T = 0 year and decreases progressively in the long term. It is also shown that ^{226}Ra makes a major contribution, i.e., above 70%, to the total excess cancer risk.

Keywords: radium-226; radon-222; life excess cancer risk

Citation: Djeufack, L.B.; Bineng, G.S.; Modibo, O.B.; Ndjana Nkoulou, J.E., II; Saïdou Correlation between Ground ^{222}Rn and ^{226}Ra and Long-Term Risk Assessment at the at the Bauxite Bearing Area of Fongo-Tongo, Western Cameroon. *Radiation* **2022**, 2, 387–404. https://doi.org/10.3390/radiation2040029

Academic Editor: Michele Guida

Received: 9 October 2022
Accepted: 9 November 2022
Published: 14 November 2022

1. Introduction

Areas with high mining potential generally represent a very interesting field for environmental monitoring before, during, and after mining. In the case of the sites hosting not-yet-exploited ore deposits, activities related to exploration led to the transfer of soil from underground to the ground surface. This action could lead to the environmental pollution by natural radioactive materials, increasing the exposure level of inhabitants to natural radiation. Moreover, human exposure to natural radiation sources is ubiquitous and inescapable. Radionuclides in the earth's crust vary from one environment to another, depending on the soil and geological profile [1]. The content and type of radioelement depend, therefore, on the bedrock [2–4]. A long exposure to the natural radionuclides

(^{226}Ra, ^{232}Th, and ^{40}K) is mainly responsible for some cancers and sometimes for the effects of genetic mutations. They constitute a real threat to human health [5–7].

Many investigations on natural radioactivity have been made in the world [8–10]. The investigation conducted in Cameroon revealed the occurrence of high levels of radioactivity in some specific areas of the country [11–13]. These high radioactivity levels are more localized in areas with uranium, thorium, and bauxite mining potential. It is the case of the natural radioactivity measurements made in Poli and Lolodorf, Douala, Fongo-Tongo, Dschang, and Ngaoundal [13–15]. They revealed high ^{238}U, ^{232}Th, and ^{40}K activity concentrations in soil compared to their corresponding world levels, as well as ^{222}Rn and ^{220}Rn concentrations in dwellings above the WHO reference level [12,16–18]. These mentioned studies showed that the ^{222}Rn level in homes depends considerably on the type of architecture, geological structure, and mineralogical composition of soil of the area [16,19]. A good correlation between ^{238}U and ^{232}Th activity concentrations in soil with ^{222}Rn and ^{220}Rn in dwellings was found in the areas, respectively [20,21].

However, these studies have not specifically examined the correlation that may exist between ^{222}Rn and ^{226}Ra activity concentrations in soil. ^{222}Rn is a direct progeny of ^{226}Ra [1]. Therefore, its concentration in soil should be proportional to that of the direct parent, ^{226}Ra. ^{222}Rn measurement was performed by using a MARKUS 10 detector to a depth of 1 m in the ground. The determination of the activity concentrations of ^{226}Ra, ^{232}Th, and ^{40}K in soil was performed with a NaI (Tl) gamma spectrometer. In addition, the ^{222}Rn and ^{226}Ra activity concentrations determined by in situ and laboratory measurements are strongly correlated, and these correlation coefficients were determined. Radiological parameters (AEED, Ra_{eq}, H_{in}, H_{ex}, ELCR, I_γ, and I_α) were determined to assess the level of public exposure to natural radioactivity in the area, and a map of the distribution of ^{226}Ra and ^{222}Rn concentrations in soil was established.

2. Materials and Methods

2.1. Study Areas

The area is located on the mountainous chain region of the Western Cameroon, specifically at the southwestern flanks of the Bamboutos Mountains [22]. The climate of the area is sub-equatorial, Cameroonian type, cold and humid, characterized by a long rainy season (March–November) and a short dry season (December–February). The average temperature and rainfall in the area are 22.5 °C and 1364.4 mm over the year, respectively [23,24]. The soils are Andic type, ferrallitic, trachytic, granitic, and basaltic [22,24,25].

This area is underlain by an extensive and thick loose mantle developed on trachyte and generally forms a differentiated geological profile, including the presence of deposits formed by new bauxite minerals; it was discovered in 1957 by BUMIFOM prospectors [26,27]. This locality is one of the main bauxite deposit sites in the western region of Cameroon. Its potential is estimated at 45 million tons and is a part of the major geological reserves of Cameroon [26,28]. Figure 1 shows a geological map of the study area.

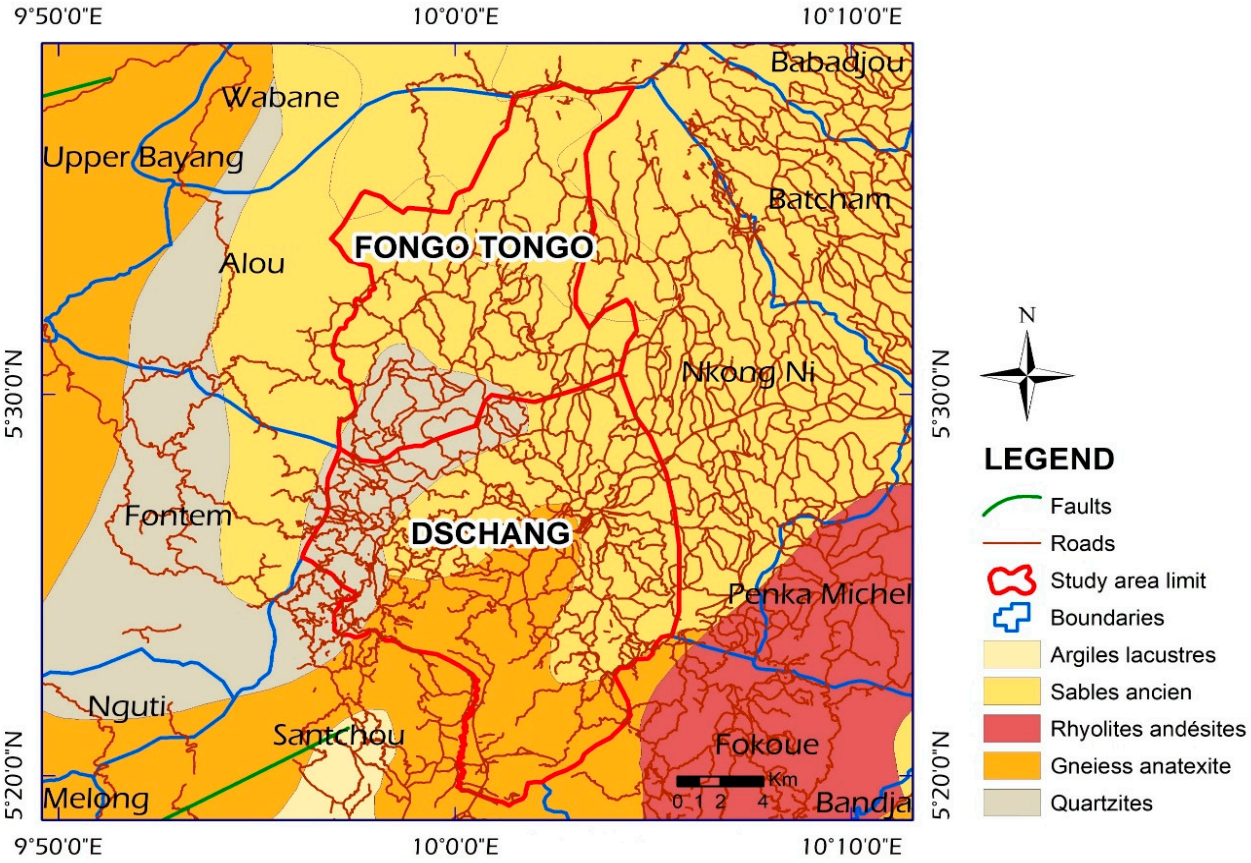

Figure 1. Soil characteristics map of the area.

2.2. Natural Radioactivity Measurements

2.2.1. Radioactivity Measurements in Laboratory

A total of twenty-seven soil samples (fifteen in Dschang and towel in Fongo-Tongo) were randomly collected for a depth between 0 and 5 cm. The samples were collected, crushed, and then dried at 100 °C for 48 h to remove moisture and mold. Then they were crushed and filtered to a size of 1 mm, transferred to Marinelli containers of 500 cm^3 each, tightly closed, and stored for at least 28 days to reach secular equilibrium between ^{222}Rn and its decay products [29,30].

^{226}Ra, ^{232}Th, and ^{40}K activity concentrations were obtained by using a NaI (Tl) scintillation spectrometer Model 802 with a crystal size of 7.6 cm × 7.6 cm and a resolution of 7.5% at 661.6 keV, with a 1024-channels multichannel analyzer. It was calibrated in energy with reference sources containing ^{60}Co (1173.23 and 1332.5 keV), ^{133}Ba (383.9 keV), ^{54}Mn (834.9 keV), ^{22}Na (511 and 1274.5 keV), and ^{137}Cs (661.6 keV) from the IAEA and in efficiency by a multi-energy standard analyzed under the same experimental conditions as the samples [31,32]. This standard is a blend of different radioactive sources, forming an energy range from 59.54 to 1836 keV [^{60} C (1173.2 and 1332.5 keV), ^{137} Cs (661.6 keV), ^{152} Eu (1407.5, 1112, 964.079, and 778.9 keV), ^{40}K (1460.8 keV), ^{137}Cs (661.6 keV), ^{208}Tl (2614.4 keV), and ^{228}Ac (940.1 keV)].

After reaching secular equilibrium between ^{222}Rn and its progeny, a gamma-ray line at 609.3 KeV of ^{214}Bi was considered to determine the activity concentration of ^{226}Ra, and a gamma-ray line at 969 KeV of ^{228}Ac used to determine that of ^{232}Th [33]. The spectra analysis was carried out by using GENIE 2000 (Canberra) software. ^{226}Ra, ^{232}Th, and ^{40}K activity concentrations in soil were determined by the following equation [17,34,35]:

$$A = \frac{N_p}{t_c \times I_\gamma(E_\gamma) \times \varepsilon(E_\gamma) \times M} \quad (1)$$

where N_P is the number of counts in a given peak area at energy, E; $\varepsilon(E_\gamma)$ the detection efficiency at energy, E; t_c is the counting time of 100,000 s; $I_\gamma(E_\gamma)$ is the number of gamma-rays per decay of that nuclide at energy, E, and M, the mass in kg, of the sample. The uncertainty on the activity concentration (ΔA) was obtained by the following equation [36,37]:

$$\frac{\Delta A}{A} = \sqrt{\left(\frac{\Delta N_p}{N_p}\right)^2 + \left(\frac{\Delta I_\gamma}{I_\gamma}\right)^2 + \left(\frac{\Delta \varepsilon}{\varepsilon}\right)^2 + \left(\frac{\Delta M}{M}\right)^2} \quad (2)$$

where ΔN, ΔI_γ, $\Delta\varepsilon$, and ΔM are the uncertainties in the count rate, emission probability found in the nuclear data tables, efficiency, and sample mass, respectively.

2.2.2. In Situ Radioactivity Measurements

They were performed simultaneously with sampling for laboratory analysis. Those measurements were made randomly at different points of the area with NucScout detector (portable Gamma Identifier-Quantifier—Dose Rate Meter) version 2018. It was installed one meter above the ground surface on a dry wooden stand. The measurement on a sample point took 45 min [38].

The NucScout is a high-sensitivity Na (Tl) gamma detector, with an integrated photo multiplier and high-voltage-supply cylindrical scintillation crystal, 2″× 2″, with an energy range of 25 keV–3 MeV (optional from 10 keV to 1.6 MeV) and resolution < 8% (Cs-137/662 keV). It works with an integrated battery. The instrument has several options such as the selection of the measurement cycle, the reading, and the calculation of the results of a measurement. It has an integrated GPS that allows users to geolocate a sampling point, or even to bring out a Maps distribution of the different measured points. The data of the different measurements obtained on the site are stored on an a USB support or on an SD card and transferred for analysis and to a PC [39]. These data are visualized with the dvision software [40]. The detector is calibrated when connected to a PC, using the dconfig software [40]. ^{226}Ra, ^{232}Th, and ^{40}K activity concentrations were obtained by using gamma lines at 609.3 KeV of ^{214} Bi, 2614 KeV of ^{208}Tl, and 1461 of ^{40}k, respectively.

2.2.3. In Situ ^{222}Rn in Soil Measurements

Measurements were taken at different locations with Markus 10 version 1.4. This instrument was developed by RADONOVA Laboratories to measure the volumic activity of ^{222}Rn in soil, with about 3 kg and 16 keV of resolution energy (under vacuum); it is an ORTEC Ultra Silicon detector with dimensions of 220 × 122 × 80 cm^3, with a pumping capacity of 1.8 L/min every 30 s, under a limiting pressure of 0.96 bar. The duration of a measurement is typically 12 min, and its battery has a capacity of about 70 measurements before being fully recharged for 8 h [41].

The principle of measurement of the device consists of two steps. The first step is the pumping phase of the gas contained in soil. This is achieved with a probe buried one meter in the ground. The gas is sucked from the ground into the measuring chamber for a short period. The pumping phase is automatically stopped when the pressure in the probe drops; when the pressure rises, the pump starts again. The pumping phase is finally stopped when a capacity of 0.91 L is reached. The next one is automatically started and consists of the measurement. The measuring chamber is immediately switched on. An electric field pushes the radon progeny into the measuring chamber, where the alpha radiation they emit is recorded. These electric pulses recorded by the sensor are amplified and then filtered in the analysis channel, which allows only the counting of pulses corresponding to the energy coming from the ^{218}Po. A latent measuring background is created in the ionization chamber of the system by filtering out the pulses from the ^{214}Po. The evolution of the measurement can be read on a screen, with each hit recorded by the sensor, until the screen displays a fixed value to signify the end of the measurement.

2.3. Radiological Hazards

2.3.1. Ambient Equivalent Dose Rates and External Effective Dose

Ambient equivalent dose rates in air at distance of one meter on the ground surface are calculated using the conversion factor of 0.0417 (nGy h^{-1})/(Bq kg^{-1})$^{-1}$ for ^{40}K, 0.462 (nGy h^{-1})/(Bq kg^{-1})$^{-1}$ for ^{226}Ra, and 0.604 (nGy h^{-1})/(Bq kg^{-1})$^{-1}$ for ^{232}Th in the following equation [1].

$$D\left(\text{nGy h}^{-1}\right) = 0.462A_{Ra} + 0.604A_{Th} + 0.0417A_{k} \quad (3)$$

where A_{Ra}, A_{Th}, and A_K are the mean concentrations of each radionuclide given in (Bq kg^{-1}). The effective dose due to external irradiation, E (mSv y^{-1}), was calculated by using the following formula [42,43]:

$$E\left(\text{mSv y}^{-1}\right) = F_c[F_{occ}F_b + (1 - F_{occ})] \times D \times T \times 10^{-6} \quad (4)$$

where F_c = 0.7 is the conversion coefficient of the absorbed dose in the air to effective dose received by adults, T is the exposure time expressed in hours, F_b (0.98) is the impact factor of the building material experimentally obtained on the site, and F_{occ} = 0.8 is the occupancy coefficient [1].

2.3.2. External and Internal Hazard Index

External Hazard Index (H_{ex})

The external hazard index was introduced to limit radiation exposure in the samples to a permissible dose-equivalent limit of 1.00 mSv y^{-1} [1,9,44], and it is assessed by Equation (5):

$$H_{ext} = \frac{A_{Ra}}{370} + \frac{A_{Th}}{259} + \frac{A_K}{4810} \leq 1 \quad (5)$$

The external hazard index must not exceed the limit of unity for the radiological risk to be insignificant. The maximum value of H_{ext} equal to unity corresponds to the upper limit of 370.00 Bq kg^{-1} of ^{226}Ra [1,9,45].

Internal Hazard Index (H_{in})

Furthermore, the deposition period of ^{222}Rn progeny in the pulmonary is also very dangerous [5,44]. In order to take this threat into account and reach the normal limit of 185 Bq kg^{-1}, the permissible value for ^{226}Ra is reduced by half to reach the limit of the unit. It is evaluated by using the following equation [44,46]:

$$H_{in} = \frac{A_{Ra}}{185} + \frac{A_{Th}}{259} + \frac{A_K}{4810} \leq 1 \quad (6)$$

2.4. Excess Lifetime Cancer Risk (ELCR)

The ELCR is the probability that an individual will contract or develop a radiation-induced cancer during his lifetime because of his exposure to ionizing radiation. It was estimated for this by using Equation (7) [9,13,47]:

$$ELCR = ELCR_{out} + ELCR_{in} \quad (7)$$

$ELCR_{out} = E_{out} \times D_L \times RF$ is the outdoor risk; $ELCR_{in} = E_{in}\ D_L \times RF$ is the indoor risk; E_{out} and E_{in} are the indoor and outdoor effective dose, respectively; DL is the average life expectancy of 70 years; and RF is the risk factor (risk of fatal cancer per mSv). In its publication 106, ICRP recommends value of RF = 0.05 $\times$ 10^{-3} mSv^{-1} for induction to stochastic effects of members to the public [5].

2.5. Excess Cancer Risk (ECR) Computer Using RESRAD-ONSITE and RESRAD-BUILD Codes

Since most dwellings in the study are constructed with locally manufactured earthen or sand bricks, the ^{40}K, ^{226}Ra, and ^{232}Th concentrations in soil are input data (contaminant on source parameters) at runtime by RESRAD-ONSITE and RESRAD-BUILD codes version 7.2 and 3.5, respectively.

RESRAD-ONSITE is used to assess the ECR due to these naturally occurring radionuclides in soil at the bauxite-bearing area of Fongo-Tongo. The site-specific characteristics of the area are listed in Table 1. The other parameters are used as defaults values [48]. Together, all the above parameters were considered in the evaluation of the risk factors.

Table 1. Input parameters for RESRAD codes.

RESRAD-ONSITE	
Parameters	Site-Specific Data
Site-specific data	25,000 m^2
Cover depth	1 m
Density of contaminated zone	1.8 cm^3 g^{-1}
Precipitation rate	0.4473 m y^{-1}
Wind speed	1.2 m s^{-1}
Well pump intake	8 m
RESRAD-BULD	
Indoor/time fraction	0.6
Number of room/occupants	1
Deposition velocity	0.01 m s^{-1}
Resuspension rate	5×10^{-7} s^{-1}
Room surface area and volume	16 m^2 and 40 m^3
Breathing rate	18 m^3 d^{-1}
Ingestion rate	44,661
Occupant location in the room	Centered
Shielding thickness	0
Type of source	Volume
Source geometry	Rectangular
Release air fraction	0.1
Radon diffusion rate	2×10^{-5} m s^{-1}
Porosity	0.1

RESRAD-BUILD allowed for the assessment of radiation doses received by a resident living or working in a house contaminated by radioactive materials. These doses are those from the different exposure pathways (external and internal, including inhalation of radon progeny inside the home). The radiological risk was estimated over the periods of 1, 10, 30, 50, 70, and 90 years of exposure. However, 85% of the dwellings in the area are made of mud bricks, usually produced on the same site, and samples of these earth bricks were analyzed to obtain the concentrations introduced as input data mentioned above. Table 1 presented the other input parameters.

2.6. Radiation Hazard Index

2.6.1. Gamma Radiation Hazard Index (I_γ)

The gamma radiation risk index was estimated from Equation (8) [47,49]:

$$I_\gamma = \frac{A_{Ra}}{300} + \frac{A_{Th}}{200} + \frac{A_K}{3000} \leq 1 \quad (8)$$

It is the index of nuclear energy level for external radiation due to specific activity of different natural radionuclides in a sample [50]. Its permissible limit is I_γ = 1 and corresponds to 0.3 mSv y^{-1}. It is used to evaluate the gamma-radiation risk level associated with naturally occurring radionuclides.

2.6.2. Alpha Radiation Hazard Index (I_α)

The excess alpha radiation following radon inhalation from building materials is determined by using Equation (9) [51,52]:

$$I_\alpha = \frac{A_{Ra}}{200} \leq 1 \quad (9)$$

The upper limit of I_α is unity because a building material with a ^{226}Ra concentration of less than 200 Bq kg^{-1} cannot cause a minimum radon concentration greater than 200 Bq m^{-3}.

3. Results and Discussion

3.1. ^{226}Ra, ^{232}Th, and ^{40}K Activity Concentrations

In Fongo-Tongo, the ^{226}Ra, ^{232}Th, and ^{40}K activity concentrations obtained by laboratory and in situ methods ranged from 106 to 170 Bq kg^{-1} and from 93 to 201 Bq kg^{-1} for ^{226}Ra; from 119 to 295 Bq kg^{-1} and from 40 to 327 Bq kg^{-1} for ^{232}Th; and from 188 to 458 Bq kg^{-1} and from 49 to 321 Bq kg^{-1} for ^{40}K.

In Dschang, the ^{226}Ra, ^{232}Th, and ^{40}K activity concentrations range from 99 to 167 Bq kg^{-1} and from 98 to 181 Bq kg^{-1} for ^{226}Ra, from 100 to 275 Bq kg^{-1} and from 139 to 309 Bq kg^{-1} for ^{232}Th; and from 198 to 297 Bq kg^{-1} and from 151 to 280 Bq kg^{-1} for ^{40}K. Figure 2 shows the box-plot distributions of these concentrations in laboratory (a) and in situ (b) for each locality and for the whole study area.

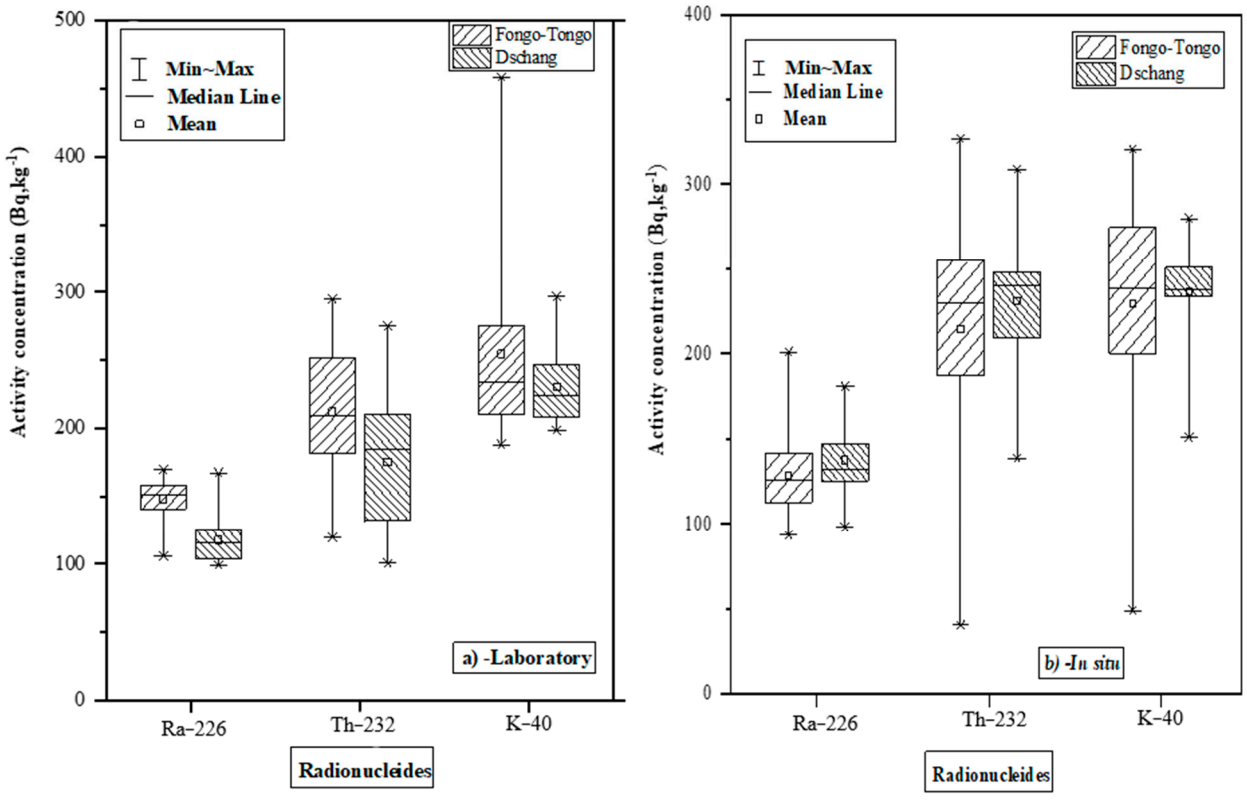

Figure 2. Boxplot distribution of activity concentration of ^{226}Ra, ^{232}Th, and ^{40}K obtained by laboratory (**a**) and in situ (**b**) measurements.

According to Table 2, 50% of sampling points have a concentration higher than 151 Bq kg^{-1}, 209 Bq kg^{-1}, and 234 Bq kg^{-1} for ^{226}Ra, ^{232}Th, and ^{40}K, respectively, in laboratory measurements. Furthermore, the in situ measurements follow a lognormal distribution. Thus, the mean value is represented by the geometric mean, whereas laboratory measurements follow a normal distribution and are represented by the arithmetic mean.

Table 2. Statistical parameters of ^{226}Ra, ^{232}Th, ^{40}K, and ^{222}Rn concentrations obtained by in situ and laboratory measurements for the localities of Dschang and Fongo-Tongo.

Locality	Parameters	Activity Concentration (Bq kg^{-1})						^{222}Rn (kBq m^{-3})
		Laboratory			In situ			
		^{226}Ra	^{232}Th	^{40}K	^{226}Ra	^{232}Th	^{40}K	
Fongo-Tongo	Min–Max	106–170	119–295	188–458	93–201	94–327	49–321	35–202
	Median	151	209	234	126	229	239	53
	AM ± SD	148 ± 23	212 ± 54	230 ± 28	-	-	-	-
	GM(GSD)	-	-	-	129 (16)	214 (67)	229 (54)	69 (8)
Dschang	Min–Max	99–167	100–275	198–297	98–181	139–309	151–280	48–255
	Median	116	185	224	132	240	238	62
	AM ± SD	118 ± 17	175 ± 46	230 ± 28	-	-	-	-
	GM(GSD)	-	-	-	138 (19)	231 (35)	237 (26)	82 (14)

AM, arithmetic mean; GM, geometric mean; SD, standard deviation; GSD, geometric standard deviation.

Soil samples analyzed in the laboratory have high concentrations of ^{226}Ra and ^{232}Th. As presented in Table 2, the minimum and maximum values of ^{226}Ra obtained in laboratory and in situ measurements are, respectively, three and five times higher than the world average value of 35 Bq kg^{-1} [1]. In the case of ^{232}Th, they are two and four times higher than the world average value of 45 Bq kg^{-1}, respectively [1]. These high values of ^{226}Ra and ^{232}Th activity concentrations are also observed for the results obtained by in situ gamma spectrometry. The minimum values of ^{226}Ra and ^{232}Th are, respectively, three and two times higher than the world average value, while the maximum values are, respectively, six and seven times higher than the world average value [1]. Furthermore, the average values of ^{40}K, as well as the maximum values for in situ and laboratory methods, are lower than 420 Bq kg^{-1}, the world average value [1].

Figure 1 shows that the investigated area extends over a geological structure covered by basaltic and trachytic granitic rocks [27,53]. The ^{226}Ra, ^{232}Th, and ^{40}K activity concentrations differ from one point to another for the two techniques used: in situ and laboratory gamma spectrometry. This can be explained by the fact that radioactivity is not uniformly distributed in the soil [**54**]. It is reported that ^{238}U, ^{232}Th, and ^{40}K have high concentrations in some rocks, such as syenite, granite, granulite, rhyolites, and plutonic [3,4,54]. The low concentrations of ^{40}K can be explained by the phenomenon of leaching and transport of potassium elements to the surface due to the effects of erosion, drainage, and an accumulation of sediments in the seabed [55]. The transfer of ores by erosion or by eruptive voice can therefore considerably modify the content and concentrations of this radionuclide in the soil. It has low concentrations in basalt [3,4,54]. According to Figure 1, the presence of the above rocks can account for considerable variation in the concentrations of these primordial radionuclides from one site to another, as shown in Figure 2.

3.2. In Situ ^{222}Rn Concentration in Soil

^{222}Rn concentrations at 1 m depth in soil, presented in Table 2, ranged from 35 to 202 kBq m^{-3}, with a mean value of 69 ± 40 kBq m^{-3}, in Fongo-Tongo; and from 48 to 255 kBq m^{-3}, with a mean value of 82 ± 56 kBq m^{-3}, in Dschang. According to Table 2, more than half of the sampled points have ^{222}Rn in soil greater than or equal to 62 kBq m^{-3} in Dschang and 53 kBq m^{-3} in Fongo-Tongo. According to Figure 3, a majority of the radon concentrations in soil are above the value of 40 kBq m^{-3}, as represented by the red line. According to the Swedish risk assessment criteria, this latter value represents the limit for which a site presents a high radon-exposure risk [56]. The difference between ^{222}Rn concentrations in soil from one location to another may be due to the geological structure and the mineralogical composition of the soil in the area [54,55]. The geological structure, the geochemical process of the soil, and the rate of gas emanation in the region are influenced by the permeability of the soil [27,28,49,53,54].

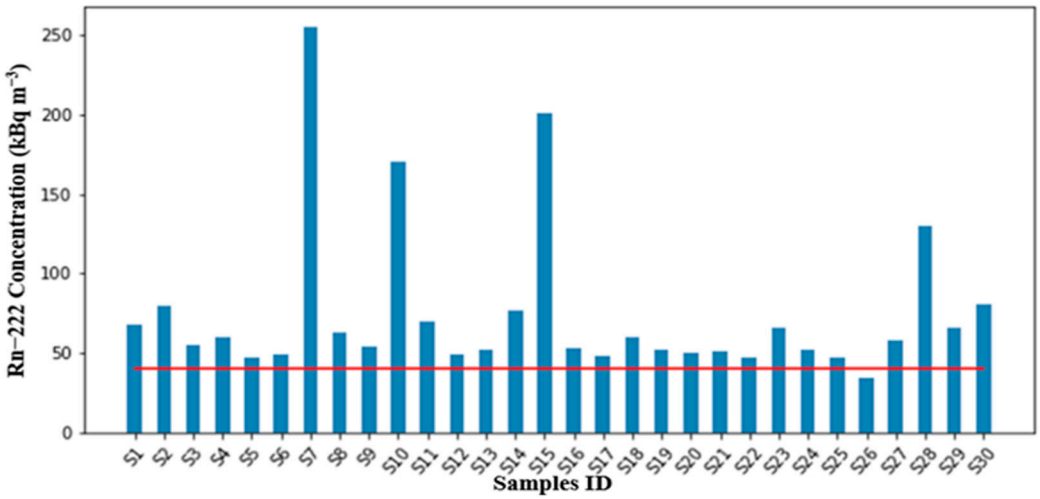

Figure 3. ^{222}Rn distribution in soil of the bauxite bearing area of Fongo-Tongo.

Table 2 shows that the average and maximum values of ^{222}Rn in soil in Dschang are higher than those in Fongo-Tongo. This is not the case with the ^{226}Ra values obtained in these two localities. This is probably due to the influence of soil moisture and porosity. In addition, the soil in the Fongo-Tongo may be more compact and moister than in Dschang [25,53]. In additional, Table 3 shows that activity concentrations of the primordial radionuclides in soil in Cameroon is higher than in some other regions of the world [51,52,57,58]. Nevertheless, ^{40}K concentrations are also high elsewhere than in the present study [46,52].

Table 3. Comparison of ^{226}Ra, ^{232}Th, ^{40}K, and ^{222}Rn activity concentration with other countries.

Country	Activity Concentration (Bq kg^{-1})			^{222}Rn (kBq m^{-3})	References
	^{226}Ra	^{232}Th	^{40}K		
Jordan	57.7 ± 5.4	18.1 ± 1.4	138.1 ± 40.8		[46]
Egypt	134.7 ± 24.1	131.8 ± 16.7	11,644 ± 550		[59]
India	116.1	43.51	300.07	-	[37]
Iraq	58.44 45.71	19.38 20.33	321.76 337.02	-	[9]
Nigeria	64.64 ± 28.10	110.18 ± 46.12	1190.10 ± 373.62		[51]
Australia	38	45	635	-	[10]
Germany	84	72	463	-	
Sweden	75	94	734		
Japan	38 ± 1	43 ± 1	590	-	[8]
Cameroon	14 ± 2	30 ± 3	103 ± 12	9 ± 2	[60]
	-	390	850	-	[14]
	124.9	157.3	670.9		[61]
	166.18	170.04	94.54		[13]
	118 ± 17 (138 ± 19) 148 ± 23 (129 ± 16)	175 ± 46 (231 ± 35) 212 ± 54 (214 ± 67)	230 ± 28 (237 ± 26) 230 ± 28 (229 ± 54)	82 ± 56 69 ± 40	Present study

3.3. Correlation between ^{222}Rn and ^{226}Ra in Soil

According to Figure 4, it is shown that ^{222}Rn concentrations in soil are directly related to those of ^{226}Ra measured at the site and in soil samples collected in the area. The R^2 = 0.88 and R^2 = 0.86 values were found between ^{222}Rn and ^{226}Ra concentrations for the laboratory method and in situ method, respectively. These high values of the coefficients obtained for each case reveal that ^{222}Rn and ^{226}Ra are strongly correlated. Similarly, the Pearson correlation coefficient determined for both sets of measurements is equal to 0.92 for the

laboratory and 0.90 for in situ. These respective Pearson correlation coefficients for the two series confirm the strong correlation between the two radionuclides.

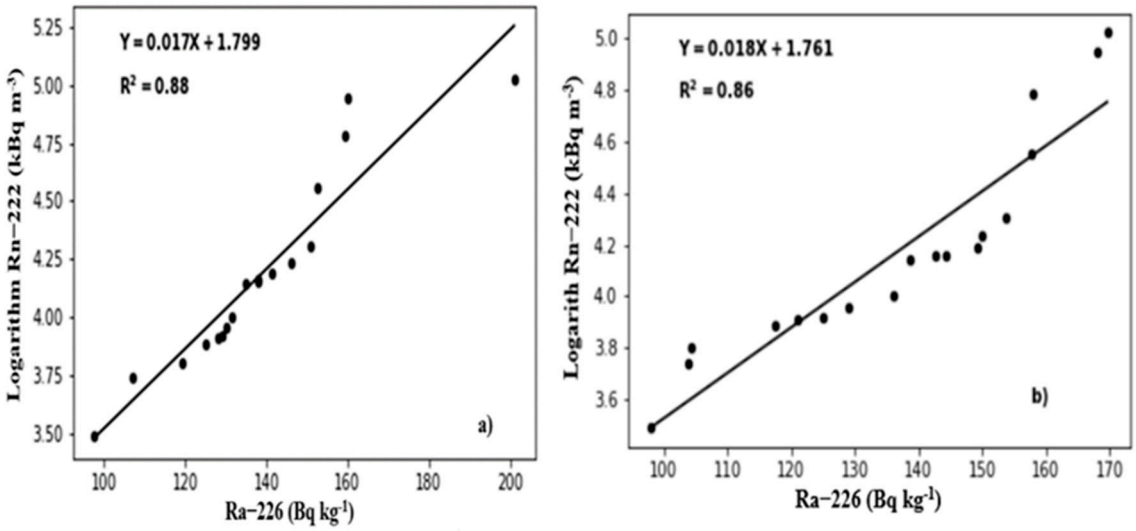

Figure 4. Correlation between ^{222}Rn/^{226}Ra concentrations in soil: (**a**) laboratory gamma-ray spectrometry and (**b**) in situ gamma-ray spectrometry.

For the values observed between 110 and 150 Bq kg^{-1} (Figure 4a) and values between 130 and 160 Bq kg−1 (Figure 4b), the residual is relatively constant, and for the extreme values, it increases slightly, which shows a dispersion of the maximum values from the median value. This can be justified by the fact that the number of samples of the different datasets is not very high to make the scatterplot dense enough and have a better regression. That is, the closer in the series values are to each other, the better correlation the coefficient and the stronger correlation intensity. This also means that, the smaller the standard deviation is between the data, the better the regression and the stronger the correlation between the two radionuclides.

The high values of ^{222}Rn concentration in soil gas at some locations certainly originate from the deep sources of permeable soil, which allows ^{222}Rn to easily escape from its cradle, which is ^{226}Ra, and migrate to the free surface of the soil. In other words, the high emanation of ^{222}Rn at a measurement point is closely related to the nature of underlying rock, geochemical process, physicochemical soil properties, and ^{226}Ra content in soil. The correlation observed between these concentrations depends on the geological structure of the area [62]. Similar results are reported in previous studies [47,63].

As shown in Figure 1, the area contains different rock formations, such as granite, basalt, gneiss, and trachyte. In addition, it is characterized by a deposit of bauxite ores [26,27]. Granite, mined in quarries in Dschang and Fongo-Tongo, is probably a potential source of ^{226}Ra distributed in the area. It is known to have a high content of uranium, thorium, and potassium at high temperatures in these rocks [54]. ^{222}Rn emanation may therefore be stronger in an area underlain by granitic bedrock.

Figure 5 shows the distribution map of ^{222}Rn and ^{226}Ra activity concentrations in the soil of the study area. It shows that the activity concentration of ^{226}Ra in soil increases with the ^{222}Rn concentration in its close proximity.

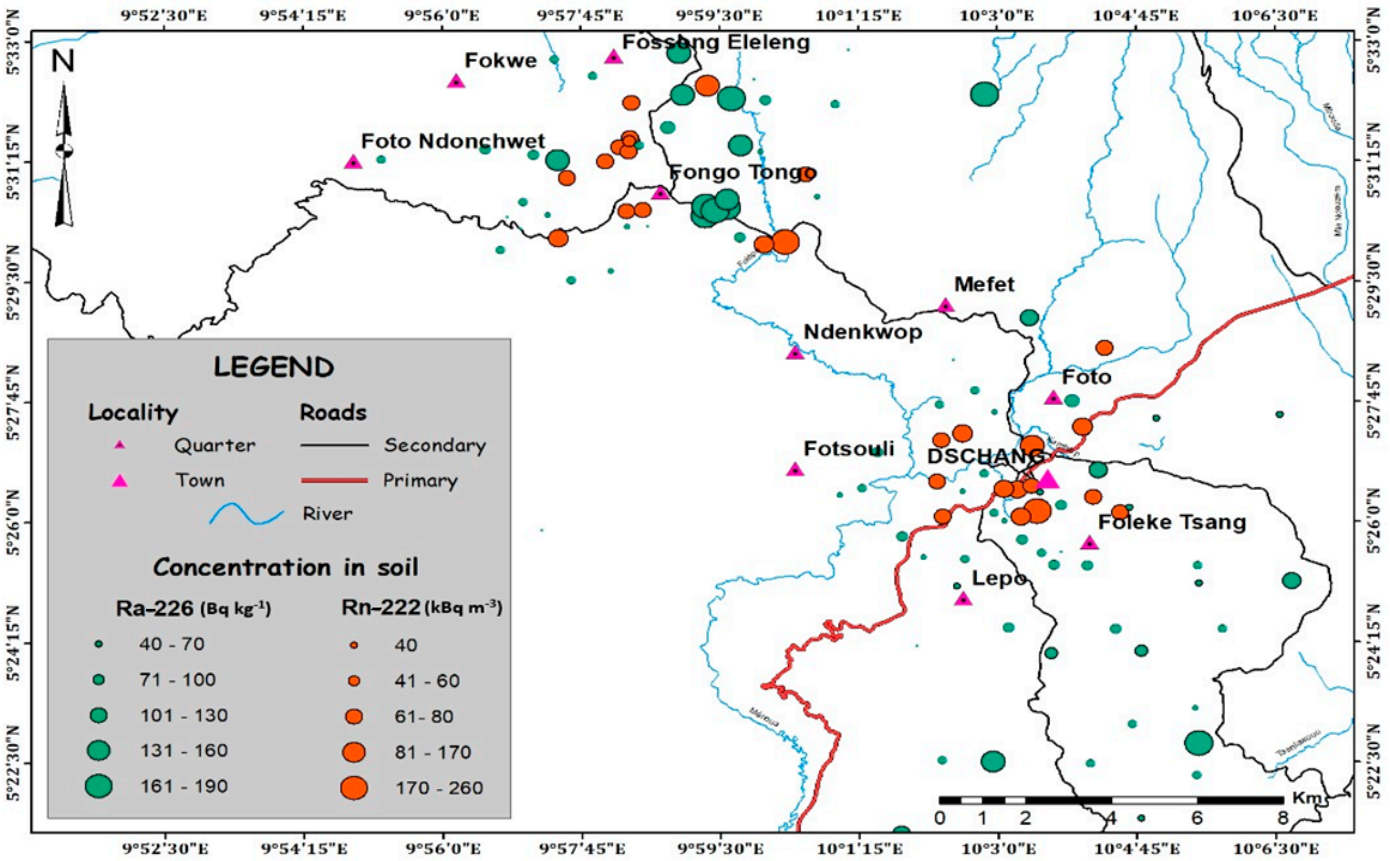

Figure 5. Map distribution of ^{222}Rn and ^{226}Ra concentrations in the soil of the study area.

3.4. Radiological Hazards

3.4.1. Ambien Equivalent Dose Rate (AEDR) and Annual External Effective Dose (AEED)

The AEED obtained in the laboratory ranged from 0.58 to 1.62 mSv y^{-1}, with a mean value of 1.27 ± 0.27 mSv y^{-1}, in Fongo-Tongo; and from 0.73 to 1.46 mSv y^{-1}, with a mean value of 1.05 ± 0.17 mSv y^{-1}, in the Dschang locality. According to Table 4 the average values for the whole study area are above the safety limit of 1.00 mSv y^{-1} [1].

Table 4. Summary of the different radiological parameters obtained in laboratory.

Locality	Fongo-Tongo					Dschang					Limit
Parameters	Min	Max	Med	AM	SD	Min	Max	Med	AM	SD	
AEDR (nGy/y)	130	265	211	207	37	119	238	172	170	31	1
AEED (mSv)	0.8	1.62	1.29	1.27	0.22	0.73	1.46	1.05	1.04	0.19	1
H_{in}	1.36	2.81	1.82	1.88	0.37	1.36	1.92	1.57	1.6	0.15	1
H_{out}	1.07	2.35	1.41	1.48	0.33	1.29	1.58	1.29	1.29	1.02	1
$ELCR_{in}$	1.68	3.4	2.71	2.67	0.47	1.53	3.06	2.21	2.18	0.4	
$ELCR_{out}$	1.12	2.26	1.81	1.78	0.31	1.02	2.04	1.47	1.46	0.27	
ELCR	2.59	5.66	4.52	4.44	0.78	2.55	5.11	3.69	3.64	0.66	
I_α	0.53	0.85	0.76	0.74	0.08	0.49	0.84	0.58	0.59	0.09	1
I_γ	1.02	2.11	1.66	1.64	0.3	0.93	1.9	1.36	1.34	0.25	1

AM, arithmetic mean; GM, geometric mean; SD, standard deviation; GSD, geometric standard deviation.

According to Table 5, the AEDR at one meter above ground surface ranged from 130 to 265 nGy h^{-1} and from 119 to 238 nGy h^{-1} at Fongo-Tongo and Dschang, respectively, with an average of 207 ± 37 nGy h^{-1} and 170 ± 31 nGy h^{-1} for soil samples analyzed in the laboratory. It ranged from 95 to 264 nGy h^{-1} and from 69 to 126 nGy h^{-1}, with a mean value of 198 ± 45 nGy h^{-1} and 96 ± 14 nGy h^{-1}, for the in situ measurement in

Fongo-Tongo and Dschang, respectively. The mean values of the current studies are all above the value set of 60 nGy h^{-1} [1].

Table 5. Summary of the different radiological parameters obtained by in situ.

Locality	Fongo-Tongo					Dschang					Limit
Parameters	**Min**	**Max**	**Med**	**AM**	**SD**	**Min**	**Max**	**Med**	**AM**	**SD**	
AEDR (nGy/y)	95	264	210	198	45	69	126	94	96	14	1
AEED (mSv)	0.58	1.62	1.27	1.22	0.28	0.42	0.77	0.58	0.59	0.08	1
H_{in}	0.9	2.01	1.65	1.57	0.32	1.25	2.04	1.68	1.68	0.19	1
H_{out}	0.56	1.64	1.3	1.22	0.29	0.92	1.64	1.32	1.31	0.16	1
$ELCR_{in}$	1.22	3.4	2.71	2.56	0.58	0.89	1.62	1.21	1.24	0.17	
$ELCR_{out}$	0.81	2.7	1.8	1.7	0.31	0.59	1.08	0.81	0.83	0.11	
ELCR	2.03	5.67	4.51	4.26	0.97	1.48	2.7	2.01	2.07	0.28	
I_{α}	0.47	1.01	0.63	0.64	0.11	0.49	0.9	0.66	0.69	0.09	1
I_{γ}	0.72	2.12	1.67	1.58	0.37	1.19	2.12	1.7	1.69	0.21	1

AM, arithmetic mean; GM, geometric mean; SD, standard deviation; GSD, geometric standard deviation.

3.4.2. External and Internal Radiation Hazard Index

External Hazard Index

The obtained values of H_{ext} are presented in Table 4. The average values are 1.48 at Fongo-Tongo and 1.32 at Dschang. H_{ext} values are greater than unity, and therefore, it can be recommended to the populations of those sites to use earth as a building construction material, except in some places where the level of natural radioactivity is relatively high.

Internal Hazard Index

The statistical parameters from H_{in} are summarized in Table 4. The maximum values of H_{in} are 2.81 and 2.04, with an average value of 1.88 and 1.68, in Fongo-Tongo and Dschang, respectively. H_{in} values are also greater than unity [64]. Nevertheless, to avoid excessive internal exposure to ^{222}Rn in these localities, the use of earth can be recommended as a building material, provided that there is good ventilation and air circulation in the rooms of the dwelling.

3.4.3. Excess Lifetime Cancer Risk (ELCR)

The ELCR statistical parameters' values obtained by gamma spectrometry in laboratory and in situ are summarized in Table 4. They ranged from 2.03×10^{-3} to 5.67×10^{-3}, with a mean value of 4.44×10^{-3}, in Fongo-Tongo; and from 1.48×10^{-3} to $5 \times 11\ 10^{-3}$, with a mean value of 3.64×10^{-3}, in Dschang. The mean values of ECR in Fongo-Tongo and Dschang were, respectively, 1.29 and 1.06 times higher than 0.29×10^{-3}, the UNSCEAR recommended limit value [1]. However, the risk values obtained could be overestimated if, in addition to the above risk, the risk due to radioactivity from building materials was taken into account, because more than 70% of the houses in the area use mainly mud bricks as building material.

3.5. Long-Term ECR Analysis Using RESRAD-ONSITE and RESRAD-BUILD Computer Codes

As shown in Figure 6, the total ECR calculated with RESRAD-ONSITE decreased progressively over the years, from the maximum value of 8.58×10^{-3} obtained at the dates T = 1 and T = 1 year to the value of 7.41×10^{-3} obtained at T = 100 years before decreasing significantly. This remarkable decreasing may be due to the self-absorption of building materials or to the process of radioactive decay [65].

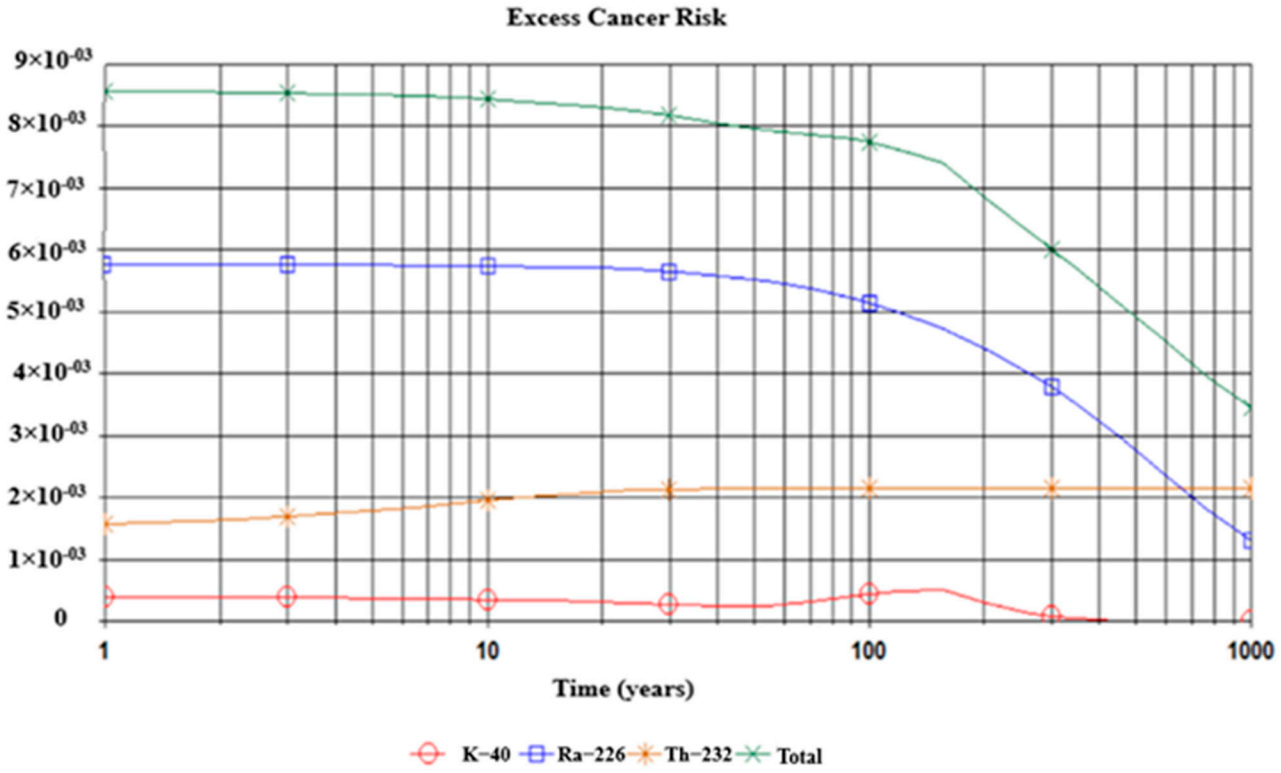

Figure 6. Long-term plotting of ECR for all exposure pathways and for each primordial radionuclide.

Similarly, ^{226}Ra is the major contributor to the total ECR at about 70% in the first year. This contribution decreases slightly over the years before dropping significantly after 100 years. The maximum value of risk due to ^{226}Ra obtained at T = 10 years is 7.372×10^{-6}. The ECR due to ^{232}Th, on the other hand, is inversely proportional to that of ^{226}Ra over the period from 1 to 40 years, where it becomes practically constant, and the maximum value obtained at T = 50 years is 9.250×10^{-6}. As for ^{40}K, its contribution to the total risk remains the smallest, but it shows some slight variations before decreasing to zero. Similar results were observed in studies conducted in the cobalt–nickel region of Lomié in Eastern Cameroon [66]. Table 5 summarizes the total ECR for initially existent radionuclides and pathways at T = 0, 1, 10, 30, 50, and 100 years.

RESRAD-BUILD assessed the total risk due to radioactivity from soil used in the manufacture of bricks as a building material. The results obtained for the different exposure routes and for each nuclide as a function of time are summarized in Table 2. The maximum value of the total excess risk obtained at T = 30 years is 5.19×10^{-2} for all the summed routes. Similarly, the value of the total excess risk for all summed nuclides obtained at T = 30 years is 1.89×10^{-2}. However, it should be noted that the external pathway is the one that contributes the most to the total excess risk. The maximum risk value for this pathway, which is 2.33×10^{-2}, was obtained at T = 30 years. Nevertheless, the decrease observed beyond 30 years for the external route would be due to the self-absorption of building materials [15,67,68]. Similar results were obtained in the work carried out in the Poli uranium region [17], in the bauxite zones of Southern Adamawa [16], and in some localities of the Centre Region, Cameroon [67].

The results presented in Table 6 show that ^{226}Ra is the main contributor to the total excess risk compared to ^{232}Th and ^{40}K. The risk due to ^{226}Ra increases progressively with time until reaching an increasing threshold after 70 years. The occurrence of this radionuclide in high concentrations in building materials increases the probability of accumulation of high indoor radon concentration [68]. Figure 7 represents the long-term total ECR for each radionuclide.

Table 6. Total ECR for initially existent radionuclides and pathways and fraction of total risk.

T (Years)	Ground	Inhalation	Radon	Plant	Meat	Milk	Soil	Total
0	1.74×10^{-3}	6.32×10^{-6}	4.89×10^{-3}	1.56×10^{-3}	2.24×10^{-4}	1.44×10^{-4}	2.22×10^{-5}	8.58×10^{-3}
1	1.74×10^{-3}	6.32×10^{-6}	4.89×10^{-3}	1.56×10^{-3}	2.24×0^{-4}	1.44×10^{-4}	2.22×10^{-5}	8.58×10^{-3}
3	1.73×10^{-3}	6.32×10^{-6}	4.87×10^{-3}	1.55×10^{-3}	2.18×10^{-4}	1.42×10^{-4}	2.22×10^{-5}	8.54×10^{-3}
10	1.72×10^{-3}	6.30×10^{-6}	4.81×10^{-3}	1.53×10^{-3}	2.06×10^{-4}	1.36×10^{-4}	2.20×10^{-5}	8.43×10^{-3}
30	1.69×10^{-3}	6.27×10^{-6}	4.67×10^{-3}	1.49×10^{-3}	1.76×10^{-4}	1.24×10^{-4}	2.17×10^{-5}	8.17×10^{-3}
100	1.60×10^{-3}	6.18×10^{-6}	4.19×10^{-3}	1.38×10^{-3}	1.16×10^{-4}	9.75×10^{-5}	2.04×10^{-5}	7.41×10^{-3}

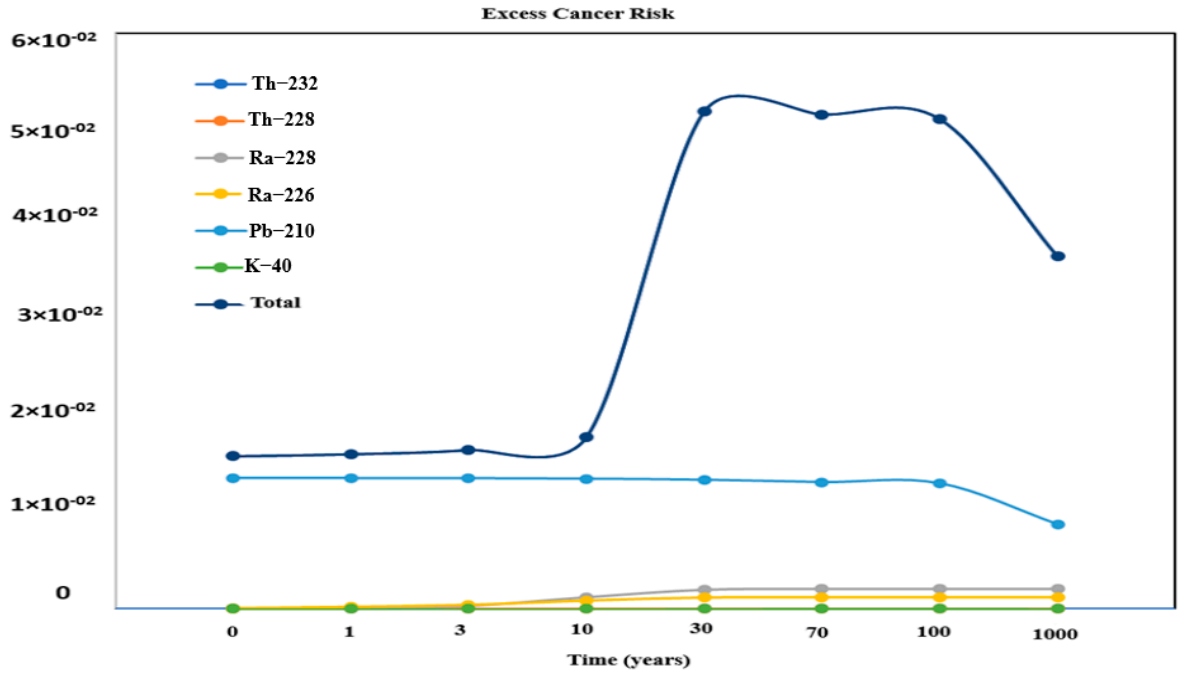

Figure 7. Long-term total excess risk for each nuclide.

According to Table 7, the pathway that contributes most to the total cancer risk is the external pathway. Like the other pathways, the risk increases until it reaches a value of 2.33×10^{-2} at T = 30 years. similarly, the total cancer risk also increases and reaches a value of 5.19×10^{-2} at the same date.

Table 7. Total risk of excess cancer for all exposure pathways.

Pathway Detail of Risks	ELCR T (Years)						
	T = 0	T = 1	T = 3	T = 10	T = 30	T = 70	T = 100
External	1.57×10^{-2}	1.59×10^{-2}	1.63×10^{-2}	1.76×10^{-2}	2.33×10^{-2}	2.32×10^{-2}	2.30×10^{-2}
Deposition	5.15×10^{-9}	5.22×10^{-9}	5.31×10^{-9}	5.64×10^{-9}	3.68×10^{-3}	3.66×10^{-3}	3.63×10^{-3}
Immersion	4.50×10^{-11}	4.54×10^{-11}	4.65×10^{-11}	5.06×10^{-10}	3.68×10^{-3}	3.66×10^{-3}	3.63×10^{-3}
Inhalation	1.18×10^{-6}	1.23×10^{-6}	1.36×10^{-6}	1.76×10^{-6}	3.01×10^{-3}	2.99×10^{-3}	2.96×10^{-3}
Radon	2.20×10^{-4}	2.27×10^{-4}	2.49×10^{-4}	3.30×10^{-4}	4.08×10^{-3}	4.06×10^{-3}	4.03×10^{-3}
Ingestion	5.39×10^{-8}	5.88×10^{-8}	6.82×10^{-8}	8.39×10^{-8}	1.89×10^{-2}	1.88×10^{-2}	1.86×10^{-2}
Total	1.59×10^{-2}	1.61×10^{-2}	1.66×10^{-2}	1.79×10^{-2}	5.19×10^{-2}	5.15×10^{-2}	5.11×10^{-2}

3.6. Radiation Hazard Index

3.6.1. Gamma Radiation Hazard Index, I_γ

The results obtained give maximum values of I_γ equal to 2.12 and 2.67 at Fongo-Tongo and equal to 2.12 and 1.90 at Dschang for in situ and laboratory measurements, respectively,

which are significantly greater than or equal to 2 to 2.7 times the maximum permissible value [50]. Similarly, the mean values of 1.69 and 1.34 at Dschang and 1.58 and 1.64 at Fongo-Tongo are also above the recommended limit. Thus, the land in the region could be exempted from all types of restrictions with respect to radiological risks, except at certain locations where I_γ is very high.

3.6.2. Alpha Radiation Hazard Index, I_α

The average values of I_α are reported in Table 4 and are below the reference limit value of unity for both study sites. Therefore, the soil bricks made at the study sites can be used as a building material in these two localities without exposing the inhabitant to a major risk of induction of lung cancer, because the I_α is below the safety limit recommended by UNSCEAR.

4. Conclusions

The current work was performed to study the ^{222}Rn and ^{226}Ra correlation that may exist in soil and assess the onsite and in-dwellings long-term ECR in the bauxite-bearing area of Fongo-Tongo. To achieve this, gamma spectrometry by in situ and laboratory was used to determine activity concentrations of ^{226}Ra in soil. A strong correlation was found between ^{226}Ra determined from the two methods and ^{222}Rn in the soil. The ^{222}Rn measurement in soil is therefore an excellent predictor of ^{226}Ra and vice versa. Radiological parameters such as AEED, H_{in}, H_{ext}, ELCR, I_γ, and I_α were also determined to assess the level of radiological exposure of the public. Their values were all higher than the various corresponding safety limits recommended by UNSCEAR. The cancer risk assessed with RESRAD-ONSITE following exposure to the various radionuclides decreases from the first to the hundredth year for all the primordial radionuclides. The risk tends toward zero after the thousandth year. The maximum value of the total cancer risk of 8.58×10^{-3} was observed at t = 1 year. It should also be noted that the contribution of ^{226}Ra to cancer risk is high compared to that of ^{232}Th. ^{226}Ra is therefore the major contributor to cancer risk. A decrease in the contribution of all exposure pathways is observed from t = 1 year to t = 100 years. The risk tends to decrease considerably after 100 years. The cancer risk due to inhalation of radon and its progeny increases and reaches a peak of 3.01×10^{-3} at t = 70 years. It should be noted that RESRAD-BUILD evaluates the risk related to radon and thoron according to the concentration of radium and thorium. Given the high concentrations of ^{232}Th in soil samples from the current study area, the contribution of thoron (^{220}Rn) to cancer risk is high. Nevertheless, the observed decrease over time for all pathways and all radionuclides could be due to the self-absorption of building materials.

Author Contributions: Conceptualization, L.B.D. and S.; methodology, L.B.D., G.S.B. and S.; software, L.B.D., O.B.M. and J.E.N.N.II validation, L.B.D., G.S.B., and S.; formal analysis, L.B.D., J.E.N.N.II and S.; writing—original draft preparation, L.B.D., O.B.M. and G.S.B.; funding acquisition, S. All authors have read and agreed to the published version of the manuscript.

Funding: This work was partly supported by the International Atomic Energy Agency (IAEA) within the framework of the Technical Cooperation (TC) Project CMR9009. The Government of Cameroon supported field works through the Public Investment Budget 2020 and 2021 of the Ministry of Scientific Research and Innovation.

Institutional Review Board Statement: Not applicable.

Informed Consent Statement: Not applicable.

Data Availability Statement: The authors confirm that the data supporting the findings of this study are available within the article.

Acknowledgments: The Ministry of Scientific Research and Innovation of Cameroon is acknowledged for funding the field works through the Public Investment Budget 2021 allocated to the Institute of Geological and Mining Research.

Conflicts of Interest: The authors declare no conflict of interest.

References

1. UNSCEAR. *Sources and Effects of Ionizing Radiation: United Nations Scientific Committee on the Effects of Atomic Radiation: UNSCEAR 2000 Report to the General Assembly, with Scientific Annexes*; United Nations: Vienna, Austria, 2000.
2. Barbarand, J.; Beaufort, D.; Benedicto, A.; Caillat, C.; Calas, G.; Cathelineau, M.; Cheilletz, A.; Cote, G.; Cuney, M.; Dacheux, N.; et al. Géologie et Chimie de l' Uranium Programme et volume des résumés. In Proceedings of the Réunion de la Société Géologique de France avec le concours d'AREVA, CNRS—INSU, PACEN, GUTEC, IDES, Université de Paris-Sud, Paris, France, 29–30 November 2011.
3. Holmes, A. Petrogenesis of katungite and its associates. *Am. Mineral.* **1950**, *35*, 772–792.
4. Bariand, J.G.P.; Cesbron, F. Métamorphiques et leurs produits d' altération, par P. Bariand, F. *Bull. Minér. Cristallogr.* **1978**, *2*, 356.
5. Paquet, F.; Bailey, M.; Leggett, R.; Lipsztein, J.; Marsh, J.; Fell, T.; Smith, T.; Nosske, D.; Eckerman, K.; Berkovski, V.; et al. ICRP Publication 137: Occupational Intakes of Radionuclides: Part 3. *Ann. ICRP* **2017**, *46*, 1–486. [CrossRef]
6. Clement, C.; Tirmarche, M.; Harrison, J.; Laurier, D.; Paquet, F.; Blanchardon, E.; Marsh, J. Part 1: Lung Cancer Risk from Radon and Progeny. *Ann. ICRP* **2010**, *40*, 11. [CrossRef] [PubMed]
7. Lindsay, R.; Newman, R.; Speelman, W. A study of airborne radon levels in Paarl houses (South Africa) and associated source terms, using electret ion chambers and gamma-ray spectrometry. *Appl. Radiat. Isot.* **2008**, *66*, 1611–1614. [CrossRef] [PubMed]
8. Hassan, N.M.; Ishikawa, T.; Hosoda, M.; Sorimachi, A.; Tokonami, S.; Fukushi, M.; Sahoo, S.K. Assessment of the natural radioactivity using two techniques for the measurement of radionuclide concentration in building materials used in Japan. *J. Radioanal. Nucl. Chem. Artic.* **2010**, *283*, 15–21. [CrossRef]
9. Mohammed, R.S.; Ahmed, R.S. Estimation of excess lifetime cancer risk and radiation hazard indices in southern Iraq. *Environ. Earth Sci.* **2017**, *76*, 303. [CrossRef]
10. Trevisi, R.; Leonardi, F.; Risica, S.; Nuccetelli, C. Updated database on natural radioactivity in building materials in Europe. *J. Environ. Radioact.* **2018**, *187*, 90–105. [CrossRef]
11. Abiama, P.E.; Tokonami, S.; Patrice, E.A. Natural Radiation Survey in the Uranium and Thorium Bearing Regions of Cameroon. 2016. Available online: https://www.researchgate.net/publication/293593746_Natural_radiation_survey_in_the_uranium_and_thorium_bearing_regions_of_Cameroon (accessed on 5 September 2022).
12. Didier, T.S.S.; Saïdou; Tokonami, S.; Hosoda, M.; Suzuki, T.; Kudo, H.; Bouba, O. Simultaneous measurements of indoor radon and thoron and inhalation dose assessment in Douala City. *Cameroon. Isot. Environ. Health Stud.* **2019**, *55*, 499–510. [CrossRef]
13. Yimele, B.C.; Ekobena, H.P.F.; Nguelem, E.J.M.; Ndontchueng, M.M.; Ben-Bolie, G.H.; Ateba, P.O. Radiation hazard of naturally occurring soil in FONGO TONGO-Cameroon. *Arab. J. Geosci.* **2019**, *12*, 233. [CrossRef]
14. Mekongtso Nguelem, E.J.M.; Ndontchueng, M.M.; Motapon, O. Determination of ^{226}Ra, ^{232}Th, ^{40}K, ^{235}U and ^{238}U activity concentration and public dose assessment in soil samples from bauxite core deposits in Western Cameroon. *SpringerPlus* **2016**, *5*, 1253. [CrossRef] [PubMed]
15. Bachirou, S.; Joseph, I.I.; Ndjana, E.; Haman, F.; Godfroy, M.; Njock, K. Natural Radiation Exposure and Radiological Hazard Analysis in a Radon-Prone Area of the Adamawa Region, Cameroon. *Radiat. Prot. Dosim.* **2022**, *198*, 74–85.
16. Saïdou; Modibo, O.B.; Emmanuel, N.N.I.J.; German, O.; Michaux, K.N.; Abba, H.Y. Indoor Radon Measurements Using Radon Track Detectors and Electret Ionization Chambers in the Bauxite-Bearing Areas of Southern Adamawa, Cameroon. *Int. J. Environ. Res. Public Health* **2020**, *17*, 6776. [CrossRef] [PubMed]
17. Saïdou; Shinji, T.; Hosoda, M.; Flore, T.S.Y.; Emmanuel, N.N.J.; Naofumi, A.; Modibo, O.B.; Joseph, P. Natural radiation exposure to the public in the uranium bearing region of Poli, Cameroon: From radioactivity measurements to external and inhalation dose assessment. *J. Geochem. Explor.* **2019**, *205*, 106350. [CrossRef]
18. Ndjana Nkoulou, J.E.; Ngoa Engola, L.; Hosoda, M.; Bongue, D.; Suzuki, T.; Kudo, H.; Kwato Njock, M.G.; Tokonami, S. Simultaneous indoor radon, thoron and thoron progeny measurements in betare-oya gold mining areas, eastern Cameroon. *Radiat. Prot. Dosim.* **2019**, *185*, 391–401. [CrossRef]
19. Bineng, G.S.; Saïdou; Tokonami, S.; Hosoda, M.; Siaka, Y.F.T.; Issa, H.; Suzuki, T.; Kudo, H.; Bouba, O. The Importance of Direct Progeny Measurements for Correct Estimation of Effective Dose Due to Radon and Thoron. *Front. Public Health* **2020**, *8*, 17. [CrossRef]
20. Saïdou; Tokonami, S.; Janik, M.; Samuel, B.G.; Abdourahimi; Emmanuel, N.N.I.J. Radon-thoron discriminative measurements in the high natural radiation areas of southwestern Cameroon. *J. Environ. Radioact.* **2015**, *150*, 242–246. [CrossRef]
21. Saïdou; Abiama, P.E.; Tokonami, S. Comparative study of natural radiation exposure to the public in three uranium and oil regions of Cameroon. *Radioprotection* **2015**, *50*, 265–271. [CrossRef]
22. Jiomeneck, P.S.T.; Tematio, P.; Wilson, M.A.; Yemefack, M. Andosolization of Soils on a Strombolian Cone at Mount Bambouto, Cameroon. *Open J. Soil Sci.* **2011**, *1*, 97–105. [CrossRef]
23. Tedonkeng, P.E. Rainfall Variability along the Southern Flank of the Bambouto Mountain (West-Cameroon). *J. Cameroon Acad. Sci.* **2008**, *8*, 45–52.
24. Tematio, P.; Kengni, L.; Bitom, D.; Hodson, M.; Fopoussi, J.; Leumbe, O.; Mpakam, H.; Tsozué, D. Soils and their distribution on Bambouto volcanic mountain, West Cameroon highland, Central Africa. *J. Afr. Earth Sci.* **2004**, *39*, 447–457. [CrossRef]
25. Kenfack, P.L.; Tematio, P.; Kwekam, M.; Ngueutchoua, G.; Njike, P.R. Evidence of a Miocene volcano-sedimentary lithostratigraphic sequence at Ngwa (Dschang Region, West Cameroon): Preliminary analyses and geodynamic interpretation. *J. Pet. Technol. Altern. Fuels*. 2011, 2, pp. 25–34. Available online: http://www.academicjournals.org/JPTAF (accessed on 1 September 2022).

26. Dongmo, F.W.N.; Yongue, R.F.; Bolarinwa, A.T.; Ngatcha, R.B.; Fuanya, C.; Kamga, M.A. *Contribution to the Study of Bauxites' Formation in the Fongo-Tongo (Western Cameroon) Sites*; Springer International Publishing: Cham, Switzerland, 2019; pp. 241–244. [CrossRef]
27. Dongmo, F.W.N.; Fouateu, R.Y.; Ntouala, R.F.D.; Lemdjou, Y.B.; Ledoux, D.C.; Bolarinwa, A.T. Geochemical, mineralogical and macroscopic facies of the Fongo-Tongo bauxite deposit western Cameroon. *Appl. Earth Sci. Trans. Inst. Min. Metall.* **2021**, *130*, 23–41. [CrossRef]
28. Tchamba, A.B.; Yongue, R.; Melo, U.C.; Kamseu, E.; Njoya, D. Caractérisation de la bauxite de HaléoDanielle (MinimMartap, Cameroun) en vue de son utilisation industrielle dans les matériaux à haute teneur en alumine. *Silic. Ind.* **2008**, *73*, 77–84.
29. Mehra, R.; Sonkawade, R.G.; Badhan, K.; Singh, S. Measurement of natural radioactivity in rock samples using gamma ray spectrometry. *Asian J. Chem.* **2009**, *21*, 212–215. [CrossRef]
30. Livens, F. Measurement of radionuclides in food and the environment. *A guidebook. J. Environ. Radioact.* **1990**, *11*, 201–202. [CrossRef]
31. Ademola, A.K.; Bello, A.K.; Adejumobi, A.C. Determination of natural radioactivity and hazard in soil samples in and around gold mining area in Itagunmodi, south-western, Nigeria. *J. Radiat. Res. Appl. Sci.* **2014**, *7*, 249–255. [CrossRef]
32. Mbonu, C.C.; Essiett, A.A.; Ben, U.C. Geospatial assessment of radiation hazard indices in soil samples from Njaba, Imo State, South-Eastern Nigeria. *Environ. Challenges* **2021**, *4*, 100117. [CrossRef]
33. Mirion Technologies (Canberra). Genie TM 2000 Software, Basic Spectroscopy. 2016. Available online: https://www.google.com/url?sa=t&rct=j&q=&esrc=s&source=web&cd=&cad=rja&uact=8&ved=2ahUKEwirucvf0qb7AhUUEVkFHczAD-gQFnoECAoQAQ&url=https%3A%2F%2Fwww3.nd.edu%2F~{}wzech%2FGenie%25202000%2520Operations%2520Manual.pdf&usg=AOvVaw0a4Hg7xAEMTZPukRCd3oLp (accessed on 23 September 2022).
34. Bineng, G.S.; Hosoda, M.; Siaka, Y.F.T.; Akata, N.; Talla, S.F.; Abiama, P.E.; Tokonami, S. External radiation exposure to the public using car-borne survey method in the uranium and thorium bearing region of Lolodorf, Cameroon External Radiation Exposure to the Public Using Car-borne Survey Method in the Uranium and Thorium Bearing Region of L. *Radiat. Environ. Med.* **2020**, *9*, 13–20.
35. Bobbo, M.O.; Saïdou; Ii, J.E.N.N.; Suzuki, T.; Kudo, H.; Hosoda, M.; Owono, L.C.O.; Tokonami, S. Occupational Natural Radiation Exposure at the Uranium Deposit of Kitongo, Cameroon. *Radioisotopes* **2019**, *68*, 621–630. [CrossRef]
36. Shouop, C.J.G.; Moyo, M.N.; Chene, G.; Mekontso, E.J.N.; Motapon, O.; Kayo, S.A.; Strivay, D. Assessment of natural radioactivity and associated radiation hazards in sand building material used in Douala Littoral Region of Cameroon, using gamma spectrometry. *Environ. Earth Sci.* **2017**, *76*, 164. [CrossRef]
37. Raghu, Y.; Ravisankar, R.; Chandrasekaran, A.; Vijayagopal, P.; Venkatraman, B. Assessment of natural radioactivity and radiological hazards in building materials used in the Tiruvannamalai District, Tamilnadu, India, using a statistical approach. *J. Taibah Univ. Sci.* **2017**, *11*, 523–533. [CrossRef]
38. SARAD GmbH. Nuc Scout, Portable Gamma Identifier—Quantifier—Dose Rate Meter. 2018. Available online: www.sarad.de/info@sarad.de (accessed on 8 September 2022).
39. SARAD GmbH. Manual Software dVISION. Wiesbadener Straße 10 D-01159 Dresden Germany. 2015. Available online: https://www.sarad.de/cms/media/docs/handbuch/Manual_dVISION_EN_16-10-15.pdf (accessed on 8 September 2022).
40. SARAD GmbH. Manual Software dCONFIG. Wiesbadener Straße 10 D-01159 Dresden DEUTSCHLAND. 2009. Available online: http://www.sarad.de/cms/media/docs/handbuch/Manual_dCONFIG_EN_21-12-12.pdf (accessed on 8 September 2022).
41. Gammadata. *User's Guide MARKUS 10 The Instrument for Determining the Radon Content in the Soil*; Gammadata: Uppsala, Sweden, 2019.
42. Agbalagba, E.; Avwiri, G.; Chad-Umoreh, Y. γ-Spectroscopy measurement of natural radioactivity and assessment of radiation hazard indices in soil samples from oil fields environment of Delta State, Nigeria. *J. Environ. Radioact.* **2012**, *109*, 64–70. [CrossRef] [PubMed]
43. Soh, S.T.; Saïdou; Hosoda, M.; Ii, J.N.N.; Akata, N.; Bouba, O.; Tokonami, S. Natural radioactivity measurements and external dose estimation by car-borne survey in Douala city, Cameroon. *Radioprotection* **2018**, *53*, 255–263. [CrossRef]
44. Penabei, S.; Bongue, D.; Maleka, P.; Dlamini, T.; Saïdou; Shouop, C.G.; Halawlaw, Y.; Ebongue, A.N.; Njock, M.K. Assessment of natural radioactivity levels and the associated radiological hazards in some building materials from Mayo-Kebbi region. *Chad. Radioprotection* **2018**, *53*, 265–278. [CrossRef]
45. Ndontchueng, M.M.; Nguelem, E.J.M.; Motapon, O.; Njinga, R.L.; Simo, A.; Guembou, J.C.S.; Yimele, B. Radiological Hazards in Soil from the Bauxite Deposits Sites in Dschang Region of Cameroon. *Br. J. Appl. Sci. Technol.* **2015**, *5*, 342–352. [CrossRef]
46. Saleh, H.; Abu Shayeb, M. Natural radioactivity distribution of southern part of Jordan (Ma'an) Soil. *Ann. Nucl. Energy* **2014**, *65*, 184–189. [CrossRef]
47. Pisapak, P.; Todorovic, N.; Bhongsuwan, T. Correlation between radon and radium concentrations in soil and estimation of natural radiation hazards in Namom district, Songkhla province (Southern Thailand). *Environ. Earth Sci.* **2017**, *76*, 139. [CrossRef]
48. Yu, C.; Zielen, A.J.; Cheng, J.J.; LePoire, D.J.; Gnanapragasam, E.; Kamboj, S.; Arnish, J.; Wallo, A., III; Williams, W.A. *User's Manual for RESRAD Version 6*; Environmental Assessment Division, Argonne National Laboratory (ANL): Lemont, IL, USA, 2001; p. 458. Available online: http://resrad.evs.anl.gov/docs/resrad6.pdf (accessed on 17 September 2022).
49. Orosun, M.M.; Usikalu, M.R.; Oyewumi, K.J.; Achuka, J.A. Radioactivity levels and transfer factor for granite mining field in Asa, North-central Nigeria. *Heliyon* **2020**, *6*, e04240. [CrossRef]

50. European Commission. *Report on Radiological Protection Principles Concerning the Natural Radioactivity of Building Materials, Radiation Protection No. 112. Directorate-General Environment, Nuclear Safety and Civil Protection*; European Commission: Brussels, Belgium, 1999.
51. Aladeniyi, K.; Olowookere, C.; Oladele, B.B. Measurement of natural radioactivity and radiological hazard evaluation in the soil samples collected from Owo, Ondo State, Nigeria. *J. Radiat. Res. Appl. Sci.* **2019**, *12*, 200–209. [CrossRef]
52. Darwish, D.; Abul-Nasr, K.; El-Khayatt, A. The assessment of natural radioactivity and its associated radiological hazards and dose parameters in granite samples from South Sinai, Egypt. *J. Radiat. Res. Appl. Sci.* **2015**, *8*, 17–25. [CrossRef]
53. Hiéronymus, B. Etude minéralogique et géochimique des formations bauxitiques de l'Ouest du Cameroun. *Cah. ORSTOM Sér. Géologie* **1973**, *5*, 97–112.
54. Curien, H. *La Radioactivité des Roches, par R. Coppens, Collection « Que Sais-Je ? » N°741, 1957*; Presses Universitaires de France: Paris, France, 1957; Volume 1.
55. Waterways, I.N. *Sediments and pollution General Considerations*; IAEA: Vienna, Austria, 1984; p. 33.
56. Boukhenfouf, W.; Boucenna, A. The radioactivity measurements in soils and fertilizers using gamma spectrometry technique. *J. Environ. Radioact.* **2011**, *102*, 336–339. [CrossRef] [PubMed]
57. Ngachin, M.; Garavaglia, M.; Giovani, C.; Njock, M.K.; Nourreddine, A. Radioactivity level and soil radon measurement of a volcanic area in Cameroon. *J. Environ. Radioact.* **2008**, *99*, 1056–1060. [CrossRef] [PubMed]
58. Nguelem, E.; Ndontchueng, M.M.; Motapon, O.; Darko, E.O.; Simo, A. Determination of ^{226}Ra,^{232}Th,^{40}K and ^{235}U in soil samples from bauxite core deposits in western Cameroon. *Radioprotection* **2016**, *51*, 199–205. [CrossRef]
59. Esan, D.T.; Sridhar, M.K.C.; Obed, R.; Ajiboye, Y.; Afolabi, O.; Olubodun, B.; Oni, O.M. Determination of Residential Soil Gas Radon Risk Indices Over the Lithological Units of a Southwestern Nigeria University. *Sci. Rep.* **2020**, *10*, 7368. [CrossRef]
60. Merdanoğlu, B.; Altınsoy, N. Radioactivity concentrations and dose assessment for soil samples from Kestanbol granite area, Turkey. *Radiat. Prot. Dosim.* **2006**, *121*, 399–405. [CrossRef]
61. Sannappa, J.; Ningappa, C.; Narasimha, K.N.P. Natural radioactivity levels in granite regions of Karnataka State. *Indian J. Pure Appl. Phys.* **2010**, *48*, 817–819.
62. Nguyen, P.T.H.; Nguyen, V.T.; Vu, N.B.; Le Cong, H. Soil radon gas in some soil types in the rainy season in Ho Chi Minh City. *Vietnam. J. Environ. Radioact.* **2018**, *193–194*, 27–35. [CrossRef]
63. Yalim, H.A.; Akkurt, I.; Ozdemir, F.B.; Unal, R.; Sandikcioglu, A.; Akkurt, A. The Measurement of Radon and Radium Concentrations in Well Water in the Afyonkarahisar area of Turkey. *Indoor Built Environ.* **2007**, *16*, 77–81. [CrossRef]
64. Petropoulos, N.; Anagnostakis, M.; Simopoulos, S. Photon attenuation, natural radioactivity content and radon exhalation rate of building materials. *J. Environ. Radioact.* **2002**, *61*, 257–269. [CrossRef]
65. Souffit, G.D.; Saïdou, S.; Modibo, O.B.; Lepoire, D.; Tokonami, S. Risk Assessment of Exposure to Natural Radiation in Soil Using RESRAD-ONSITE and RESRAD-BIOTA in the Cobalt-Nickel Bearing Areas of Lomié in Eastern Cameroon. *Radiation* **2022**, *2*, 177–192. [CrossRef]
66. Ii, J.E.N.N.; Manga, A.; Saïdou; German, O.; Sainz-Fernandez, C.; Kwato Njock, M.G. Natural radioactivity in building materials, indoor radon measurements, and assessment of the associated risk indicators in some localities of the Centre Region. *Cameroon. Environ. Sci. Pollut. Res.* **2022**, *29*, 54842–54854. [CrossRef]
67. Risica, S.; Bolzan, C.; Nuccetelli, C. Radioactivity in building materials: Room model analysis and experimental methods. *Sci. Total Environ.* **2001**, *272*, 119–126. [CrossRef]
68. Souffit, G.D.; Valdes, M.J.; Modibo, O.B.; Flore, T.S.Y.; Félix, B.A.J.; Saïdou; Tokonami, S. Radon Risk Assessment and Correlation Study of Indoor Radon, Radium-226, and Radon in Soil at the Cobalt–Nickel Bearing Area of Lomié, Eastern Cameroon. *Water Air Soil Pollut.* **2022**, *233*, 196. [CrossRef]